March 2018

The Role of the Metallochaperone HypA in the Acid Survival and Activities of Nickel Enzymes in Helicobacter pylori

Heidi Hu
University of Massachusetts Amherst

THE ROLE OF THE METALLOCHAPERONE HYPA IN THE ACID SURVIVAL AND ACTIVITIES OF NICKEL ENZYMES IN *HELICOBACTER PYLORI*

A Dissertation Presented

by

HEIDI QIAOYI HU

Submitted to the Graduate School of the
University of Massachusetts Amherst in partial fulfillment
of the requirements for the degree of

DOCTOR OF PHILOSOPHY

February 2018

Program of Molecular and Cellular Biology

THE ROLE OF THE METALLOCHAPERONE HYPA IN THE ACID SURVIVAL AND ACTIVITIES OF NICKEL ENZYMES IN *HELICOBACTER PYLORI*

A Dissertation Presented

by

HEIDI QIAOYI HU

Approved as to style and content by:

_____
Michael J. Maroney, Chair

_____
Michael J. Knapp, Member

_____
Jeanne A. Hardy, Member

_____
Peter Chien, Member

_____
Scott C. Garman, Leader
Molecular and Cellular Biology Graduate Program

_____
John Lopes, Director
Interdepartmental Graduate Programs

ACKNOWLEDGMENTS

I must thank my collaborators, the Merrell Lab, at the Uniformed Services University of the Health Sciences (Bethesda, Maryland) for their work on the acid survival of *hypA* variant strains of *H. pylori*. I also enjoyed working with our collaborators at Stefano Ciurli's Lab, at the University of Bologna (Bologna, Italy) on the NMR structures of HypA. The hospitality and insight they have shown me are greatly appreciated.

Big thanks to Lizz Bartlett and IALS Biophysical Characterization Core Facility, where I collected my ITC, SEC-MALS, and thermophoresis data. I also acknowledge the beamline scientists, "Nerik", Matt, Riti, and "Ferik", who made sure we did not break the beam while collecting XAS data at SSRL beamline 7-3 and 9-3; and at NSLS (formerly) beamline X3B.

I appreciate the interdisciplinary groups at UMass Amherst, including MCB, CBI, and Protein Homeostasis/M2M. I am grateful for the meaningful discussions and the platforms for sharing our research and expertise with one another, which ultimately made me a better researcher. I would also like to thank my colleagues and friends at the LSL and LGRT, especially the Knapp Lab, the Hardy Lab, the Chien Lab, the Hebert Lab, the Vierling Lab, and the Gierasch Lab for sharing their equipment, space, expertise, and the occasional hugs as needed.

I would like to thank my advisor, Professor Mike Maroney, for accepting me into his group and for his patience, guidance, and discussions through the past eight years. I also appreciate my dissertation committee, Professors Mike Knapp, Jeanne Hardy, and Peter Chien, who have provided helpful guidance through this process.

Many thanks to the past and present members of the Maroney lab, who are instrumental for not only teaching me research skills, but also the dedication and mental fortitude required to finishing my PhD studies. The serious lab mates, especially my "research mother" Professor Khadine Higgins, have always been there to support me through helpful research discussions and through bouts of serious self-doubt. Special thanks for the silly-fun members of the lab, especially "Captain" Dr. Carolyn Carr and "Cute-Tiffany" Hsin-Ting Huang, for indulging me in serious discussions about research, sci-fi, politics, and silly life antics, which uplifted my spirits and provided much-needed laughter to lab life.

I am grateful for the wonderful teachers who have encouraged me and help shape my interest in science. Mr. Brenner and Ms. Kenney first sparked my interest in biology and chemistry through not only helpful instructions, but immense kindness and understanding. Dr. Martha Richmond and Dr. Rachel Kipp helped me solidify my interest in the colorful world of transition metals in biology and then further encouraged me to go to grad school.

I am thankful for the encouragement and support of friends and family throughout my graduate career. My mom and sister have been immeasurably supportive in my pursuit of graduate studies. Also, my not so little brother, who taught me the importance of enjoying life daily while still pursuing bigger dreams. I am so thankful to my friends, who have supported me throughout my graduate career and for not asking me when I will graduate in the last few months!

Most importantly, I must thank my fiancé, Hector, who has showered me with love and support throughout the past twelve years, and has been driving back and forth between Woburn and Amherst week after week for seven years.

ABSTRACT

THE ROLE OF THE METALLOCHAPERONE HYPA IN THE ACID SURVIVAL AND ACTIVITIES OF NICKEL ENZYMES IN *HELICOBACTER PYLORI*

FEBRUARY 2018

HEIDI Q. HU, B.S., SUFFOLK UNIVERSITY

Ph.D., UNIVERSITY OF MASSACHUSETTS AMHERST

Directed by: Professor Michael J. Maroney

Helicobacter pylori is a bacterium that has colonized the human gastric mucosa of over 50% of the world population. Persistent infection can cause gastritis, peptic ulcers, and cancers. The ability of *H. pylori* to colonize the acidic environment of the human stomach is dependent on the activity of the nickel containing enzymes, urease and NiFe-hydrogenase. The nickel metallochaperone, HypA, was previously shown to be required for the full activity of both enzymes. In addition to a Ni-binding site, HypA also contains a structural Zn site, which has been characterized to alter its averaged structure depending on pH and the presence of nickel.

Site-directed mutagenesis of the HypA Zn- and Ni-binding residues were used to elucidate mechanistic details in the involvement of HypA in Ni-delivery to enzymatic targets. Cellular studies were conducted to characterize the acid survival and enzymatic activities in a panel of *hypA* isogenic strains of *H. pylori* in collaboration with geneticists at the Uniformed Services University of Health Sciences (Bethesda, MD). *In vitro* studies were conducted on purified HypA variant proteins, correlating structural changes to the metal binding sites, and further probing the biophysical interactions with Ni(II) and protein binding partners.

Our studies indicated that NiFe-hydrogenase was not required for acid survival in *H. pylori* cultures. Only mutations of the conserved Cys residues in the HypA Zn site were found to exhibit varying degrees of acid sensitivity and loss of activity in Ni-containing enzymes. The same Cys residues were found to be important for the maturation of both urease and NiFe-

hydrogenase, indicating that these residues were critical for the function of HypA as a metallochaperone. Our mutagenesis studies found that Ni(II) binds to HypA at the N-terminus, coordinating the N-terminal amine of Met1 as an essential ligand, the loss of which lead to acid sensitivity and loss of enzymatic activities in isogenic strain. We also found that protein-protein interactions between HypA and dimeric UreE (an essential Ni-metallochaperone for urease) were enhanced in the presence of Ni(II) in both neutral and acidic conditions. Further, the presence of HypA protected UreE from degradation. Taken together, we concluded that HypA is acting as a co-metallochaperone along with dimeric UreE in Ni-delivery for urease maturation.

TABLE OF CONTENTS

Page

LIST OF TABLES

LIST OF FIGURES

CHAPTER 1

INTRODUCTION

1.1 Helicobacter pylori Persistence

Helicobacter pylori is a gram-negative bacterium that colonizes human gastric mucosa. Physicians first isolated and characterized *H. pylori* in the 1980s as a causative agent for peptic ulcers.[1] In the decades following its discovery, it was revealed as a prevalent human pathogen that has infected more than half of the world population.[2] Genetic studies indicated the pathogen co-evolved with human populations and may contribute some benefits,[3, 4] such as lower risk of esophageal cancers, celiac disease, allergy, and asthma.[5-7] However, untreated infections can persist for decades and develop into gastric cancers in a small percentage of infected individuals.[5, 8] With such high infection rates, stomach cancers accounted for 8.8% of estimated cancer related deaths in 2012, with up to 90% of new cases were attributed to chronic *H. pylori* infections.[9]

Despite high prevalence of colonization in the population, *H. pylori* infections are asymptomatic and remain untreated in most individuals leading to persistent infections and increased cancer risks.[10] The bacteria utilize a series of adaptations to maintain persistent infection in the stomach, which includes multiple strategies for acid adaptation[11] and immune evasions[12] that may induce virulence or bestow benefits to asymptomatic carriers (Figure 1.1).

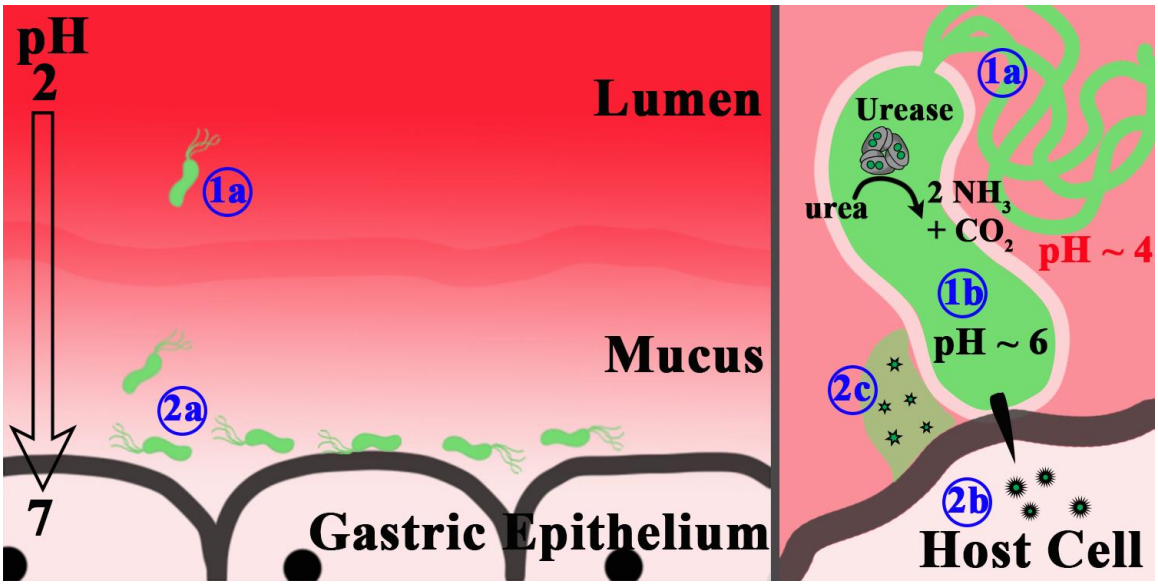

Figure 1.1: *H. pylori* strategy for persistent gastric colonization.
One major strategy is acid acclimation include (1a) motility and chemotaxis towards neutral pH in the mucus layer and (1b) rapid neutralization of cytoplasmic pH using the urease enzyme activity. Another strategy is immune system evasion involving (2a) avoiding constant attachment to host cells, effector proteins or nucleic acids (2b) injected into host cells through the bacteria type IV secretion system and/or (2c) secreted to induce host anti-inflammatory response.

1.1.1 Acid Adaptations

Despite colonizing the acidic niche of the human stomach, *H. pylori* is an acid-acclimated neutralophilic bacterium.[13] *H. pylori* grow best under neutral and microaerophilic conditions *in vitro*.[14] Unlike other acid-tolerant neutralophiles, such as *Escherichia coli* and *Salmonella typhimurium*, which are only able to survive passing through the acidic stomach environment, *H. pylori* form dense colonies and persist for decades.[11-13] This acclimation requires *H. pylori* to maintain the periplasmic and cytoplasmic pH close to neutral in acidic medium to allow for growth and division (Figure 1.1).[13]

1.1.1.1 Regulation

The acidity of the human stomach varies based on location and food buffering, the colonizing bacteria must be ready to respond to ever changing acidic stress. Hence, persistent colonization by *H. pylori* requires acclimation to both acute and chronic response to acid stress.[11] In chronic resistance to acid stress, the bacterium relies on transcriptional up-regulations of acid

acclimation genes,[11] which is largely controlled by the ArsR/S two-component system, with cross-talk to other regulatory systems such as the nickel regulatory system.[11, 15-17] The multi-domain ArsS integral membrane protein spans the cytoplasmic membrane, allowing for pH-sensing in the periplasm and corresponding phosphorylation cascade in the cytoplasm.[15] Acidic pH in the periplasm activates the ArsS histidine kinase activity in the cytoplasm by autophosphorylation and subsequent phosphorylation of the response regulator ArsR.[18] P-ArsR binds to the promoter region of multiple acid-responsive genes and regulates transcription.[15-18] Transcripts must then be translated into proteins that perform functions to adapt to acidic pH, which is a slow process. In contrast, acute acid stress in *H. pylori* is handled by being in a constant state of readiness with constitutive expression of a large arsenal acid resistant proteins,[12] which expedite the relief of acid stress.

H. pylori transcriptional response to acid stress has been studied under different conditions in several studies,[19-23] in addition to similar proteomic studies.[24, 25] Although some identified targets appear to be dependent on growth conditions, most studies agree on several acid acclimation adaptation strategies including motility and ammonia production.

1.1.1.2 Oxidative Damage Resistance

Robust DNA repair pathways and diverse antioxidant systems in *H. pylori* afford additional protection from the acidic environment.[12] *H. pylori* express a diverse repertoire of proteins for detoxifying reactive oxygen species such as superoxide dismutase (SOD), catalase (KatA), and peroxiredoxins such as AhpC.[26] Additionally, the pathogen reduces host nitric oxide production by host cells with arginase activity.[12, 26, 27] However, many homologues of oxidative stress regulators commonly found in bacteria are absent in the *H. pylori* genome.[26] Proteomic analysis of O_2-stressed *H. pylori* confirmed by time-dependent RT-PCR analysis indicated transcriptional up-regulation of SOD and down-regulation of AhpC over a period of 8 – 48 hours.[28, 29] Chronic acid stressed proteomic and transcriptomic studies in *H. pylori* show similar regulation profiles for SOD and AhpC.[22-24] The oxygen- and acid-responsive expression of

antioxidant proteins in *H. pylori* protects the pathogen against both oxidative stress from the host immune system and increased cellular damage caused by acid stress.[12, 26]

DNA repair proteins such as RecA, that are classically up-regulated in bacterial SOS response under cell stress, are constitutively active in *H. pylori*,[30] and contribute to efficient colonization.[31] Instead of a classic SOS response to DNA damage, *H. pylori* up-regulates natural competence,[32, 33] presumably to increase genetic diversification.[12] In individuals with persistent infection, this response may contribute to the increased cancer risk because it increases the potential of acquiring additional virulence genes by *H. pylori*, particularly in individuals with multiple strain infections.[10] The constitutively active antioxidant and DNA repair mechanisms in *H. pylori* indicate a state of stress-readiness in response to a rapidly changing acidic environment of the stomach constituting both acute and persistent acid resistance.

1.1.1.3 Motility

Upon initial introduction of *H. pylori* to the human stomach, the bacteria are exposed to the highly acidic lumen (pH ~2).[13, 34] *H. pylori* can only able to survive for minutes under this harsh luminal pH and must quickly migrate into the mucus layer (pH ~5) where most colonies are found.[11, 35] Chemotactic migration towards neutral pH niches have been demonstrated both *in vitro* and *in vivo* (Figure 1.1).[19, 35] Acidic growth induced transcriptional up-regulation of motility and chemotaxis genes,[19-21] which has been confirmed to be essential for efficient gastric colonization.[36-39]

1.1.1.4 Ammonia Production

The constant readiness strategy is also used by *H. pylori* as a defense against acute acid stress by having a consistent supply of apo-urease (Figure 1.1). Apo-urease represents approximately 10% of all nascent protein synthesized by *H. pylori* grown under both neutral conditions and under acid stress.[40] The apo-enzyme remains inactive until the di-nickel active site is assembled, which requires the accessory proteins encoded in the *ureEFGH* genes as well as *hypA* and *hypB*[41] (discussed in Section 1.2.5). Active urease catalyzes the hydrolysis of urea to

ammonia and carbamate, which spontaneously degrades to another molecule of ammonia and carbon dioxide,[42] resulting in the following net reaction[34]:

$$(NH_2)_2CO + H_2O \rightarrow CO_2 + 2\,NH_3 \qquad \text{Eq. 1.1}$$

All NH_3 produced is protonated to NH_4^+ (pK_a ~ 9.4) removing H^+ in the cytoplasm in large quantities and effectively neutralizes the cytoplasmic pH of the bacterium.[11, 34] Core urease genes *ureAB* as well as associated accessory proteins are required for acid survival in the presence of urea, and are up-regulated during acid stress.[11]

Transcriptional up-regulation also included the *ureI* gene, which is located between the *ureAB* genes (for the core enzyme) and *ureEFGH* genes (for maturation proteins).[43] The gene product, UreI, is a proton-gated transmembrane channel that transports urea (the substrate for urease) into the cytoplasm from the periplasmic space under acid stress.[11, 43] Disruption of the UreI channel results in loss of acid acclimation in *H. pylori*.[44-46] Thus, the activity of the massive quantity of urease produced by *H. pylori* is regulated in at least three levels: by acid-responsive (1) transcriptional up-regulation[19-23] and (2) substrate availability from UreI[44-46]; and by Ni^{2+} availability and accessory protein interactions required for (3) post-translational maturation.[11, 43] By synthesizing a large supply of apo-urease and then tightly controlling its activity, the bacterium is constantly ready for acute acid stress, but also guards against over alkalization of the cytoplasm from overproduction of NH_3/NH_4^+ by urease. Additional NH_3/NH_4^+ derives from the hydrolysis of short-chain amides by aliphatic amidases: AmiE and AmiF.[11] The *amiE* and *amiF* genes are transcriptionally up-regulated in response to acid stress.[19-23]

The robust NH_3/NH_4^+ production pathways in *H. pylori* are accompanied by specialized NH_4^+ utilization/dispersal system.[11] NH_4^+ produced by urease have been shown to be incorporated into amino acids.[47] However, many of the genes associated with nitrogen assimilation are missing from the *H. pylori* genome.[11] The glutamate (Glu) and glutamine (Gln) synthesis pathways occurs through the activities of glutamate dehydrogenase and glutamine synthetase.[11] However, the aspartate (Asp) and asparagine (Asn) synthesis pathway is missing from the *H. pylori* genome.[11]

Instead, the bacterium first deamidates Asn in the periplasm, and then transports the resulting Asp into the cytoplasm.[48] The same deamidation and transport system also exists for Gln/Glu, and are the only pathways for *H. pylori* to uptake these amino acids.[48] These deamidation enzymes/transporters pathways allows *H. pylori* to buffer the periplasm by preventing additional NH_3/NH_4^+ from entering the cytoplasm.[11, 48] These NH_3/NH_4^+ utilization enzymes have been shown to improve acid tolerance in *H. pylori*.[49]

1.1.1.5 Periplasm Buffering

Growing and dividing in acidic medium requires *H. pylori* to buffer both the cytoplasmic and periplasmic pH to maintain proper proton motive force.[13, 34] In addition to deamidation of Asn and Gln in the periplasm, *H. pylori* also expresses two carbonic anhydrase enzymes that catalyzes the pH-dependent interconversion of CO_2 and HCO_3^+.[50, 51] These catalysts of the dehydration/hydration reaction are pH-dependent and therefore buffer the pH of the periplasmic space at ~6.[11, 50]

1.1.2 Immune Evasion

Most *H. pylori* colonies are found in the mucus layer close to the gastric epithelium surface with less than 30% attaching to the tissue (Figure 1.1).[35] Avoidance of attachment to the host cell surface promotes the key strategy of avoiding detection by the host immune system and corresponding pro-inflammatory response.[35] In addition to avoidance, *H. pylori* also preferentially activate anti-inflammatory responses in the host innate immune response system.[12]

Attachment of *H. pylori* to cell surfaces trigger host detection and inflammatory responses, to which the bacteria respond by secreting/injecting various toxins that alter the host immune response and nutrient recruitment (Figure 1.1).[12] Some of these toxins have been found to skew host T cell responses, which have been linked to the mechanism of reduced of allergic responses in asymptomatic hosts.[12] Other toxins, such as those encoded in the cytotoxin-associated gene (*cag*) pathogenicity island (PAI) have been extensively studied and linked to the increased virulence and cancer risks.[10] The *cag* PAI encode multiple gene products, including a

bacterial type IV secretion system (T4SS) that is used for horizontal gene transfer and to inject bacterial proteins and nucleic acids into host cells.[10, 12] CagA is the most well-studied gene product from the *cag* PAI and has been shown to be phosphorylated by kinases within the host cell and then subsequently altering host cell signaling.[10, 12]

The translocation of CagA into host cells from *H. pylori*, increased infection rates, and host cell transformations, have been linked to the strains with high NiFe-hydrogenase (H_2ase) activity.[52] H_2ases catalyze the reversible oxidation of molecular hydrogen:

$$H_2 \leftrightharpoons 2\,H^+ + 2\,e^- \qquad \text{Eq. 1.2}$$

The *H. pylori* H_2ase has been characterized as a membrane-bound respiratory enzyme that oxidizes molecular H_2 (presumed to be produced by other intestinal flora) as an alternate source of energy.[53] It is also the only other known Ni containing enzyme in *H. pylori* (in addition to urease), with accompanying accessory proteins required for enzyme maturation, some of which are shared with urease (discussed in Sections 1.2 and 1.3).[43]

1.2 Nickel Trafficking

Reactive transition metals such as Cr, Mn, Fe, Co, Ni, and Cu are not available as free ions within the cell because they can mediate oxidative damage to DNA, proteins, and lipids.[54] Instead, cellular metal contents are tightly regulated through metal trafficking systems.[55] Transition metals that do not serve as enzymatic co-factors within a cell are treated as toxic substances and quickly sequestered or exported.[55] For cells producing enzymatic targets that require a specific metal co-factor, a metal trafficking system for that specific metal controls the availability within the cell.[55] For *H. pylori*, Ni is a required co-factor for the enzymatic activities of NiFe-H_2ase and urease (affecting energy usage and acid acclimation), and therefore an important resource that is controlled by a specific Ni-trafficking system (Figure 1.2).[43, 56]

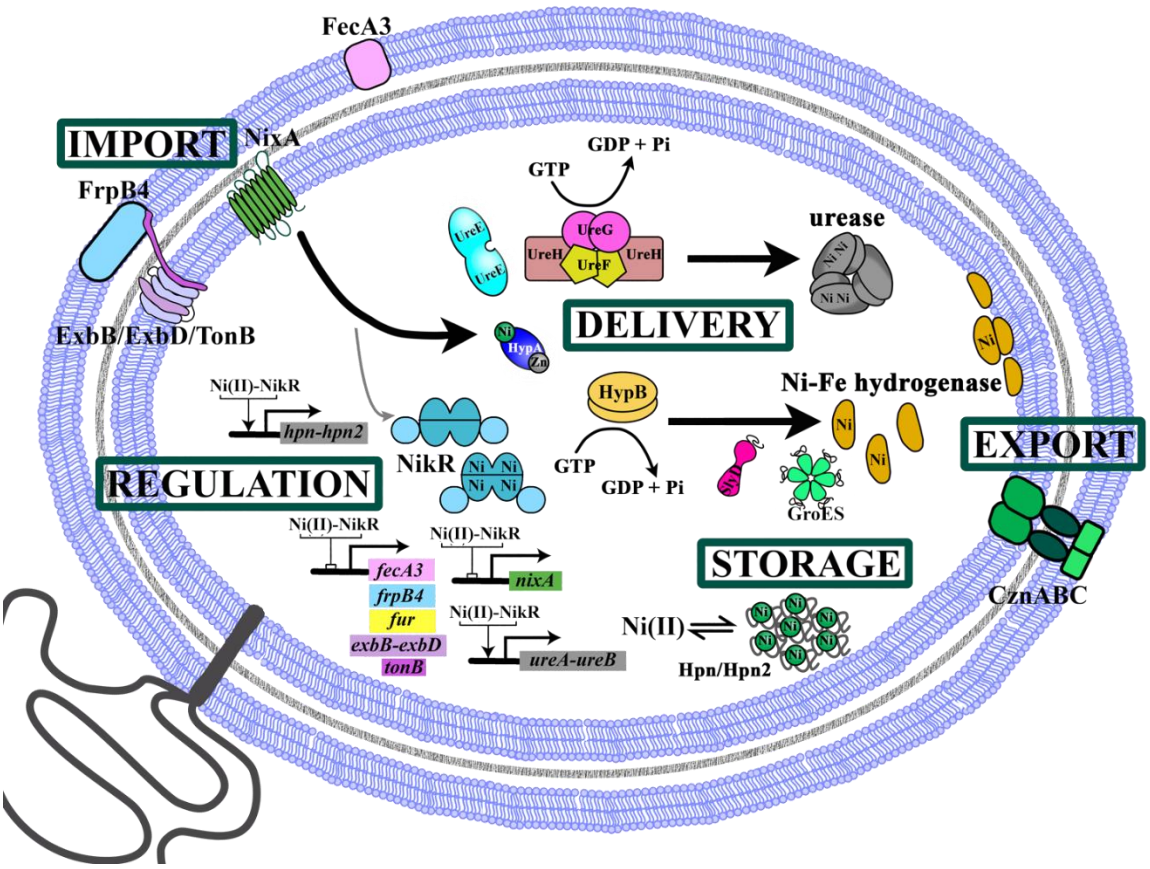

Figure 1.2: Select Nickel trafficking components in *H. pylori*.

Like other metal trafficking systems, the Ni-trafficking system in *H. pylori* contained proteins for the import, export , and storage of Ni, as well as accessory proteins for the target-specific delivery of Ni co-factor, and protein(s) to regulate the transcription of the Ni-trafficking proteins (Figure 1.2).[56]

1.2.1 Regulation

The *H. pylori* genome coded for a well-characterized Ni-responsive regulator (NikR), which has been targeted for Ni-responsive transcriptomic studies in this organism.[57] A surprising number of genes found in Ni- and *nikR*-responsive transcriptomic studies overlapped with iron-responsive genes in the same organism.[58, 59] A number of genes in the Ni-trafficking system were additionally regulated by acid stress.[17, 20, 21, 46, 60, 61]

The homo-tetrameric *H. pylori* NikR bound to AT-rich promoter regions of the genome,[62] which can result in activation or repression of targeted genes.[57, 61-64] Like other characterized

NikR proteins, Ni bound to *H. pylori* NikR with high affinity (nM – pM range).[62, 65] The whole array of accessory protein genes: *hypA, hypB, slyD,* and *ureE,* has been shown to be required to compete for Ni-binding with NikR to prevent premature down-regulation of the Ni-importer genes.[66] DNA-binding affinity has generally been characterized for Ni-bound NikR with apparent dissociation constant (K_d) ranging from low to high nM.[62, 67] DNA-binding has also been reported for NikR bound to metals other than Ni (Zn and Co).[67] Unlike other NikR proteins, both apo- and Ni-bound states *H. pylori* NikR have been shown to bind targeted DNA elements with some selectivity at neutral or acidic pH conditions.[68]

Ni-dependent and NikR-targeted transcriptome studies show that NikR can both up- and down-regulate various transcripts in response to Ni(II) treatment (Figure 1.2).[57] This is unusual compared to other well-studied NikR proteins, such as *E. coli* NikR.[56] Surprisingly, Ni-NikR down-regulates the transcription of genes that lead to the expression of the enzymatic target, NiFe-H_2ase,[57] but not of accessory protein known to be involved in NiFe-H_2ase maturation (*hypA, hypB, slyD, and groES)* [57] Unsurprisingly, Ni-NikR down-regulated known Ni-importer genes such as *nixA, fecA3, frpB4,* and *exbBD/tonB*.[57, 61] It also down-regulated the transcription of the iron-responsive regulator, *fur*, in response to Ni.[57, 61] These Ni-importers were also down-regulated in response to acid, demonstrating the intermingled network of transcriptional regulation by acid, iron, and Ni.[19-21]

NikR bound to its own promoter region only under Ni-bound and low pH conditions as shown by deoxyribonuclease (DNase) footprinting.[68] This binding presumably promotes its own transcription in acid shock and Ni-rich conditions, although this *in vitro* acid-responsive transcriptional response has not been confirmed in transcriptomic studies.[19-23]

Ni-NikR promotes the transcription of the genes *ureAB*, which promotes the expression of apo-urease, but not of the associated accessory proteins.[57] It has been shown that although the full *ureAB-IEFGH* transcript may be synthesized at all pH levels, but the resulting mRNA was cleaved and degraded at neutral pH within the accessory protein transcript.[69] The *ureAB* and

ureIEFGH gene has also been shown to be transcriptionally regulated by acid.[19-21] Ni-NikR also up-regulates transcripts coding for the Ni-storage proteins Hpn and Hpn2.[57]

Curiously, many of the genes coding for accessory proteins involved in the Ni-delivery and maturation of Ni-enzymes (*ureIEFGH*, *hypA*, and *hypB*) were not found to be transcriptionally regulated by NikR. Instead, these accessory proteins were transcriptionally up-regulated in response to acid stress.[19-21] Potentially, the mRNA of *ureIEFGH* may be post-transcriptionally degraded too rapidly to be detected in Ni/NikR-dependent transcriptomic studies.[69]

1.2.2 Import

Known nickel importers in *H. pylori* include both outer and inner membrane components that import nickel or nickel-complexes into the periplasm or the cytoplasm, respectively (Figure 1.2) which were all transcriptionally down-regulated by Ni-NikR.[57, 61, 70] At the inner membrane, a Ni-permease NixA has been shown to specifically transport Ni^{2+} into the cytoplasm at high affinity.[71] However, interruption of the *nixA* gene only reduces urease activity by about 50%, which alluded to a yet undiscovered Ni-importer at the inner membrane level.[11, 43]

Many of the outer membrane Ni-importers are also linked to the Fe-trafficking pathway. Outer membrane importers FecA3 and FrpB4 were both originally identified as importers of Fe-siderophore complexes, which were energized by the TonB/ExbB/ExbD complexes.[58] However, in *H. pylori* the genes encoding these outer membrane importers have been found to be differentially regulated by Ni and NikR, by acid, and by the iron responsive regulator, Fur.[11] Ni-, Fe-, and pH-dependent studies on deletion strains of these outer membrane importers indicate that these energy-dependent outer membrane transporters import Fe-complexes at neutral conditions, and import Ni-complexes under acid stress and low Ni conditions.[72] A putative ABC-type Ni-complex transporter in the outer membrane has been identified in crystallographic studies as CeuE-ABC,[73] as a Ni- or Co-complex importer. Binding studies indicated that the importer bind to Ni-$(L\text{-}His)_2$,[73] similar to the *E. coli* ABC-type Ni-importer NikABCDE.[74]

1.2.3 Export

The gene cluster *cznCBA* in the *H. pylori* genome were identified as functional homologues of a metal efflux pump that convey cadmium, zinc, and nickel (Czn) resistance to the cell as well as modulate urease activity.[75] The *cznA* gene is homologous to inner membrane cation-proton antiporters in other organisms, and deletions of either *cznA* or *cznC* genes resulted in increased urease activity.[75] Additionally, recombinant CznB and CznC proteins both bind to Ni-NTA resin.[75] Together, the complex was postulated to be a proton-driven exporter of Ni^{2+} as a mechanism for down-regulating urease activity,[75] presumably to prevent urease activity from making the cytoplasm alkaline. The *cznCBA* cluster has not been identified amongst genes reported to be transcriptional regulated by Ni and NikR or by acid in literature. Since the exporter also exports other toxic metals, regulation may be controlled by a yet unidentified metal responsive regulator, analogous to the NikR/RcnR regulatory pair for import/export of Ni in *E. coli*.[56]

1.2.4 Storage

Two genes in the *H. pylori* genome have been identified as metal storage proteins, *hpn* and *hpn2* (also known as *hpnl* for *hpn*-like) that increased whole cell Ni-content in growth on Ni-supplemented media.[76] These two proteins have been shown to be transcriptionally up-regulated in response to Ni and NikR,[57, 61] but only *hpn2* was found to be up-regulated by acid.[21] Both of these proteins are small (7 – 8 kDa) His-rich proteins, with Hpn2 also rich in Gln, that form larger oligomers with each monomer binding from 2 – 5 units of metal.[76] The Hpn protein have been shown to interact with Hpn2, the accessory/delivery proteins HypA and HypB, and the urease small subunit UreA, either directly or indirectly.[76] His-rich motifs are also found in accessory/delivery proteins SlyD and GroES (discussed in 1.2.5.3).

1.2.5 Delivery

Delivery of Ni cofactors to enzymatic targets is accomplished by accessory proteins that are specific for each enzyme target as well as for each metal cofactor.[43, 56] Typically, these are

organized as an operon for each enzyme target such as the *ureIEFGH* operon in *H. pylori* that is specifically required for the maturation of urease.[43] The genes coding for accessory proteins required for the maturation of NiFe-H_2ase are not organized as a discrete cluster. Instead, *hypBCD* is organized as a discrete cluster away from a second cluster of *hypEF*, and leaving *hypA* by itself in yet another location in the genome.[43, 77] The genes *hypCDEF* have been characterized to be involved in iron incorporation in *E. coli* NiFe-H_2ase and not considered part of the Ni-trafficking system.[43] Still other genes, *slyD* and *groES* have been linked to the maturation of NiFe-H_2ase and urease, but are not required for activity.[78, 79]

1.2.5.1 Ni-chaperones

Metallochaperones are a class of accessory proteins that specifically escort the metal cofactor to a specific enzyme target, which prevents the presence of free metal ions inside the cell and provides enzyme specificity.[55] This requires the metallochaperone to bind the target metal with a moderate affinity (facilitating bind and release) and to participate in protein-protein interactions (providing enzyme specificity). In *H. pylori* HypA and $UreE_2$ are the Ni-chaperones for NiFe-H_2ase and Urease, respectively.[43] Unlike other well characterized metallochaperones, HypA is required for the activity of both NiFe-H_2ase and urease under conditions where Ni is not supplemented in the growth media.[80]

The *ureE* gene encoded in *H. pylori* genome is essential for urease activity for cells grown under Ni-limiting or Ni-excess conditions.[43, 81] The corresponding gene product is a 39-kDa homodimer, $UreE_2$, with a single 6-coordinate Ni site at the dimer interface involving residues His102 and His152 and ligands from the solvent.[82] The His152 ligand in *H. pylori* $UreE_2$ is typically disordered in crystal structures, and located near the C-terminal region of the protein that is known to degrade over time.[82-85] The low number of Ni-site (one per dimer) of *H. pylori* $UreE_2$ is unusual compared to orthologues found in *K. aerogenes* and *B. pasteurii*, which bound six and two Ni per dimer, respectively.[41, 43, 86] The increased number of $UreE_2$ Ni sites in these organisms are accompanied by increased number of histidine residues at the C-terminal regions.[43,

[86] Urease activity is increased in variant strains by encoding additional poly-His tails to the C-terminus of the endogenous *ureE* gene, demonstrating the improved Ni-sequestration in $UreE_2$ increases urease activity.[86] It has been suggested that the reduced number of Ni sites in *H. pylori* $UreE_2$ is a mechanism for controlling the activity of the abundant apo-urease within the cell, where urease made up approximately 10% of total protein in *H. pylori* and only ~0.1% in *K. aerogenes*.[43] Despite only having one Ni site per dimer, *H. pylori* $UreE_2$ binds Ni with high affinity (K_d ~ 0.15 μM),[83] and has been demonstrated to be required for sequestering Ni away from NikR and preventing premature shut down of the Ni-import pathway.[66]

H. pylori $UreE_2$ directly interacts with other urease accessory proteins, including UreG (discussed in Section 1.2.5.2) and HypA (Section 1.3.3) in facilitating Ni-delivery to urease.[41, 43] It has been suggested that $UreE_2$ becomes part of a macromolecular complex in urease maturation like in *K. aerogenes*,[41, 43] however crystallographic and biochemical evidence suggests otherwise (discussed in Section 1.2.5.2).[87]

The other known Ni-chaperone in *H. pylori* is HypA, the structure and protein-protein interactions of which have been extensively studied and are discussed in Section 1.3.

1.2.5.2 GTPases and other Accessory Proteins

H. pylori HypB and UreG belong to the SIMIBI (for signal recognition particle, MinD, and BioD) class of P-loop GTPase involved in the Ni-insertion into NiFe-H_2ase and urease.[88] Enzymatic activities of NiFe-H_2ase and urease in the deletion strains of *hypB* or *ureG* indicate that *ureG* is required for urease activity, and *hypB* is required for both NiFe-H_2ase and urease activity in cells grown without Ni supplementation.[80, 89] Abolishing the GTPase activities in HypB or UreG by site directed mutagenesis resulted in lack of NiFe-H_2ase and urease activities.[89] Like other SIMIBI class of GTPases, UreG exhibit dimerization-dependent enhancement of GTP hydrolysis, which is dependent on the presence of Ni (or Zn) and nucleotide, but additionally enhanced by bicarbonate.[83, 87, 90, 91] HypB GTP hydrolysis was also enhanced under conditions that favor dimerization which requires Ni and nucleotide, but additionally enhanced by potassium.

Both HypB and UreG bind one Ni per dimer at the dimeric interface. Ni bound to UreG with much lower affinity (K_d ~ 10 μM) than Zn (K_d ~ 0.33 μM),[92] which forms a pyramidal site at the dimer interface involving two Cys ligands and two His ligands along with a buffer anion.[91] The crystal structure of dimeric HypB (PDB ID: 4LPS) shows Ni-binding to four Cys residues at the dimer interface,[93] with a moderate affinity (K_d ~ 1 μM) (discussed in APPENDIX 1).

H. pylori HypB and UreG directly interact with Ni-chaperones HypA and $UreE_2$, respectively, presumably facilitating GTP hydrolysis and Ni-insertion into NiFe-H_2ase and urease.[43] The direct interaction of HypB with HypA has been observed in cross-linking studies[94] and corresponded to low affinity binding (K_d ~ 60 μM) (discussed in Section 1.3.3).[95] Direct binding of UreG to $UreE_2$ has a moderate affinity (K_d ~ 4 μM),[83] and other methods suggest HypA competes with UreG for binding to $UreE_2$ (discussed in Section 1.3.3).[96]

H. pylori UreG has also been structurally characterized as part of a macromolecular urease maturation complex additionally involving UreF and UreH.[87] Unlike the maturation complexes in *K. aerogenes*, the *H. pylori* urease maturation complex involves the prior formation of UreH-$UreF_2$-UreH' precomplex, onto which the $UreG_2$ complex docks on the $UreF_2$ interface (Figure 1.3).[87] Size exclusion chromatography coupled with multi-angle light scattering (SEC-MALS) studies suggest that bicarbonate stimulated GTP hydrolysis induces the dissociation of $UreG_2$ from the macromolecular complex; with subsequent metal analysis also indicating Ni dissociation from $UreG_2$.[87] These observations suggested that GTP-hydrolysis in $UreG_2$ has multiple functional implications (discussed in Section 1.3.3). Where the role of UreF and UreH (UreD in *K. aerogenes*) orthologous is known,[41] the functional role of these proteins has not been studied in detail in *H. pylori*, where the difference in maturation complex organization suggest different roles for these proteins.[87] This is supported by tandem affinity pull-down studies using affinity tagged UreA, where UreA interactions with UreG and HypB was observed but not with UreF or ureH.[97]

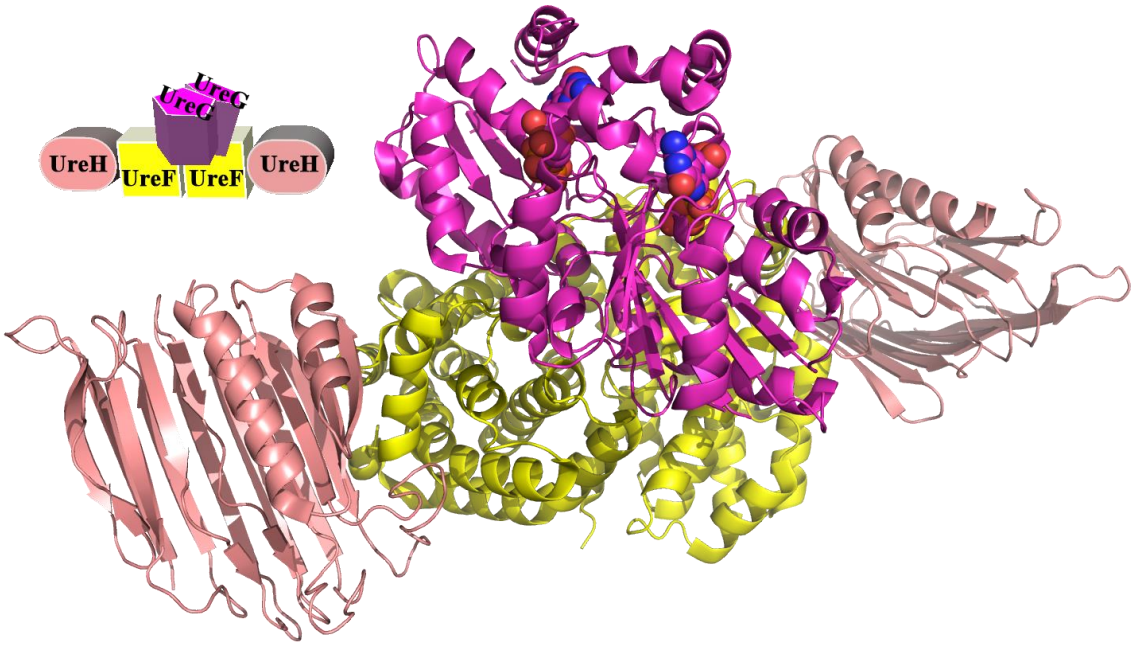

Figure 1.3: *H. pylori* UreG/UreF/UreH complex
Crystal structure of urease maturation complex demonstrating $UreG_2$ docked on top of $UreF_2$, which is flanked by UreH on each side (PDB ID: 4HI0).[87]

1.2.5.3 Folding Chaperone and Ni-storage

H. pylori genes *slyD* and *groES* coded for proteins that have both folding chaperone domains as well as metal binding domains rich in Cys and His residues.[78, 98] The His- and Cys-rich tails in the corresponding SlyD and GroES proteins have been characterized to increase Ni-tolerance and potentially convey some Ni-storage function,[78, 98] but were not transcriptionally regulated by Ni-NikR.[57] GroES Ni-sequestration contributes to the Ni-insertion into NiFe-H2ase, but not urease.[78]

The SlyD protein also contains a prolyl isomerase activity domain in addition to folding chaperone and metal binding domains.[79] SlyD has been shown enhance urease activity by competing for Ni with *H. pylori* NikR (along with the rest of the urease accessory proteins), therefore preventing shut down of Ni-importers.[66] The deletion of both *slyD* and *hypA* is resulted in the transcript reduction of Ni-importer genes, but not of each gene individually, which suggests these two genes shared some function *in vivo*.[66] One possible role shared by HypA and SlyD may

be to supply Ni to HypB through protein-protein interaction, as the direct interaction between SlyD and HypB has been demonstrated to enhance HypB GTP-hydrolysis.[98] SlyD has also been studied in its capacity to transform host cells either as an external treatment (simulating excreted toxic protein),[99] or expressed inside host cells (to simulate SlyD protein injected by the bacterial T4SS into host cells).[100]

1.3 The Unique *H. pylori* Metallochaperone HypA

1.3.1 The *hypA* gene required for two Ni-enzymes in *H. pylori*

The *hypA*, or homologous genes, are found in of all organisms that express NiFe-H_2ase with the gene product generally characterized as a Ni-metallochaperone specifically for NiFe-H_2ase maturation.[43, 56] In *H. pylori*, the *hypA* gene was found to be additionally required for the maturation of urease under Ni-limiting conditions.[66, 80] The *hypA*-requirement for urease maturation is abolished in Ni-supplemented media (1 – 5 μM $NiCl_2$).[80] Additionally, cross-linking studies showed the purified HypA protein directly interacts with the urease-specific Ni-chaperone $UreE_2$.[81] The dual role of HypA in Ni-enzyme maturation led to extensive studies of this protein.

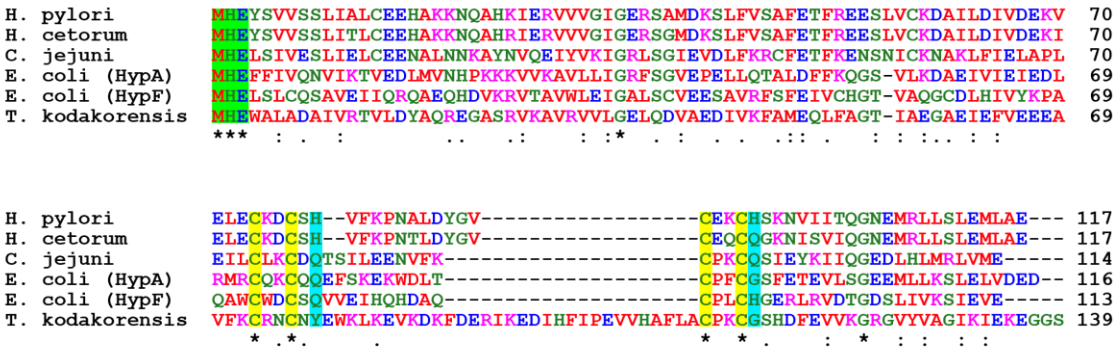

Figure 1.4: Multiple sequence alignment of HypA proteins.
The conserved nickel binding site at the N-terminus are highlighted in green, the conserved CXXC zinc binding motifs are highlighted in yellow, and the non-conserved flanking His residues at the zinc binding site highlighted in cyan. Rigidly conserved (*****), moderately conserved (**:**), and slightly (**.**) conserved residues are as marked at the bottom of the sequences.

1.3.2 Metal Sites

The *hypA* gene codes for a small protein with only 113 amino acids (13 kDa) that has been shown to directly bind to Ni, Zn, $UreE_2$, HypB, and Hpn.[76, 81, 94, 101] Multiple sequence alignments of the HypA amino acid sequence with orthologs reveal the location of two conserved metal sites (Figure 1.4). The N-terminal MHE-motif constitutes part of the Ni site and two CXXC motifs make up the structural Zn site of the protein. Structural studies of the Ni site by X-ray absorption spectroscopy (XAS) demonstrated a 6-coordinate paramagnetic site with all N/O (nitrogen or oxygen) ligands of which at least one is an imidazole, presumably His2.[101, 102] However, nuclear magnetic resonance (NMR) studies of Ni-titration into the N-terminal extended HypA variant (extra Gly-Ser residues at the N-terminus remaining from cleavage of affinity tag, henceforth known as GSHypA) shows a diamagnetic, and therefore planar site (Figure 1.5).[103] We hypothesized the change in Ni site structure in this N-terminal extension HypA variant is caused by the loss of N-terminal amine ligation, which will be tested with another N-terminal extension variant of HypA (discussed in CHAPTER 2 and CHAPTER 3).

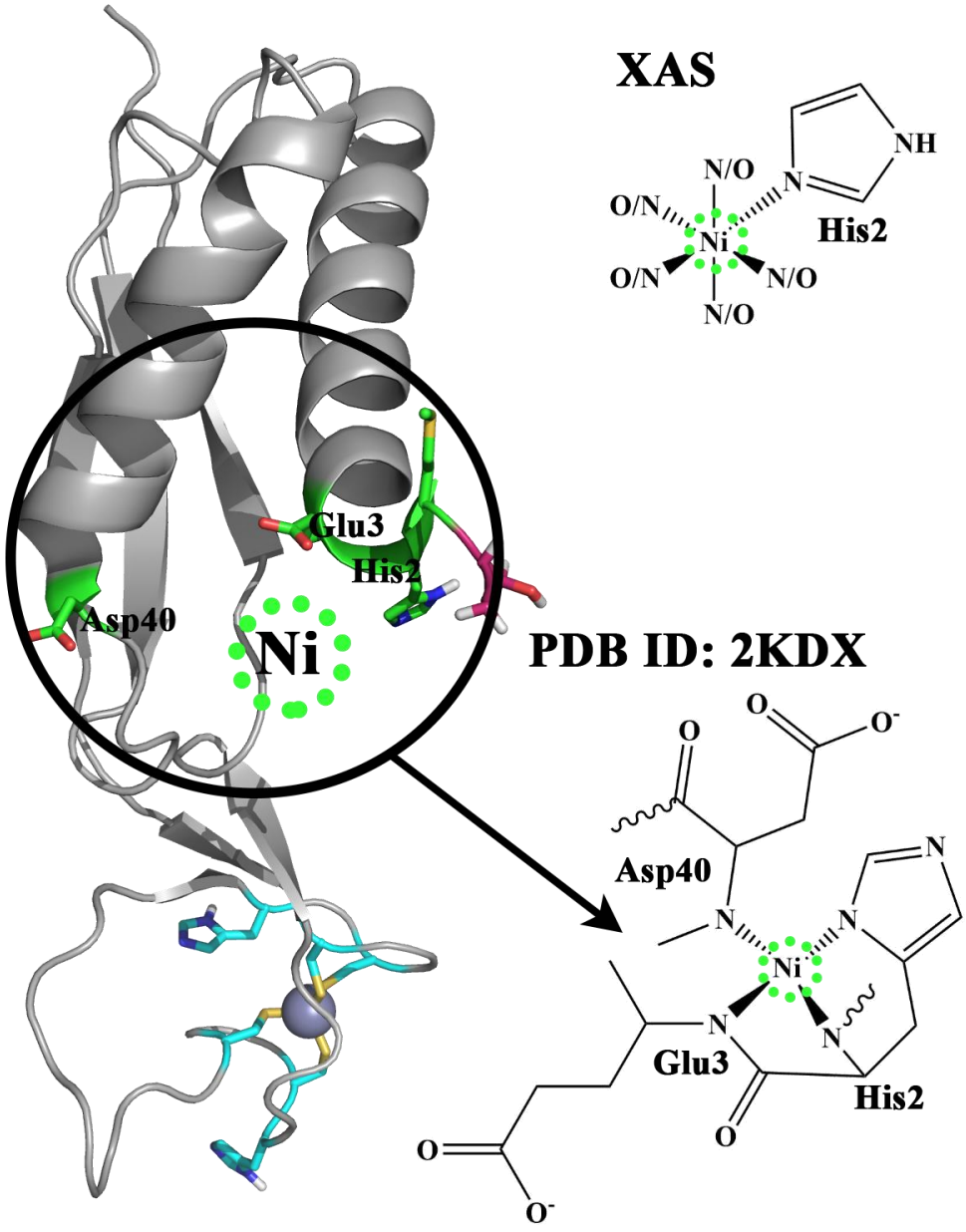

Figure 1.5: Planar and 6-coordinate HypA nickel sites.
The 6-coordinate and paramagnetic Ni site was characterized in native HypA by XAS.[101, 102] NMR structure (PDB ID: 2KDX) of GSHypA was characterized to have a planar and diamagnetic Ni site.[103] Cartoon representation of the GSHypA structure is shown in gray, where the sidechains of the non-native N-terminal overhang and the Ni- and Zn-binding residues are represented in sticks and colored. The nitrogen (blue), oxygen (red), sulfur (yellow), and hydrogen (white) atoms are colored the same in all sidechains, whereas the carbon atoms are colored differently for Ni-binding residues (green), Zn-binding residues (cyan), and non-native (magenta) residues.

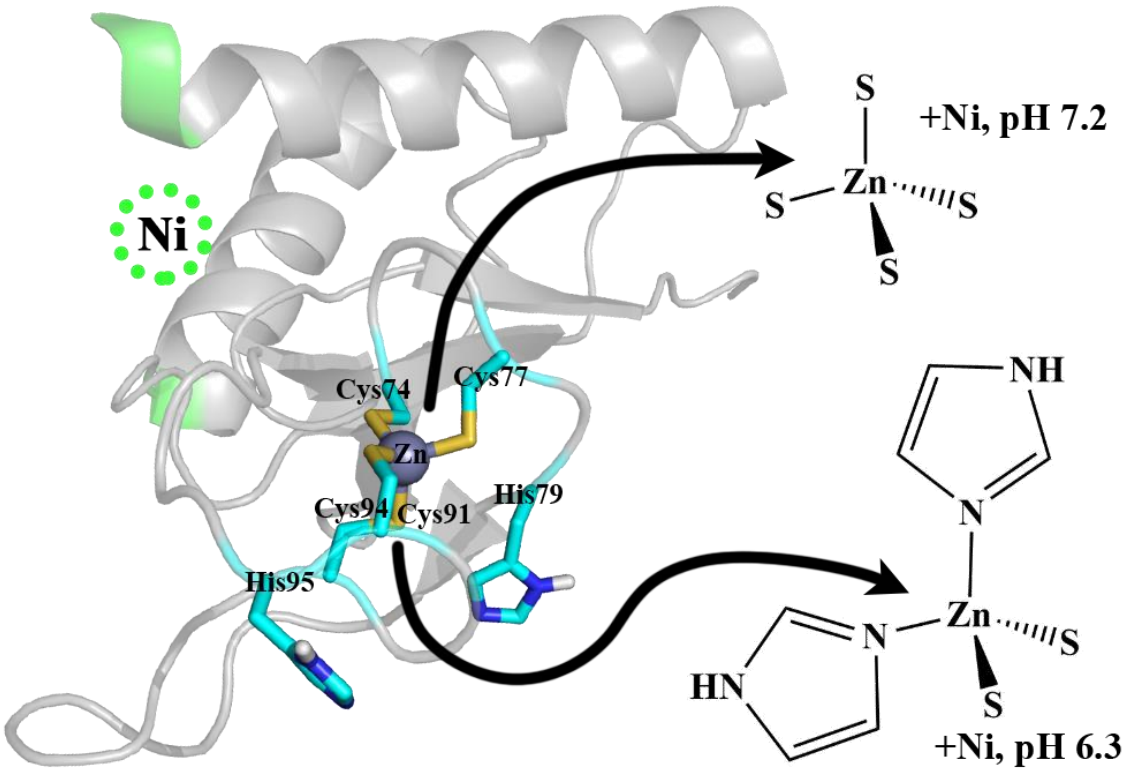

Figure 1.6: Ni- and pH-dependent dynamics HypA zinc site.
View of Zn-binding site from the cartoon representation of GSHypA the NMR structure (PDB ID: 2KDX)[103] in gray. The proposed Ni-binding residue are shown in green. The Zn-binding residues are as labeled with the sidechains represented in sticks with the carbon (cyan), nitrogen (blue), sulfur (yellow), and hydrogen (white) atoms shown in colors. Corresponding pH- and Ni-dependent average structures of the HypA Zn sites as previously characterized by XAS[101, 102] are shown to the right.

The two invariant CXXC Zn-binding motifs in *H. pylori* HypA are flanked by two adjacent His residues (Figure 1.4). The average structure of the Zn site in WT-HypA was shown to vary in a pH- and Ni-dependent fashion (Figure 1.6).[102] At pH 7.2 (simulating the cytoplasmic pH of *H. pylori* living in near neutral conditions) with or without Ni-bound, the averaged Zn site consist of four Cys ligands.[101, 102] At pH 6.3 (simulating the cytoplasmic pH of *H. pylori* experiencing acid shock conditions), the averaged Zn site consist of one His and three Cys ligands without Ni-bound; and further changes to two His and two Cys ligands with Ni-bound.[101, 102] Site-directed mutagenesis studies have been conducted on the structure of the HypA Zn-site.[102] Each of the Cys or His residues were mutated to Ala (loss of ligand); and each of the Cys residues

were additionally mutated to Asp (ligand substitution).[102] XAS studies of these Zn site variants show that any Cys mutations resulted in an average structure of two His and two Cys ligands, like the WT-HypA Zn-site structure at pH 6.3 with Ni-bound.[102] Any mutation to the flanking His residues resulted in an average Zn site structure of a four Cys ligands, like the WT-HypA Zn site structure at pH 7.2 with Ni-bound.[102] Lysate from Δ*hypA* strains of *H. pylori* treated with reconstituted WT-HypA or His-mutated Zn site variant proteins recovered urease activity, but treatment with reconstituted Cys-mutated Zn site variant HypA protein did not rescue urease activity.[102] The Zn site variant strains of *H. pylori* were additionally constructed and the role of the HypA dynamic Zn site in Ni-enzyme maturation and acid survival were tested (discussed in CHAPTER 3).

1.3.3 Protein-protein interactions

HypA interactions with protein partners HypB and $UreE_2$ have been characterized by cross-linking and NMR studies. [81, 94 95, 104] Interaction of purified *H. pylori* HypA and HypB proteins were first studied in chemical cross-linking studies where a heterodimeric complex (HypB-HypA) was observed.[94] Subsequent studies of the HypA-HypB interaction were conducted using the N-terminal extension variant GSHypA. Isothermal titration calorimetry (ITC) studies of the GSHypA binding to HypB indicated weak binding (K_d ~ 60μM) between the two proteins.[95] NMR studies of GSHypA found that residues perturbed by interaction with HypB were the same as those perturbed by Ni-binding, indicating that HypA interacted with HypB close to its Ni-binding site.[95] It was unclear whether the N-terminal extension in GSHypA affected the binding between the two proteins, particularly since the HypA-HypB interaction interface has been mapped to the Ni-binding domain (discussed in APPENDIX 1). Mutagenesis studies of HypB indicate that the N-terminal 24-residues were critical for interaction with HypA, which were well away from the metal- and GTP-binding residues.[95] Ni-binding has been reported to both increase and decrease GTP-hydrolysis in HypB[93, 95, 105] and the effect of HypA on GTP-hydrolysis has not been reported (discussed in APPENDIX 1).

Direct interaction between purified *H. pylori* HypA and $UreE_2$ was first characterized in chemical cross-linking studies, from which a heterodimeric complex (HypA-UreE resolved at 34 kDa on SDS-PAGE) was observed.[81] The presence of a 34-kDa heterodimer of HypA-UreE but not the HypA-$UreE_2$ heterotrimeric complex in denaturing conditions indicated that the conditions used did not promote cross-link formation between the dimeric $UreE_2$ species. Biolayer interferometry (BLI) and surface plasmon resonance (SPR) were also used for studies of the HypA and $UreE_2$ interaction. These studies were carried out at neutral pH without reducing agents (in buffer containing 10 mM HEPES, pH 7.4, 150 mM NaCl, 0.01% Surfactant P-20) with the smaller HypA (13 kDa) tethered to a surface and then $UreE_2$ were flowed over HypA-tethered surfaces where binding was detected. These methods identified complex and strong interactions between $UreE_2$ and tethered-HypA assigned to a high affinity binding (K_d ~ 5.4 nM) and subsequent conformational change (K_d ~ 1 μM), which is unaffected by the presence of Ni or Zn.[96] Additionally, BLI studies show that HypA outcompeted UreG for binding to $UreE_2$, however metal-dependent dimer formation of UreG indicated a multiple step interaction.[96]

Indeed, studies using the N-terminal extension variant GSHypA found the opposite effect, where the Ni-bound GSHypA-$UreE_2$ complex dissociated in the presence of UreG and GTP, where a $UreG_2$-$UreE_2$ complex forms in its place.[90] These results indicated that $UreE_2$ does not form heterocomplex with both UreG and HypA simultaneously, but rather bind to either one or the other.[96] Mutagenesis studies of $UreE_2$ identified the C-terminal motif (residues 158 – 170) as the interaction interface with GSHypA.[104] NMR studies of GSHypA identified the Ni-binding domain as the interaction interface with $UreE_2$.[104] Additionally, ITC was used to monitor the binding occurring with titration of GSHypA into $UreE_2$. These titration experiments were performed at neutral pH without reducing agent (in buffer containing 20 mM HEPES, 100 mM NaCl, pH 7.2), where either apoGSHypA, apo-ZnGSHypA or Ni-ZnGSHypA were titrated into apo-$UreE_2$ or Ni-$UreE_2$. These titrations found that GSHypA bound to $UreE_2$ in a single observable binding event with moderate affinity (K_d ~ 1 – 2 μM), which were unaffected by the

presence of metals. It is unclear whether the HypA-$UreE_2$ interactions were affected by N-terminal modification in GSHypA variant protein or in response to acid shock (discussed in CHAPTER 3 and CHAPTER 4).

The requirement for HypA in urease maturation in *H. pylori* has been hypothesized to involve Ni-transfer to $UreE_2$.[90, 106] Ni-transfer from GSHypA to full length $UreE_2$ (treated with a light-dependent protein crosslinking moiety that has Ni-dependent fluorescence) was demonstrated after separation of the two proteins on SDS-PAGE.[104] However, separation of the GSHypA-$UreE_2$ complex did not occur under non-denaturing conditions with or without the presence of metals, and has only been observed in the presence of $UreG_2$ and GTP.[90, 104] These trends indicate the mechanistic involvement of HypA in urease maturation is more complex than simple Ni-transfer from HypA to $UreE_2$ (discussed in CHAPTER 4).

1.4 References

1. Marshall, B. J., and Warren, J. R. (1984) Unidentified curved bacilli in the stomach of patients with gastritis and peptic ulceration, *Lancet 1*, 1311-1315

2. Eusebi, L. H., Zagari, R. M., and Bazzoli, F. (2014) Epidemiology of Helicobacter pylori infection, *Helicobacter 19 Suppl 1*, 1-5. (10.1111/hel.12165)

3. Moodley, Y., Linz, B., Bond, R. P., Nieuwoudt, M., Soodyall, H., Schlebusch, C. M., Bernhoft, S., Hale, J., Suerbaum, S., Mugisha, L., van der Merwe, S. W., and Achtman, M. (2012) Age of the association between Helicobacter pylori and man, *PLoS Pathog 8*, e1002693. (10.1371/journal.ppat.1002693)

4. Kodaman, N., Pazos, A., Schneider, B. G., Piazuelo, M. B., Mera, R., Sobota, R. S., Sicinschi, L. A., Shaffer, C. L., Romero-Gallo, J., de Sablet, T., Harder, R. H., Bravo, L. E., Peek, R. M., Jr., Wilson, K. T., Cover, T. L., Williams, S. M., and Correa, P. (2014) Human and Helicobacter pylori coevolution shapes the risk of gastric disease, *Proc Natl Acad Sci U S A 111*, 1455-1460. (10.1073/pnas.1318093111)

5. Sonnenberg, A. (2013) Review article: historic changes of Helicobacter pylori-associated diseases, *Aliment Pharmacol Ther 38*, 329-342. (10.1111/apt.12380)

6. Lebwohl, B., Blaser, M. J., Ludvigsson, J. F., Green, P. H., Rundle, A., Sonnenberg, A., and Genta, R. M. (2013) Decreased risk of celiac disease in patients with Helicobacter pylori colonization, *Am J Epidemiol 178*, 1721-1730. (10.1093/aje/kwt234)

7. Arnold, I. C., Dehzad, N., Reuter, S., Martin, H., Becher, B., Taube, C., and Muller, A. (2011) Helicobacter pylori infection prevents allergic asthma in mouse models through the induction of regulatory T cells, *J Clin Invest 121*, 3088-3093. (10.1172/JCI45041)

8. Peek, R. M., Jr., and Blaser, M. J. (2002) Helicobacter pylori and gastrointestinal tract adenocarcinomas, *Nat Rev Cancer 2*, 28-37. (10.1038/nrc703)

9. Torre, L. A., Bray, F., Siegel, R. L., Ferlay, J., Lortet-Tieulent, J., and Jemal, A. (2015) Global cancer statistics, 2012, *CA Cancer J Clin 65*, 87-108. (10.3322/caac.21262)

10. Wroblewski, L. E., Peek, R. M., Jr., and Wilson, K. T. (2010) Helicobacter pylori and gastric cancer: factors that modulate disease risk, *Clinical microbiology reviews 23*, 713-739. (10.1128/CMR.00011-10)

11. Fischer, F., and De Reuse, H. (2016) Adaptation of *Helicobacter pylori* Metabolism to Persistent Gastric Colonization, In *Helicobacter pylori Research From Bench to Bedside* (Steffen Backert, Y. Y., Ed.), pp 29-56, Springer, Japan.

12. Salama, N. R., Hartung, M. L., and Muller, A. (2013) Life in the human stomach: persistence strategies of the bacterial pathogen Helicobacter pylori, *Nat Rev Microbiol 11*, 385-399. (10.1038/nrmicro3016)

13. Sachs, G., Weeks, D. L., Wen, Y., Marcus, E. A., Scott, D. R., and Melchers, K. (2005) Acid acclimation by Helicobacter pylori, *Physiology 20*, 429-438. (DOI 10.1152/physiol.00032.2005)

14. Goodwin, C. S., and Armstrong, J. A. (1990) Microbiological aspects of Helicobacter pylori (Campylobacter pylori), *Eur J Clin Microbiol Infect Dis 9*, 1-13

15. Pflock, M., Finsterer, N., Joseph, B., Mollenkopf, H., Meyer, T. F., and Beier, D. (2006) Characterization of the ArsRS regulon of Helicobacter pylori, involved in acid adaptation, *Journal of bacteriology 188*, 3449-3462. (10.1128/JB.188.10.3449-3462.2006)

16. Wen, Y., Feng, J., Scott, D. R., Marcus, E. A., and Sachs, G. (2007) The HP0165-HP0166 two-component system (ArsRS) regulates acid-induced expression of HP1186 alpha-carbonic anhydrase in Helicobacter pylori by activating the pH-dependent promoter, *Journal of bacteriology 189*, 2426-2434. (10.1128/JB.01492-06)

17. Carpenter, B. M., West, A. L., Gancz, H., Servetas, S. L., Pich, O. Q., Gilbreath, J. J., Hallinger, D. R., Forsyth, M. H., Merrell, D. S., and Michel, S. L. (2015) Crosstalk between the HpArsRS two-component system and HpNikR is necessary for maximal activation of urease transcription, *Front Microbiol 6*, 558. (10.3389/fmicb.2015.00558)

18. Pflock, M., Kennard, S., Delany, I., Scarlato, V., and Beier, D. (2005) Acid-induced activation of the urease promoters is mediated directly by the ArsRS two-component system of Helicobacter pylori, *Infect Immun 73*, 6437-6445. (10.1128/IAI.73.10.6437-6445.2005)

19. Merrell, D. S., Goodrich, M. L., Otto, G., Tompkins, L. S., and Falkow, S. (2003) pH-regulated gene expression of the gastric pathogen Helicobacter pylori, *Infect Immun 71*, 3529-3539

20. Wen, Y., Marcus, E. A., Matrubutham, U., Gleeson, M. A., Scott, D. R., and Sachs, G. (2003) Acid-Adaptive Genes of Helicobacter pylori, *Infection and Immunity 71*, 5921-5939. (10.1128/iai.71.10.5921-5939.2003)

21. Bury-Mone, S., Thiberge, J. M., Contreras, M., Maitournam, A., Labigne, A., and De Reuse, H. (2004) Responsiveness to acidity via metal ion regulators mediates virulence in the gastric pathogen Helicobacter pylori, *Molecular microbiology 53*, 623-638. (10.1111/j.1365-2958.2004.04137.x)

22. Allan, E., Clayton, C. L., McLaren, A., Wallace, D. M., and Wren, B. W. (2001) Characterization of the low-pH responses of Helicobacter pylori using genomic DNA arrays, *Microbiology 147*, 2285-2292. (10.1099/00221287-147-8-2285)

23. Ang, S., Lee, C. Z., Peck, K., Sindici, M., Matrubutham, U., Gleeson, M. A., and Wang, J. T. (2001) Acid-induced gene expression in Helicobacter pylori: study in genomic scale by microarray, *Infect Immun 69*, 1679-1686. (10.1128/IAI.69.3.1679-1686.2001)

24. Slonczewski, J. L., McGee, D. J., Phillips, J., Kirkpatrick, C., and Mobley, H. L. (2000) pH-dependent protein profiles of Helicobacter pylori analyzed by two-dimensional gels, *Helicobacter 5*, 240-247

25. Shao, C., Zhang, Q., Tang, W., Qu, W., Zhou, Y., Sun, Y., Yu, H., and Jia, J. (2008) The changes of proteomes components of Helicobacter pylori in response to acid stress without urea, *Journal of microbiology 46*, 331-337. (10.1007/s12275-008-0062-x)

26. Wang, G., Alamuri, P., and Maier, R. J. (2006) The diverse antioxidant systems of Helicobacter pylori, *Molecular microbiology 61*, 847-860. (10.1111/j.1365-2958.2006.05302.x)

27. Gobert, A. P., and Wilson, K. T. (2016) The Immune Battle against Helicobacter pylori Infection: NO Offense, *Trends Microbiol 24*, 366-376. (10.1016/j.tim.2016.02.005)

28. Chuang, M. H., Wu, M. S., Lin, J. T., and Chiou, S. H. (2005) Proteomic analysis of proteins expressed by Helicobacter pylori under oxidative stress, *Proteomics 5*, 3895-3901. (10.1002/pmic.200401232)

29. Liu, Z. F., Chen, C. Y., Tang, W., Zhang, J. Y., Gong, Y. Q., and Jia, J. H. (2006) Gene-expression profiles in gastric epithelial cells stimulated with spiral and coccoid Helicobacter pylori, *J Med Microbiol 55*, 1009-1015. (10.1099/jmm.0.46456-0)

30. Orillard, E., Radicella, J. P., and Marsin, S. (2011) Biochemical and cellular characterization of Helicobacter pylori RecA, a protein with high-level constitutive expression, *Journal of bacteriology 193*, 6490-6497. (10.1128/JB.05646-11)

31. Dorer, M. S., Sessler, T. H., and Salama, N. R. (2011) Recombination and DNA repair in Helicobacter pylori, *Annu Rev Microbiol 65*, 329-348. (10.1146/annurev-micro-090110-102931)

32. Dorer, M. S., Fero, J., and Salama, N. R. (2010) DNA damage triggers genetic exchange in Helicobacter pylori, *PLoS Pathog 6*, e1001026. (10.1371/journal.ppat.1001026)

33. Dorer, M. S., Cohen, I. E., Sessler, T. H., Fero, J., and Salama, N. R. (2013) Natural competence promotes Helicobacter pylori chronic infection, *Infect Immun 81*, 209-215. (10.1128/IAI.01042-12)

34. Scott, D., Weeks, D., Melchers, K., and Sachs, G. (1998) The life and death of Helicobacter pylori, *Gut 43 Suppl 1*, S56-60

35. Schreiber, S., Konradt, M., Groll, C., Scheid, P., Hanauer, G., Werling, H. O., Josenhans, C., and Suerbaum, S. (2004) The spatial orientation of Helicobacter pylori in the gastric mucus, *Proc Natl Acad Sci U S A 101*, 5024-5029. (10.1073/pnas.0308386101)

36. Eaton, K. A., Suerbaum, S., Josenhans, C., and Krakowka, S. (1996) Colonization of gnotobiotic piglets by Helicobacter pylori deficient in two flagellin genes, *Infect Immun 64*, 2445-2448

37. Foynes, S., Dorrell, N., Ward, S. J., Stabler, R. A., McColm, A. A., Rycroft, A. N., and Wren, B. W. (2000) Helicobacter pylori possesses two CheY response regulators and a histidine kinase sensor, CheA, which are essential for chemotaxis and colonization of the gastric mucosa, *Infect Immun 68*, 2016-2023

38. Croxen, M. A., Sisson, G., Melano, R., and Hoffman, P. S. (2006) The Helicobacter pylori chemotaxis receptor TlpB (HP0103) is required for pH taxis and for colonization of the gastric mucosa, *Journal of bacteriology 188*, 2656-2665. (10.1128/JB.188.7.2656-2665.2006)

39. Ottemann, K. M., and Lowenthal, A. C. (2002) Helicobacter pylori uses motility for initial colonization and to attain robust infection, *Infect Immun 70*, 1984-1990

40. Bauerfeind, P., Garner, R., Dunn, B. E., and Mobley, H. L. T. (1997) Synthesis and activity of Helicobacter pylori urease and catalase at low pH, *Gut 40*, 25-30

41. Farrugia, M. A., Macomber, L., and Hausinger, R. P. (2013) Biosynthesis of the Urease Metallocenter, *Journal of Biological Chemistry 288*, 13178-13185. (10.1074/jbc.R112.446526)

42. Maroney, M. J., and Ciurli, S. (2014) Nonredox nickel enzymes, *Chemical reviews 114*, 4206-4228. (10.1021/cr4004488)

43. Maier, R. J., Benoit, S. L., and Seshadri, S. (2007) Nickel-binding and accessory proteins facilitating Ni-enzyme maturation in Helicobacter pylori, *Biometals : an international journal on the role of metal ions in biology, biochemistry, and medicine 20*, 655-664. (10.1007/s10534-006-9061-8)

44. Skouloubris, S., Thiberge, J. M., Labigne, A., and De Reuse, H. (1998) The Helicobacter pylori UreI protein is not involved in urease activity but is essential for bacterial survival in vivo, *Infect Immun 66*, 4517-4521

45. Scott, D. R., Marcus, E. A., Weeks, D. L., Lee, A., Melchers, K., and Sachs, G. (2000) Expression of the Helicobacter pylori ureI gene is required for acidic pH activation of cytoplasmic urease, *Infect Immun 68*, 470-477

46. Bury-Mone, S., Skouloubris, S., Labigne, A., and De Reuse, H. (2001) The Helicobacter pylori UreI protein: role in adaptation to acidity and identification of residues essential for its activity and for acid activation, *Molecular microbiology 42*, 1021-1034

47. Williams, C. L., Preston, T., Hossack, M., Slater, C., and McColl, K. E. (1996) Helicobacter pylori utilises urea for amino acid synthesis, *FEMS Immunol Med Microbiol 13*, 87-94

48. Leduc, D., Gallaud, J., Stingl, K., and de Reuse, H. (2010) Coupled amino acid deamidase-transport systems essential for Helicobacter pylori colonization, *Infect Immun 78*, 2782-2792. (10.1128/IAI.00149-10)

49. Miller, E. F., and Maier, R. J. (2014) Ammonium metabolism enzymes aid Helicobacter pylori acid resistance, *Journal of bacteriology 196*, 3074-3081. (10.1128/JB.01423-13)

50. Marcus, E. A., Moshfegh, A. P., Sachs, G., and Scott, D. R. (2005) The periplasmic alpha-carbonic anhydrase activity of Helicobacter pylori is essential for acid acclimation, *Journal of bacteriology 187*, 729-738. (10.1128/JB.187.2.729-738.2005)

51. Bury-Mone, S., Mendz, G. L., Ball, G. E., Thibonnier, M., Stingl, K., Ecobichon, C., Ave, P., Huerre, M., Labigne, A., Thiberge, J. M., and De Reuse, H. (2008) Roles of alpha and beta carbonic anhydrases of Helicobacter pylori in the urease-dependent response to acidity and in colonization of the murine gastric mucosa, *Infect Immun 76*, 497-509. (10.1128/IAI.00993-07)

52. Wang, G., Romero-Gallo, J., Benoit, S. L., Piazuelo, M. B., Dominguez, R. L., Morgan, D. R., Peek, R. M., Jr., and Maier, R. J. (2016) Hydrogen Metabolism in Helicobacter pylori Plays a Role in Gastric Carcinogenesis through Facilitating CagA Translocation, *MBio 7*. (10.1128/mBio.01022-16)

53. Olson, J. W., and Maier, R. J. (2002) Molecular hydrogen as an energy source for Helicobacter pylori, *Science 298*, 1788-1790. (10.1126/science.1077123)

54. Stohs, S. J., and Bagchi, D. (1995) Oxidative mechanisms in the toxicity of metal ions, *Free Radic Biol Med 18*, 321-336

55. Ba, L. A., Doering, M., Burkholz, T., and Jacob, C. (2009) Metal trafficking: from maintaining the metal homeostasis to future drug design, *Metallomics : integrated biometal science 1*, 292-311. (10.1039/b904533c)

56. Higgins, K. A., Carr, C. E., and Maroney, M. J. (2012) Specific metal recognition in nickel trafficking, *Biochemistry 51*, 7816-7832. (10.1021/bi300981m)

57. Contreras, M., Thiberge, J. M., Mandrand-Berthelot, M. A., and Labigne, A. (2003) Characterization of the roles of NikR, a nickel-responsive pleiotropic autoregulator of Helicobacter pylori, *Molecular microbiology 49*, 947-963

58. Merrell, D. S., Thompson, L. J., Kim, C. C., Mitchell, H., Tompkins, L. S., Lee, A., and Falkow, S. (2003) Growth phase-dependent response of Helicobacter pylori to iron starvation, *Infect Immun 71*, 6510-6525

59. Miles, S., Carpenter, B. M., Gancz, H., and Merrell, D. S. (2010) Helicobacter pylori apo-Fur regulation appears unconserved across species, *Journal of microbiology 48*, 378-386. (10.1007/s12275-010-0022-0)

60. van Vliet, A. H., Ernst, F. D., and Kusters, J. G. (2004) NikR-mediated regulation of Helicobacter pylori acid adaptation, *Trends Microbiol 12*, 489-494. (10.1016/j.tim.2004.09.005)

61. Muller, C., Bahlawane, C., Aubert, S., Delay, C. M., Schauer, K., Michaud-Soret, I., and De Reuse, H. (2011) Hierarchical regulation of the NikR-mediated nickel response in Helicobacter pylori, *Nucleic acids research 39*, 7564-7575. (10.1093/nar/gkr460)

62. Abraham, L. O., Li, Y., and Zamble, D. B. (2006) The metal- and DNA-binding activities of Helicobacter pylori NikR, *Journal of inorganic biochemistry 100*, 1005-1014. (10.1016/j.jinorgbio.2005.10.014)

63. Ernst, F. D., Kuipers, E. J., Heijens, A., Sarwari, R., Stoof, J., Penn, C. W., Kusters, J. G., and van Vliet, A. H. (2005) The nickel-responsive regulator NikR controls activation and repression of gene transcription in Helicobacter pylori, *Infect Immun 73*, 7252-7258. (10.1128/IAI.73.11.7252-7258.2005)

64. Dian, C., Schauer, K., Kapp, U., McSweeney, S. M., Labigne, A., and Terradot, L. (2006) Structural basis of the nickel response in Helicobacter pylori: crystal structures of HpNikR in Apo and nickel-bound states, *Journal of molecular biology 361*, 715-730. (10.1016/j.jmb.2006.06.058)

65. Zambelli, B., Bellucci, M., Danielli, A., Scarlato, V., and Ciurli, S. (2007) The Ni2+ binding properties of Helicobacter pylori NikR, *Chemical communications*, 3649-3651. (10.1039/b706025d)

66. Benanti, E. L., and Chivers, P. T. (2009) An intact urease assembly pathway is required to compete with NikR for nickel ions in Helicobacter pylori, *Journal of bacteriology 191*, 2405-2408. (10.1128/JB.01657-08)

67. Zambelli, B., Danielli, A., Romagnoli, S., Neyroz, P., Ciurli, S., and Scarlato, V. (2008) High-affinity Ni2+ binding selectively promotes binding of Helicobacter pylori NikR to its target urease promoter, *Journal of molecular biology 383*, 1129-1143. (10.1016/j.jmb.2008.08.066)

68. Li, Y., and Zamble, D. B. (2009) pH-responsive DNA-binding activity of Helicobacter pylori NikR, *Biochemistry 48*, 2486-2496. (10.1021/bi801742r)

69. Akada, J. K., Shirai, M., Takeuchi, H., Tsuda, M., and Nakazawa, T. (2000) Identification of the urease operon in Helicobacter pylori and its control by mRNA decay in response to pH, *Molecular microbiology 36*, 1071-1084

70. Ernst, F. D., Stoof, J., Horrevoets, W. M., Kuipers, E. J., Kusters, J. G., and van Vliet, A. H. (2006) NikR mediates nickel-responsive transcriptional repression of the Helicobacter pylori outer membrane proteins FecA3 (HP1400) and FrpB4 (HP1512), *Infect Immun 74*, 6821-6828. (10.1128/IAI.01196-06)

71. Mobley, H. L., Garner, R. M., and Bauerfeind, P. (1995) Helicobacter pylori nickel-transport gene nixA: synthesis of catalytically active urease in Escherichia coli independent of growth conditions, *Molecular microbiology 16*, 97-109

72. Schauer, K., Gouget, B., Carriere, M., Labigne, A., and de Reuse, H. (2007) Novel nickel transport mechanism across the bacterial outer membrane energized by the TonB/ExbB/ExbD machinery, *Molecular microbiology 63*, 1054-1068. (10.1111/j.1365-2958.2006.05578.x)

73. Shaik, M. M., Cendron, L., Salamina, M., Ruzzene, M., and Zanotti, G. (2014) Helicobacter pylori periplasmic receptor CeuE (HP1561) modulates its nickel affinity via organic metallophores, *Molecular microbiology 91*, 724-735. (10.1111/mmi.12487)

74. Chivers, P. T., Benanti, E. L., Heil-Chapdelaine, V., Iwig, J. S., and Rowe, J. L. (2012) Identification of Ni-(L-His)(2) as a substrate for NikABCDE-dependent nickel uptake in Escherichia coli, *Metallomics : integrated biometal science 4*, 1043-1050. (10.1039/c2mt20139a)

75. Stahler, F. N., Odenbreit, S., Haas, R., Wilrich, J., Van Vliet, A. H., Kusters, J. G., Kist, M., and Bereswill, S. (2006) The novel Helicobacter pylori CznABC metal efflux pump is required for cadmium, zinc, and nickel resistance, urease modulation, and gastric colonization, *Infect Immun 74*, 3845-3852. (10.1128/IAI.02025-05)

76. Vinella, D., Fischer, F., Vorontsov, E., Gallaud, J., Malosse, C., Michel, V., Cavazza, C., Robbe-Saule, M., Richaud, P., Chamot-Rooke, J., Brochier-Armanet, C., and De Reuse, H. (2015) Evolution of Helicobacter: Acquisition by Gastric Species of Two Histidine-Rich Proteins Essential for Colonization, *PLoS Pathog 11*, e1005312. (10.1371/journal.ppat.1005312)

77. Tomb, J. F., White, O., Kerlavage, A. R., Clayton, R. A., Sutton, G. G., Fleischmann, R. D., Ketchum, K. A., Klenk, H. P., Gill, S., Dougherty, B. A., Nelson, K., Quackenbush, J., Zhou, L., Kirkness, E. F., Peterson, S., Loftus, B., Richardson, D., Dodson, R., Khalak, H. G., Glodek, A., McKenney, K., Fitzegerald, L. M., Lee, N., Adams, M. D., Hickey, E. K., Berg, D. E., Gocayne, J. D., Utterback, T. R., Peterson, J. D., Kelley, J. M., Cotton, M. D., Weidman, J. M., Fujii, C., Bowman, C., Watthey, L., Wallin, E., Hayes, W. S., Borodovsky, M., Karp, P. D., Smith, H. O., Fraser, C. M., and Venter, J. C. (1997) The complete genome sequence of the gastric pathogen Helicobacter pylori, *Nature 388*, 539-547. (10.1038/41483)

78. Schauer, K., Muller, C., Carriere, M., Labigne, A., Cavazza, C., and De Reuse, H. (2010) The Helicobacter pylori GroES cochaperonin HspA functions as a specialized nickel chaperone and sequestration protein through its unique C-terminal extension, *Journal of bacteriology 192*, 1231-1237. (10.1128/JB.01216-09)

79. Cheng, T., Li, H., Xia, W., and Sun, H. (2012) Multifaceted SlyD from Helicobacter pylori: implication in [NiFe] hydrogenase maturation, *Journal of biological inorganic chemistry : JBIC : a publication of the Society of Biological Inorganic Chemistry 17*, 331-343. (10.1007/s00775-011-0855-y)

80. Olson, J. W., Mehta, N. S., and Maier, R. J. (2001) Requirement of nickel metabolism proteins HypA and HypB for full activity of both hydrogenase and urease in Helicobacter pylori (vol 39, pg 176, 2001), *Molecular microbiology 40*, 270-270. (DOI 10.1046/j.1365-2958.2001.02397.x)

81. Benoit, S. L., Mehta, N., Weinberg, M. V., Maier, C., and Maier, R. J. (2007) Interaction between the Helicobacter pylori accessory proteins HypA and UreE is needed for urease maturation, *Microbiology 153*, 1474-1482. (10.1099/mic.0.2006/003228-0)

82. Banaszak, K., Martin-Diaconescu, V., Bellucci, M., Zambelli, B., Rypniewski, W., Maroney, M. J., and Ciurli, S. (2012) Crystallographic and X-ray absorption spectroscopic characterization of Helicobacter pylori UreE bound to Ni(2)(+) and Zn(2)(+) reveals a role for the disordered C-terminal arm in metal trafficking, *The Biochemical journal 441*, 1017-1026. (10.1042/BJ20111659)

83. Bellucci, M., Zambelli, B., Musiani, F., Turano, P., and Ciurli, S. (2009) Helicobacter pylori UreE, a urease accessory protein: specific Ni(2+)- and Zn(2+)-binding properties and interaction with its cognate UreG, *The Biochemical journal 422*, 91-100. (10.1042/BJ20090434)

84. Shi, R., Munger, C., Asinas, A., Benoit, S. L., Miller, E., Matte, A., Maier, R. J., and Cygler, M. (2010) Crystal structures of apo and metal-bound forms of the UreE protein from Helicobacter pylori: role of multiple metal binding sites, *Biochemistry 49*, 7080-7088. (10.1021/bi100372h)

85. Hu, H. Q., Johnson, R. C., Merrell, D. S., and Maroney, M. J. (2017) Nickel Ligation of the N-Terminal Amine of HypA Is Required for Urease Maturation in Helicobacter pylori, *Biochemistry 56*, 1105-1116. (10.1021/acs.biochem.6b00912)

86. Benoit, S., and Maier, R. J. (2003) Dependence of Helicobacter pylori Urease Activity on the Nickel-Sequestering Ability of the UreE Accessory Protein, *Journal of bacteriology 185*, 4787-4795. (10.1128/jb.185.16.4787-4795.2003)

87. Fong, Y. H., Wong, H. C., Yuen, M. H., Lau, P. H., Chen, Y. W., and Wong, K. B. (2013) Structure of UreG/UreF/UreH complex reveals how urease accessory proteins facilitate maturation of Helicobacter pylori urease, *PLoS Biol 11*, e1001678. (10.1371/journal.pbio.1001678)

88. Leipe, D. D., Wolf, Y. I., Koonin, E. V., and Aravind, L. (2002) Classification and evolution of P-loop GTPases and related ATPases, *Journal of molecular biology 317*, 41-72. (10.1006/jmbi.2001.5378)

89. Mehta, N., Benoit, S., and Maier, R. J. (2003) Roles of conserved nucleotide-binding domains in accessory proteins, HypB and UreG, in the maturation of nickel-enzymes required for efficient Helicobacter pylori colonization, *Microbial Pathogenesis 35*, 229-234. (10.1016/s0882-4010(03)00151-7)

90. Yang, X., Li, H., Lai, T. P., and Sun, H. (2015) UreE-UreG complex facilitates nickel transfer and preactivates GTPase of UreG in Helicobacter pylori, *The Journal of biological chemistry 290*, 12474-12485. (10.1074/jbc.M114.632364)

91. Martin-Diaconescu, V., Bellucci, M., Musiani, F., Ciurli, S., and Maroney, M. J. (2012) Unraveling the Helicobacter pylori UreG zinc binding site using X-ray absorption spectroscopy (XAS) and structural modeling, *Journal of biological inorganic chemistry : JBIC : a publication of the Society of Biological Inorganic Chemistry 17*, 353-361. (10.1007/s00775-011-0857-9)

92. Zambelli, B., Turano, P., Musiani, F., Neyroz, P., and Ciurli, S. (2009) Zn2+-linked dimerization of UreG from Helicobacter pylori, a chaperone involved in nickel trafficking and urease activation, *Proteins 74*, 222-239. (10.1002/prot.22205)

93. Sydor, A. M., Lebrette, H., Ariyakumaran, R., Cavazza, C., and Zamble, D. B. (2014) Relationship between Ni(II) and Zn(II) coordination and nucleotide binding by the Helicobacter pylori [NiFe]-hydrogenase and urease maturation factor HypB, *The Journal of biological chemistry 289*, 3828-3841. (10.1074/jbc.M113.502781)

94. Mehta, N., Olson, J. W., and Maier, R. J. (2003) Characterization of Helicobacter pylori Nickel Metabolism Accessory Proteins Needed for Maturation of both Urease and Hydrogenase, *Journal of bacteriology 185*, 726-734. (10.1128/jb.185.3.726-734.2003)

95. Xia, W., Li, H., Yang, X., Wong, K. B., and Sun, H. (2012) Metallo-GTPase HypB from Helicobacter pylori and its interaction with nickel chaperone protein HypA, *The Journal of biological chemistry 287*, 6753-6763. (10.1074/jbc.M111.287581)

96. Benoit, S. L., McMurry, J. L., Hill, S. A., and Maier, R. J. (2012) Helicobacter pylori hydrogenase accessory protein HypA and urease accessory protein UreG compete with each other for UreE recognition, *Biochimica et biophysica acta 1820*, 1519-1525. (10.1016/j.bbagen.2012.06.002)

97. Stingl, K., Schauer, K., Ecobichon, C., Labigne, A., Lenormand, P., Rousselle, J. C., Namane, A., and de Reuse, H. (2008) In Vivo Interactome of Helicobacter pylori Urease Revealed by Tandem Affinity Purification, *Mol Cell Proteomics 7*, 2429-2441. (DOI 10.1074/mcp.M800160-MCP200)

98. Cheng, T., Li, H., Yang, X., Xia, W., and Sun, H. (2013) Interaction of SlyD with HypB of Helicobacter pylori facilitates nickel trafficking, *Metallomics : integrated biometal science 5*, 804-807. (10.1039/c3mt00014a)

99. Kang, D., Gong, Y., Zhu, Y., Li, A., Dong, N., Piao, Y., and Yuan, Y. (2013) The biological activity of H. pylori SlyD in vitro, *Helicobacter 18*, 347-355. (10.1111/hel.12057)

100. Zhu, Y., Chen, M., Gong, Y., Liu, Z., Li, A., Kang, D., Han, F., Liu, J., Liu, J., and Yuan, Y. (2015) Helicobacter pylori FKBP-type PPIase promotes gastric epithelial cell proliferation and anchorage-independent growth through activation of ERK-mediated mitogenic signaling pathway, *FEMS Microbiol Lett 362*. (10.1093/femsle/fnv023)

101. Kennedy, D. C., Herbst, R. W., Iwig, J. S., Chivers, P. T., and Maroney, M. J. (2007) A dynamic Zn site in Helicobacter pylori HypA: A potential mechanism for metal-specific protein activity, *J Am Chem Soc 129*, 16-17. (Doi 10.1021/Ja066958x)

102. Herbst, R. W., Perovic, I., Martin-Diaconescu, V., O'Brien, K., Chivers, P. T., Pochapsky, S. S., Pochapsky, T. C., and Maroney, M. J. (2010) Communication between the Zinc and Nickel Sites in Dimeric HypA: Metal Recognition and pH Sensing, *J Am Chem Soc 132*, 10338-10351. (Doi 10.1021/Ja1005724)

103. Xia, W., Li, H. Y., Sze, K. H., and Sun, H. Z. (2009) Structure of a Nickel Chaperone, HypA, from Helicobacter pylori Reveals Two Distinct Metal Binding Sites, *J Am Chem Soc 131*, 10031-10040. (Doi 10.1021/Ja900543y)

104. Yang, X., Li, H., Cheng, T., Xia, W., Lai, Y. T., and Sun, H. (2014) Nickel translocation between metallochaperones HypA and UreE in Helicobacter pylori, *Metallomics : integrated biometal science 6*, 1731-1736. (10.1039/c4mt00134f)

105. Sydor, A. M., Liu, J., and Zamble, D. B. (2011) Effects of metal on the biochemical properties of Helicobacter pylori HypB, a maturation factor of [NiFe]-hydrogenase and urease, *Journal of bacteriology 193*, 1359-1368. (10.1128/JB.01333-10)

106. Ge, R. G., Wang, D. X., Hao, M. C., and Sun, X. S. (2013) Nickel trafficking system responsible for urease maturation in Helicobacter pylori, *World journal of gastroenterology : WJG 19*, 8211-8218. (10.3748/wjg.v19.i45.8211)

CHAPTER 2

HYDROGENASE ACTIVITY DOES NOT CONTRIBUTE TO *HELICOBACTER PYLORI* ACID SURVIVAL

Portions of this chapter has been published: Faith C. Blum; Heidi Q. Hu; Stephanie L. Servetas; Stéphane L. Benoit; Robert J. Maier; Michael J. Maroney; and D. Scott Merrell. Structure-function analyses of metal-binding sites of HypA reveal residues important for hydrogenase maturation in *Helicobacter pylori*. *PLOS ONE*, 2017.

2.1 Introduction

Helicobacter pylori is a prevalent human pathogen that colonizes the gastric mucosa and chronic infection is associated with development of stomach ulcers and cancers (discussed in CHAPTER 1, Section 1.1).[1, 2] Ni-dependent enzymes urease and NiFe-hydrogenase (H_2ase) have been associated with its ability for infecting the acidic environment of the human stomach.[3, 4]

Despite thriving in the acidic human stomach, *H. pylori* is not an acidophile and thus, must acclimate to the low pH environment found in the stomach (discussed in CHAPTER 1, Section 1.1.1).[5] This is in large part accomplished by urease (discussed in CHAPTER 1, Section 1.1.1.4), which neutralizes the gastric microenvironment and buffers the bacterial cytoplasm by catalyzing the conversion of urea into ammonia and carbon dioxide.[5-7] The importance of urease in the *H. pylori* life cycle is evidenced by the fact that this enzyme represents approximately 10% of the total protein syntheses in the cell.[8] As such, urease represents a major nickel sink within *H. pylori*. Insertion of the Ni cofactors into the urease active site requires the accessory proteins UreEFGH, as well as HypA and HypB, which are typically associated with the insertion of Ni into NiFe-H_2ase.[9, 10]

H_2ase and urease, therefore, compete for maturation within *H. pylori*, as both enzymes require the accessory proteins HypA and HypB for inserting the Ni co-factor into their active sites (discussed in Sections 1.2.5.1 and 1.3). NiFe-H_2ase is the only other known Ni-containing enzyme in *H. pylori*.[11] H_2ases catalyzes the reversible oxidation of molecular hydrogen: $H_2 \leftrightharpoons 2\,H^+ + 2\,e^-$. However, the *H. pylori* NiFe- H_2ase has been categorized as an H_2-uptake type H_2ase.[12] The oxidation of H_2 (presumed to be produced by the intestinal flora of the host) by

H_2ase was thought to be an alternate source of energy for *H. pylori*.[12] The heterotrimeric H_2ase complex is composed of HydA, the small subunit that contains multiple [Fe-S] clusters; HydB, the large subunit that contains the [NiFe] site; and HydC, a membrane-anchored *b*-type cytochrome.[13] Deletion of *hyd* results in reduced colonization in animal models, which is attributed to the inability of the mutants to use H_2 as an energy source within the animal host.[12] The energy generated by H_2 oxidation is intricately linked to powering the *H. pylori* type IV secretion systems (T4SS), which is used for horizontal gene transfer and injection of the CagA cytotoxin and other effectors into host cells and surrounding tissues to modify the host immune response.[14]

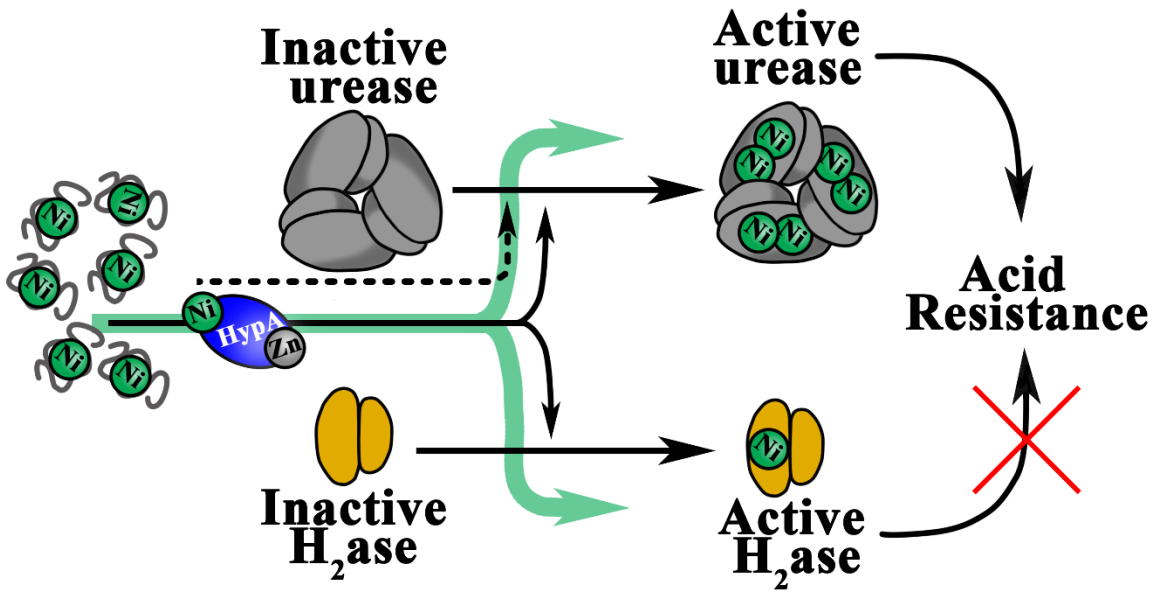

Figure 2.1: Contributions of Ni enzyme maturation pathways in *H. pylori* to acid resistance. HypA distributes Ni cofactors (green circles) within *H. pylori* to enzyme targets urease and H_2ase. Insertion of Ni into urease can occur under Ni abundant conditions in the absence of HypA (dash line); but H_2ase maturation cannot be accomplished without HypA. Activation of urease contributes to acid resistance, but H_2ase activity is herein shown not to contribute to acid resistance (red X). Figure reproduced from Blum *et. al. PLOS ONE*, 2017, 12, e0183260[15].

Proper Ni- and Zn-coordination of the HypA Ni-metallochaperone has been shown to be required for the activation of both urease and H_2ase in *H. pylori*[10, 16] (extensively characterized and discussed in CHAPTER 3). Despite its pivotal role in regulating the activity of both known Ni-dependent enzymes, the transcription of the *hypA* gene was not regulated by Ni,[17] but is

instead up-regulated in response to acid stress (discussed in Section 1.2.1).[18-20] This acid-dependent up-regulation of *hypA* potentially contributes to the maturation for both Ni-containing enzymes (Figure 2.1). Where the role of urease in acid stress response has been extensively characterized in *H. pylori*,[4, 6, 21] it is unclear whether H_2ase also play a role. H_2ase mutant strains exhibit impaired acid resistance in *Escherichia coli* K-12,[22, 23] *salmonella enterica* serovar Typhimurium,[24] and *shigella flexneri*.[25] However, to our knowledge the role of *H. pylori* H_2ase in acid resistance has not yet been investigated.

2.2 Results

2.2.1 Enzyme activities of Δ*hydB* variant strain of *H. pylori*

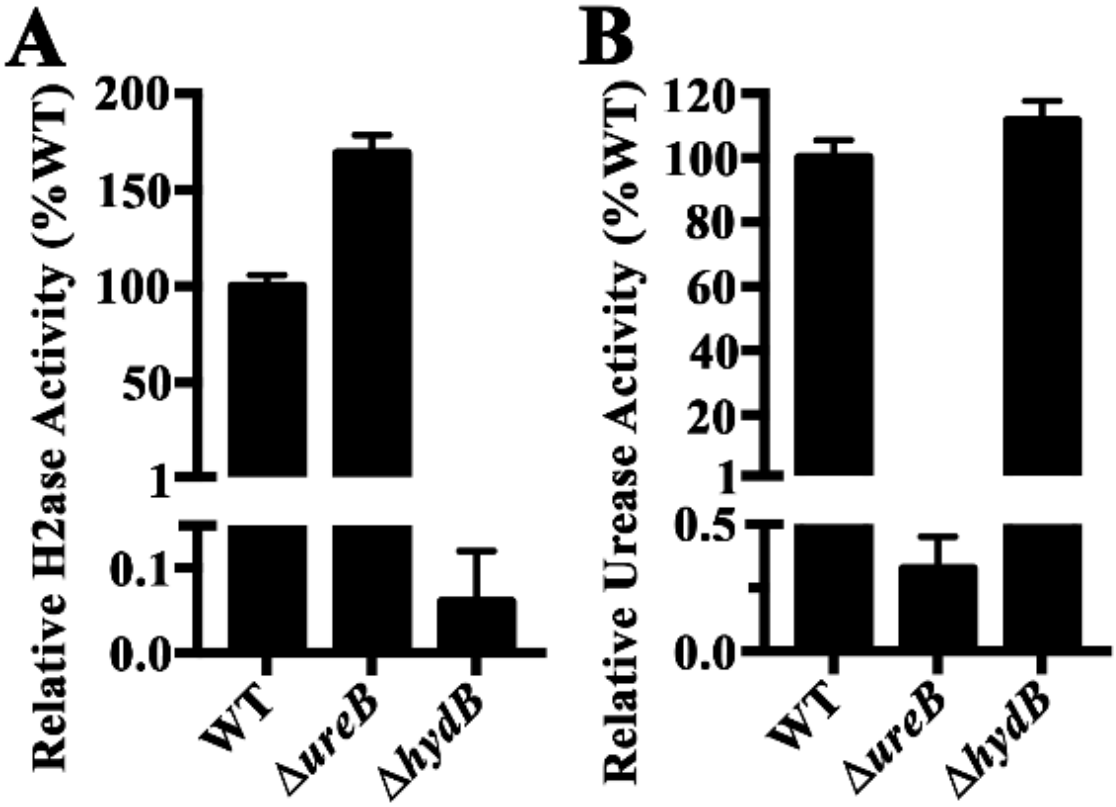

Figure 2.2: *H. pylori* Δ*hydB* has no detectable H_2ase activity and WT-like urease activity. Cell lysates of the G27 wild-type strain (WT), urease mutant strain (Δ*ureB*), and H_2ase mutant strain (Δ*hydB*) were used to measure (A) H_2ase activity by measuring the rate of H_2-oxidation and (B) urease activity by measuring the rate of NH_3 production. The enzyme activities in each strain were normalized against the total protein in the lysate to obtain the specific activity, and then further normalized against the specific activity of the WT-strain to obtain the relative activity as %WT. Three biological replicates were tested for each strain, and the mean and standard deviation are graphed. Figure reproduced from Blum *et. al. PLOS ONE*, 2017, 12, e0183260[15].

To determine the role of the H_2ase in *H. pylori* acid resistance, a deletion mutation of *hydB* in the G27 strain background was generated. The H_2 oxidation activity in the lysates of the Δ*hydB* strain were measured using a methyl violet assay; the parental WT strain and a urease mutant strain (Δ*ureB*) were included as controls (Figure 2.2A). As expected,[10, 12] the Δ*hydB* strain did not exhibit H_2ase activity (H_2 oxidation < 0.1% of WT, similar to buffer alone). Unexpectedly, the Δ*ureB* strain showed increased H_2ase activity as compared to that of WT; this increased activity was consistent across all experiments (range of 130-170%). To confirm that deletion of H_2ase had no effect on urease activity as previously described,[16] urease activity was measured using a modified phenol-hypochlorite assay for NH_3 production (Figure 2.2B). The Δ*hydB* strain exhibited urease activity similar to the parent WT strain.

2.2.2 H_2ase does not contribute to acid resistance in *H. pylori*

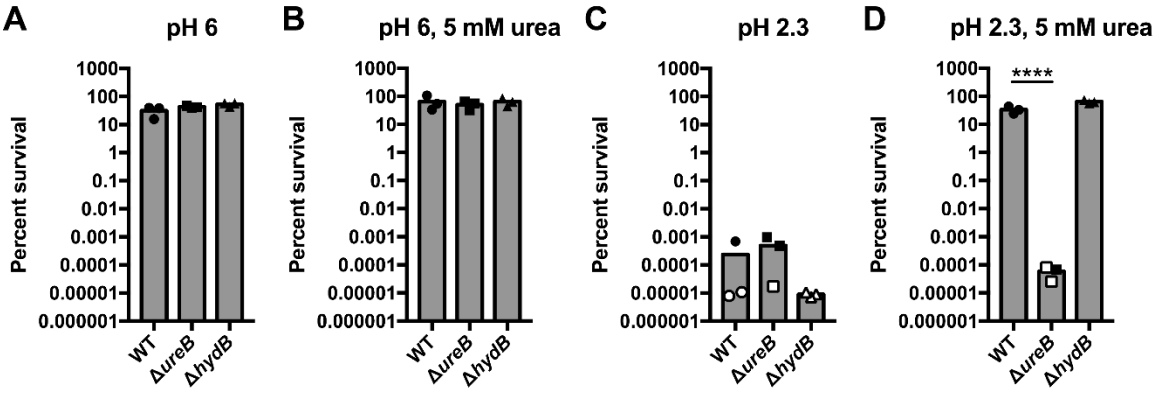

Figure 2.3: Δ*hydB* strain of *H. pylori* G27 is not attenuated for acid survival.
The wild-type (WT) strain, urease mutant strain (Δ*ureB*), and hydrogenase mutant strain (Δ*hydB*) were incubated for 1 hour in PBS adjusted to pH 6.0 (A and B) or to pH 2.3 (C and D), in the absence (A and C) or presence (B and D) of 5 mM urea. The number of colony-forming units (CFU) was measured at 0 min (T_0) and at 60 min (T_{60}), and percent survival was calculated as CFU at T_{60} divided by CFU at T_0. Data from individual biological replicates are shown as points, with the bar plotted at the mean. Open symbols indicate that no bacteria were recovered and thus, the CFU are plotted as a function of the limit of detection (100 CFU/mL). Three biological replicates were performed. For panels A-C, a one-way ANOVA followed by Dunnett's test for multiple comparisons was performed; the comparison was made only to WT. In panel D, the same statistical tests were performed on the log-transformed data. **** = $p < 0.0001$. Figure reproduced from Blum *et. al. PLOS ONE*, 2017, 12, e0183260 [15].

The contribution of H_2ase to *H. pylori* acid resistance was assessed after exposure of bacteria to pH 6.0 or pH 2.3 buffers for one hour in the presence or absence of 5 mM urea, and then measuring the surviving colony forming units (CFU). All strains survived at pH 6.0, independent of the presence or absence of urea (Figure 2.3AB). Conversely, at pH 2.3 without urea, all strains exhibited significantly impaired survival (limit of detection [LOD] = 100, Figure 2.3C). At pH 2.3 in the presence of urea, the Δ*ureB* strain was extremely acid sensitive, which was expected since the Δ*ureB* strain is unable to utilize urea to neutralize low pH. In contrast, survival of the WT and Δ*hydB* strains was comparable. This result confirmed the *ex vivo* urease activities measured in the corresponding strains (Figure 2.3D). Thus, unlike in other pathogenic bacteria, H_2ase appears to play no role in acid resistance in *H. pylori*.

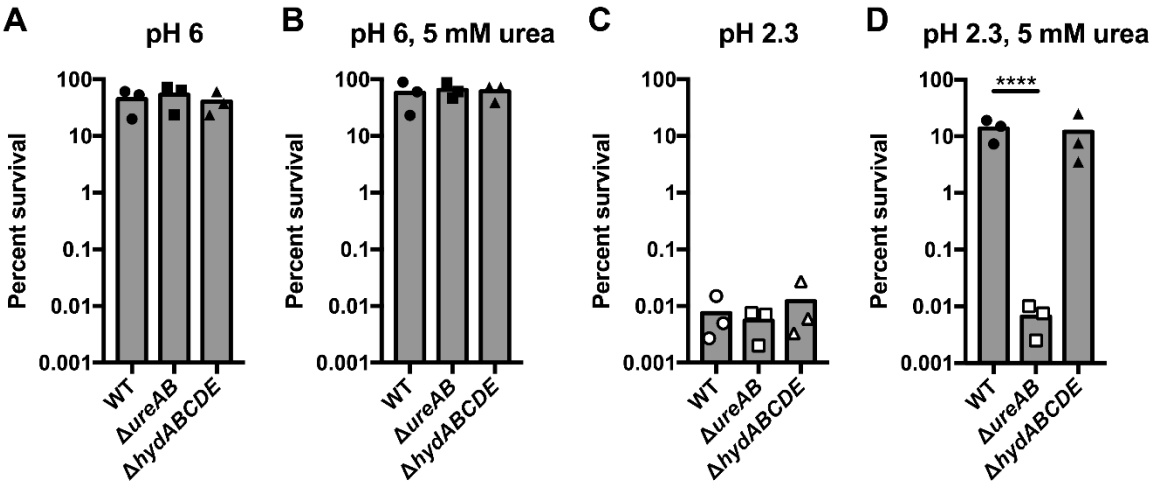

Figure 2.4: Δ*hydABCDE* strain of *H. pylori* 26695 is not attenuated for acid survival.
The wild-type (WT) 26695 strain, urease mutant strain (Δ*ureAB*), and H_2ase mutant strain (Δ*hydABCDE*) were incubated for 1 hour in PBS adjusted to pH 6.0 (A and B) or to pH 2.3 (C and D), in the absence (A and C) or presence (B and D) of 5 mM urea. The number of colony-forming units (CFU) was measured at 0 min (T_0) and at 60 min (T_{60}), and percent survival was calculated as CFU at T_{60} divided by CFU at T_0. Data from individual biological replicates are shown as points, with the bar plotted at the mean. Open symbols indicate that no bacteria were recovered and thus, the CFU are plotted as a function of the limit of detection (1000 CFU/mL). Three biological replicates were performed. For panels A-C, a one-way ANOVA followed by Dunnett's test for multiple comparisons was performed; the comparison was made only to WT. In panel D, the same statistical tests were performed on the log-transformed data. **** = $p < 0.0001$. Figure reproduced from Blum *et. al. PLOS ONE*, 2017, 12, e0183260 [15].

Given the high degree of genetic diversity seen between strains of *H. pylori*,[26, 27] these results were verified in an additional *H. pylori* strain. The Δ*hydABCDE* mutant strain,[28] previously constructed from *H. pylori* 26695 as the parent WT strain, in addition to a urease-negative control (Δ*ureAB*) were tested for acid survival. As shown in Figure 2.4, the results obtained with the 26695 strain background were comparable to those obtained with G27. *En masse*, these data indicate that H_2ase does not contribute to the acid resistance of *H. pylori*.

2.3 Discussion

Mutation of H_2ase or urease resulted in the expected loss of each respective enzymatic activity (Figure 2.2).[29] Unexpectedly, the deletion of *ureB* consistently resulted in an increase in H_2ase activity above that seen in the wild-type parental strain (Figure 2.2A). Interestingly, the reverse did not hold true; deletion of H_2ase resulted in only a slight increase (~12%) in urease activity in the G27 background (Figure 2.2B), as was previously observed in the 26695 background.[16] Both the urease and the H_2ase maturation pathways require intracellular nickel and the accessory proteins HypA and HypB.[10] However, urease is the major nickel sink,[8, 30] suggesting that the equilibrium between the two pathways favors urease. Deletion of urease is hypothesized to increase the Ni available to the H_2ase maturation pathway, resulting in an increase in H_2ase activity. While deletion of H_2ase also increases the Ni available to the urease maturation pathway, however to a much lesser extent, therefore only a small increase of urease activity was observed in the Δ*hydB* strains.

Though a role for H_2ase in acid resistance has been shown in several other pathogenic bacteria, the [NiFe] uptake-type H_2ase of *H. pylori* does not appear to contribute to acid resistance (Figure 2.1, Figure 2.3, Figure 2.4). Though the reason for this variation across pathogens is not completely clear, several interesting differences across the various species are apparent. For example, *Salmonella enterica* serovar Typhimurium carries three H_2 uptake-type H_2ases (*hya*, *hyb* and *hyd*), in addition to two H_2-evolving H_2ases (*hyc* and *hyf*). Deletion of *hya*, but not *hyb* or *hyd*, results in loss of acid resistance and impaired survival inside macrophages.[24]

Though the exact mechanism by which Hya contributes to the acid stress response of *S.* Typhimurium is unknown, a mechanism involving energy conservation by Hya via recycling of H_2 produced by Hyc has been proposed.[24, 31, 32] Similarly, in *Shigella flexneri*, deletion of the hydrogen-uptake-type H_2ase *hya* results in an acid sensitive mutant strain,[25] while in *Escherichia coli*, deletion of the hydrogen-evolving H_2ase encoded by *hyc* results in acid sensitivity in anaerobic growth conditions.[23] It is worth noting that each of these other pathogens that rely on a H_2ase for acid resistance have limited mechanisms for dealing with acid stress as compared to urease activity in *H. pylori*. Indeed, acid neutralization is accomplished quickly by *H. pylori* urease; when incubated in unbuffered HCl as low as pH 3, *H. pylori* increases the pH to neutral within 1 min.[8] Despite living in the human stomach, *H. pylori* is not an acidophile, and appears to synthesize a large amount of urease (up to 10% of the nascent protein content) for protection against a sudden decrease in pH.[8] With such a robust mechanism for acid neutralization, and so much energy committed to urease synthesis and nickel sequestration, perhaps *H. pylori* simply does not need to dedicate a second nickel-containing enzyme (H_2ase) to cope with acid stress.

A loss of acid resistance was observed in strains of *H. pylori* lacking urease, but not in strains lacking H_2ase (Figure 2.3 and Figure 2.4). Previous studies have shown that H_2ase mutant strains of *H. pylori* are deficient for colonization in mouse and Mongolian gerbil models of infection.[12, 14] The degree of deficiency varies depending on the animal model and/or *H. pylori* strain background.[12, 14] Given the lack of a pH-sensitive phenotype, the role of H_2ase during *H. pylori* animal infection may solely be the previously proposed utilization of H_2 as an energy source.[12] The energy generated by robust H_2 oxidation activity was associated with increased incidents of gastric carcinogenesis in Mongolian gerbil infection models, likely by increasing the translocation of the CagA cytotoxin into host cells, which was demonstrated *ex vivo*.[14] The translocation of CagA, as well as other effectors, through associated T4SS into host cells or surrounding tissues has been known to modulate the host immune system.[33, 34] CagA translocation promoted denser initial infections (2 – 6 weeks post inoculation), but increases host inflammatory

responses with prolonged colonization (12 weeks), accompanied by development of gastric cancers in Mongolian gerbil infection models.[14] Thus, diverting Ni and HypA toward the H_2ase maturation pathway does not contribute to acid acclimation in *H. pylori*, but instead boost initial infection efficiencies[12, 14] by powering the translocation of CagA.[14]

2.4 Method

2.4.1 Bacterial growth

Growth of G27 background strains of *H. pylori* were performed at the Merrell Lab, part of the Department of Microbiology and Immunology at the Uniformed Services University of Health Sciences, Bethesda, MD. Growth of 26695 background strains of *H. pylori* were performed at the Maier Lab, part of the Department of Microbiology at the University of Georgia, Athens, GA. Strains are listed and described in Table 2.1. *H. pylori* strains were maintained at -80°C in brain heart infusion (BHI) broth (BD) supplemented with 20% (v/v) glycerol (CalBioChem) and 10% (v/v) fetal bovine serum (FBS, Gibco). *H. pylori* G27 and G27-derived strains were grown on 4.4% (w/v) Columbia agar (Acumedia) supplemented with 5% (v/v) horse blood (HemoStat), 0.2% (w/v) β-cyclodextrin (Sigma), 10 μg/mL vancomycin (Amresco), 2.5 U/mL polymyxin B sulfate (Sigma), and 8 μg/mL amphotericin B (Amresco). Liquid growth of G27 strains was accomplished in Brucella broth (Acumedia) supplemented with 10% (v/v) FBS and 10 μg/mL vancomycin. G27 cultures were grown at 37°C under microaerophilic conditions (10% CO_2, 5% O_2, and N_2 as balance) achieved using an Anoxomat (Advanced Instruments Inc). *H. pylori* 26695 and 26695-derived strains were grown on Brucella agar plates (Becton Dickinson) supplemented with 10% sheep blood (Hemostat) in CO_2 incubators (Thermo Scientific) under microaerophilic conditions (5% CO_2, 4% O_2, and N_2 as balance). Liquid growth of 26695 strains was performed in BHI broth supplemented with 0.4% β-cyclodextrin (Sigma) under microaerophilic conditions (5% CO_2, 5% O_2, and N_2 as balance). For both strains, selection was performed with 25 μg/mL kanamycin (Gibco) or 30 μg/mL chloramphenicol (Sigma), as appropriate. Liquid *H. pylori* cultures were grown with shaking at 110 RPM. *Escherichia coli*

Top10 cells were grown at 37°C on 4% LB agar plates (MoBio) or in liquid in LB broth (Invitrogen) with shaking at 225 RPM. Selection was performed with 100 µg/mL ampicillin (Affymetrix).

Table 2.1: Strains, plasmids, and primers used in this study

Strains	**Description**	**Reference**
DSM1	G27 WT	[35]
DSM43	G27 Δ*ureB* (Δ*ureB::kan*), Kan^R	[36]
DSM1569	*E. coli* TOP10 containing pDSM1569, Kan^R	This study
DSM1570	G27 Δ*hydB* (Δ*hydB::kan*), Kan^R	This study
26695	WT	[37]
SLB1333	26695 Δ*ureAB* (Δ*ureAB::cat*), Cm^R	This study
SLB1166	26695 Δ*hydABCDE* (Δ*hydABCDE::cat*), Cm^R	[28]
Plasmids	**Description**	**Reference**
pDSM199	pTM117 vector with Kan^R gene	[38]
pDSM1569	pGEM T-Easy vector with KanR gene fused with sequence upstream and downstream of *hydB*	This study
Primers	**Sequence (5′-3′)**	**Reference**
hydB_us_F	GCAATGTGCTTTATTACTTGATG	This study
hydB_us_R	GTTAGTCACCCGGGTACCGAGCTCGACATGTTAA TCCCTTACTCTTTG	This study
hydB_ds_F	CTAGAGTCGACCTGCAGGCATGCAAGGGACACGC ATGGATAAAATG	This study
hydB_ds_R	GGTTATGGTTATACCAAAGAATGA	This study
NP_kan_F	GAGCTCGGTACCCGGGTGACTAACTAGGAGGAAT AAATG	[39]
NP_kan_R	CTTGCATGCCTGCAGGTCGACTCTAGAGGATCCCC GGGTCATTATTCCCTCCAGGTACTA	[39]
hydB_conf_F	CCAGTTAAGGAGTGGCG	This study
hydB_conf_R	GGATATTTCCAATGCCTAAAATTAG	This study
ureABR2	TCCCTAAAGGGATTTTCAAGATGT	[40]
ureCAMF2	CCCAGTTTGTCGCACTGATAACCATGTGTTCGTGG ATGGCAA	[40]
C1	GATATAGATTGAAAAGTGGAT	[40]
C2	TTATCAGTGCGACAAACTGGG	[40]
ureCAMR1	ATCCACTTTTCAATCTATATCATTCTCCTATTCTTA AAGTGTTTT	[40]
ureABF1	CATGGGGGCGTGGTGGATTA	[40]

Table reproduced from Blum *et. al. PLOS ONE*, 2017, 12, e0183260 [15].

2.4.2 Mutant construction of Δ*hydB* and Δ*ureAB*

Construction of Δ*hydB* and Δ*ureAB* strains in the G27 *H. pylori* background strains were performed at the Merrell Lab, part of the Department of Microbiology and Immunology at the Uniformed Services University of Health Sciences, Bethesda, MD. Construction of Δ*ureAB* strain in the 26695 *H. pylori* background strains were performed at the Maier Lab, part of the Department of Microbiology at the University of Georgia, Athens, GA. A Δ*hydB* deletion insertion strain containing a *kan* cassette replacing the coding sequence for *hydB* (HPG27_ RS03075) was constructed as follows. *H. pylori* G27 (Table 2.1) genomic DNA was used as a template for polymerase chain reaction (PCR) to amplify fragments of DNA flanking *hydB*. The primer pair hydB_us_F and hydB_us_R was used to amplify a 490-bp fragment upstream of *hydB* (containing coding sequence for *hydA*). The upstream primer contained an additional 24-bp complementary sequence to the 5′ sequence of the *kan* cassette. The primer pair hydB_ds_F and hydB_ds_R was used to amplify a 683-bp fragment downstream of *hydB* (containing coding sequence for *hydC*); the forward primer contained an additional 26-bp sequence that was complementary to the end of the *kan* cassette. Primer pairs NP_kan_F and NP_kan_R were used to amplify *aphA3*, which encodes a Kan^R gene, from pDSM199. The three fragments were assembled using splicing-by-overlap-extension (SOE) PCR. The spliced PCR product was ligated into the pGEM-T Easy vector (Promega) and transformed into *E. coli* TOP10 cells. Transformants were selected with ampicillin and screened for growth of white colonies on X-gal and IPTG. The desired SOE product was confirmed by Sanger sequencing. The plasmid containing the sequenced product was named pDSM1569, and the *E. coli* strain containing pDSM1569 was named DSM1569. The 2061-bp SOE product was amplified from *E. coli* using primers that annealed to the backbone of the plasmid, and 500 ng of the resulting linear DNA was transformed into *H. pylori* G27. Transformants were selected for on HBA plates containing kanamycin. Incorporation of the *kan* cassette to replace *hydB* was confirmed by Sanger sequencing using hydB_conf_F and hydB_conf_R primers. The resultant mutant strain was

named DSM1570 (Table 2.1). A Δ*ureAB* deletion insertion strain containing a *cat* cassette replacing the coding sequence for *ureAB* (HP0073 and HP0072) was constructed in *H. pylori* 26695 using a SOE PCR method as described previously.[40]

2.4.3 Hydrogenase activity

H_2ase activity of *H. pylori* strains were performed at the Maroney Lab, part of the Department of Chemistry and Program of Molecular and Cellular Biology at the University of Massachusetts Amherst, Amherst, MA. Hydrogen oxidation activity was measured at room temperature (~23˚C) using whole cell lysates of various *H. pylori* strains. Cells were grown as previously described[29] and approximately 10^8 cells were pelleted and frozen at -80˚C prior to lysis. Upon thawing, cells were resuspended in 750 µL of ice-cold *H. pylori* lysis buffer (50 mM HEPES at pH 7.0 with 1 mM phenylmethansulfonyl fluoride (PMSF)) and then kept on ice during lysis by pulsed sonication (500 Hz) at 40% amplitude for 14 seconds. H_2 consumption was measured as previously described[41] with slight modifications. Briefly, an aliquot of whole cell lysate was used to test H_2 oxidation activity by monitoring the reduction of methyl viologen (MV) inside an anaerobic chamber (COY Labs, Grass Lake, MI) with a constant atmosphere of primarily N_2 with 3 – 4 % H_2 and 0 – 20 ppm O_2. Oxidized-MV (colorless) is the electron acceptor in the H_2 oxidation reaction catalyzed by H_2ase in the lysate resulting in reduced-MV (blue). The appearance of reduced-MV was monitored at $A_{578\ nm}$ ($\varepsilon = 9.78\ mM^{-1} \bullet cm^{-1}$)[42] where two reduced-MV were expected for every H_2 oxidized.[41] The reaction was initiated by adding 30 µL of whole cell lysate to 1 mL of deoxygenated H_2ase Reaction Buffer (50 mM Tris-HCl, 2 mM methyl viologen, pH 8.0) in a glass vial. After an initial lag time, the reaction mixture was transferred to a quartz cuvette and the appearance of methyl viologen reduction was monitored at $A_{578\ nm}$ for 45 – 150 minutes, of which the slope of the linear increase in absorbance over time is taken as the rate. The lag is due to anaerobic activation that occurs upon exhaustion of trace oxygen levels.[43] Reaction initiated by lysis buffer alone was used to correct for background activity/instrument drift, which is in the same order of magnitude (H_2-OX ~10^{-8} µmol/min) as the

Δ*hydB* strain (where no activity was expected) and less than 1% of any other strains tested. The specific H_2 oxidation activity was obtained by normalizing against the total protein in the whole cell lysate. Three biological replicates were tested for each strain (unless otherwise noted) and the specific H_2 oxidation activity of each strain was normalized against the activity of the wild-type strain to obtain percent H_2ase activity relative to wild-type.

2.4.4 Urease activity

Urease activity of *H. pylori* strains were performed at the Maroney Lab, part of the Department of Chemistry and Program of Molecular and Cellular Biology at the University of Massachusetts Amherst, Amherst, MA. Urease activity assays of whole cell extracts of *H. pylori* wild-type, Δ*ureB*, and Δ*hydB* strains were performed as previously described.[29] Briefly, for each strain, overnight liquid cultures of *H. pylori* were used to inoculate 5 mL liquid cultures to an optical density at 600 nm (OD_{600}) of 0.05, and then allowed to grow for 22 hr. At that point, the OD was measured and 1 OD unit of *H. pylori* was pelleted by centrifugation. The supernatants were removed and the bacterial pellets were stored at -20°C until ready for urease assays. The frozen cells were thawed and resuspended in 750 µL of ice-cold lysis buffer (HEPES buffer at pH 7.0, 1 mM PMSF, and 1x protease inhibitor cocktail). Resuspended cells were kept on ice during lysis, which was performed by sonication at 70% power for 6 pulses (2 sec each). The lysate was centrifuged at 15,000 x *g* for 10 min to remove insoluble material from the soluble whole cell extracts. The protein concentration of soluble whole cell extracts was determined by Bradford assays using the Pierce Coomassie Protein Assay Kit (Thermo Fisher Scientific). Urease activity was determined using a modified phenol-hypochlorite method (Section 2.4.4), which measures the amount of ammonia released from the soluble whole cell extract in the presence of urea.[44, 45] Five µL of whole cell extract was added to 245 µL of urease reaction buffer (50 mM HEPES, 25 mM urea, at pH 7.0), and incubated at 37ºC for 20 min to allow for ammonia production. The reaction was quenched by the sequential addition of 375 µL of phenol-hypochlorite buffer A (100 mM phenol, 167.8 mM sodium nitroprusside) and of 375 mL of phenol-hypochlorite buffer B

(125 mM NaOH, 0.044% NaClO). The assay mixture was incubated at 37ºC for 30 minutes to allow for color development, due to the conversion of phenol to indophenol, and measured at $A_{625\ nm}$. Assays were performed alongside a standard curve created using known amounts of ammonium chloride in place of the whole cell extract. The specific urease activity was determined by calculating the nmol of ammonia produced per µg of total protein in each whole cell extract. Relative urease activity of each strain was determined by normalizing against the specific activity of the wild-type strain to obtain percent urease activity relative to wild-type. Three biological replicates were tested for each strain.

2.4.5 Acid survival assay

Acid survival of G27 background strains of *H. pylori* were performed at the Merrell Lab, part of the Department of Microbiology and Immunology at the Uniformed Services University of Health Sciences, Bethesda, MD. Acid survival of 26695 background strains of *H. pylori* were performed at the Maier Lab, part of the Department of Microbiology at the University of Georgia, Athens, GA. Liquid cultures of *H. pylori* G27 were inoculated to an OD_{600} of 0.05 from an overnight starter liquid culture and were then grown for 18-19 h to an OD_{600} of approximately 0.9-1.0. 1-mL aliquots were pelleted at 2500-3000 x *g* and were resuspended in 1 mL phosphate buffered saline (PBS) at pH 6.0 or pH 2.3, and with or without supplementation with 5 mM urea. To prepare the resuspension solutions, urea was added from a freshly made 100 mM (in PBS) stock, as appropriate, and the pH of the solutions was adjusted using 6 M HCl. Immediately after resuspension, a 100-µL aliquot of *H. pylori* was removed, serially diluted in Brucella broth to 10^{-7}, and 10 µL aliquots of each dilution were plated to determine the colony-forming units (CFU) at T_0 for each condition. The remaining *H. pylori* were incubated at 37°C for 1 h with shaking. At 1 h, a second 100-µL aliquot was removed, serially diluted, and plated to determine the CFU at T_{60} for each condition. CFU counts were quantified after 4-5 d of growth. A similar protocol was used to monitor acid survival of the 26695 strains with the following minor exceptions. Liquid cultures of 26695 wild-type and mutant strains were grown for 26-30 h to an OD_{600} of

approximately 0.34-0.42. Cells were serially diluted up to 10^{-5} in PBS at pH 7.3 and 10 µL of the 10^{-1} - 10^{-5} dilutions were plated in triplicate. Percent survival was calculated for each strain and condition using the equation T_{60} / T_0 x 100%. Three biological replicates were performed for each isolate and for each strain background.

2.5 References

1. Eusebi, L. H., Zagari, R. M., and Bazzoli, F. (2014) Epidemiology of Helicobacter pylori infection, *Helicobacter 19 Suppl 1*, 1-5. (10.1111/hel.12165)

2. Sonnenberg, A. (2013) Review article: historic changes of Helicobacter pylori-associated diseases, *Aliment Pharmacol Ther 38*, 329-342. (10.1111/apt.12380)

3. Eaton, K. A., Brooks, C. L., Morgan, D. R., and Krakowka, S. (1991) Essential Role of Urease in Pathogenesis of Gastritis Induced by Helicobacter-Pylori in Gnotobiotic Piglets, *Infection and Immunity 59*, 2470-2475

4. Tsuda, M., Karita, M., Morshed, M. G., Okita, K., and Nakazawa, T. (1994) A urease-negative mutant of Helicobacter pylori constructed by allelic exchange mutagenesis lacks the ability to colonize the nude mouse stomach, *Infect Immun 62*, 3586-3589

5. Sachs, G., Weeks, D. L., Wen, Y., Marcus, E. A., Scott, D. R., and Melchers, K. (2005) Acid acclimation by Helicobacter pylori, *Physiology 20*, 429-438. (DOI 10.1152/physiol.00032.2005)

6. Marshall, B. J., Barrett, L. J., Prakash, C., McCallum, R. W., and Guerrant, R. L. (1990) Urea protects Helicobacter (Campylobacter) pylori from the bactericidal effect of acid, *Gastroenterology 99*, 697-702

7. Maroney, M. J., and Ciurli, S. (2014) Nonredox nickel enzymes, *Chemical reviews 114*, 4206-4228. (10.1021/cr4004488)

8. Bauerfeind, P., Garner, R., Dunn, B. E., and Mobley, H. L. T. (1997) Synthesis and activity of Helicobacter pylori urease and catalase at low pH, *Gut 40*, 25-30

9. Farrugia, M. A., Macomber, L., and Hausinger, R. P. (2013) Biosynthesis of the Urease Metallocenter, *Journal of Biological Chemistry 288*, 13178-13185. (10.1074/jbc.R112.446526)

10. Olson, J. W., Mehta, N. S., and Maier, R. J. (2001) Requirement of nickel metabolism proteins HypA and HypB for full activity of both hydrogenase and urease in Helicobacter pylori (vol 39, pg 176, 2001), *Molecular microbiology 40*, 270-270. (DOI 10.1046/j.1365-2958.2001.02397.x)

11. Maier, R. J., Benoit, S. L., and Seshadri, S. (2007) Nickel-binding and accessory proteins facilitating Ni-enzyme maturation in Helicobacter pylori, *Biometals : an international journal on the role of metal ions in biology, biochemistry, and medicine 20*, 655-664. (10.1007/s10534-006-9061-8)

12. Olson, J. W., and Maier, R. J. (2002) Molecular hydrogen as an energy source for Helicobacter pylori, *Science 298*, 1788-1790. (10.1126/science.1077123)

13. Benoit, S. L., and Maier, R. J. (2008) Hydrogen and nickel metabolism in helicobacter species, *Ann N Y Acad Sci 1125*, 242-251. (10.1196/annals.1419.014)

14. Wang, G., Romero-Gallo, J., Benoit, S. L., Piazuelo, M. B., Dominguez, R. L., Morgan, D. R., Peek, R. M., Jr., and Maier, R. J. (2016) Hydrogen Metabolism in Helicobacter pylori Plays a Role in Gastric Carcinogenesis through Facilitating CagA Translocation, *MBio 7*. (10.1128/mBio.01022-16)

15. Blum, F. C., Hu, H. Q., Servetas, S. L., Benoit, S. L., Maier, R. J., Maroney, M. J., and Merrell, D. S. (2017) Structure-function analyses of metal-binding sites of HypA reveal residues important for hydrogenase maturation in Helicobacter pylori, *PloS one 12*, e0183260. (10.1371/journal.pone.0183260)

16. Benanti, E. L., and Chivers, P. T. (2009) An intact urease assembly pathway is required to compete with NikR for nickel ions in Helicobacter pylori, *Journal of bacteriology 191*, 2405-2408. (10.1128/JB.01657-08)

17. Contreras, M., Thiberge, J. M., Mandrand-Berthelot, M. A., and Labigne, A. (2003) Characterization of the roles of NikR, a nickel-responsive pleiotropic autoregulator of Helicobacter pylori, *Molecular microbiology 49*, 947-963

18. Merrell, D. S., Goodrich, M. L., Otto, G., Tompkins, L. S., and Falkow, S. (2003) pH-regulated gene expression of the gastric pathogen Helicobacter pylori, *Infect Immun 71*, 3529-3539

19. Wen, Y., Marcus, E. A., Matrubutham, U., Gleeson, M. A., Scott, D. R., and Sachs, G. (2003) Acid-Adaptive Genes of Helicobacter pylori, *Infection and Immunity 71*, 5921-5939. (10.1128/iai.71.10.5921-5939.2003)

20. Bury-Mone, S., Thiberge, J. M., Contreras, M., Maitournam, A., Labigne, A., and De Reuse, H. (2004) Responsiveness to acidity via metal ion regulators mediates virulence in the gastric pathogen Helicobacter pylori, *Molecular microbiology 53*, 623-638. (10.1111/j.1365-2958.2004.04137.x)

21. Eaton, K. A., and Krakowka, S. (1994) Effect of Gastric Ph on Urease-Dependent Colonization of Gnotobiotic Piglets by Helicobacter-Pylori, *Infection and Immunity 62*, 3604-3607

22. Hayes, E. T., Wilks, J. C., Sanfilippo, P., Yohannes, E., Tate, D. P., Jones, B. D., Radmacher, M. D., BonDurant, S. S., and Slonczewski, J. L. (2006) Oxygen limitation modulates pH regulation of catabolism and hydrogenases, multidrug transporters, and envelope composition in Escherichia coli K-12, *BMC Microbiol 6*, 89. (10.1186/1471-2180-6-89)

23. Noguchi, K., Riggins, D. P., Eldahan, K. C., Kitko, R. D., and Slonczewski, J. L. (2010) Hydrogenase-3 contributes to anaerobic acid resistance of Escherichia coli, *PloS one 5*, e10132. (10.1371/journal.pone.0010132)

24. Zbell, A. L., Benoit, S. L., and Maier, R. J. (2007) Differential expression of NiFe uptake-type hydrogenase genes in Salmonella enterica serovar Typhimurium, *Microbiology 153*, 3508-3516. (10.1099/mic.0.2007/009027-0)

25. McNorton, M. M., and Maier, R. J. (2012) Roles of H2 uptake hydrogenases in Shigella flexneri acid tolerance, *Microbiology 158*, 2204-2212. (10.1099/mic.0.058248-0)

26. Kang, J., and Blaser, M. J. (2006) Bacterial populations as perfect gases: genomic integrity and diversification tensions in Helicobacter pylori, *Nat Rev Microbiol 4*, 826-836. (10.1038/nrmicro1528)

27. Salama, N., Guillemin, K., McDaniel, T. K., Sherlock, G., Tompkins, L., and Falkow, S. (2000) A whole-genome microarray reveals genetic diversity among Helicobacter pylori strains, *Proc Natl Acad Sci U S A 97*, 14668-14673. (10.1073/pnas.97.26.14668)

28. Benoit, S. L., and Maier, R. J. (2014) Twin-arginine translocation system in Helicobacter pylori: TatC, but not TatB, is essential for viability, *MBio 5*, e01016-01013. (10.1128/mBio.01016-13)

29. Johnson, R. C., Hu, H. Q., Merrell, D. S., and Maroney, M. J. (2015) Dynamic HypA zinc site is essential for acid viability and proper urease maturation in Helicobacter pylori, *Metallomics : integrated biometal science 7*, 674-682. (10.1039/c4mt00306c)

30. Benoit, S. L., Mehta, N., Weinberg, M. V., Maier, C., and Maier, R. J. (2007) Interaction between the Helicobacter pylori accessory proteins HypA and UreE is needed for urease maturation, *Microbiology 153*, 1474-1482. (10.1099/mic.0.2006/003228-0)

31. Sawers, R. G., Jamieson, D. J., Higgins, C. F., and Boxer, D. H. (1986) Characterization and physiological roles of membrane-bound hydrogenase isoenzymes from Salmonella typhimurium, *Journal of bacteriology 168*, 398-404

32. Maier, R. J., Olczak, A., Maier, S., Soni, S., and Gunn, J. (2004) Respiratory hydrogen use by Salmonella enterica serovar Typhimurium is essential for virulence, *Infect Immun 72*, 6294-6299. (10.1128/IAI.72.11.6294-6299.2004)

33. Wroblewski, L. E., Peek, R. M., Jr., and Wilson, K. T. (2010) Helicobacter pylori and gastric cancer: factors that modulate disease risk, *Clinical microbiology reviews 23*, 713-739. (10.1128/CMR.00011-10)

34. Salama, N. R., Hartung, M. L., and Muller, A. (2013) Life in the human stomach: persistence strategies of the bacterial pathogen Helicobacter pylori, *Nat Rev Microbiol 11*, 385-399. (10.1038/nrmicro3016)

35. Baltrus, D. A., Amieva, M. R., Covacci, A., Lowe, T. M., Merrell, D. S., Ottemann, K. M., Stein, M., Salama, N. R., and Guillemin, K. (2009) The Complete Genome Sequence of Helicobacter pylori Strain G27, *Journal of bacteriology 191*, 447-448. (10.1128/Jb.01416-08)

36. Joyce, E. A., Gilbert, J. V., Eaton, K. A., Plaut, A., and Wright, A. (2001) Differential gene expression from two transcriptional units in the cag pathogenicity island of Helicobacter pylori, *Infection and Immunity 69*, 4202-4209

37. Tomb, J. F., White, O., Kerlavage, A. R., Clayton, R. A., Sutton, G. G., Fleischmann, R. D., Ketchum, K. A., Klenk, H. P., Gill, S., Dougherty, B. A., Nelson, K., Quackenbush, J., Zhou, L., Kirkness, E. F., Peterson, S., Loftus, B., Richardson, D., Dodson, R., Khalak, H. G., Glodek, A., McKenney, K., Fitzegerald, L. M., Lee, N., Adams, M. D., Hickey, E. K., Berg, D. E., Gocayne, J. D., Utterback, T. R., Peterson, J. D., Kelley, J. M., Cotton, M. D., Weidman, J. M., Fujii, C., Bowman, C., Watthey, L., Wallin, E., Hayes, W. S., Borodovsky, M., Karp, P. D., Smith, H. O., Fraser, C. M., and Venter, J. C. (1997) The complete genome sequence of the gastric pathogen Helicobacter pylori, *Nature 388*, 539-547. (10.1038/41483)

38. Carpenter, B. M., McDaniel, T. K., Whitmire, J. M., Gancz, H., Guidotti, S., Censini, S., and Merrell, D. S. (2007) Expanding the Helicobacter pylori genetic toolbox: modification of an endogenous plasmid for use as a transcriptional reporter and complementation vector, *Appl Environ Microbiol 73*, 7506-7514. (10.1128/AEM.01084-07)

39. Menard, R., Sansonetti, P. J., and Parsot, C. (1993) Nonpolar mutagenesis of the ipa genes defines IpaB, IpaC, and IpaD as effectors of Shigella flexneri entry into epithelial cells, *Journal of bacteriology 175*, 5899-5906

40. Tan, S., and Berg, D. E. (2004) Motility of urease-deficient derivatives of Helicobacter pylori, *Journal of bacteriology 186*, 885-888

41. Boyer, M. E., Stapleton, J. A., Kuchenreuther, J. M., Wang, C. W., and Swartz, J. R. (2008) Cell-free synthesis and maturation of [FeFe] hydrogenases, *Biotechnol Bioeng 99*, 59-67

42. Park, D. H., Laivenieks, M., Guettler, M. V., Jain, M. K., and Zeikus, J. G. (1999) Microbial utilization of electrically reduced neutral red as the sole electron donor for growth and metabolite production, *Appl Environ Microb 65*, 2912-2917

43. Maier, R. J., Fu, C., Gilbert, J., Moshiri, F., Olson, J., and Plaut, A. G. (1996) Hydrogen uptake hydrogenase in Helicobacter pylori, *FEMS Microbiol Lett 141*, 71-76

44. Weatherburn, M. W. (1967) Phenol-Hypochlorite Reaction for Determination of Ammonia, *Anal Chem 39*, 971-&. (Doi 10.1021/Ac60252a045)

45. McGee, D. J., May, C. A., Garner, R. M., Himpsl, J. M., and Mobley, H. L. (1999) Isolation of Helicobacter pylori genes that modulate urease activity, *Journal of bacteriology 181*, 2477-2484

CHAPTER 3

HYPA METAL BINDING RESIDUES AFFECT *HELICOBACTER PYLORI* UREASE ACTIVITIES AND ACID SURVIVAL

Portions of this chapter have been published: (1) Johnson, R. C, Hu, H. Q., Merrell, D. S., and Maroney, M. J. (2015) Dynamic HypA zinc site is essential for acid viability and proper urease maturation in *Helicobacter pylori*. *Metallomics 7*, 674 – 682. (2) Hu, H. Q., Johnson, R. C., Merrell, D. S., and Maroney, M. J. (2017) Nickel Ligation of the N-Terminal Amine of HypA Is Required for Urease Maturation in *Helicobacter pylori. Biochemistry 56*, 1105 – 1116. (3) Blum, F. C., Hu, H. Q., Servetas, S. L., Benoit, S. L., Maier, R. J., Maroney, M. J., and Merrell, D. S. (2017) Structure-function analyses of metal-binding sites of HypA reveal residues important for hydrogenase maturation in *Helicobacter pylori*. *Plos one 12*, e0183260.

3.1 Introduction

The HypA metallochaperone is found in all bacteria that express NiFe-H_2ase and is typically associated with Ni-insertion into that enzyme, however it is also required for full activation of urease activity in *H. pylori*.[1] The *H. pylori* HypA protein has been extensively studied and discussed in detail in 1.3. Briefly, the small HypA protein (13 kDa) contains two metal sites and interacts with several proteins in the nickel trafficking pathway.[2] Specifically, it directly interacts with urease accessory protein, $UreE_2$, which has been linked to its requirement for urease activation.[3-6]

The *H. pylori* HypA structural Zn is coordinated by two conserved CXXC motifs with flanking His residues, and the Ni is coordinated by the conserved N-terminal MHE-motif (Figure 1.4).[7-10] Coordination of the structural Zn have been previously demonstrated to alternate between $Zn(Cys)_4$ at neutral pH and $Zn(Cys)_2(His)_2$ at acidic pH with Ni-bound (Figure 1.6).[8] Cys residues in the *H. pylori* HypA conserved CXXC motifs have been systematically mutated to Ala (to simulate loss-of-ligand) and to Asp (to simulate ligand-substitution) in the Zn site. The non-conserved flanking His residues in the Zn site have also been mutated to Ala individually. Structural characterizations of these protein variants concluded the loss or substitution of any Cys or His residues in the HypA Zn site resulted in loss of dynamics in the Zn site structure, in which the variants no longer alternate between the $Zn(Cys)_4$ and $Zn(Cys)_2(His)_2$ structure in a pH- and Ni-dependent manner.[9, 11]

The *H. pylori* HypA Ni site was also investigated to resolve a controversy regarding the coordination and magnetic properties of the site. The unmodified HypA Ni site has been shown to be 6-coordinate and paramagnetic,[8] but the Ni site of the N-terminally modified GSHypA (residues Gly-Ser remained after cleavage of affinity tag) was shown to be 4-coordinate and diamagnetic (Figure 1.5).[10] The difference in Ni sites point to the N-terminal amine of HypA as a potential Ni ligand and its importance in determining the overall structure of the site. Site-directed mutagenesis was used to extend the N-terminus of the HypA protein by inserting a Leu residue between the conserved Met1 and His2, creating the Met1_His2insLeu variant (hereafter known as L2*-HypA). N-terminal extension strategies have been successfully used to probe the ligation of N-terminal amine in Ni-containing proteins, such as RcnR and Ni-SOD.[12, 13] The side-by-side comparison of the Ni site structures, magnetic properties and cellular response of the WT- and L2*-HypA would clarify the controversial HypA Ni site as well as establish the role of the N-terminal amine in Ni-ligation.[14]

In collaboration with the Merrell lab at the Uniformed Services University of Health Sciences (Bethesda, MD), the cellular responses to the HypA variants were investigated by replacing the intrinsic *hypA* gene in *H. pylori* strain G27[15] with the coding sequence for the metal site variant HypA proteins. These corresponding *hypA* isostrains if *H. pylori* were then tested for acid survival as well as urease and H_2ase activities. Although H_2ase activity has been shown to be non-essential for the acid survival of *H. pylori*[16] as described in CHAPTER 2, it is still an important indicator of HypA function as a metallochaperone.

In addition to the *hypA* metal site variant strains, several control strains were produced from the parental G27 *H. pylori*, including the *hypA::kan-sacB*, the *hypA*-restorant, and Δ*ureB* strains.[11, 15, 17] The *hypA::kan-sacB* strain contains an interrupted *hypA* gene, and therefore does not produce functional HypA protein.[11] The *hypA*-restorant (hereafter known as *hypA*-R) strain of which the native *hypA* coding sequence was replaced by another copy of the WT-*hypA*, controls for genetic manipulations of the *hypA* gene and is expected to behave like the WT parent strain.[11]

The Δ*ureB* strain, in which the gene coding for the large subunit of urease (*ureB*) is interrupted, does not have a functional urease, and is therefore not expected to survive acid shock or have urease activity.[11, 17]

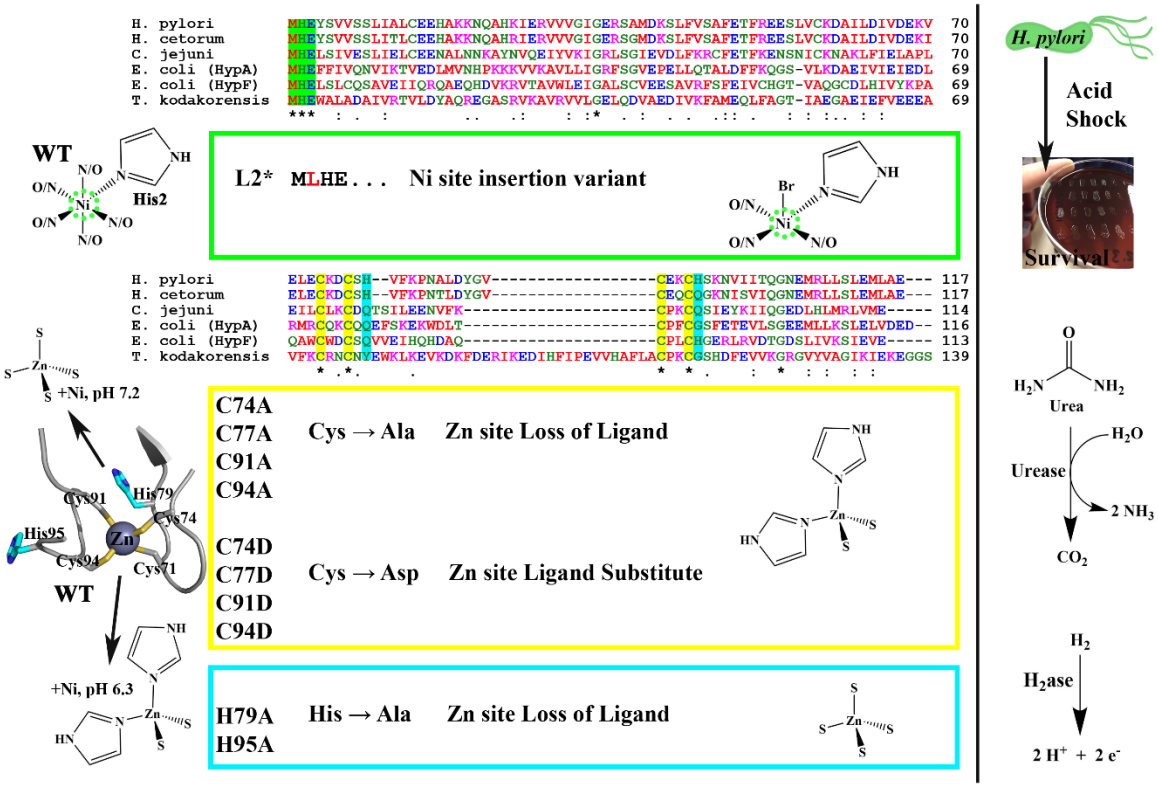

Figure 3.1: Summary of *H. pylori* metal site variants and strategies
Multiple protein sequence alignment of HypA homologues performed by the Clustal Omega 1.2.1 algorithm. The residues are colored by properties of the side chain for hydrophobic (red), acidic (blue), basic (magenta), and other (green) type side chains. Rigidly (*), moderately (:), or slightly (.) conserved residues are marked below the alignment. Positions of the metal site variant are highlighted in green for Ni site, and in yellow and cyan for Zn site. Metal site variants described in this chapter are shown in corresponding colored boxes. WT metal sites previously characterized by XAS are shown on the left.[8, 9] Cellular response characterization strategies of *H. pylori* variant strains are shown on the right.

3.2 Results

3.2.1 Zn site variants

A total of 10 Zn site variants strains were tested for cellular response by characterization of each strain for acid survival, urease activity, and H_2ase activity as summarized in Figure 3.1.

3.2.1.1 Acid survival

The 10 Zn site variant strains were grown along with the four control strains: the parent WT (G27) strain, *hypA::kan-sacB*, *hypA*-R, and Δ*ureB*, in acid survival challenge for one hour with or without urea supplement. All 14 of these *H. pylori* strains showed similar robust survival profiles when exposed to pH 6 in the presence or absence of 5mM urea (Figure 3.2AB). Conversely, when exposed to pH 2.3, all of the *H. pylori* strains, including the WT, showed a dramatic decrease in survival; less than 0.01% of the inoculum survived at pH 2.3 in the absence of urea (Figure 3.2C). However, when urea was supplemented to the pH 2.3 buffer, we began to detect differences in acid resistance across the various strains (Figure 3.2D). As expected, the WT *H. pylori* strain and the *hypA*-R were able to efficiently utilize the supplemented urea as a substrate for the urease system and survive the acidic challenge. Also, as expected the urease deficient *ΔureB* strain was incredibly acid sensitive; no surviving bacteria were detected (limit of detection 500 CFU/mL equating to 0.0001% survival). The *hypA::kan-sacB* strain that carried an insertion in the *hypA* coding sequence was also deficient in its ability to resist acidic stress (< 3% survival). This result confirmed previous studies that indicated that *hypA* is necessary for efficient urease activity.[1, 4, 18] For the various Zn-binding site mutants, mutation of Cys77, His79, and His95 of HypA resulted in no changes in acid resistance. Conversely, significant decrease in acid resistance, as compared to the wild type strain, were observed for the C74D, C91A, and C94A mutant strains: 17.6%, 2.1% and 1.7% average survival, respectively. This finding suggests that these zinc-binding site residues play a critical role in acid survival, presumably by affecting the ability of HypA to provide nickel to the urease maturation pathway.

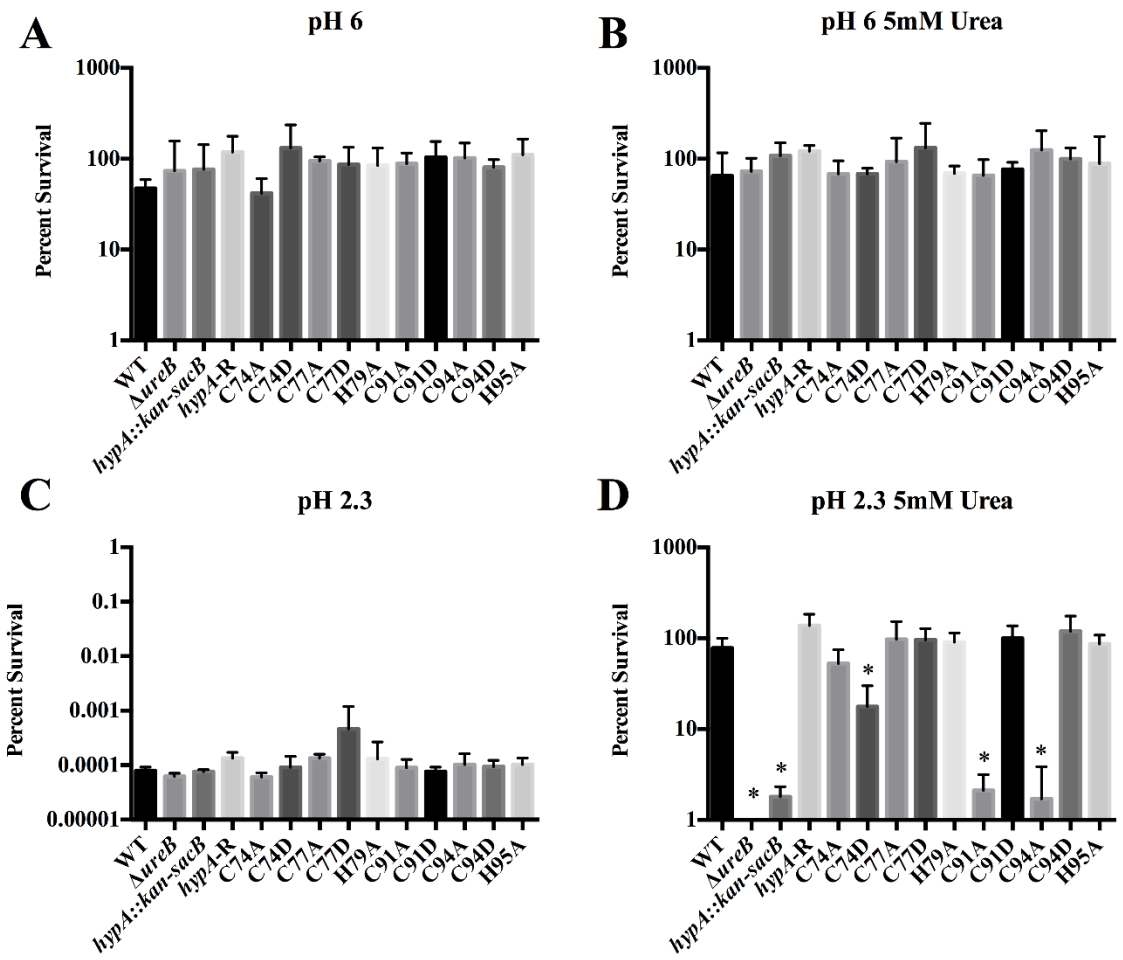

Figure 3.2: Acid survival of *H. pylori hypA* Zn site variant strains
A decrease in acid survival was observed for specific amino acid mutations in the HypA protein Zn site. The *hypA* variant strains and controls were exposed to various acid shock environment for 1 hour: pH 6 (A), pH 6 containing 5 mM urea (B), pH 2.3 (C), and pH 2.3 containing 5 mM urea (D). Percent survival was calculated for each strain. The data shown represent mean ± standard deviation. A* indicates that acid resistance was significantly reduced when compared to wild type ($p < 0.01$, one-way ANOVA followed by Dunnett's test for multiple comparisons.) Figure from [Johnson, *et. al. Metallomics*, **7**, 674-682 (2015) [11] reprinted by permission of The Royal Society of Chemistry.

3.2.1.2 Urease activities

The acid survival data suggested that the C74, C91 and C94 residues play a critical role in the ability of HypA to facilitate urease maturation.[1, 4, 18] We next directly investigated urease activity of each of the 10 Zn-binding site mutants of *hypA*, along with the Δ*ureB*, the *hypA::kan-sacB*, the *hypA*-R and WT strains. The *hypA*-R strain showed three-fold less urease activity than

the WT *H. pylori* strain, which may be a consequence of genetic manipulation. Consequently, urease activities were normalized to the *hypA*-R strain. Since the Δ*ureB* strain of *H. pylori* is missing the nickel-containing β subunit of the urease enzyme and should have no urease activity,[17] the average urease activity of the Δ*ureB* strain was subtracted from the measurements of all strains to correct for any background levels of ammonia present in whole cell extract.

As shown in Figure 3.3, we identified two classes of mutations of the HypA structural zinc site, those that had no effect on urease activity (WT-like), and those that decreased urease activity. This latter class can be subdivided into moderately deficient and severely deficient (*hypA::kan-sacB*-like) subclasses. Mutations of non-conserved His residues (H79A and H95A) that flanked the HypA CXXC motifs resulted in strains that retained WT-like activity, suggesting that these His residues are not important for urease maturation. In contrast, all mutations involving Cys residues in the HypA CXXC motifs were deficient in urease activity to some extent (less than 15% compared with the *hypA*-R strain), indicating the importance of the Cys residues in the proper function of HypA in the urease maturation pathway. Comparisons of the urease activities in the Cys mutant strains with the *hypA::kan-sacB* stain revealed more subtle phenotypes. The activity of C77D, C91D, and C94D were statistically different ($p < 0.05$) from the *hypA::kan-sacB* strain (12 – 13% compared with the *hypA*-R strain) constituting a moderately deficient phenotype (Figure 3.3A). The remaining Cys mutants, C74A, C74D, C77A, C91A, and C94A, showed activity levels similar to the *hypA::kan-sacB* strain (> 4% compared with *hypA*-R strain). These urease activity results corroborate the acid survival phenotypes, where C74D, C91A, and C94A mutants were found to be both acid-sensitive and severely deficient in urease activity. Contrary to the acid survival results, C74A and C77A mutants which were not acid sensitive under our test conditions, but were found to be severely deficient in urease activity. These findings suggest that, although all Cys residues in the CXXC motifs are important for proper HypA function in the urease maturation pathway, there is a gradient of importance based on the residue position as well as the type of mutation.

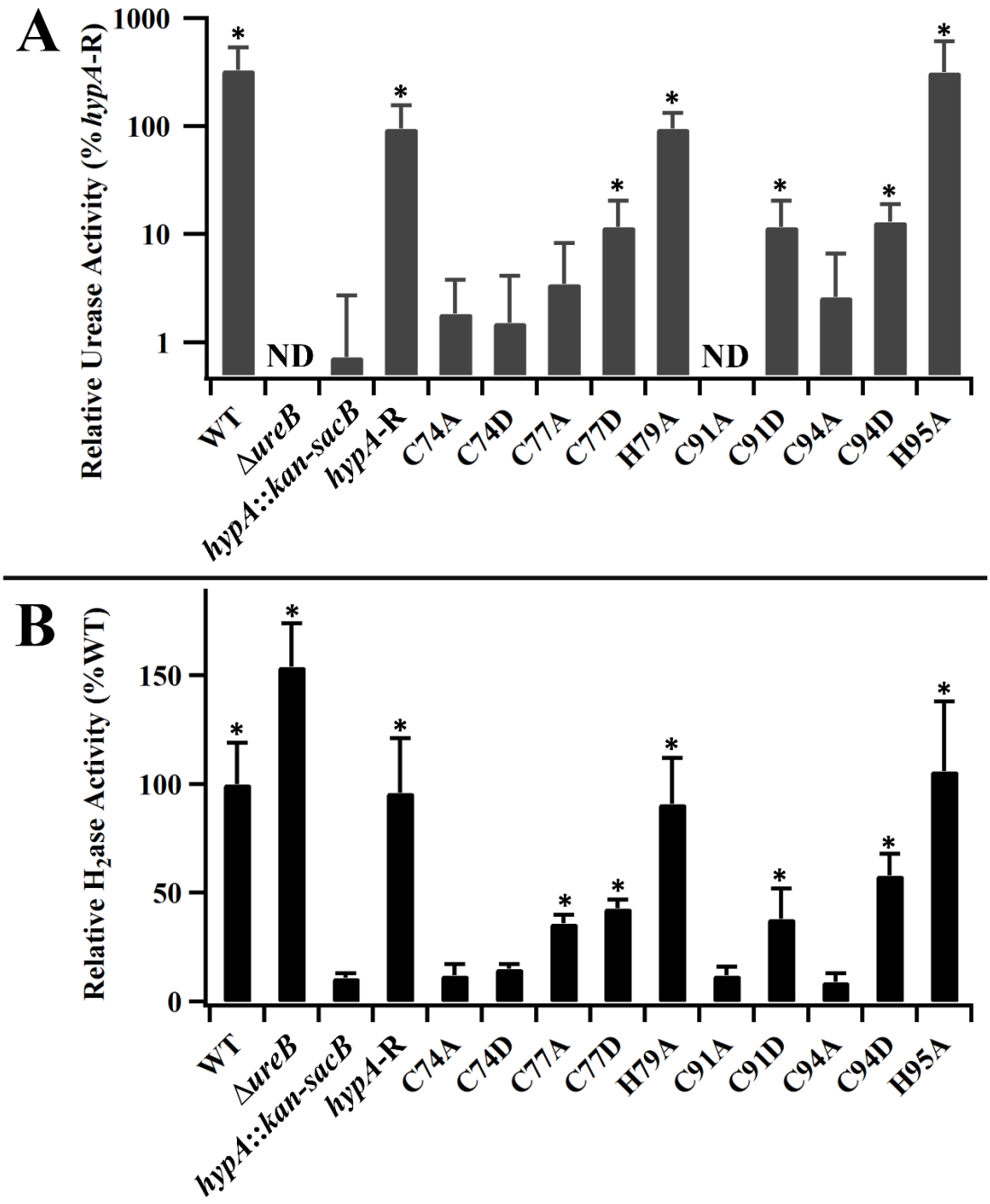

Figure 3.3: Urease and H_2ase activities of *hypA* Zn site variant strains
The urease activities of each *hypA* Zn site variant and control strains were measured, the activity of the Δ*ureB* strain (less than 1%) was subtracted from each as background, and then the data was normalized against the activity of the *hypA*-R strain (A). The H_2 oxidation from each strain of *H. pylori* was normalized against the activity of the WT strain (B). A * indicates activity that was significantly different from the *hypA*::*kan-sacB* control ($p < 0.05$), and ND = none detected. Panel A was previously published in [Johnson, *et. al. Metallomics*, 2015, **7**, 674-682 [11] and reproduced by permission of The Royal Society of Chemistry. Panel B was reproduced from [Blum *et. al. PLOS ONE*, 12, e0183260 (2017) [16].

3.2.1.3 Hydrogenase Activity

The H_2ase activities of the Zn site variant strains of *H. pylori* were also investigated. Although H_2ase is not required for acid survival in *H. pylori*[16] (discussed in CHAPTER 2), its activity still contribute to the metabolism and virulence of the pathogen (discussed in Section 1.1.2).[19, 20] Since HypA is a known Ni-metallochaperone involved in H_2ase activation (discussed in Section 1.3),[2, 21] the H_2ase activities of the Zn site variant *hypA* strains in comparison to urease activities of the same strains should reveal the role of specific residues in proper function.

The overall activities of the Zn site variant strains are summarized in Figure 3.3B, in comparison to WT, Δ*ureB*, *hypA::kan-sacB*, and *hypA-R* control strains. The relative (to WT strain G27) specific H_2ase activities of the Zn site variant strains can also be separated into two different categories, which are either (1) unaffected or (2) H_2ase-deficient in activities. The latter group can be subcategorized into mildly or severely deficient in H_2ase activities. Mutations of the non-conserved His residues (H79A and H95A) that flanked the HypA Zn site did not affect H_2ase activity (91% and 106% of WT activity, respectively), and are similar to the control strain *hypA-R* (96% of WT). This confirmed observations from the urease activities, indicating that the His residues are not important for the overall function of HypA as a metallochaperone. The H_2ase activity of the Δ*ureB* strain is 154% of WT; the increase in activity could be a result of the lack of urease in this strain to compete for the Ni co-factor and therefore increases the Ni-availability for H_2ase activation. All mutations to the conserved Cys residues in the HypA CXXC motifs resulted in deficiency in H_2ase activity. Amongst these strain, C74A, C74D, C91A, and C94A were subcategorized as severely deficient in H_2ase activity (9 – 15% of WT), and C77A, C77D, C91D, and C94D were mildly deficient in H_2ase activity (36 – 68% of WT). These trends conform to the urease activity pattern observed in the same *hypA* variant strains, confirming that the conserved Cys residues are more important for the function of HypA than the flanking His residues.

3.2.2 Ni site N-terminal extension variant (L2*)

The N-terminal extension variant, L2*-HypA, was characterized *in vitro* for overall protein properties as well as Ni site structure and magnetic properties.[14] The L2*-*hypA* variant strain of *H. pylori* was also assessed for acid survival, urease activity, and H_2ase activity.[14]

3.2.2.1 L2* mutation did not alter protein properties

To ensure that the insertion of Leu into the N-terminal MHE-motif did not disrupt the overall fold of the purified HypA protein variant, the secondary and quaternary structures of purified WT- and L2*-HypA were investigated. Circular dichroism of purified WT-HypA and L2*-HypA proteins show that the N-terminal mutation has not disrupted the mostly α-helical characteristics of the purified protein (Figure 3.4A) either with or without Ni bound. These results show that the L2*-HypA variant has not altered its overall fold as compared to WT.

To further analyze the overall size and shape of the purified HypA, size exclusion chromatography in combination with multi-angle light scattering (SEC-MALS) was used to analyze both the molecular weight and the hydrodynamic radius of the purified HypA proteins. Previously, SEC was used to estimate the "size" of HypA in solution based on its elution volume in comparison to known molecular weight standards. However, elution volume from a SEC column is dependent on the hydrodynamic radius of the eluted molecule, and the estimated "molecular weight" calculated from standard curve assumed that the eluted molecule is approximately globular shape. HypA has been reported to have an elongated shape with two distinct lobes in the solution NMR structure of *H. pylori* HypA (PDB ID: 2KDX)[10] and in the crystal structure of *T. kodakarensis* HypA(PDB ID: 3A43).[22] Therefore, elution volume alone is an unreliable method for estimating "size" of the HypA protein, and have led to the HypA protein being reported as a solution dimer in the past.[7, 23] Using elution volume alone, HypA was estimated to be ~23 kDa for both WT- and L2*-HypA, based on a calibration curve using known molecular weight standards, which is consistent with a solution dimer (the calculated monomeric molecular weight of WT-HypA is 13.2 kDa). MALS calculates absolute molecular mass based on

light scattering properties of the molecule, independent of the hydrodynamic radius or shape.[24] Using MALS analysis, the absolute mass of WT- and L2*-HypA were calculated to be 13.01 ± 0.007 and 13.37 ± 0.021 kDa respectively (Figure 3.4B), which is consistent with a monomeric solution structure for both WT- and L2*-HypA. The similarity between WT- and L2*-HypA in CD spectroscopy and SEC-MALS analyses confirmed that the overall fold and oligomeric structure of the overall protein was not altered in the L2*-HypA variant.

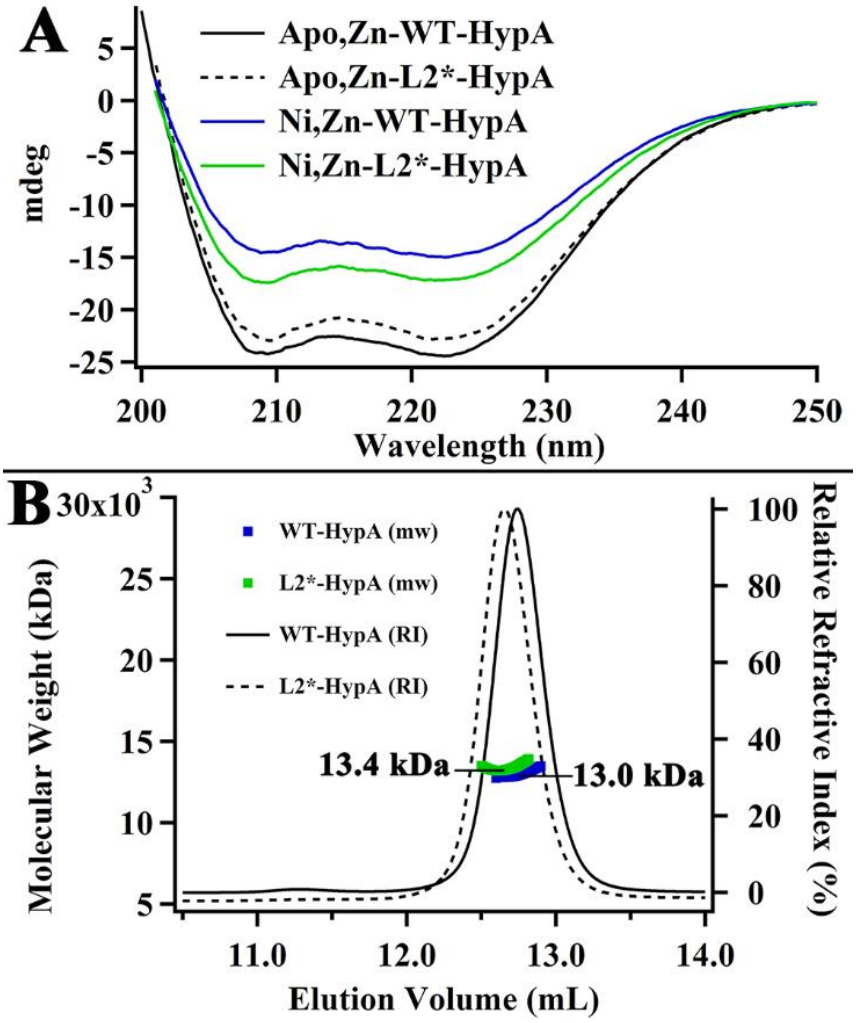

Figure 3.4: CD and SEC-MALS characterization of WT- and L2*-HypA
Comparison of CD and SEC-MALS characterization of WT- and L2*-HypA indicate that insertion mutation did not alter the general secondary and quaternary structure of the protein. Figures reprinted with permission from [Hu, *et. al. Biochemistry*, 56, 1105-1115 (2017) [14]. Copy right 2017 American Chemical Society.

3.2.2.2 L2* mutation changes Ni-coordination

The controversy over the HypA Ni-binding site structure in the literature points to the unmodified WT-HypA Ni site having a six-coordinate and therefore paramagnetic site,[8, 9] and the N-terminally modified GSHypA variant (PDB: 2KDX) having a four-coordinate planar and diamagnetic site.[10] Direct comparison of the structures of the Ni sites in WT- and L2*-HypA by XAS was made to investigate the role of the N-terminal amine as a potential ligand in the Ni site of WT-HypA.

Comparison of the Ni K-edge x-ray absorption near-edge structure (XANES) region of the XAS spectra obtained from WT-HypA and L2*-HypA Ni(II) complexes in NaBr buffer show a clear difference that corresponds to a change in the coordination number/geometry of the Ni site (Figure 3.5A). Typically, two types of high-energy bound-transitions may be observed in the pre-edge XANES region of the XAS spectra of Ni(II) complexes.[25] These features are associated with transitions involving promotion of a 1s electron into the 3d manifold (1s → 3d) or into the $4p_z$ orbital (1s → $4p_z$) of the Ni(II) complex and are observed near 8331 and 8336 eV, respectively.[25] In the case of Ni-WT-HypA, no discernable pre-edge features were observed. The small (unresolved) 1s → 3d (plus shakedown) transition is consistent with a centrosymmetric Ni(II) site, and the absence of a peak associated with a 1s → $4p_z$ transition rules out a four-coordinate planar site.[25] The XANES analysis is therefore consistent with a six-coordinate Ni site in WT-HypA, in agreement with the paramagnetism associated with the site by Evans magnetic susceptibility measurements (see below).

In contrast, a clear feature corresponding to a 1s → $4p_z$ transition (plus shakedown) is observed on the Ni-L2*-HypA K-edge that indicated the loss of at least one axial ligand from the Ni site compared to WT-HypA (Figure 3.5A, inset).[25] The 1s → $4p_z$ feature in the Ni-L2*-HypA spectrum appears as an unresolved shoulder on the Ni K-edge, and is therefore more consistent with a five-coordinate pyramidal geometry than with a four-coordinate planar complex, where a resolved maximum is expected.[25] A second set of Ni K-edge XAS data were collected on a Ni-

L2*-HypA sample in NaCl buffer (20 mM HEPES, 200 mM NaCl, 1mM TCEP, pH 7.2) to rule out buffer effects on the geometry of the Ni site. The similarity of the XANES spectra in NaCl and NaBr buffers (Figure 3.5B) indicates the geometries of the Ni site was not affected by buffer, and confirms the five-coordinate pyramidal Ni(II) structural assignment in L2*-HypA.

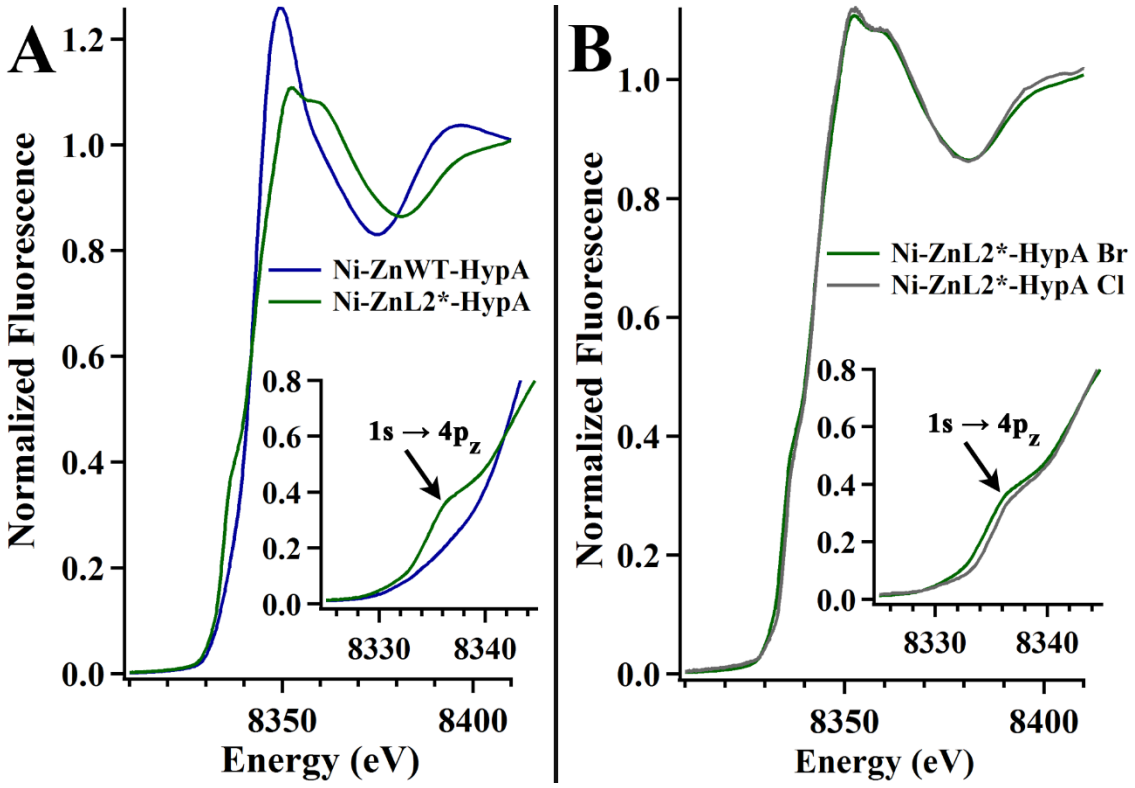

Figure 3.5: Ni K-edge XANES overlay of HypA complexes
Ni K-edge XANES region overlay of WT- and L2*-HypA (A) bound to Ni and Zn in NaBr buffer; and of the L2*-HypA bound to both Ni and Zn in NaBr or NaCl buffer (B), with the pre-edge regions shown in inset. Figure reproduced with permission from [Hu, *et. al. Biochemistry*, 56, 1105-1115 (2017) [14]]. Copy right 2017 American Chemical Society.

Six-coordinate Ni(II) complexes with octahedral geometry are invariably high-spin with S = 2, while four-coordinate planar Ni(II) complexes are invariably low-spin and diamagnetic.[26] Five-coordinate complexes may be either high- or low- spin depending on the relative strengths of the axial and in-plane ligand fields.[25] Magnetic susceptibility measurements using Evans' NMR method[27, 28] (Section 3.4.12) show that the WT-HypA Ni complex is high-spin (μ = 3.52 μ_B, well within the range typically observed for Ni(II) complexes: μ = 2.8 – 4.0 μ_B [26]). In contrast, the Ni(II) complex of L2*-HypA protein is diamagnetic.

3.2.2.3 Loss of two Ni protein ligands occurs in L2*-HypA

To further characterize the changes in the Ni site structure in WT- and L2*-HypA proteins, the EXAFS regions of the XAS spectra were analyzed. One limitation of EXAFS analysis is that the models cannot distinguish scattering atoms with Z ± 1, which means the structural models cannot easily distinguish between a N- vs. O-donor ligand, or a S-donor vs. a Cl^- ligand.[29] Fits were generated using parameters for N-donors and are represented as N/O in Table 3.1 to emphasize this lack of distinction. To address the issue of S vs. Cl ligation, samples were prepared in a buffer containing NaBr, rather than NaCl. This practice increases the confidence of models containing S ligand donors, and can also identify solvent accessible metal sites in those cases where Br^- becomes a ligand.

Models to interpret the EXAFS data were developed beginning with the coordination number determined by XANES and magnetic studies (see in 3.2.2.2 above). Models were developed by first using single-scattering analysis. Multiple-scattering scaffolds were added to the best single-scattering models to account for features in the FT-EXAFS spectra arising from the second and third coordination sphere scattering atoms resulting from the coordination of His imidazole ligands (depicted in Figure 3.6, and described in method Section 3.4.9) as previously described.[30, 31] Imidazoles were fit as rigid rings with a single adjustable distance. Integer numbers of rings were added to "count" the number of imidazole ligands. A separate model was developed that incorporated a rigid, bidentate 1,2-ethylenediammine-like unit (depicted in Figure 3.6, and described in methods Section 3.4.9) similar to the bidentate coordination of α-ketoglutarate Fe-binding in nonheme Fe(II) enzymes used in prior models.[32, 33] This model simulates the formation of five-membered chelate rings that form when the binding of the N-terminal amine is accompanied by backbone amide binding, which lead to the ordering of second coordination sphere C atoms similar to prior models of backbone amidate ligation in the active site of NiSOD.[34, 35]

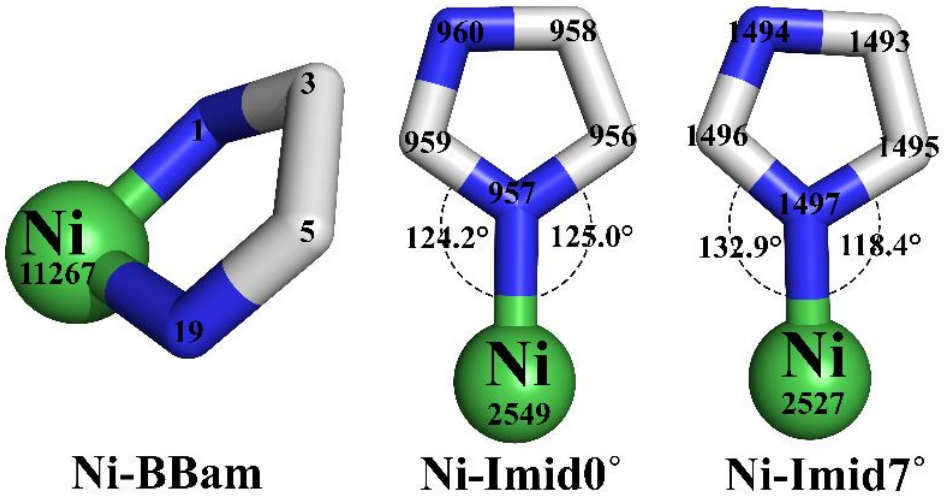

Figure 3.6: Pictorial representations of multiple scattering scaffolds
Multiple scattering scaffolds were used for calculating the scattering paths for fitting the Ni-WT- and L2*-HypA EXAFS data (described in detail in the method Section 3.4.9). Green sphere represents Ni atom, blue sticks represent nitrogen, and white sticks represent carbon with the atom ID number labeled on each atom as identified in the corresponding crystal structures.[36, 37] The angle between the Ni to the coordinated nitrogen and the adjacent carbon on the imidazole rings are labeled, and α is the difference between these two angles divided by two, indicated here as 0˚ or 7˚ tilt. Figure reproduced with permission from [Hu, *et. al. Biochemistry*, 56, 1105-1115 (2017) [14]]. Copy right 2017 American Chemical Society.

Table 3.1: XANES and EXAFS Analysis of WT- and L2*-HypA Ni complexes

	XANES analysis				EXAFS analysis[a]				
HypA	K-edge Energy (eV)	1s →3d peak area (x10^{-2} eV)	1s → 4p$_z$ observed	Coordination Number	Shell	r (Å)	σ^2 (x10^{-3} Å^2)	ΔE$_o$ (eV)	R factor (%)
WT	8342.8	<0.05	no	6	1N/O	2.21(5)	4(8)	2(1)	3.53
					3N/O (1 Imid0˚)	2.08(2)	3(2)		
					BBAm	1.92(3)	6(3)		
					BBAm	1.97(3)			
L2*	8342.5	<0.05	yes	5	1N/O	2.04(3)	4(4)	0(1)	3.49
					1Br	2.42(2)	11(3)		
					1 Imid7˚	1.94(4)	5(5)		
					BBAm	1.82(1)	1(1)		

[a] Uncertainties in the fitted parameters are shown in parentheses.
Table reproduced with permission from [Hu, *et. al. Biochemistry*, 56, 1105-1115 (2017) [14]]. Copy right 2017 American Chemical Society.

The best fit for Ni-WT-HypA EXAFS is a six-coordinate complex (Figure 3.7A, Table 3.1; with alternate fits in APPENDIX 2, Table A2.1) with exclusively N/O-donor ligands at distances ranging from 1.92 – 2.21 Å, and includes multiple-scattering paths that describe an imidazole with 0˚ tilt (Imid0˚) and binding of one bidentate backbone amide (BBAm) unit. The inclusion of the BBAm was required to generate a fit with a R-factor < 5 %. Although both imidazole ligands and five-membered chelate rings feature carbon atoms in the second coordination sphere at similar Ni-C distances, the two ligands are distinguished by scattering from atoms in the third coordination sphere (C and N) that contribute to scattering intensities between 3 – 4 Å (uncorrected for phase shifts) FT-EXAFS (Figure 3.6), and exist only for imidazole ligation. The imidazole in the Ni-WT-HypA fit likely arises from Ni binding to the His2 sidechain, which has been shown to be critical to Ni- binding and function.[7]

The L2*-HypA Ni-EXAFS obtained in buffer NaBr was modeled as a 5-coordinate Ni(II) site that featured one Br^- ligand at a Ni-Br distance of 2.42 ± 0.2 Å and four N/O-donor ligands ranging from 1.82 – 2.04 Å, and included multiple-scattering paths that were consistent with one imidazole ligand with a 7˚tilt (Imid7˚) and a bidentate BBAm unit (Figure 3.7B, Table 3.1; with additional fits in APPENDIX 2, Table A2.2). The multiple-scattering paths used to fit the WT-HypA EXAFS are mostly preserved in the L2*-HypA Ni site (although at slightly different distances and angles), including the bidentate backbone N coordination and a His imidazole. However, the BBAm unit is not required to generate a fit to the L2*-HypA data with an R-factor < 5 %, though the alternative fit requires the presence of two His imidazole ligands (see additional fits in Table A2.2). It is not clear where the second His imidazole would come from, and the single His fit is consistent with the nickel occupying the same locus (the N-terminus) of the protein as in WT-HypA and preserving the coordination of the His2 sidechain. In comparison with the WT-HypA Ni site structure, two N/O-donor ligands were lost, one of which was substituted by a Br^- ligand originating from the buffer in L2*-HypA. The bromide scattering atom is required to generate a fit with an R-factor < 5 % when BBAm is used to model backbone N

coordination. Additionally, a systematic shortening of the average distances of Ni-N/O ligation by 0.14 Å in the Ni-L2*-HypA complex is consistent with the observed spin-state change measured by Evans' NMR method (Section 3.4.12).

To confirm the 5-coordinate fitting model with exogenous Br^- ligand, the EXAFS of a Ni-L2*-HypA sample in buffer with NaCl was analyzed. The best 5-coordinate model for this data set include the bidentate BBAm scaffold, as well as a S/Cl-donor at a reasonable distance of 2.25 Å, consistent with the XANES analysis and the best fits in NaBr buffer. A S/Cl donor is required to generate a fit with R-factor < 5 % (APPENDIX 2, Table A2.3 and Figure A2.1).

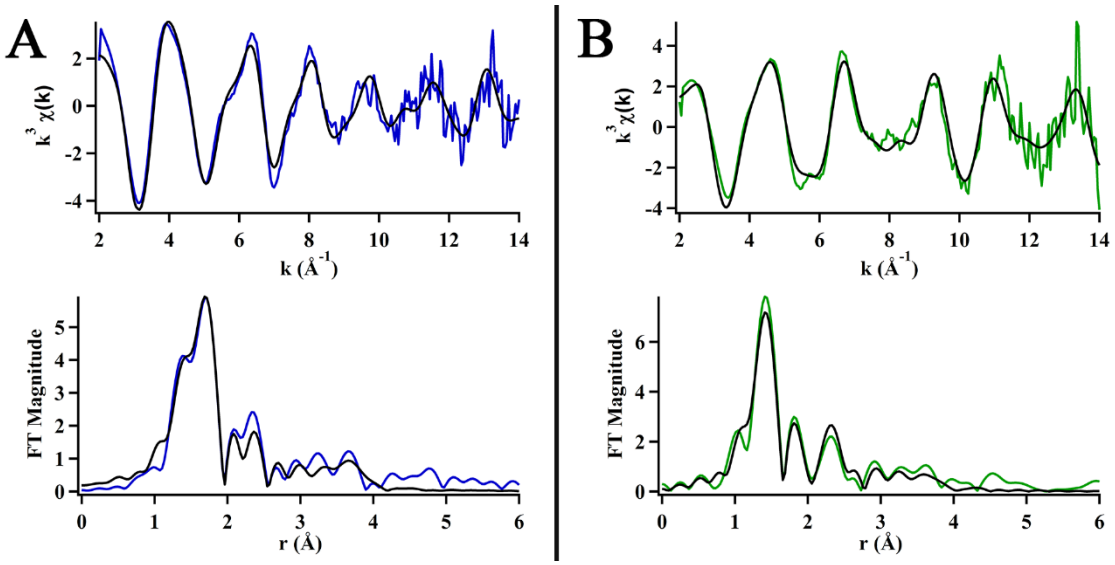

Figure 3.7: Ni K-edge EXAFS overlay of HypA complexes
Data (color) and best fit models (black) of the Ni K-edge EXAFS represented in k^3-weighted unfiltered data (top) and Fourier-transformed (k = 2 – 14 $Å^{-1}$) data uncorrected for phase shifts (bottom) for (A) Ni-ZnWT-HypA and (B) Ni-ZnL2*-HypA in 20 mM HEPES, 200 mM NaBr, and 1 mM TCEP (pH 7.2). Figures reprinted with permission from [Hu, *et. al. Biochemistry*, 56, 1105-1115 (2017) [*14*]. Copy right 2017 American Chemical Society.

3.2.2.4 The Zn site in L2*-HypA is unchanged compared to WT

In addition to the Ni K-edge, the Zn K-edge XAS spectra were also obtained for Ni- and Zn-bound WT- and L2*-HypA and confirm that Zn site coordination involving two conserved CXXC motifs is unperturbed in L2*-HypA. The Zn K-edge XANES spectra of WT- and L2*-HypA overlay well, indicating that no significant change in geometry at the Zn site has occurred

(APPENDIX 2, Table A2.4, and Figure A2.2). The zinc EXAFS spectra for both WT- and L2*-HypA were best fitted with a model featuring four S-donors with Zn-S distances of ~2.34 Å and an imidazole ligand with a 2˚ tilt (Imid2˚) at a distance of 2.18 Å, although acceptable fits with exclusively Cys ligands are also consistent with the data (APPENDIX 2, Table A2.4, and Figure A2.2). Possible coordination of the flanking His residue demonstrates that the dynamic nature of the HypA Zn site is preserved in WT- and L2*-HypA.[11, 23]

3.2.2.5 L2*-*hypA* variant *H. pylori* strain is acid sensitive

To investigate the cellular effect of the N-terminal extension of the HypA protein in *H. pylori*, the chromosomal *hypA* gene was replaced with the coding sequence for L2*-HypA. This mutant strain (DSM1475) expresses the L2*-HypA protein under the control of the endogenous promoter (see method Section 3.4.2). As the *hypA* gene has been shown to be vital for urease activity in *H. pylori*,[38] and therefore an integral part of the acid survival mechanism, the urea-dependent acid survival was assessed for this variant strain. *H. pylori* strains were challenged for one hour at mild (pH 6) or harsh (pH 2.3) acidic shock conditions either with or without urea supplement, and then plated to assess for surviving colony-forming units (CFU). In addition to the L2*-*hypA* strain, the parental WT strain, the *ΔureB* strain where a subunit of the urease enzyme has been deleted, the *hypA::kan-sacB* strain where the *hypA* gene was interrupted, and the *hypA-R* strain where the *hypA* gene was restored after deletion were tested concurrently as controls (Figure 3.8). Under mild acid shock conditions, all tested strains survived with or without urea supplement (Figure 3.8AB). Without urea supplement, harsh acid shock was lethal for all strains tested (Figure 3.8C). At harsh acid shock conditions with urea supplement, distinct phenotypes for each strain were revealed with WT and *hypA-R* strains each exhibiting unimpaired acid survival, whereas the acid survival of L2*-*hypA* strain along with the *hypA::kan-sacB* and *ΔureB* strains were significantly reduced compared to WT ($p < 0.0001$) (Figure 3.8D). To further confirm the results obtained with the L2*-*hypA* mutant, the strain was independently remade and

tested in a single replicate of the acid survival assay; this mutant strain displayed similar acid survival phenotype as the original L2*-*hypA* mutant strain (data not shown).

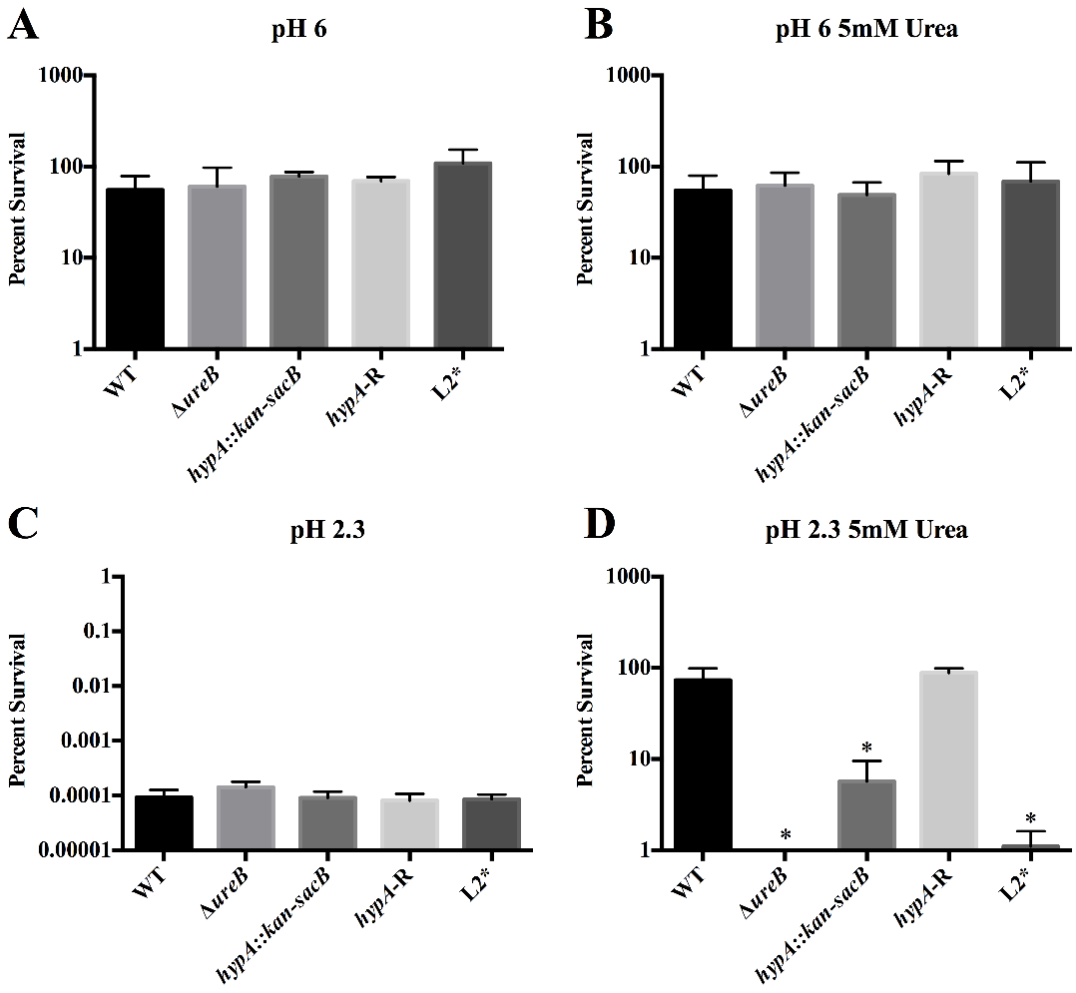

Figure 3.8: Acid survival of L2*-*hypA* variant *H. pylori* strain
H. pylori strains were exposed to PBS for 1 hour at pH 6 or 2.3 with or without 5 mM urea: (A) pH 6, (B) pH 6 with 5 mM urea, (C) pH 2.3, and (D) pH 2.3 with 5 mM urea. Each bar represents the mean percent survival ± the standard deviation. * = acid survival that was significantly reduced compared to that of wild type ($p < 0.0001$; one-way analysis of variance followed by Dunnett's test for multiple comparisons). Figures reprinted with permission from [Hu, *et. al. Biochemistry*, 56, 1105-1115 (2017) [14]. Copy right 2017 American Chemical Society.

3.2.2.6 L2*-*hypA* variant strains of *H. pylori* is deficient in urease and H_2ase activity

To confirm that the acid sensitive phenotype in L2*-*hypA* strain was a result of urease deficiency, urease activity was measured using a modified phenol-hypochlorite assay for NH_3 production. In 30 minutes, the clarified lysates of *H. pylori* strains produced 109, 0.47, 0.77, 86,

and 0.33 nmol NH_3 per μg of total protein for WT, Δ*ureB*, *hypA*::*kan-sacB*, *hypA*-R, and L2*-*hypA* strains respectively. These results confirmed the trend observed in acid survival tests, with *hypA-R* strain having WT-like urease activity, whereas L2*-*hypA* strain along with negative control strains *ΔureB* and *hypA::kan-sacB* had less than 1% of WT relative urease activity (Figure 3.9A). These results show that insertion of a single Leu residue into the N-terminal Ni-binding motif of HypA (L2*-*hypA* variant) is sufficient to nearly eliminate urease activity and to severely impair urea-dependent acid survival of *H. pylori*.

H_2ase activity of the L2*-*hypA* strain of *H. pylori* as well as accompanying controls were assessed (Figure 3.9B) and compared to the corresponding urease activity. The control strains *hypA*-R and Δ*ureB* exhibited H_2ase activity levels similar to the WT parental strain at 92% and 128% of WT, respectively. In contrast, the H_2ase activity of L2*- *hypA* variant strain was comparable to the *hypA*::*kan-sacB* strain, where no functional *hypA* gene is present. This confirms that the L2*-*hypA* variant strain lacks H_2ase activity as well as urease activity, indicating that proper Ni-ligation in HypA is required for its function as a Ni metallochaperone.

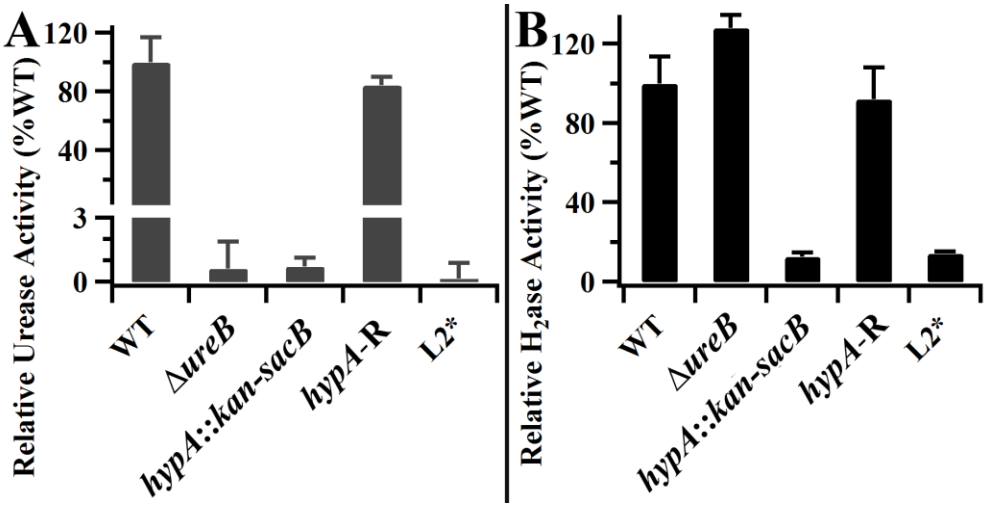

Figure 3.9: Urease and H_2ase activities of L2*-*hypA* variant and control strains
The urease activities of L2*-*hypA* variant and control strains were measured and then normalized against the activities of the WT strain (A). The H_2 oxidation from each strain of *H. pylori* was normalized against the activity of the WT strain (B). Each bar represents the average ± standard deviation of three technical replicates from two independent growths. Panel A was previously published and reproduced with permission from [Hu, *et. al. Biochemistry*, 56, 1105-1115 (2017) [14]. Copy right 2017 American Chemical Society. Panel B was reproduced from [Blum *et. al. PLOS ONE*, 12, e0183260 (2017) [16].

3.2.2.7 L2*-HypA retains protein-protein interaction with UreE but loses Ni-binding affinity

The L2*-*hypA* strain could lead to cellular urease deficiency by two potential mechanisms. Firstly, the L2*-HypA mutation could disrupt protein-protein interactions between HypA and the known interaction partner, dimeric UreE, in the urease maturation pathway.[4] Alternatively, insertion of a Leu at the N-terminal MHE-motif could disrupt the Ni-binding properties of HypA directly. These mechanisms are not mutually exclusive, and both would result in impaired Ni delivery and the loss of urease activity and acid survival phenotype that is observed for the L2* *hypA* strain.

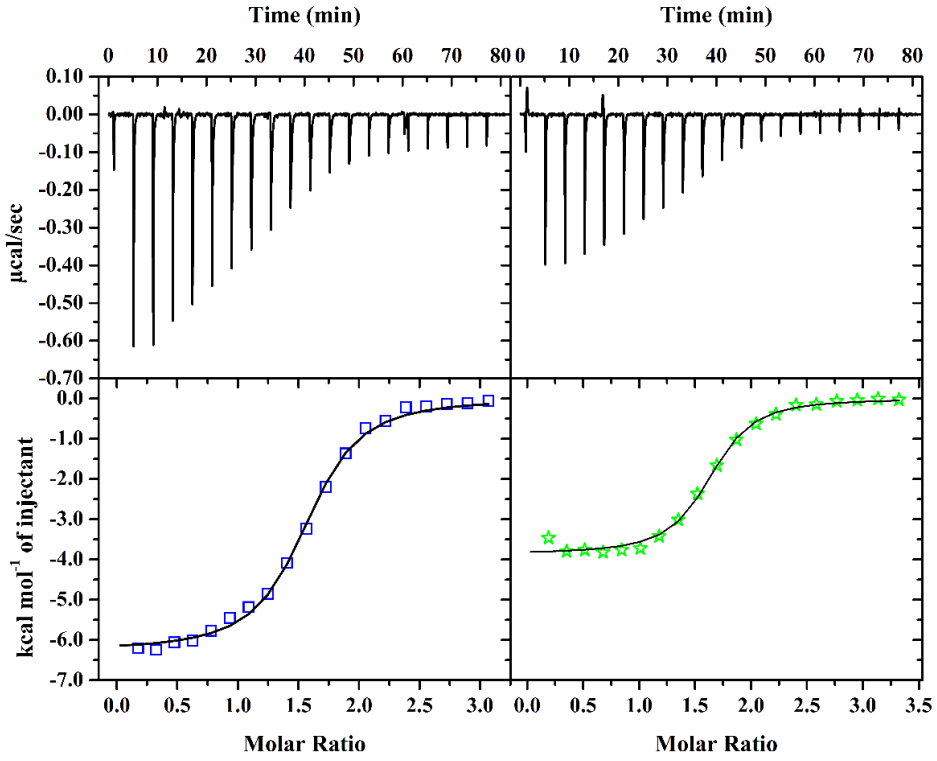

Figure 3.10: Binding of WT- and L2*-HypA to UreE dimer by ITC
Binding curves of WT-HypA (left) or L2*-HypA (right) to WT-UreE dimer measured by isothermal titration calorimetry (ITC) in buffer consisting of 20 mM HEPES, 200 mM NaCl, and 1 mM TCEP (pH 7.2). The top panels show the heat response from each injection, which are integrated to generate the enthalpy of binding plotted in the bottom panels [WT (squares) and L2* (stars)]. Binding of WT- and L2*-HypA to the UreE WT dimer is each fitted to OneSite models as described in the text. Figures reprinted with permission from [Hu, *et. al. Biochemistry*, 56, 1105-1115 (2017) [14]. Copy right 2017 American Chemical Society.

To assess whether the L2* mutation of HypA affected protein-protein interaction between HypA and UreE, binding of purified HypA to UreE was monitored using isothermal titration calorimetry (ITC). Concentrated WT- or L2*-HypA proteins were injected into WT-UreE dimers[30, 39] and the change in heat from each injection was integrated and the resulting binding curve was fitted to OneSite models (see method Section 3.4.10, Figure 3.10A). The number of sites (*N*) in each case was fitted to be ~1.5 HypA per UreE dimer. The larger than expected value of *N* (HypA:UreE dimer >1) is likely due to the tendency of *H. pylori* UreE protein to degrade slowly over time at the C-terminal Ni-binding motif. This degradation was previously observed in mass spectrometry of purified UreE and was reported as a cause for the disorder of the C-terminal region in crystal structures. [30, 40] The degradation was also observed in SDS-PAGE, resulting in a lower molecular weight band, which was carefully monitored post-titration to ensure that full-length UreE is comparable in each titration (APPENDIX 2, Figure A2.3). The degradation of UreE makes the concentration of full-length UreE in a sample uncertain and invariably less than expected, thus complicating an accurate determination of *N*. Despite the larger than expected *N* values, WT- and L2*-HypA binding to UreE dimer were fitted to similar *N* values (1.5 ± 0.1 and 1.6 ± 0.2) and affinities (with apparent K_d values of 0.96 ± 0.09 and 0.69 ± 0.11 μM respectively, Table 3.2). This finding suggests that the L2* variant did not disrupt the protein-protein interactions with the urease maturation pathway (through dimeric UreE).

Table 3.2: Apparent Binding to HypA as Measured by ITC

binding partner	HypA	K_d (μM)	*N*	ΔH (kcal/mol)
UreE (dimer)	WT	0.96 ± 0.94	1.5 ± 0.1	-6.27 ± 0.06
	L2*	0.69 ± 0.11	1.6 ± 0.2	-3.86 ± 0.06
Ni	WT	1.0 ± 0.2	0.88 ± 0.01	-4.99 ± 0.07
	L2*	59 ± 12	0.39 ± 0.07	-1.30 ± 0.29

Table was previously published and reproduced with permission from [Hu, *et. al. Biochemistry*, 56, 1105-1115 (2017) [14]. Copy right 2017 American Chemical Society.

Another mechanism by which L2*-HypA could hinder urease maturation is through lowering the ability of HypA to bind Ni. This was also addressed using ITC to measure the difference in Ni binding affinity between WT- and L2*-HypA. ITC titrations involving injection of $NiCl_2$ (dissolved in the same buffer as the protein) into the respective HypA protein, where the heat of injection was monitored and integrated. The resulting binding curves were each fitted to OneSite models (see method Section 3.4.10). The results indicated that WT-HypA bound approximately one nickel per protein (N = 0.88 ± 0.01) with an apparent K_d of 1.0 ± 0.2 μM (Figure 3.11, Table 3.2), which is consistent with prior studies.[9] Titration of $NiCl_2$ into L2*-HypA at the same concentrations resulted in curves that did not reach saturation after the addition of two equivalents of Ni (data not shown), indicating a much lower Ni affinity for L2*-HypA. A more concentrated $NiCl_2$ solution was subsequently used for the L2*-HypA titration to push the titration to apparent saturation. The resulting heat of binding was best fitted with a OneSite model with an apparent K_d = 59 ± 12 μM and N = 0.39 ± 0.07 (Figure 3.11 right, Table 3.2).

However, it clear that the amount of heat generated by Ni binding to L2*-HypA is very small, making K_d and N difficult to measure. For this reason, the Ni-binding affinities of WT- and L2*-HypA, were also measured by $NiCl_2$ titration into HypA protein solutions monitored by changes in absorbance in the UV-Vis spectra. The absorption spectra of samples with a constant concentration of WT or L2*-HypA mixed with increasing concentrations of Ni^{2+} (dissolved in the same buffer) were measured. The apparent K_d was calculated from the change in absorption maxima in response to total Ni concentration (see Method Section 3.4.11, Figure 3.12). The apparent K_d was calculated to be 1.1 ± 1.0 μM for Ni-binding to WT-HypA, corroborating the ITC data. The apparent K_d was calculated to be 27 ± 4 μM for Ni-binding to L2*-HypA, which is of the same order of magnitude as the value found using ITC, and ~ 20-fold greater than WT. Thus, inserting a Leu residue into the Ni-binding motif of HypA (L2*-HypA) significantly

decreases its ability to bind Ni, rendering it unable to deliver this metal efficiently to the urease maturation pathway.

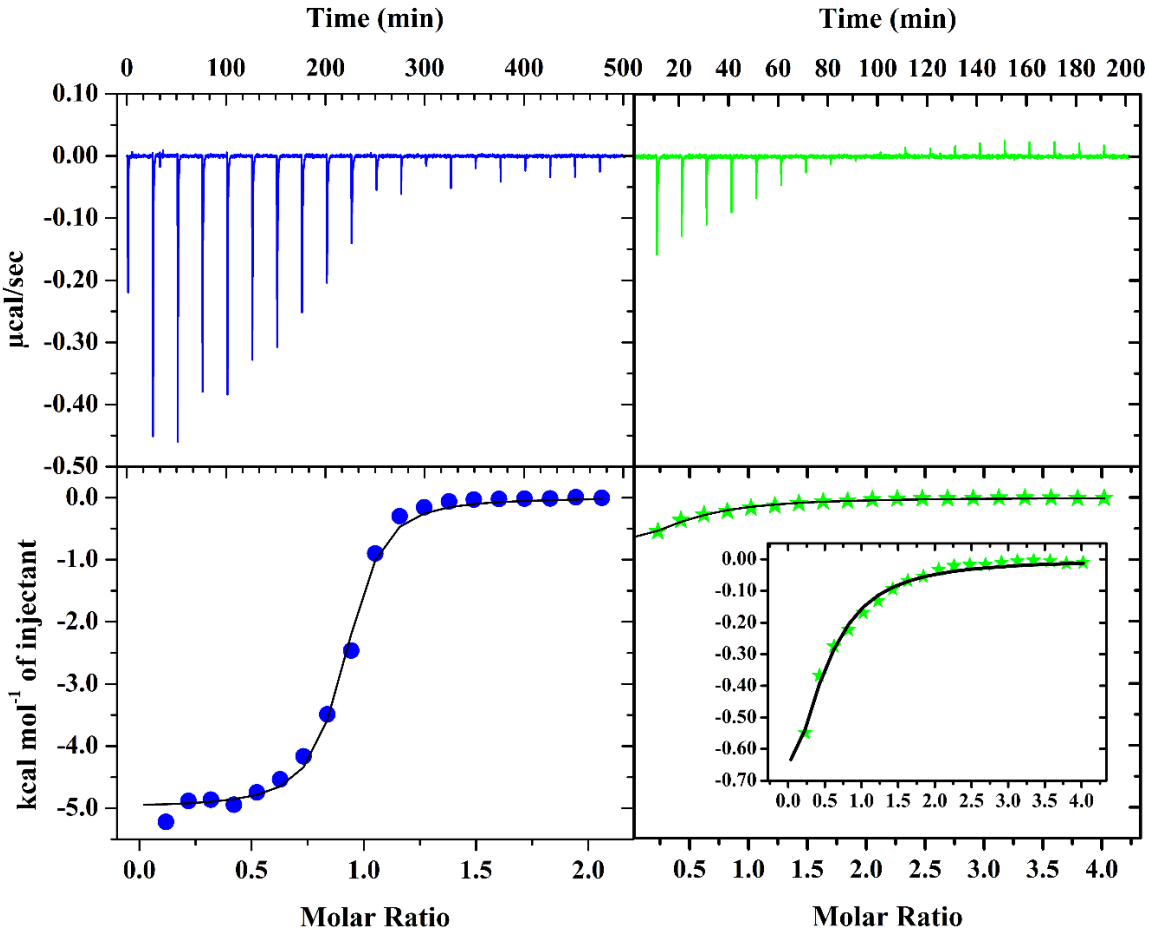

Figure 3.11: Ni^{2+} binding to WT- and L2*-HypA measured by ITC
ITC binding curves of titrations of Ni into WT-HypA (blue) and L2*-HypA (green) in a buffer consisting of 20 mM HEPES, 200 mM NaCl, 1 mM TCEP (pH 7.2). The top panels show the heat response of each injection, which are integrated to generate the enthalpy of binding plots in the bottom panels [WT (circles) and L2* (stars)]. The binding curves are graphed to the same scale on the y-axes for WT- and L2*-HypA to emphasize the difference in enthalpy response with a more appropriately scaled y-axis for Ni-L2* binding also shown (inset). Binding Ni to WT- and L2*-HypA is fitted to a OneSite models in both cases, as described in the text. Figures reprinted with permission from [Hu, *et. al. Biochemistry*, 56, 1105-1115 (2017) [*14*]. Copy right 2017 American Chemical Society.

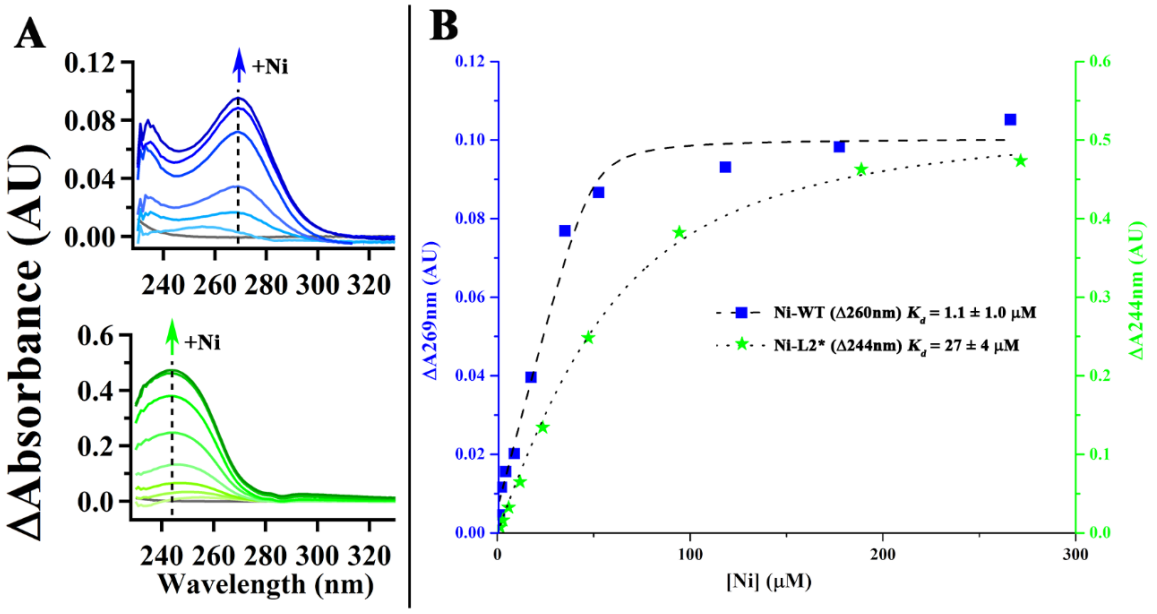

Figure 3.12: Ni^{2+} binding to WT- and L2*-HypA measured by UV absorption
Ni^{2+} addition to 50 μM of Apo-ZnWT- and Apo-ZnL2*-HypA monitored by UV-Vis absorption. (A) Spectra of Apo-ZnHypA are shown in gray and are subtracted from the Ni-ZnHypA spectra of WT- (top, blue) and L2*-HypA (bottom, green), where the Ni-dependent absorption maxima at 269 nm and 244 nm respectively. (B) Ni titration curve of WT- and L2*-HypA obtained from plotting the change in absorption at the maxima are against the total nickel concentration with fits for K_d shown as dashed (WT) and dotted (L2*) lines (see methods Section 3.4.11 for detailed fitting procedures). Figures reprinted with permission from [Hu, *et. al. Biochemistry*, 56, 1105-1115 (2017) [14]. Copy right 2017 American Chemical Society.

3.3 Discussion

H. pylori is a prevalent human pathogen that colonizes the acidic stomach using multiple adaptations (discussed in detail in Section 1.1.1).[41] One of the most prominent adaptations for acid acclimation is the use of the Ni-dependent enzyme urease (discussed in Section 1.1.1.4).[41, 42] Briefly, urease catalyzes the hydrolysis of urea to carbon dioxide and ammonia, which neutralize the cytoplasmic and periplasmic pH of the bacteria under acid shock conditions.[43] Up to 10% of the total protein synthesized by the bacteria is urease to ensure for fast response to acid exposure.[44] However, under neutral conditions, excessive activation of urease can over alkalinize the internal pH of the bacteria leading to cell death. Therefore, the activity of urease is regulated at multiple levels in response to acid shock and Ni availability (discussed in CHAPTER 1).[42] Assembly of the di-nickel active site requires several accessory proteins (discussed in Section

1.2.5), which include the Ni-metallochaperones UreE and HypA.[43] HypA is also involved in Ni-acquisition for the only other Ni-dependent enzyme in *H. pylori*, NiFe-H_2ase.[2]

Properties of the HypA protein have been extensively studied and are discussed in detail in Section 1.3. Briefly, HypA contains a structural Zn site that coordinates the metal by two conserved CXXC motifs and features non-conserved flanking His residues; and a Ni site at the conserved N-terminal MHE-motif.[8-10] The work described in this chapter probed the functional consequences of properly constructed Zn and Ni binding sites, as well as identifying key ligands.[11, 14]

3.3.1 Dynamics of the HypA Zn site

The structural Zn sites in HypA were previously shown to change coordination in a pH and nickel-dependent manner, adopting a $Zn(Cys)_4$ conformation at neutral pH (7.2), and a $Zn(Cys)_2(His)_2$ conformation at more acidic pH (6.3) (Figure 3.1) in the presence of Ni.[8, 9] These two structures were correlated with other physical properties of HypA, including nickel binding stoichiometry and thermal stability, with the lower pH form associated with greater thermal stability.[9] Mutagenesis studies revealed that altering any Cys residue in the two CXXC motifs (to Ala or Asp) resulted in adoption of the acidic conformation ($Zn(Cys)_2(His_2)$), and any mutation of the flanking His residues resulted in the neutral conformation ($Zn(Cys)_4$), in the presence of Ni at both pH values, as determined by EXAFS analysis.[9] The loss of pH-responsive dynamics in the HypA Zn site variants were important tools for probing the role of HypA in urease and H_2ase maturation within the cell and in acid survival.

Urease activities of clarified lysate from *H. pylori hypA* Zn site variant strains correlate well with previous *in vitro* studies employing addition of purified HypA proteins to whole cell extract from a *ΔhypA* mutant strain of *H. pylori*.[9] Results of the HypA protein add-back studies show a general decrease in urease activity upon addition of the zinc site variants relative to addition of wild type HypA protein, and a generally greater effect associated with Cys mutants as compared to His mutants.[9] The urease activity of clarified lysate of *H. pylori* Zn site *hypA* variant

strains presented here reveal two distinct phenotypes: WT-like urease activity, represented by His mutants, and urease-deficient strains associated with Cys-mutants. The H_2ase activity of these strains closely mirror the urease activity, with the His variants exhibiting WT-like H_2ase activity, and Cys variants showing H_2ase deficiency. These two classes of mutants correspond to the $Zn(Cys)_4$ or $Zn(Cys)_2(His)_2$ conformations, respectively. Our data indicate that, a deficient HypA metallochaperone is deficient for both target enzymes, and that a properly constructed Zn site is essential for Ni delivery to either target, which suggest that all Cys residues in the HypA Zn site are important in the maturation of urease and H_2ase in *H. pylori*. These results are consistent with a model in which lower levels of enzyme activation are associated with the $Zn(Cys)_2(His)_2$ structural conformation, or the loss of access to the $Zn(Cys)_4$ structure.

Among the Cys mutations, there were two levels of enzymatic activities observed: a moderate decrease that was generally associated with ligand substitution variants (Cys → Asp); and severe decrease in activity generally associated with loss of ligand mutations (Cys → Ala). This trend suggests that at least part of the difference lies in coordination of the CXXC motifs. A Cys→Asp mutation involves the substitution of a Cys thiolate ligand by a carboxylate. Thus, the Cys → Asp substitution provides a mechanism to access a $Zn(Cys)_3$Asp site that favors the wild type-like $Zn(Cys)_4$ conformation, which appears to preserve greater HypA function in moderately affected mutants. Exceptions to this trend was observed for position C74, where both C74A and C74D resulted in severe deficiency in enzymatic activities (see below for additional discussion). Another exception was observed in the C77A variant, which was severely deficient in urease activity but only moderately affected in H_2ase activity, indicating its potential role in differentiating the activation between the two Ni-dependent enzymes.

Acid survival studies of Zn site *hypA* variant strains corroborated that mutation of the His residues did not affect acid survival. However, although most Cys mutations of *hypA* resulted in lower urease activities, only three (C91A, C94A, and C74D) were shown to be acid sensitive under the experimental conditions used in this study. This discrepancy suggests that WT-like

urease activity is not required for acid survival under the conditions used in this study (30 minutes at pH 2.3 and with 5mM urea supplement). Of the three Cys variants identified to be acid sensitive, C74 occupied a unique position and phenotype (discussed in more detail below). Interestingly, acid sensitivity was detected for the loss of Zn ligands in C91 and C94 (Cys → Ala mutation), but not for ligand substitutions (C91D and C94D *hypA* variant strains had WT-like acid survival). This suggests a positional difference in the two CXXC motifs, where the lack of Zn coordination in the second CXXC motif (C91 and C94) is more deleterious compared to the first CXXC motif (C74 and C77). No clear reason is apparent for the functional differences observed for the two CXXC motifs, although it is worth noting that two of the four Cys residues in the CXXC motifs were substituted by His at acidic pH (as previously shown by EXAFS analysis)[9] while the other two remain bound to anchor the Zn site. This pair-wise difference may account for the functional difference noted in the two CXXC motifs, however, more structural information is required to definitively assign the role of each CXXC motifs.

It is clear from both the enzyme activity data and acid survival data that Cys74 is a special position among the Cys variants. It is the only position where the Cys → Asp mutation results in a less acid viable strain than the Cys →Ala mutation, and the only position where urease activity of the Ala variant is higher than the Asp variant. The NMR structure of GSHypA shows that the Zn site is formed by a loop that begins with Cys74 and ends with Cys94. However, the terminal Cys residues in the loop differ in that Cys94 is flanked by a His residue and Cys74 is not. The lack of an alternative ligand (in the form of a flanking His residue) could make Cys74 mutations a more vulnerable position, particularly if it plays an anchoring role, the loss of which may result in a more severe phenotype due to destabilization of the entire structural zinc site.

Altering the HypA structural zinc site by point mutations also severely affects urease and H_2ase maturation and acid survival of *H. pylori*. These findings suggest that protein structural dynamics, reflected in the HypA Zn site structure, may result in subtle alterations of the overall

HypA fold, ultimately leading to a gradient in urease and H_2ase enzymatic activities that varies with cellular pH and Ni availability.

3.3.2 N-terminal amine of the HypA Ni site

Protein and cell-based studies of the N-terminal insertion variant, L2*-HypA, lead to the conclusion that proper Ni-binding by HypA is critical for its function as a Ni-chaperone in the urease maturation pathway. Proper Ni-binding requires the unmodified MHE-motif at the N-terminus of HypA (likely by coordinating the N-terminal amine). Deficiency in urease activity and acid survival of the L2*-*hypA* mutant strain of *H. pylori* does not appear to result from interruption of protein-protein interactions with the urease maturation pathway, as the apparent affinities of WT-HypA and L2*-HypA binding to WT-UreE dimer were found to be similar (3.2.2.7). Instead, the apparent affinity of L2*-HypA for Ni(II) ions was found to be reduced by at least 20-fold compared to WT-HypA (3.2.2.7). This "loss of Ni-binding affinity" mechanism to account for the observed loss of function in urease maturation is corroborated by the structural changes found for the Ni-binding site in L2*-HypA (discussed below).

The identification of the proper Ni-binding site in HypA has been controversial. From multiple sequence analysis to mutagenesis studies, Ni bound to HypA at the conserved N-terminal MHE-motif, involving His2 as one of the ligands.[4, 7, 10] However, the geometry of the Ni-binding site and the identity of the other Ni ligands from this Ni metallochaperone were not clear. Our lab previously identified the unmodified WT-HypA as having a six-coordinate site involving exclusively N/O-donor ligands that include 1 – 2 imidazoles.[8, 9] Xia *et. al.*, working with the N-terminal extended GSHypA that contained the intact MHE sequence (resulting from a 2-residue overhang from cleavage of an N-terminal affinity tag) proposed a four-coordinate planar site involving the His2 side-chain and three additional backbone amides from His2, Glu3, and Asp40 (depicted in Figure 3.13C).[10] In the studies presented here, the unmodified WT-HypA protein is consistent with the six-coordinate site with one His imidazole and where the scattering attributed to a putative second histidine is now attributed to chelate ring formation involving backbone

amide coordination (depicted in Figure 3.13A). The N-terminal extension variant protein, L2*-HypA, bound Ni at the same locus as WT-HypA, but having lost two N/O-donor protein ligands it adopted a pyramidal five-coordinate geometry with the additional ligand being a Br^- contributed from the buffer system (depicted in Figure 3.13B). The direct comparison between the Ni sites in unmodified WT-HypA and the variant protein with an N-terminal extension (L2*-HypA) demonstrated that the N-terminal amine of HypA is clearly involved in Ni binding.

The L2*-HypA Ni site structure described here is also consistent with the data from the N-terminally modified GSHypA protein (PDB: 2KDX), which was proposed to have a four-coordinate (planar) Ni site based on the fact that it is diamagnetic (lack of paramagnetic line-broadening) and on chemical shift perturbations observed by $^1H^{15}N$-HSQC experiments upon Ni(II) titration into a sample that identified four ligands.[10] In the case of the L2*-HypA Ni(II) complex, the same set of ligands that were proposed in the 2KDX structure could be used to describe the best-fit for the Ni site with the addition of a Br^- in the axial position from the buffer system (depicted in Figure 3.13B). While the NMR experiment clearly establishes that the Ni(II) site is diamagnetic in GSHypA, it does not establish a four-coordinate planar geometry because the technique is blind to non-protein ligands. Despite the five-coordinate pyramidal geometry, Ni(II) binding to the L2*-HypA protein variant results in a diamagnetic low-spin Ni(II) site. In determining the ligands involved in Ni binding, Xia *et al.* would not have been able to determine the involvement of non-protein ligands in coordinating the Ni site using NMR and therefore concluded that the N-terminally modified GSHypA Ni site is planar in geometry.[10] Xia *et al.* also concluded that all other conserved Glu, Asp, and His residues are quite far away from the N-terminus of the protein in the 2KDX structure and therefore are unlikely to be involved in formation of the six-coordinate Ni site in WT-HypA.[10] However, the proximity of Glu3 and Asp40 was established in their experiments through backbone amide binding in forming the planar Ni site.[10] Having established the N-terminal amine as one of the ligands in WT-HypA, in addition to the His2 side chain and backbone amide, the missing three ligands are proposed to be

the sidechains of Glu3 and Asp40 as well as an additional backbone amide residue (most likely from Glu3). This proposed Ni site structure for WT-HypA is depicted in Figure 3.13A. The binding of Glu3 and Asp40 sidechains and neutral amides would result in a charge neutral complex. The use of the N-terminal amine, and both the sidechain and backbone amides of His2 and Glu3 would firmly establish the rigidly conserved MHE-motif for Ni binding in HypA.

One crystallographically characterized example of the HypA Ni-binding site is available from the *T. kodakarensis* KOD1 (PDB ID: 5AUN and 5AUO) in a complex with the ATP-binding form of HypB from the same organism in two distinct nucleotide-bound forms (ATP and ADP analogs).[45] Each Ni site features HypA in planar four-coordinate geometry with ligands comprised of the N-terminal amine, the backbone amide of His2, and the sidechains of His2 and His98 (His79 in *H. pylori* HypA), the latter of which is pushed into the Ni-binding site by HypB binding close to the HypA Zn site.[45] Since the *H. pylori* HypA Zn-binding region is much more compact compared to the *T. kodakarensis* site (see multiple sequence alignment in Figure 3.1), it is unlikely that the His residues in the Zn site would ever be able to coordinate the distant Ni site. Additionally, H79A and H95A *hypA* variant strains did not exhibit deficiencies in acid survival, urease activity, or H_2ase activity; which would be expected if one of the His residues at the *H. pylori* HypA Zn site was involved in Ni-coordination, either alone or as part of a functional protein complex.

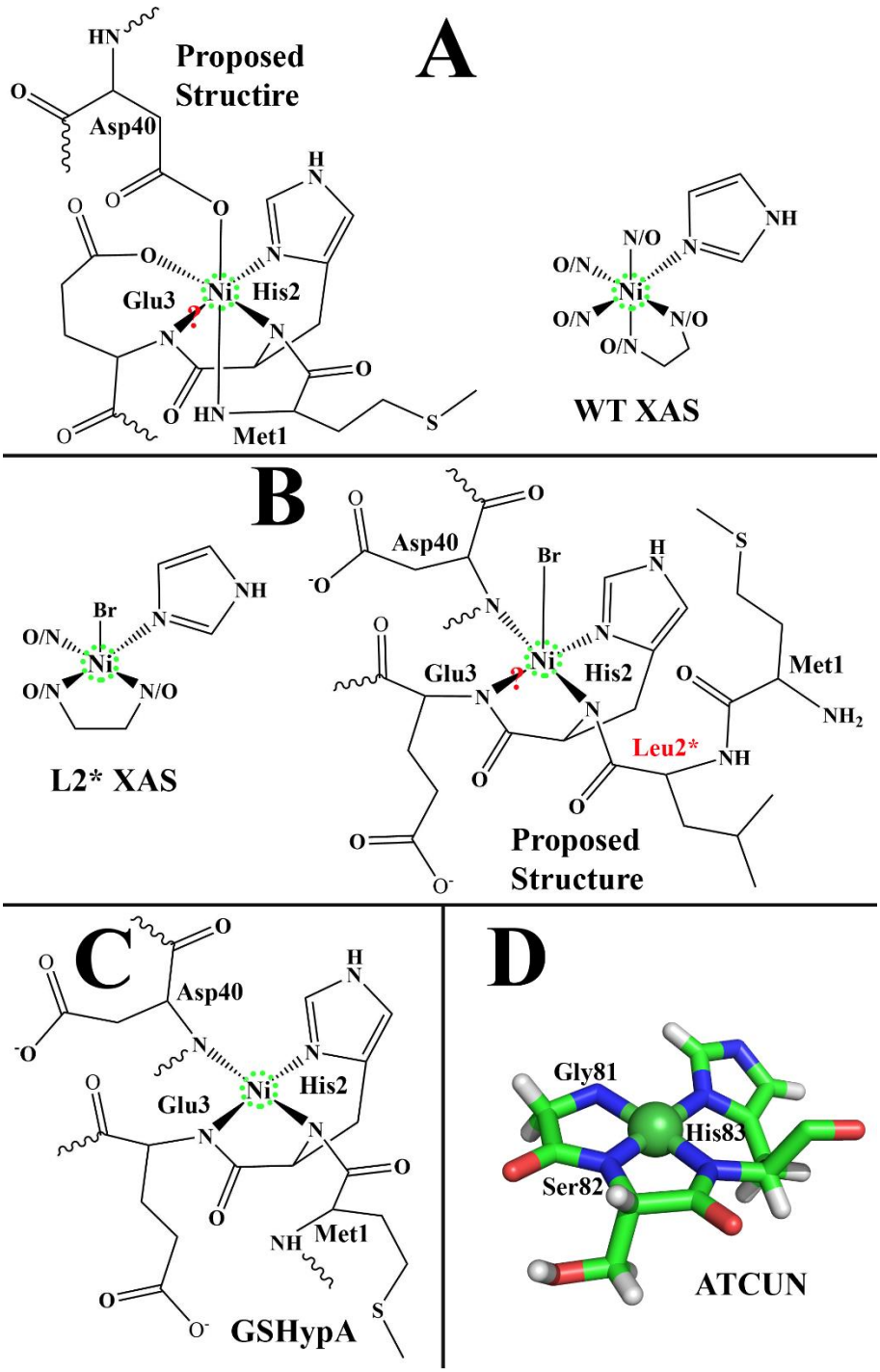

Figure 3.13: Summary of proposed HypA Ni site structures
Proposed Ni site structures for WT-HypA (A) and L2*-HypA (B) based on the analysis of XAS data. The Ni site structure for GSHypA (C) as proposed by Xia *et. al.* from NMR studies (PDB ID: 2KDX) of the N-terminal extension variant.[10] N-terminus of the SH3 mutant domain of c-SRC tyrosine kinase (PDB ID: 4OMO) solved by x-ray diffraction,[46] demonstrating the Ni-bound ATCUN motif in a protein.

The planar, and therefore diamagnetic, *T. kodakarensis* HypA Ni site resembles other classic N-terminal Ni-binding motifs. Use of the N-terminal amine as a metal ligand is unusual in metalloproteins, but more common in Ni and Cu proteins. Coordination of Ni(II) in the N-terminus of proteins and peptides has been most extensively studied in the classic amino terminal Cu(II) and Ni(II) (ATCUN)-motifs. The ATCUN-motif was first described in albumin, which is amongst the major transporters of Cu(II) and Ni(II) in serum.[47] The motif has since been described in several other peptides such as human protamine 2, histatin 5, heuromedin C, and hepcidin, of which the physiological evidence of Cu(II) and Ni(II) binding has yet to be confirmed.[47, 48] Additionally, small molecule mimics and protein/peptide engineering studies have shown that ATCUN-motifs are associated with DNA-cleavage activities.[47, 49, 50] Despite the high stability and tight binding of the ATCUN metal site [K_d ~1 pM for Cu(II) and 150 nM for Ni(II)], the ATCUN metal site structure has yet to be crystallized in albumin and is presumed to contain multiple conformations even in crystals.[48] Instead, most of the structural information on ATCUN motifs has been derived from small molecule and oligopeptide mimics,[48-51] although a high-resolution crystal structure of the Ni-bound ATCUN motif (depicted in Figure 3.13D) at the N-terminus of a protein is available for SH3 mutant domain of c-SRC tyrosine kinase from *G. gallus* (PDB ID 4OMO).[46] The classic ATCUN-motif has a strictly conserved His-residue in the third position and binds metals using the N-terminal amine, backbone amide N-donors from the second and third amino acid, and the His-imidazole sidechain, forming two chelate rings, one 5-membered and one 6-membered, with the metal in a distorted four-coordinate planar geometry.[47, 48, 50] This stable planar structure excluded sidechain coordination from the first two amino acids of the motif.[48]

Despite binding Ni(II) at the N-terminus, the WT-HypA Ni site structure is distinct from the classic ATCUN-motif in several ways. Like the ATCUN-motif, Ni(II) binds to HypA with the N-terminal three-residue motif (MHE-) through the N-terminal amine and likely the backbone amides of His2 and Glu3 as well as the imidazole sidechain of His2. However, Ni-coordination to

the MHE-motif forces one of these N/O-donor ligands into an axial position (as depicted in Figure 3.13A), instead of favoring the rigid planar structure found in the classic Ni-ATCUN site. The axial coordination of an N/O-donor, such as His imidazole, may favor a high-spin configuration, which also favors a 6-coordinate Ni(II) site, instead of the planar four-coordinate low-spin Ni-ATCUN structure. Like the ATCUN-motif, the HypA MHE-motif is associated with known Ni-transporter activity, although with a much more modest K_d (~ 1 μM, *vide supra*), which allows for more appropriate Ni metallochaperone activity inside the cell. With the L2*-HypA variant, the conserved His2 residue is shifted to the third position (MLHE-) to more closely resemble the classic ATCUN motif.

Despite having a more ATCUN-like metal binding motif, the L2*-HypA variant did not exhibit the tight Ni(II) binding that is associated with the ATCUN complexes like albumin,[48] although albumin Ni-binding has not been measured under similar conditions. The reason for the decreased affinity is not clear; one possibility lies with the difference in protein structure. In HypA proteins, the N-terminus is associated with a helical structure that would be perturbed by Ni binding, effectively lowering the affinity relative to the unstructured N-termini in albumin structures.[48] Another possibility is that the protonation state of the amide N-donors is important. If one or more amides is left protonated in the L2*HypA structure, this would decrease Ni affinity and enhance the binding of an additional anion, such as Br^- or Cl^-. In any case, the L2*-HypA Ni site is low-spin, like the Ni-ATCUN site, indicating that it can adopt a similar planar coordination of the four protein ligands. In five-coordinate Ni(II) complexes, the relative ligand field of the ligands in the basal plane vs. the axial ligand determines the spin-state. Addition of a Br^- ligand, a weak field ligand, leads to a pyramidal geometry, but retains the low-spin configuration.

In addition to the ATCUN-motif, there are several examples of proteins that bind Ni(II) at the N-terminus, specifically coordinating the N-terminal amine. One such example is the N-terminal high affinity site in *E. coli* HypB (absent in *H. pylori* HypB), which binds Ni(II) through a CXXCGC motif at the N-terminus, coordinating the N-terminal amine and the three S-Cys in a

planar geometry.[52] Another such example is *S. coelicolor* nickel superoxide dismutase (NiSOD), which binds Ni(II) through the N-terminal amine of His1, the backbone amide of Cys2, and the sidechains of Cys2 and Cys6, with the sidechain imidazole of His1 also bound in the Ni(III) state.[37, 53, 54] Both the *E. coli* HypB N-terminal motif and NiSOD Ni binding sites have been referred to as "ATCUN-like" in literature due to the binding of the N-terminal amine and planar geometry.[35, 37, 52] Another example of Ni-binding at the N-terminus can be found in *E. coli* RcnR, a Ni(II)-/Co(II)-responsive transcriptional regulator, which binds Ni(II) with the N-terminal amine of Ser2 (Met1 is cleaved in *E. coli*) in a 6-coordinate site, where there is no evidence of backbone amide binding thus far.[12] Thus, Ni(II) binding at the N-terminal amine has been found in proteins with vastly different functions and metal coordination: metal transporters/chaperones (*e.g.*, albumin (planar)[48] and HypA (6-coordinate)), both redox-active and inactive enzymes (*e.g.*, NiSOD (planar/pyramidal)[37] and *Ec*HypB N-terminal Ni-motif (planar)[52]), and a metal-responsive transcriptional regulator (RcnR (6-coordinate)[12]), demonstrating the N-terminal amine is a common and important ligand for Ni(II)-binding in biology overall.

One mechanism for controlling cellular urease activity in *H. pylori* is through modulation of urease maturation via nickel insertion into apo-urease.[42, 55, 56] Apo-urease is produced in large quantities (10% of all synthesized protein[44]) but remains largely in the apo form.[38, 42] Increases in enzyme activity are correlated with Ni available in the media.[42, 55, 56] Beyond Ni availability, acid conditions also strongly enhance urease activity, but urease transcription is only marginally increased.[57, 58] Thus, nickelation of the apo-protein is employed to boost urease activity under acidic conditions.[42] With respect to the accessory proteins involved in Ni incorporation, the roles of the hydrogenase proteins HypA and HypB and the urease protein UreE are quite distinct. Both the Ni-binding deficient *hypA* H2A mutant[4, 7] and the nucleotide-binding deficient *hypB* K59A mutant[59] were reported to lack urease activity, but this defect could be complemented by Ni supplementation in the media, consistent with their roles in Ni(II) transport and delivery, and implying that under high Ni concentration some Ni is available to UreE. In contrast, Ni

supplementation could not rescue the urease-deficient phenotype in either the *ΔureE* mutant[4] or the *ureG* K14A mutant (nucleotide-binding deficient UreG).[59] Hence urease maturation specifically requires the urease cascade, but not HypA and HypB when excess Ni is present.

With Ni-binding to WT-HypA having only a modest Ni-binding affinity at (K_d ~1 μM) (*vide supra*) and *H. pylori* having a full cascade of urease maturation accessory proteins UreEFGH,[60] why would the full maturation of urease require the hydrogenase maturation accessory proteins HypA and HypB? Specifically, why is HypA Ni-binding necessary for Ni transport and delivery to the urease maturation pathway? One possibility is that HypA and HypB provide an additional pathway for Ni incorporation that is triggered under acidic conditions that supplements a low basal level provided by *H. pylori* UreE alone. In fact, *H. pylori* appears to restrict Ni incorporation into urease by UreEFGH by lowering in the Ni-binding properties of UreE. The poor Ni-sequestration ability of *H. pylori* UreE compared to homologues (such as *K. aerogenes* UreE, which has a poly-His tail) has been studied.[61] Incorporation of a poly-His tail into *H. pylori* UreE has been shown to increase the Ni-sequestration ability and the urease activity in the absence of HypA or HypB proteins.[61] Under acidic conditions, HypA and HypB could provide a higher level of Ni incorporation into UreE by 1) increasing the local concentration of Ni by formation of a complex with HypA and HypB, or 2) by simply enhancing the affinity of UreE for Ni in a complex with HypA and HypB. The former mechanism is suggested by the known HypA-UreE complex formation,[3, 4] and by protein structural changes that accompany changes in the Zn site structure at pH 6.3.[8, 9] The latter mechanism is supported by the increase in Ni affinity that occurs in the HypA and HypB complex in *T. kodakaraensis.*[45]

These prior studies along with our own study point to the role of the hydrogenase maturation accessory protein HypA in the acquisition and delivery of Ni to the urease maturation pathway under non-abundant Ni conditions (without Ni supplementation). Instead of enhancing the Ni-sequestration ability of the urease cascade, HypA is recruited from the hydrogenase maturation pathway to sequester Ni for the urease maturation pathway; in doing so they assert a

higher level of control over Ni availability to the urease maturation pathway. Due to the high level of Apo-urease synthesized under both acidic and neutral conditions[44], the higher level of Ni control could hypothetically be employed to finely tune the urease activity of *H. pylori* to prevent an alkaline internal pH or depletion of urea in the cytoplasm under neutral conditions. However, this fine-tuning mechanism would impose acid sensitivity to the strains where the ability of HypA to bind Ni is impaired as is the case in the H2A *hypA* strain[4, 7] and the L2* *hypA* strain.

3.4 Methods

3.4.1 *H. pylori* growth conditions

Growth of G27 background strains of *H. pylori* were performed at the Merrell Lab, part of the Department of Microbiology and Immunology at the Uniformed Services University of Health Sciences, Bethesda, MD. All *H. pylori* strains were maintained at -80°C in brain heart infusion broth (Becton Dickinson) supplemented with 10% fetal bovine serum (FBS) and 20% glycerol and were cultivated on horse blood agar (HBA) medium containing 4% Columbia agar base (Neogen Corp), 5% defibrinated horse blood (HemoStat Laboratories, Dixon, CA), 0.2% β-cyclodextrin (Sigma), 10 μg/mL of vancomycin (Amresco), 2.5 U/mL of polymyxin B (Sigma), 5 μg/mL of trimethoprim (Sigma), and 5 μg/mL of amphotericin B (Amresco). Where required, 5% sucrose was added to HBA for selection of sucrose sensitive strains. Liquid growth of *H. pylori* was performed in Brucella broth (Neogen Corp) with 10% FBS and 10μg/mL of vancomycin. All *H. pylori* cultures were grown under microaerobic conditions (5% O_2, 10% CO_2, and 85% N_2) at 37°C with 100rpm shaking for liquid cultures. *H. pylori* strain G27 was used for all experiments[15]. *Escherichia coli* Top10 cells were either grown on LB agar or in LB liquid medium with shaking at 225rpm. Kanamycin (25μg/mL) and ampicillin (100μg/mL) were used for bacterial selection.

Table 3.3: List of primers in this study

Primers	Sequence (5'-3')	Reference
HypA_Up_F	CCGCTTTGATTCAGATGGGGTG	This study
HypA_Up_R*	*TCTAGA*AAGCTTGCGATCGCTCGAGACTCTAAAAGTCTCAAACGCGCTC	This study
HypA_Dn_F*	*CTCGAG*CGATCGCAAGCTTCTAGAGAATCTTTGGTGTGTAAAGACGC	This study
HypA_Dn_R	GCAAAACGCTGCGGTATTGC	This study
Kan_SacB_F*	GTGGG*CTCGAG*CCCGGGCGAACCATTTGAGGTGA	This study
Kan_SacB_R*	GCGCG*TCTAGA*TATAAGCCCATTTTCATGC	This study
HypA_Confirm_F	GGCTAACGAGCGTGGATAAG	This study
HypA_Confirm_R	GCACTCACTAAAATCGTGGGC	This study
HypA_seq_F	CTAAAGCGGTAACCACATCCG	This study
L2_F	GGGGCTAATTTAAAGATTAAGGTTTAGTATGCTCCATGAATACTCGGTCG	This study
PhypA_R	GCGTTCAATTCTTCTTGCATCGGTTTTTATTCCGCTAACATTTCTAAAGAC	This study
HypA2_Up_F	GCGATTGAGCAAAACGGC	This study
HypA2_Up_R	ACTAAACCTTAATCTTTAAATTAGCCCC	This study
HypA2_Dn_F	AAACCGATGCAAGAAGAATTGAACGC	This study
HypA2_Dn_R	GGTTTTGGACTTGATAGAGCTTG	This study
HypA_L2*_F	CTCCATGAATACTCGGTCGTTTC	This study
HypA_L2*_R2	CGAGTATTCATGGAGCATATGTATATCTCC	This study
HypA_C74A_F	GGTTGAATTAGAAGCCAAGGATTGTTCGCATGTTTTTAAGCCTAACGCG	[9], This study
HypA_C74A_R	CGCGTTAGGCTTAAAAACATGCGAACAATCCTTGGCTTCTAATTCAACC	[9], This study
HypA_C74D_F	GGTTGAATTAGAAGACAAGGATTGTTCGCATGTTTTTAAGCCTAACGCG	[9], This study
HypA_C74D_R	CGCGTTAGGCTTAAAAACATGCGAACAATCCTTGTCTTCTAATTCAACC	[9], This study
HypA_C77A_F	GAATTAGAATGCAAGGATGCTTCGCATGTTTTTAAGCCTAACGCGC	[9], This study
HypA_C77A_R	GCGCGTTAGGCTTAAAAACATGCGAAGCATCCTTGCATTCTAATT	[9], This study
HypA_C77D_F	GAATTAGAATGCAAGGATGATTCGCATGTTTTTAAGCCTAACGCGC	[9], This study
HypA_C77D_R	GCGCGTAGGCTTAAAAACATGCGAATCATCCTTGCATTCTAATTC	[9], This study
HypA_H79A_F	GCAAGGATTGTTCGGCTGTTTTTAAGCCTAACGCGCTAG	[9], This study
HypA_H79A_R	GTTAGGCTTAAAAACAGCCGAACAC	This study
HypA_C91A_F	GCGCTAGATTATGGGGTGGCTGAGAAATGCCACAGC	[9], This study
HypA_C91A_R	GCTGTGGCATTTCTCAGCCACCCCATAATCTAGCGC	[9], This study
HypA_C91D_F	CGCCGTAGATTATGGGGTGGATGAGAAATGCCACAGC	[9], This study
HypA_C91D_R	GCTGTGGCACTTTCTCATCCACCCCATAATCTAGCGCG	[9], This study
HypA_C94A_F	GGTGTGTGAGAAAGCCCACAGCAAG	This study
HypA_C94A_R	AACATTCTTGCTGTGGGCTTTCTCAC	This study
HypA_C94D_F	GGGGTGTGTGAGAAAGACCACAGCAAGAATGTTATTATCAC	[9], This study
HypA_C94D_R	GTGATAATAACATTCTTGCTGTGGTCTTTCTCACACACCCC	[9], This study
HypA_H95A_F	GTGTGTGAGAAATGCGCCAGCAAGAATGTTATTATC	[9], This study

*Restriction enzyme sites are italicized (XhoI or XbaI)

Underline denotes nucleotide changes made to the pJI110 (wild type *hypA*) plasmid

Table combined from previous publications [Johnson, *et. al. Metallomics*, 7, 674-682 (2015) [11] reproduced with permission of The Royal Society of Chemistry, and [Hu, *et. al. Biochemistry*, 56, 1105-1115 (2017) [14], copy right 2017 American Chemical Society.

Table 3.4: List of plasmids and *H. pylori* strains in this study

Strains	**Description**	**Reference**
DSM1	G27 WT	[62]
DSM43	G27 Δ*ureB* Kan^R	[63], This study
DSM1283	G27 *hypA*::*kan-sacB* Kan^R Suc^S	This study
DSM1295	G27 *hypA* restorant	This study
DSM1296	G27 *hypA* C74A	This study
DSM1297	G27 *hypA* C94D	This study
DSM1298	G27 *hypA* C91A	This study
DSM1299	G27 *hypA* C91D	This study
DSM1300	G27 *hypA* H95A	This study
DSM1301	G27 *hypA* C74D	This study
DSM1363	G27 *hypA* C77A	This study
DSM1364	G27 *hypA* C77D	This study
DSM1365	G27 *hypA* H79A	This study
DSM1366	G27 *hypA* C94A	This study
DSM1475	G27 *hypA* L2*	This study
Plasmids	**Description**	**Reference**
pDSM3	pKSF-II	[64]
pDSM32	pEJ22	[63]
pJI110	pET22b(+) vector with *hypA* WT coding sequence	[8, 9], This study
pET22b-HypA(C74A)	pET22b(+) vector with *hypA* C74A coding sequence	This study
pET22b-HypA(C74D)	pET22b(+) vector with *hypA* C74D coding sequence	This study
pET22b-HypA(C77A)	pET22b(+) vector with *hypA* C77A coding sequence	This study
pET22b-HypA(C77D)	pET22b(+) vector with *hypA* C77D coding sequence	This study
pET22b-HypA(H79A)	pET22b(+) vector with *hypA* H95A coding sequence	This study
pET22b-HypA(C91A)	pET22b(+) vector with *hypA* C91A coding sequence	This study
pET22b-HypA(C91D)	pET22b(+) vector with *hypA* C91D coding sequence	This study
pET22b-HypA(C94A)	pET22b(+) vector with *hypA* C94A coding sequence	This study
pET22b-HypA(C94D)	pET22b(+) vector with *hypA* C94D coding sequence	This study
pET22b-HypA(H95A)	pET22b(+) vector with *hypA* H95A coding sequence	This study
pET22b-hypA(L2*)	pET22b(+) vector with *hypA* L2* coding sequence	This study

Table combined from previous publications [Johnson, *et. al. Metallomics*, 7, 674-682 (2015) [11] reproduced with permission of The Royal Society of Chemistry, and [Hu, *et. al. Biochemistry*, 56, 1105-1115 (2017) [14], copy right 2017 American Chemical Society.

3.4.2 Mutant *hypA* Construction

Construction of *H. pylori hypA* strains were performed at the Merrell Lab, part of the Department of Microbiology and Immunology at the Uniformed Services University of Health Sciences, Bethesda, MD. *H. pylori* G27 genomic DNA was used as the template for mutant construct development. A *hypA* mutant strain containing a *kan-sacB* cassette insertion was constructed as follows. The HypA_Up_F and HypA_Up_R primers (Table 3.3) were used to amplify a 556-base pair segment of DNA that spanned 398 base pairs upstream of *hypA* (HPG27_832) and 158 base pairs into the *hypA* coding region. Additionally, the HypA_Dn_F and HypA_Dn_R primers (Table 3.3) were used to amplify a 532-base pair region that began at nucleotide position 160 of *hypA* and spanned 337 base pairs downstream of the *hypA* stop codon. The HypA_Up_R and HypA_Dn_F primers were designed to contain identical flanking sequences, which contained XhoI and XbaI restriction enzyme sites. Thus, the upstream and downstream amplicons were next fused together utilizing splicing by overlap extension (SOE) PCR[65]. The resulting spliced product was cloned into the pGEM-T easy vector (Promega) and transformed into *E. coli* Top10 cells. The *kan-sacB* cassette[64], which confers resistance to kanamycin and sensitivity to sucrose, was amplified from pKSF-II[64] using primers Kan_SacB_F and Kan_SacB_R, which were designed to incorporate a XhoI and XbaI restriction site, respectively. The resulting fragment was digested with XhoI and XbaI and was then inserted between the spliced *hypA* fragments that had been similarly digested. The resulting construct was then transformed into *H. pylori* G27 and transformants were selected on HBA plates containing kanamycin. Successful insertion of the *kan-sacB* cassette into the *hypA* gene was confirmed by PCR and sequencing using the HypA_Confirm_F/R and HypA_seq_F/R primers, respectively. The resulting mutant strain was named DSM1283.

3.4.3 Site-directed mutagenesis

Site-directed mutagenesis constructed within pET-22b(+) vectors for the purpose of protein overexpression were performed at the Maroney Lab, part of the Department of Chemistry

and Program of Molecular and Cellular Biology at the University of Massachusetts Amherst, Amherst, MA. Mutagenesis performed within the G27 *H. pylori* genome were performed at the Merrell Lab, part of the Department of Microbiology and Immunology at the Uniformed Services University of Health Sciences, Bethesda, MD.

Mutations of the cysteines in the HypA CXXC motifs (Cys71, Cys74, Cys91 and Cys94) to alanine or aspartic acid and the flanking histidines (His79 and His95) to alanine were constructed by polymerase chain reaction (PCR) using the PJI110 plasmid (wild type *hypA* sequence carried on the pET-22b(+) vector, Table 3.4) as a template.[66] The PJI110 plasmid was transformed into NovaBlue (Novagen) competent cells and then re-isolated using the Axyprep Plasmid MiniPrep Kit (Axygen) and used as the DNA template in all subsequent PCR reactions. PCR primers were designed to incorporate the desired mutations and are listed in Table 3.3. Reactions were carried out in 50μL volumes using 1ng of template DNA and 2.5ng or 2μM of each primer per reaction. Successful PCR amplifications were confirmed by 0.8% agarose gel electrophoresis, and then methylated PJI110 template was digested with 20 units of DpnI (New England Biolabs) for 1 hour at 37°C. The resulting PCR mixture was transformed into NovaBlue competent cells. Single colonies were selected and grown to saturation in 5mL liquid cultures of LB-Miller (Fisher Scientific) media supplemented with ampicillin at 37°C. Cells were pelleted by centrifugation at 6,000 g for 5 minutes and plasmids were isolated using the Axyprep Plasmid MiniPrep Kit. Successful mutations were confirmed by plasmid sequencing (GENEWIZ, Inc.) and listed in Table 3.4

The L2* mutation was also constructed on the PJI110[8] plasmid background using two rounds of sequential polymerase chain reactions (PCR) with the Q5 High-Fidelity DNA polymerase (New England Biolabs). In the first round of PCR, 0.5μM of HypA_L2*_F primer (Table 3.3) was used to amplify the forward strand of the template DNA containing the L2* mutation. The second primer, HypA_L2*_R2 (Table 3.3), was added to the product of the first

round of PCR mixture for a second round of PCR to amplify the complimentary strand of the DNA template. The presence of linear double stranded PCR product was confirmed by 0.8% agarose gel electrophoresis. The resulting mixture was digested with DpnI (New England Biolabs) for 1 h at 37˚C to remove methylated PJI110 plasmid DNA, and then ligated for 30 min at 25˚C using T4 ligase (New England Biolabs). The resulting reaction mixture was transformed into NovaBlue (Novagen) competent cells and multiple single colonies were isolated from LB-Agar plates supplemented with 100 μg/mL ampicillin (Amp) and then amplified in liquid cultures. The mutated plasmid DNA from three separate single colonies were purified using the GeneJET plasmid DNA miniprep kit (Thermos Scientific) and then sequenced (Genwiz) to confirm the presence of the L2* mutation and successful creation of the pET22b-hypA(L2*) plasmid (Table 3.4) for this study.

We utilized the wild-type or mutant HypA pET-22b (+) plasmids, which each contained the entire HypA coding region, to move the mutant constructs of interest into the *H. pylori* chromosome. Each of the constructs was individually transformed into DSM1283, and double crossover events in which the *kan-sacB* cassette was replaced by the mutagenized *hypA* gene carried on the pET-22b (+) vector were selected for based on sucrose resistance. Sucrose resistant transformants were screened for kanamycin sensitivity and proper integration of the *hypA* construct was confirmed by PCR and sequencing using the HypA_Confirm_F/R and HypA_seq_F/R primers, respectively. In total, *H. pylori* mutant strains were made that contained the following *hypA* mutations (Table 3.4): C74A (DSM1296), C74D (DSM1301), C77A (DSM1363), C77D (DSM1364), H79A (DSM1365), C91A (DSM1298), C91D (DSM1299), C94A (DSM1366), C94D (DSM1297), and H95A (DSM1300). In addition, a *hypA*-restorant (*hypA*-R; DSM1295) in which the *kan-sacB* cassette was replaced by the wild type *hypA* gene was also created in order to control for any defects that may have resulted due to genetic manipulation.

The L2*-*hypA* mutant, which contains a leucine insertion in between the methionine and histidine in the conserved MHE nickel binding motif, was constructed in a similar fashion with slight modifications.[11] Briefly, the *hypA* gene containing the L2* mutation was initially PCR amplified from the pET22b-hypA(L2*) vector with the L2_F and PhypA_R primers (Table 3.3), which were each designed to have extensions to be used in subsequent splicing by overlap extension (SOE) reactions.[67] To increase the likelihood of recombination events before and after the 2nd amino acid position of L2*-*hypA*, a 442 base pair upstream DNA fragment and a 451 base pair downstream DNA fragment were added to either end of the mutated hypA amplicon using SOE PCR.[67] Wild type *H. pylori* G27 (DSM1) genomic DNA was used as template to PCR amplify the upstream and downstream regions using the HypA2_Up_F / HypA2_Up_R and HypA2_Dn_F / HypA2_Dn_R primer pairs, respectively. These products were then spliced to the L2*-*hypA* fragment by SOE reaction. The resulting "upstream-L2*-*hypA*-downstream" SOE construct was then transformed into the interrupted *hypA* mutant (DSM1283). Replacement of the *kan-sacB* cassette in DSM1283 with the mutated *hypA* gene was selected for by plating on HBA agar containing 5% sucrose. Sucrose resistant colonies were subsequently screened for kanamycin sensitivity. Proper integration of the mutated *hypA* gene was confirmed by PCR and sequencing using the HypA_Confirm_F and HypA_Confirm_R primers and HypA_seq_F and HypA_seq_R primers. The newly created L2*-*hypA* strain was named DSM1475 (Table 3.3).

3.4.4 Acid resistance testing

Acid survival of G27 background strains of *H. pylori* were performed at the Merrell Lab, part of the Department of Microbiology and Immunology at the Uniformed Services University of Health Sciences, Bethesda, MD. Each of the ten *hypA* Zn site *H. pylori* mutants were tested for acid resistance. Additionally, the wild type *H. pylori* strain, the *hypA::kan-sacB* mutant, and the *hypA* restorant were included as controls. Furthermore, a urease-deficient mutant of *H. pylori* (DSM43) in which the kanamycin resistance cassette replaced the *ureB* subunit was used as a positive control for acid sensitivity; DSM43 was created by transforming wild type *H. pylori* with

vector pEJ22 as previously described.[17] Assays were conducted as follows: 20mL liquid cultures of *H. pylori* were inoculated to an optical density (600nm) of 0.05 from overnight liquid grown bacterial cells and then allowed to grow for approximately 19 hours. 1mL aliquots were removed from the culture and pelleted by centrifugation. The supernatants were removed and the bacterial pellet was re-suspended in 1mL of phosphate buffered saline (PBS) at pH 6 or 2.3, with or without supplementation with 5mM urea. Immediately after the bacterial pellets were re-suspended, an aliquot was removed, serially diluted in Brucella broth and plated on HBA plates to determine colony forming units (CFU) per milliliter. The cultures were then incubated in 1.5mL capped tubes for 1 hour at 37°C. At this point, a second aliquot was removed from the cultures, immediately serially diluted, and plated to determine CFU/mL as described above. Percent survival after 1-hour incubation in the various PBS solutions was determined for each bacterial strain. At least three biological replicates were performed for each strain.

Additionally, the L2*-*hypA* mutant (DSM1475), Wild type G27 (DSM1), the interrupted *hypA* mutant (DSM1283), the *hypA* restorant (DSM1295), and urease-deficient mutant of *H. pylori* (DSM43) was tested for acid survival as described above. At least three biological replicates were performed for each strain. Furthermore, to ensure reproducibility, a second, biologically independent L2* *hypA* mutant was created in *H. pylori* G27 in an identical fashion as described above and tested for acid viability also. Similar phenotypes were found for each independently derived strain.

3.4.5 Urease activity

Urease activities were determined for each of the ten *hypA* Zn site variants, the wild type *H. pylori* strain, the *hypA::kan-sacB* mutant, and the *hypA* restorant strain. For each strain, 8mL liquid cultures of *H. pylori* were inoculated to an optical density (600nm) of 0.05 from overnight liquid grown bacterial cells and then allowed to grow for approximately 22 hours. At that point, 1mL aliquots were removed from the culture and pelleted by centrifugation (~10^8 cells). The supernatants were removed and the bacterial pellets were stored at -20°C until ready for urease

assays. The frozen cells were thawed and then re-suspended in 750µL of ice-cold HEPES buffer (pH 7.0), 1mM phenylmethylsulfonyl fluoride (PMSF) (MP Biomedicals, LLC), and 1X protease inhibitor cocktail (Sigma-Aldrich) and then lysed by sonication at 70% power for 6 pulses (2-second each) on ice. Lysate was centrifuged at 15,000-g for 10 minutes to remove insoluble fractions from soluble whole cell extracts. Soluble whole cell extracts were kept at 4°C for up to one month and insoluble fractions were stored at -20°C. Total protein concentration in soluble whole cell extract was assessed by Bradford Assay using the Coomassie Protein Assay Kit (Thermo Scientific).

Urease activities for each strain were determined using a modified phenol-hypochlorite method to assay the amount of ammonia released in the soluble whole cell extract of *H. pylori* lysate in the presence of urea[68, 69]_ENREF_24. For each strain, 5µL of whole cell extract was added to 245µL of urease reaction buffer (50mM HEPES, 25mM Urea, pH 7.0), and incubated at 37°C for 20 minutes to allow for ammonia production. The reaction was quenched with the sequential addition of 375µL of phenol-hypochlorite buffer A (100mM phenol, 167.8µM sodium nitroprusside) and then the addition of 375µL of phenol-hypochlorite buffer B (125mM NaOH, 0.044% NaClO); samples were mixed with quick vortexing after the addition of each buffer. The assay mixture was incubated at 37°C for 30 minutes to allow for color development (the conversion of ammonia to indophenol) and the absorbance was evaluated at 625nm. Assays were performed alongside a standard curve created using known amounts of ammonium chloride (0.24 – 500nmol) in place of whole cell extract.

The urease activity of *ΔureB* strain was set as background and subtracted from the activity of each *hypA* Zn site variant and corresponding control strains. After background subtraction, the relative urease activity (% *hypA*-R) of the *hypA* Zn site variants and corresponding control strains were normalized to the *hypA*-restorant (*hypA*-R; DSM1295) *H.*

pylori as 100%. All experiments were performed in triplicate with two independently grown cultures.

The urease activities of the L2*-*hypA* mutant (DSM1475) and corresponding control strains: Wild type G27 (DSM1), the interrupted *hypA* mutant (DSM1283), the *hypA* restorant (DSM1295), and the urease-deficient mutant *ΔureB* (DSM43) was performed as a separate group as described above and then normalized using an alternate method. The total protein concentration of whole cell extracts was determined by Bradford assays using the Pierce Coomassie Protein Assay Kit (ThermoFisher Scientific). The specific urease activity was determined by calculating the nmol of ammonia produced per μg of total protein in each whole cell extract. Relative specific activity (%WT) of the L2*-*hypA* strain and corresponding control strains were determined by normalizing the specific activity against wild type as 100%. All experiments were performed in triplicates with two independently grown cultures, each displaying similar relative specific activity.

3.4.6 Hydrogenase activity

H_2ase activities for *hypA* Zn site variant strains, L2*-*hypA* variant strains, and accompanying controls were performed as described in CHAPTER 2, Section 2.4.3.

3.4.7 Protein overexpression and purification

Sequence-confirmed PJI110 or pET22b-*hypA*(L2*) plasmid was transformed into DL41(DE3)pLysS[70] competent cells and then plated on LB-Agar plates supplemented with Amp and chloramphenicol (Cam), and stored at 4 ˚C and used for protein overexpression for up to one month. A single colony from the plate was transferred to 150 mL of 25 g/L sterilized liquid LB Miller media (LabExpress) supplemented with Amp and Cam and grown at 37 ˚C with shaking (200 rpm) until saturation (>6 h). The culture was scaled up to 2 L of sterilized liquid LB media supplemented with Amp by inoculation with 20 mL of the saturated culture followed by growth at 37 ˚C and 200 rpm until the OD_{600} was ~0.6 (approximately 3.5 h). The cells were then induced to overexpress protein by the addition of 0.8 mM of isopropyl β-D-1-thiogalactopyranoside

(IPTG) (Carbosynth Limited) for 3 h. The culture was then harvested by centrifugation at 5,500 x g for 8 min and then resuspended in Buffer QA (20 mM Tris, 1 mM TCEP, pH 7.2) at a final volume of 10 mL per liter of culture grown. A final concentration of 1 mM phenylmethylsulfonyl fluoride (PMSF) protease inhibitor was added to the resuspended culture and then stored at -80 ˚C for up to one year.

Cells were thawed in a 37 ˚C water bath, and were lysed upon one freeze-thaw cycle due to the expression of T7 lysozyme from the pLysS plasmid from the cell line. Upon thawing, 2 mM of PMSF was added to the cell lysate and then genomic DNA from the lysate was clarified by the addition of 20 μL of 10 mg/mL DNase I (Worthington) per liter of cell culture followed by digestion for 30 min at 37 ˚C in a water bath. The lysate was clarified by centrifugation at 15,000 x g for 30 min, and the soluble protein was separated from the pellet and then filtered through a 0.22 μm membrane filter prior to purification.

An AKTA FPLC (GE Healthcare) was used to purify HypA protein from clarified cell lysate using a three-column protocol. In the first step, clarified lysate from 3 L of cell culture was combined and then diluted to 50 mL using Buffer QA. This was applied to a Q Sepharose Fast Flow (GE Healthcare) column (12 mL geometric column volume) that had been washed with Buffer QB (20 mM Tris, 1 M NaCl, 1 mM TCEP, pH 7.2) and then equilibrated with Buffer QA. The column was washed with four column volumes of 3% Buffer QB, and then the bound protein was eluted using a linear gradient of 3 – 30% Buffer QB over 10 column volumes, with the HypA protein eluting off the column at 15 – 23% Buffer QB. The remaining bound protein was removed by an additional 5 column volumes of 100% Buffer QB prior to re-equilibrating the column for more purification. Fractions from the Q Sepharose column that contain HypA protein were identified by 16% SDS-PAGE, and then pooled together for further purification.

Two additional columns were used to concentrate and then purify the HypA protein. The fractions from the Q Sepharose column that contained HypA were diluted to 50 mL (~3 times

dilution) with Buffer QA, and then applied onto a pre-packed 1 mL HiTrap QXL column (GE Healthcare) pre-washed with Buffer QB and then equilibrated with Buffer QA. The column was washed with 5 column volumes of 7% Buffer QB to remove loosely bound protein, and then HypA and other proteins were eluted in a single 3 mL fraction with 50% Buffer QB. The concentrated HypA proteins were further purified by using the HiLoad 16/60 Superdex 75 Prep Grade (GE Healthcare) gel filtration column (120 mL geometric column volume) pre-equilibrated with Buffer GF (20 mM HEPES, 200 mM NaCl, 1 mM TCEP, pH 7.2). HypA separates from other cellular proteins in a resolved peak centered around 95 mL. The purity of the HypA protein was confirmed by 16% SDS-PAGE and quantified using the Odyssey CLx Imaging System (LI-COR). Only protein samples with greater than 90% purity were used for experiments. The expressions of the desired HypA proteins were confirmed by LC-MS using an Agilent 1100 HPLC with a BioBasic-8 column (Thermo Scientific) and a QSTAR XL MS/MS system (Applied Biosystems). The theoretical mass of WT-HypA protein is 13202.2 Da and the experimental mass was determined to be 13202.03 Da. The theoretical mass of L2*-HypA protein is 13315.3 Da and the experimental mass was determined to be 13315.21 Da.

The concentration of HypA proteins in buffer was determined by the absorption at 280 nm using and extinction coefficient of 3250 M^{-1} cm^{-1} per monomer (previously determined by amino acid analysis as 6500 M^{-1} cm^{-1} per dimer[23]) using a Agilent/HP 8453 UV-Vis spectrophotometer. The metal content of purified HypA proteins was analyzed by ICP-OES and confirmed to contain approximately one zinc per protein for both WT- and L2*-HypA.

3.4.8 XAS sample preparation and data collection

Nickel complexes of HypA for XAS were prepared in Buffer XBr (20 mM HEPES, 200 mM NaBr, 1 mM TCEP, pH 7.2) or Buffer GF unless otherwise noted. For samples prepared in Buffer XBr, purified HypA proteins (>90% pure by SDS-PAGE) were diluted to between 100 – 250 μM in concentration (1.5 – 4 mL in volume) and then rapidly buffer exchanged into Buffer XBr using two consecutive 10 mL Zeba Spin Desalting columns with 7-kDa MWCO (Thermo

Fisher Scientific) and pre-equilibrated with Buffer XBr. The concentration of the HypA protein in Buffer XBr was measured again to account for any sample loss or dilution.

The metal content of a 10 mM $Ni(OAc)_2$ stock solution was confirmed by ICP-OES and then used for reconstituting the HypA protein in the desired buffer. A total of two molar-equivalents of $Ni(OAc)_2$ from the stock was added to the HypA protein in four aliquots at room temperature, allowing for 15 – 20 min equilibration between additions and an additional 30 min after the final metal addition to allow for proper metal binding. Chelex 100 (sodium form, Sigma) resin was added to the Ni-HypA complex at equal volume to the protein and gently agitated at room temperature for 45 min to remove any unbound Ni(II) ions from solution. The Ni-HypA complex was removed from the resin either by pipette or by filtration through a 0.22 μm membrane filter. The resulting Ni-HypA complex was concentrated using Amicon Ultra-0.5 mL 3-kDa MWCO (EMD Millipore) at 10,000 x g to 1 – 3 mM. The exact concentration of the HypA protein in the concentrated Ni-HypA complex was determined by absorption at 280 nm after treating with 15 mM EDTA for 10 min at 60˚C. The final metal content of the Ni-HypA complex was measured by ICP-OES and used to calculate the final Ni:Zn:HypA ratios, which were 1.1:1.0:1 for WT-HypA in Buffer XBr; 0.63:1.2:1 for WT-HypA in Buffer GF; 0.8:1.4:1 for L2*-HypA in both Buffer XBr and Buffer GF. The Ni content of the final flow through from Ni-HypA centrifugal concentrating was analyzed by ICP-OES and determined to be at least 500-folds less than the concentration of Ni in the Ni-HypA complex in each sample. The Ni-HypA complexes were mixed with sterile 80% glycerol to a final glycerol concentration of 11 – 15% as a glassing agent. The samples were loaded into Kapton-taped polycarbonate sample holders and then rapidly frozen in liquid nitrogen and then stored at -80˚C until ready for XAS data collection.

XAS at the Ni and Zn K-edges of WT- and L2*-HypA in Buffer XBr were collected at the National Synchrotron Light Source (NSLS) of the Brookhaven National Labs using the dedicated ring conditions and optics at beamline X3B. Ni and Zn K-edges of WT-HypA in Buffer GF were collected at the Stanford Synchrotron Radiation Lightsource (SSRL) at the SLAC

National Accelerator Laboratory using the dedicated ring conditions and optics at beamline 7-3. For XAS collected at NSLS, data were collected on frozen samples in kapton-taped polycarbonate holders immobilized in an aluminum sample clamp under vacuum and cooled to ~40 K with a helium displex cryostat. XAS was collected under ring conditions of 2.8 GeV and 120 – 300 mA with a sagittally focused Si (111) double crystal monochromator. X-ray fluorescence was collected with a 31-element Ge fluorescence detector (Canberra) with a 3 μm Z-1 filter installed between the detector and the sample to minimize scattering.

For XAS data collected at SSRL, frozen samples in kapton-taped polycarbonate holders were immobilized by aluminum prongs and cooled to ~10 K using a liquid helium cryostat. XAS was collected under ring conditions of 3 GeV and 450 – 500 mA with a Si (220) double-crystal monochromator. X-ray fluorescence data were collected with a 30-element Ge detector (Canberra) with a 3 μm Z-1 filter and Soller slits installed between the detector and the sample to minimize scattering.

X-ray fluorescence data for Ni and Zn K-edges of WT- and L2*-HypA were collected concurrently with the relevant metal foil in transmission mode for energy calibration. X-ray Absorption Near Edge Structure (XANES) data were collected from -200 to +200 eV relative to the metal K-edge, and Extended X-ray Absorption Fine Structure (EXAFS) were collected to 15*k* above the K-edge.

3.4.9 XAS data reduction and analysis

XAS data processing and normalization were performed using the Sixpack[71] software package for the Ni K-edge and the Athena program (part of the Demeter[72] suite of XAS analysis software package) for the Zn K-edge spectra. The data are an average of 8 – 10 scans at the Ni K-edges and 5 – 8 scans at the Zn K-edges. Fluorescence channels from each scan were visually scrutinized and bad channels were deleted. K-edge energy calibrations were performed for each scan by assigning the first inflection point in the first-derivative spectra of the metal foils to

8331.6 eV for Ni and 9660.7 eV for Zn. Additional energy alignments were performed for Zn K-edge spectra by aligning each subsequent scan of the Zn foil to the first scan using the auto align feature of Athena to correct for apparent monochromator slipping. The fluorescence channels from all scans were averaged, and the averaged spectra were normalized using the *AUTOBK*[73] algorithm. The normalization and background correction routine involved setting the K-edge energy (E_0) to 8340 eV for Ni and 9670 eV for Zn with a R_{bkg} of 1 and a *k*-weight of 3, and then normalizing the edge step to 1 between the pre-edge and post-edge. A linear or Gaussian function was used for fitting the pre-edge range of -200 to -50 eV and quadratic functions were used for fitting the post-edge range of -50 to +860 eV relative to E_0. The data were converted to *k*-space using the relationship $k = \left[\frac{2m_e(E-E_0)}{\hbar^2}\right]^{\frac{1}{2}}$, where m_e is the mass of the election and $\hbar$ is Plank's constant divided by 2π. The EXAFS data were extracted by setting a polynomial spline with 7 – 8 knots between the *k* range of 2 – 14 $Å^{-1}$, resulting in $\chi(k)$ data. The $\chi(k)$ data for Ni K-edge data or the normalized and background corrected spectra for Zn K-edge data were exported for further analysis and fitting using the Artemis program (part of Demeter[72]).

The XANES region of the Ni spectra were analysis for pre-edge peak areas using EXAFs123[74] as previously described.[12] Briefly, the baseline of the spectra were fitted with cubic function with the edge jump fitted to a 75% Gaussian and 25% Lorenzian function. Transitions occurring prior to the edge jump (~8 eV below E_0) were taken as the 1s→3d transition and fitted with a Gaussian function with the area under the curve taken as the pre-edge peak area. Additionally, 1s → $4p_z$ transitions were observed in some spectra but were not fitted accurately due to overlap with the rising edge.

EXAFS analysis were performed using the Artemis[72] software, which employs the IFEFFIT[75] engine to fit scattering paths to the conventional EXAFS equation (below) using phase and amplitude parameters generated by FEFF6[76]:

$$\chi(k) = \sum_j \frac{N_j f_j(k) e^{-2k^2\sigma_j^2}}{kr_j^2} \sin[2kr_j + \delta_j(k)] \quad \text{Eq. 3.1}$$

With respect to the neighbor scattering atom, *f(k)* is the scattering amplitude, and *δ(k)* is the phase-shift; *r* is the distance σ^2 is the mean-square disorder of the distance; *N* is the coordination number.

All data sets were fitted in *r*-space, where the $\chi(k)$ data were Fourier-transformed using the Hanning window function for *k* range of 2 – 14 $Å^{-1}$. For each model, an amplitude correction factor (S_0^2) set to 0.9 and a single value of E_0 was used, with the adjustable parameter of ΔE_0 at an initial value of 0 eV. A systematic combination of Ni-N/O, Ni-S, and Ni-Br scattering paths at distances (r_{eff}) between 1.8 and 2.3 Å were fitted to the data for approximation of the first coordination sphere. For each shell of scattering paths in a fit model, separate sets adjustable parameters: Δr_{eff} and σ^2 were used, with initial guess values of 0 Å and 0.003 $Å^2$ respectively.

The r-space data were fit to models built using a bottom-up approach that involved systematic combinations of integer numbers of N- and S-donor ligands, as well as possible Br^- or Cl^- ligation from the buffer. A total of up to seven ligands were fitted in the r = 1 – 2.5 Å range (roughly the first coordination sphere) using these combinations. The best fits from the first coordination combinations were then further refined by adding scattering atoms in the second and third coordination spheres that are ordered by metal-ligand bonds, and fit using multiple-scattering parameters to arrive at the best statistical (based on the R-factor, reduced χ^2, and σ^2) and scientifically sound fits. The best fits for the Ni site of HypA in XBr buffer were selected from an accumulation of 298 and 426 individual fits for WT and L2* respectively. The best fits for the Ni site of L2*-HypA in Buffer GF (NaCl) were selected from 309 individual fits.

Multiple-scattering ligands include His imidazoles and five-membered chelate rings that form when two adjacent backbone amide N-donors are ligated from the protein (BBAm). Multiple-scattering paths for imidazoles and BBAm five-membered chelate rings were calculated from coordinates obtained from high resolution protein crystal structures (less than 1.4 Å) from

the protein data bank (PDB). For each Ni-imidazole or Ni-BBAm FEFF calculation, scattering paths with amplitude ratio greater than 15% were used for fitting. Calculated multiple-scattering paths from either imidazole or BBAm shared the same adjustable distance (Δr_{eff}) and disorder (σ^2) parameters, effectively treating the entire multiple-scattering scaffold as a rigid entity where all the atoms move together as a unit. Due to this rigid treatment of fitting His-imidazole ligands, a change in angle of Ni-imidazole binding may cause dramatic changes in the disorder parameter (σ^2) associated with the scattering scaffold. To compensate for this, metal-imidazole scattering is fitted using FEFF paths calculated for imidazole binding at two different tilt angles (α) with respect to the absorbing metal. Ni-imidazole with tilt angles of 0˚ and 7˚ were obtained from PDB ID 1Q5Y,[36] as depicted in Figure 3.6, and Zn-imidazole at α=2˚ and α=8˚ originated from PDB ID 1Q0E.[77] With ordered atoms at three bonds away from the absorber, metal-imidazole scattering have characteristic intensities visible at ~4Å in the non-phase corrected *r*-space data, which is absent from multiple scattering from bidentate backbone amide binding (see Figure 3.6). Therefore, a separate FEFF calculation was performed to generate multiple scatting paths for bidentate binding of backbone amides from the polypeptide chain to the Ni absorbing atom (Ni-BBAm) using coordinates originated from PDB ID 1T6U[37] (Figure 3.7). The number of His-imidazoles bound to the absorbing metal atom is increased by integer numbers using the same bottom-up approach to improve the final fitting model. The Ni-BBAm multiple scattering scaffold was used to replace of two Ni-N/O ligands in select fits to improve/refine the final fitting model.

To evaluate goodness of fit between different fitting models, IFEFFIT minimizes three different fit parameters: *R*-factor, χ^2, and *Reduced* χ^2. The *R*-factor evaluates the misfit relative to the data size and is defined as:

$$R = \frac{\sum_{i=1}^{N}\left\{\left[Re\left(\chi_{data}(r_i)-\chi_{model}(r_i)\right)\right]^2+\left[Im\left(\chi_{data}(r_i)-\chi_{model}(r_i)\right)\right]^2\right\}}{\sum_{i=1}^{N}\left\{\left[Re\left(\chi_{data_i}(r_i)\right)\right]^2+\left[Im\left(\chi_{data}(r_i)\right)\right]^2\right\}} \qquad \text{Eq. 3.2}$$

Where $\chi(r_i)$is the Fourier-transformed EXAFS data or model function, *Re( )* is the real, and *Im( )* is the imaginary parts of the EXAFS Fourier transform. The *R*-factor is directly proportional to the statistical parameter χ^2 and related to the $Reduced\ \chi^2$, which are defined as:

$$\chi^2 = \frac{N_{idp}}{N_{pt}\varepsilon^2}\sum_{i=1}^{N}\left\{\left[Re\left(\chi_{data}(r_i) - \chi_{model}(r_i)\right)\right]^2 + \left[Im\left(\chi_{data}(r_i) - \chi_{model}(r_i)\right)\right]^2\right\} \quad \text{Eq. 3.3}$$

$$Reduced\ \chi^2 = \frac{\chi^2}{N_{idp} - N_{var}} \quad \text{Eq. 3.4}$$

N_{idp} is the number of independent data points defined as $N_{idp} \cong {(2\Delta r \Delta k)}/{\pi}$, with Δr as the fitting range in *r*-space, Δk is the fitting range in *k*-space. N_{pt} is the number point in the fitting range, ε is the estimated uncertainty of the data, and N_{var} is the number of adjustable parameters in the model. *R*-factor and $Reduced\ \chi^2$ were both considered in comparing different models fit to the same $\chi(r)$ data. Whereas increasing the number of adjustable parameters would generally improve the *R*-factor, the $Reduced\ \chi^2$ would go through a minimum and then increase indicating the model is overfitting the data.[75]

3.4.10 Isothermal titration calorimetry (ITC)

ITC was used to measure the heat released by Ni-binding to HypA proteins, and the protein-protein interactions between HypA and UreE using the Auto-ITC200 (Microcal/Malvern). The instrument has a cell volume of 200 μL and a syringe volume of 40 μL, which were filled by robotic arms from plates stored at 4˚C prior to the start of the experiment. All titrations were performed in Buffer GF (20 mM HEPES, 200 mM NaCl, 1 mM TCEP, pH 7.2) at 25˚C with the reference cell filled with Buffer GF. All purified proteins (WT- and L2*-HypA and WT-UreE) used for titrations were confirmed to be greater than 90% pure by SDS-PAGE. Concentrated proteins were rapidly buffer exchanged into Buffer GF using 0.5 mL Zeba Spin Desalting columns with 7-kDa MWCO pre-equilibrated with Buffer GF and then diluted to the appropriate concentration as needed for titration immediately before ITC experiments. The Zn:HypA ratios were confirmed by ICP-OES to be between 0.8 – 1.0 in all proteins used for ITC, and metal:WT-

UreE ratio were confirmed to be less than 0.05 (Ni or Zn) in all ITC experiments. For Ni to HypA titrations, $NiCl_2$ was dissolved in MilliQ water from a 500-mM stock solution and then diluted into Buffer GF at the appropriate concentrations for ITC experiments (~1.5 – 2.5 mM). The exact concentrations of Ni in Buffer GF used for titrations were confirmed by ICP-OES and used for fitting the data.

For each ITC experiment, 20 injections were made from the syringe into the cell and the change in heat was monitored by the instrument. The initial injection contained only 0.4 μL and was used to minimize the equilibration artifacts sometimes observed with the first injection and was not included in fitting the data. All subsequent injections at 2.0 μL each were used for fitting the titration curve in each experiment. For Ni titration into WT-HypA, the spacing between injections were set to 1,500 sec due to initial observations of a slow return to baseline. For Ni titration into L2*-HypA the spacing between injections were reduced to 600 sec. For WT-HypA or L2*-HypA titrations into WT-UreE dimer, the spacing between injections were further reduced to 240 sec. Experimental titrations were accompanied by corresponding reference/control titrations of the titrants (either Ni or HypA protein) into Buffer GF in the cell, the resulting heats of which were used to establish the corresponding baseline corrections used for fitting the ΔH data. Experimental titrations were performed at least twice using separately prepared proteins and each produced similar result.

The resulting data were fitted using the MicroCal analysis module in Origin7.0. First, the heat released from titration experiments were baseline corrected and then integrated to produce the corresponding ΔH curve. The ΔH curve for each experiment was corrected by subtracting the average ΔH from the reference titration. The ΔH curve was fitted with the OneSite model to find the apparent K_a (multiple fitting models were attempted for each set of experimental data and in each case the OneSite model produced the best χ^2 value). The apparent K_d values reported are the inverse of the K_a values obtained from each fit.

3.4.11 UV-Vis absorption for Ni-HypA titration

For Ni-titration into Apo-ZnHypA protein monitored by UV-Vis, a series of samples were prepared with equal concentration of HypA protein (~50 μM) and varying concentrations of Ni (400 – 1 μM) in Buffer UV (20 mM HEPES, 200 mM NaCl, pH 7.2). First, concentrated Apo-ZnWT-HypA and L2*-HypA were rapidly desalted into Buffer UV and the Zn:HypA ratio were confirmed by ICP-OES to be 0.8 in each sample. Proteins were diluted to ~50-70 μM using Buffer UV and then equal volumes were distributed to separate 1.7-mL centrifuge tubes. The $NiCl_2$ used for the experiment was diluted to 10 mM in Buffer UV (from a 500-mM stock in water), with the actual concentration of the Ni confirmed by ICP-OES. Decreasing concentrations of Ni in Buffer UV were serially diluted (2:3 and 1:1) from the 10-mM stock. For WT-HypA, 5 μL of the serially diluted $NiCl_2$ solution was added to 115 μL of ~50 μM producing a 12-point dilution series with the final Ni concentration ranging from 400 μM to 1.10 μM. For L2*-HypA, 30 μL of the serially diluted $NiCl_2$ solution was added to 90 μL of ~70 μM of protein 15-point dilution series with Ni concentration ranging from 2.4mM to 1.48 μM (Ni-L2*-HypA samples beyond 271 μM precipitated prior to data collection). Equal volumes of Buffer UV alone were added to each respective HypA aliquot to produce the Apo-ZnHypA background in each series. From this, the final concentration of WT- and L2*-HypA in the Ni-titration series were determined to be 49.1 μM and 51.9 μM respectively. All samples were gently agitated at room temperature for one hour prior to UV-Vis measurement using an Agilent/HP 8453 UV-Vis spectrophotometer. The respective Apo-ZnHypA spectra of the of WT- and L2*- were subtracted from each of the spectra in the Ni-HypA titration series producing the difference spectra with Ni-dependent increases in absorption observed at 269 nm and 244 nm, respectively. These Δ-absorbance for Ni-WT- and Ni-L2*-HypA were graphed against the concentrations of Ni in each dilution series to produce the titration curve. The titration curve was fitted with the quadratic from of the mass action function using the following equation:

$$f(M) = P_{free} + \frac{PM - P_{free}}{2} * \left(P + M + K_d - \sqrt{(P + M + K_d)^2 - 4 * P * M}\right) \quad \text{Eq. 3.5}$$

with the adjustable parameters of *M* as the concentration of Ni, P_{free} is the fraction of Apo-ZnHypA, *PM* is the fraction of Ni-ZnHypA, and *P* is the concentration of total HypA (which is constant and fixed to 49.1 and 51.9 μM for WT and L2*-HypA respectively). Leaving the apparent dissociation constant, K_d, as the only unknown in the equations.

3.4.12 Magnetic susceptibility

Magnetic susceptibility of the Ni binding site in WT-HypA and L2* protein was assessed by Evans method with slight modification from previously described.[8] All samples and standards were prepared in a D_2O buffer containing 20 mM HEPES, 200 mM NaCl, 1mM TCEP, pD 7.1, filtered (0.22 μm membrane). $NiCl_2$ in buffer was used as a paramagnetic standard and $K_2Ni(CN)_4$ in buffer was used as a diamagnetic standard to determine the effective magnetic moment (μ_{eff}) from 1mM of paramagnetic Ni(II). Protein samples were prepared by buffer exchanging the WT- or L2*- Apo-ZnHypA protein into the D_2O buffer. Metallation of proteins were performed as described in the XAS sample preparation (Section 3.4.8) using $NiCl_2$ stocks dissolved in D_2O buffer, and then concentrated to 1.14 mM and 1.28mM respectively for Ni-ZnWT-HypA and Ni-ZnL2*-HypA. The metal concentrations of Standards and proteins samples were confirmed by metal analysis using ICP-OES. The final Ni:Zn:HypA ratios for Ni-ZnWT-HypA was 0.97:0.7:1, and for Ni-ZnL2*-HypA was 1.05:0.75:1.

Evans method was performed by collecting ^1H NMR on samples concurrently with the reference D_2O buffer on a Bruker Avance III 400 instrument. The standards or samples were placed in NMR tubes with a coaxial insert (Wilmad-LabGlass) filled with the reference D_2O buffer. Separation in the HDO peak (in Hz) was used to confirm the presence of a paramagnetic metal site (where a single HDO peak was observed for diamagnetic samples) and to calculate the μ_{eff} in each sample. Diamagnetic corrections of ligands in protein samples were determined from

WT- and L2*-Apo-ZnHypA samples. The following equations were used to calculate the paramagnetic properties of Ni sites in WT-Ni-ZnHypA:

$$\chi_g = \frac{-3\,\Delta\nu}{4\,\pi\,\nu_0\,m} + \chi_0 \quad \text{Eq. 3.6}$$

$$\chi_M = \chi_g\,M \quad \text{Eq. 3.7}$$

$$\chi_M^* = \chi_M - \sum\chi_L \quad \text{Eq. 3.8}$$

$$\mu_{eff} = 2.83\sqrt{\chi_M^*\,T} \quad \text{Eq. 3.9}$$

Given χ_g is the mass susceptibility of the metal ion, $\Delta\nu$ is the peak separation (Hz); ν_0 is the frequency of the spectrometer (Hz); m is the concentration of the sample (g/mL); χ_0 is the mass susceptibility of solvent (csg); M is the compound molecular weight (g/mol); χ_M* is the molar susceptibility of the metal ion; χ_L is diamagnetic correction for ligands; μ_{eff} is the effective magnetic moment; T is the absolute temperature (K).

3.4.13 Circular dichroism

Circular Dichroism (CD) spectroscopy of purified HypA proteins was performed on a Jasco J-715 spectropolarimeter. All spectra were taken of 20μM purified HypA proteins (> 90 %) loaded into quartz cuvettes with a 1mm path length in buffer with 10mM Tris, 100mM NaCl, 1mM TCEP, pH 7.2. Ni-bound protein was prepared using the same method as described for XAS sample preparation and the Ni:Zn:HypA ratio for WT was 1.0:0.74:1.0; and for L2* was 0.75:0.94:1.0. An average of four scans were taken of each sample at 20 ˚C with scan speeds of 20nm/min and step size of 2nm. Spectra of buffer alone were also taken using the same scan parameters using the same cuvette and then subtracted from the protein spectra to produce the final figure as shown in Figure 3.4.

3.4.14 Size Exclusion Chromatography/Multi-Angle Light Scattering (SEC-MALS)

SEC-MALS was performed using a combination of an Agilent HPLC running a Superdex 75 10/300GL (GE Healthcare Life Sciences) attached to the DAWN HELEOS II (Wyatt Technology) and the Optilab T-rEX (Wyatt Technology). Experiments were performed at 25 ˚C,

with the system was equilibrated with Buffer GF (20 mM HEPES, 200 mM NaCl, 1mM TCEP, pH 7.2) at 0.2 mL/min and then purified HypA protein was injected at 100 μL of 98 μM for L2*-HypA and 100 μL of 120 μM for WT-HypA. Proteins eluting off the column were monitored by UV absorbance (280 nm) on the HPLC, and for multi-angle (16 angles ranging from 13 – 157.8˚) light scattering with the DAWN HELEOS II at 664nm, as well as for RI with the Optilab T-tEX at 658 nm. Peak data were processed using the Astra 6 software package (Wyatt) with light-scattering peaks fitted with the Zimm model with a dn/dc value of 0.185 ml/g (typically recommended value for a range of proteins by Wyatt manual) to deduce the absolute mass of the peak. To ensure that the data processing method used was accurate in measuring the absolute mass of the proteins, the experiment and data processing procedures were used to calculate the mass of bovine serum albumin (expected 66.5 kDa, SEC-MALS 66.2 kDa), *H. pylori* HypB (expected 27.2 kDa, SEC-MALS 27.1 kDa), and *H. pylori* UreE dimer (expected 38.8 kDa, SEC-MALS 39.7 kDa), all of which were accurate in calculating the molecular weight of the peak.

Additionally, the same LC method was used to calculate the elution volume of known molecular weight standards (Sigma) for gel filtration chromatography using blue dextran (void volume), albumin (66 kDa), carbonic anhydrase (29 kDa), cytochrome C (12.4 kDa), and aprotinin (6.5 kDa). The elution volumes of each protein standard were used to construct a calibration curve for protein molecular weights, by which HypA protein was measured. Using this traditional calibration curve for size exclusion chromatography obtained from retention times of molecular weight standards WT- and L2*-HypA was calculated to have an apparently molecular weight of 21.7 and 22.7 kDa (data not shown), which is consistent with a dimeric quaternary structure. However, MALS analysis calculates the mass of HypA WT and L2* to be 13.01 ± 0.007 and 13.37 ± 0.021 kDa respectively (Figure 3.4), which is consistent with monomeric HypA. Additional SEC-MALS experiments of other proteins including BSA, *H.*

pylori HypB, and UreE confirms that MALS analysis correctly calculates the molecular weights of globular proteins (data not shown).

3.4.15 Inductively Coupled Plasma Optical Emission Spectrometry (ICP-OES)

Metal analysis was performed on protein samples and metal solutions using a Perkin-Elmer Optima DV4300 ICP-OES instrument. The instrument was blanked with MilliQ water and then calibrated with 0.1 – 10.0 ppm standards of Ni, Cu, and Zn diluted from known ICP analytical standards (Sigma) in MilliQ water to ensure linearity and consistency in response. Metal solutions samples were prepared by diluting the stock solution to an expected metal content between 1.0 – 3.0 ppm with a known amount of MilliQ water. The ratio of the actual metal content of the sample to the expected metal content multiplied by the expected metal concentration and dilution factor is taken as the actual concentration of the stock solution. Protein samples were prepared by first accurately measuring the protein concentration, and then diluting the sample to an expected metal content of 0.5 – 1.0 ppm metal (assuming 1:1 binding of protein-to-metal) with a known amount of MilliQ water. The ratio of the actual metal content of the protein sample to the expected metal content of the sample is taken as the metal:protein ratio.

3.5 References

1. Olson, J. W., Mehta, N. S., and Maier, R. J. (2001) Requirement of nickel metabolism proteins HypA and HypB for full activity of both hydrogenase and urease in Helicobacter pylori, *Molecular microbiology 39*, 176-182

2. Higgins, K. A., Carr, C. E., and Maroney, M. J. (2012) Specific metal recognition in nickel trafficking, *Biochemistry 51*, 7816-7832. (10.1021/bi300981m)

3. Benoit, S. L., McMurry, J. L., Hill, S. A., and Maier, R. J. (2012) Helicobacter pylori hydrogenase accessory protein HypA and urease accessory protein UreG compete with each other for UreE recognition, *Biochimica et biophysica acta 1820*, 1519-1525. (10.1016/j.bbagen.2012.06.002)

4. Benoit, S. L., Mehta, N., Weinberg, M. V., Maier, C., and Maier, R. J. (2007) Interaction between the Helicobacter pylori accessory proteins HypA and UreE is needed for urease maturation, *Microbiology 153*, 1474-1482. (10.1099/mic.0.2006/003228-0)

5. Yang, X., Li, H., Lai, T. P., and Sun, H. (2015) UreE-UreG complex facilitates nickel transfer and preactivates GTPase of UreG in Helicobacter pylori, *The Journal of biological chemistry 290*, 12474-12485. (10.1074/jbc.M114.632364)

6. Yang, X., Li, H., Cheng, T., Xia, W., Lai, Y. T., and Sun, H. (2014) Nickel translocation between metallochaperones HypA and UreE in Helicobacter pylori, *Metallomics : integrated biometal science 6*, 1731-1736. (10.1039/c4mt00134f)

7. Mehta, N., Olson, J. W., and Maier, R. J. (2003) Characterization of Helicobacter pylori Nickel Metabolism Accessory Proteins Needed for Maturation of both Urease and Hydrogenase, *Journal of bacteriology 185*, 726-734. (10.1128/jb.185.3.726-734.2003)

8. Kennedy, D. C., Herbst, R. W., Iwig, J. S., Chivers, P. T., and Maroney, M. J. (2007) A dynamic Zn site in Helicobacter pylori HypA: A potential mechanism for metal-specific protein activity, *J Am Chem Soc 129*, 16-17. (Doi 10.1021/Ja066958x)

9. Herbst, R. W., Perovic, I., Martin-Diaconescu, V., O'Brien, K., Chivers, P. T., Pochapsky, S. S., Pochapsky, T. C., and Maroney, M. J. (2010) Communication between the Zinc and Nickel Sites in Dimeric HypA: Metal Recognition and pH Sensing, *J Am Chem Soc 132*, 10338-10351. (Doi 10.1021/Ja1005724)

10. Xia, W., Li, H. Y., Sze, K. H., and Sun, H. Z. (2009) Structure of a Nickel Chaperone, HypA, from Helicobacter pylori Reveals Two Distinct Metal Binding Sites, *J Am Chem Soc 131*, 10031-10040. (Doi 10.1021/Ja900543y)

11. Johnson, R. C., Hu, H. Q., Merrell, D. S., and Maroney, M. J. (2015) Dynamic HypA zinc site is essential for acid viability and proper urease maturation in Helicobacter pylori, *Metallomics : integrated biometal science 7*, 674-682. (10.1039/c4mt00306c)

12. Higgins, K. A., Chivers, P. T., and Maroney, M. J. (2012) Role of the N-terminus in determining metal-specific responses in the E. coli Ni- and Co-responsive metalloregulator, RcnR, *J Am Chem Soc 134*, 7081-7093. (10.1021/ja300834b)

13. Ryan, K. C., Guce, A. I., Johnson, O. E., Brunold, T. C., Cabelli, D. E., Garman, S. C., and Maroney, M. J. (2015) Nickel superoxide dismutase: structural and functional roles of His1 and its H-bonding network, *Biochemistry 54*, 1016-1027. (10.1021/bi501258u)

14. Hu, H. Q., Johnson, R. C., Merrell, D. S., and Maroney, M. J. (2017) Nickel Ligation of the N-Terminal Amine of HypA Is Required for Urease Maturation in Helicobacter pylori, *Biochemistry 56*, 1105-1116. (10.1021/acs.biochem.6b00912)

15. Baltrus, D. A., Amieva, M. R., Covacci, A., Lowe, T. M., Merrell, D. S., Ottemann, K. M., Stein, M., Salama, N. R., and Guillemin, K. (2009) The complete genome sequence of Helicobacter pylori strain G27, *J Bacteriol 191*, 447-448. (10.1128/JB.01416-08)

16. Blum, F. C., Hu, H. Q., Servetas, S. L., Benoit, S. L., Maier, R. J., Maroney, M. J., and Merrell, D. S. (2017) Structure-function analyses of metal-binding sites of HypA reveal residues important for hydrogenase maturation in Helicobacter pylori, *PloS one 12*, e0183260. (10.1371/journal.pone.0183260)

17. Joyce, E. A., Gilbert, J. V., Eaton, K. A., Plaut, A., and Wright, A. (2001) Differential gene expression from two transcriptional units in the cag pathogenicity island of Helicobacter pylori, *Infection and immunity 69*, 4202-4209. (10.1128/IAI.69.7.4202-4209.2001)

18. Mehta, N., Olson, J. W., and Maier, R. J. (2003) Characterization of Helicobacter pylori nickel metabolism accessory proteins needed for maturation of both urease and hydrogenase, *Journal of bacteriology 185*, 726-734

19. Olson, J. W., and Maier, R. J. (2002) Molecular hydrogen as an energy source for Helicobacter pylori, *Science 298*, 1788-1790. (10.1126/science.1077123)

20. Wang, G., Romero-Gallo, J., Benoit, S. L., Piazuelo, M. B., Dominguez, R. L., Morgan, D. R., Peek, R. M., Jr., and Maier, R. J. (2016) Hydrogen Metabolism in Helicobacter pylori Plays a Role in Gastric Carcinogenesis through Facilitating CagA Translocation, *MBio 7*. (10.1128/mBio.01022-16)

21. Maier, R. J., Benoit, S. L., and Seshadri, S. (2007) Nickel-binding and accessory proteins facilitating Ni-enzyme maturation in Helicobacter pylori, *Biometals : an international journal on the role of metal ions in biology, biochemistry, and medicine 20*, 655-664. (10.1007/s10534-006-9061-8)

22. Watanabe, S., Arai, T., Matsumi, R., Atomi, H., Imanaka, T., and Miki, K. (2009) Crystal structure of HypA, a nickel-binding metallochaperone for [NiFe] hydrogenase maturation, *Journal of molecular biology 394*, 448-459. (10.1016/j.jmb.2009.09.030)

23. Herbst, R. W. (2010) Structure and Function in a Nickel Metallochaperone, HypA and Nickel Dependent Superoxide Dismutase, In *Department of Chemistry*, p 184, University of Massachusetts Amherst, UMASS Amherst.

24. Andersson, M., Wittgren, B., and Wahlund, K. G. (2003) Accuracy in multiangle light scattering measurements for molar mass and radius estimations. Model calculations and experiments, *Anal Chem 75*, 4279-4291

25. Colpas, G. J., Maroney, M. J., Bagyinka, C., Kumar, M., Willis, W. S., Suib, S. L., Baidya, N., and Mascharak, P. K. (1991) X-Ray Spectroscopic Studies of Nickel-Complexes, with Application to the Structure of Nickel Sites in Hydrogenases, *Inorg Chem 30*, 920-928. (Doi 10.1021/Ic00005a010)

26. Lewis, J., and Wilkins, R. G. (1960) *Modern coordination chemistry: principles and methods*, Interscience Publishers, New York,.

27. Evans, D. F. (1959) The Determination of the Paramagnetic Susceptibility of Substances in Solution by Nuclear Magnetic Resonance, *J Chem Soc*, 2003-2005. (Doi 10.1039/Jr9590002003)

28. Schubert, E. M. (1992) Utilizing the Evans Method with a Superconducting Nmr Spectrometer in the Undergraduate Laboratory, *J Chem Educ 69*, 62-62

29. Yano, J., and Yachandra, V. K. (2009) X-ray absorption spectroscopy, *Photosynthesis research 102*, 241-254. (10.1007/s11120-009-9473-8)

30. Banaszak, K., Martin-Diaconescu, V., Bellucci, M., Zambelli, B., Rypniewski, W., Maroney, M. J., and Ciurli, S. (2012) Crystallographic and X-ray absorption spectroscopic characterization of Helicobacter pylori UreE bound to Ni(2)(+) and Zn(2)(+) reveals a role for the disordered C-terminal arm in metal trafficking, *The Biochemical journal 441*, 1017-1026. (10.1042/BJ20111659)

31. Martin-Diaconescu, V., Bellucci, M., Musiani, F., Ciurli, S., and Maroney, M. J. (2012) Unraveling the Helicobacter pylori UreG zinc binding site using X-ray absorption spectroscopy (XAS) and structural modeling, *Journal of biological inorganic chemistry : JBIC : a publication of the Society of Biological Inorganic Chemistry 17*, 353-361. (10.1007/s00775-011-0857-9)

32. Giri, N. C., Sun, H., Chen, H., Costa, M., and Maroney, M. J. (2011) X-ray absorption spectroscopy structural investigation of early intermediates in the mechanism of DNA repair by human ABH2, *Biochemistry 50*, 5067-5076. (10.1021/bi101668x)

33. Giri, N. C. (2013) Structural Investigations of Early Intermediates and Nickel Inhibition Complexes of Human DNA and Histone Demethylases, In *Chemistry*, p 343, University of Massachusetts Amherst, UMASS Amherst.

34. Ryan, K. C. (2013) Investigation of the Structure/Function Relationship in Nickel Containing Superoxide Dismutase, In *Chemistry*, p 259, University of Massachusetts Amherst, UMASS Amherst.

35. Campecino, J. O., Dudycz, L. W., Tumelty, D., Berg, V., Cabelli, D. E., and Maroney, M. J. (2015) A Semisynthetic Strategy Leads to Alteration of the Backbone Amidate Ligand in the NiSOD Active Site, *J Am Chem Soc 137*, 9044-9052

36. Schreiter, E. R., Sintchak, M. D., Guo, Y., Chivers, P. T., Sauer, R. T., and Drennan, C. L. (2003) Crystal structure of the nickel-responsive transcription factor NikR, *Nature structural biology 10*, 794-799. (10.1038/nsb985)

37. Barondeau, D. P., Kassmann, C. J., Bruns, C. K., Tainer, J. A., and Getzoff, E. D. (2004) Nickel superoxide dismutase structure and mechanism, *Biochemistry 43*, 8038-8047. (10.1012/bi0496081)

38. Olson, J. W., Mehta, N. S., and Maier, R. J. (2001) Requirement of nickel metabolism proteins HypA and HypB for full activity of both hydrogenase and urease in Helicobacter pylori (vol 39, pg 176, 2001), *Molecular microbiology 40*, 270-270. (DOI 10.1046/j.1365-2958.2001.02397.x)

39. Bellucci, M., Zambelli, B., Musiani, F., Turano, P., and Ciurli, S. (2009) Helicobacter pylori UreE, a urease accessory protein: specific Ni(2+)- and Zn(2+)-binding properties and interaction with its cognate UreG, *The Biochemical journal 422*, 91-100. (10.1042/BJ20090434)

40. Shi, R., Munger, C., Asinas, A., Benoit, S. L., Miller, E., Matte, A., Maier, R. J., and Cygler, M. (2010) Crystal structures of apo and metal-bound forms of the UreE protein from Helicobacter pylori: role of multiple metal binding sites, *Biochemistry 49*, 7080-7088. (10.1021/bi100372h)

41. Fischer, F., and De Reuse, H. (2016) Adaptation of *Helicobacter pylori* Metabolism to Persistent Gastric Colonization, In *Helicobacter pylori Research From Bench to Bedside* (Steffen Backert, Y. Y., Ed.), pp 29-56, Springer, Japan.

42. Stingl, K., and De Reuse, H. (2005) Staying alive overdosed: how does Helicobacter pylori control urease activity?, *International journal of medical microbiology : IJMM 295*, 307-315. (10.1016/j.ijmm.2005.06.006)

43. Farrugia, M. A., Macomber, L., and Hausinger, R. P. (2013) Biosynthesis of the Urease Metallocenter, *Journal of Biological Chemistry 288*, 13178-13185. (10.1074/jbc.R112.446526)

44. Bauerfeind, P., Garner, R., Dunn, B. E., and Mobley, H. L. T. (1997) Synthesis and activity of Helicobacter pylori urease and catalase at low pH, *Gut 40*, 25-30

45. Watanabe, S., Kawashima, T., Nishitani, Y., Kanai, T., Wada, T., Inaba, K., Atomi, H., Imanaka, T., and Miki, K. (2015) Structural basis of a Ni acquisition cycle for [NiFe] hydrogenase by Ni-metallochaperone HypA and its enhancer, *Proc Natl Acad Sci U S A 112*, 7701-7706. (10.1073/pnas.1503102112)

46. Bacarizo, J., Martinez-Rodriguez, S., Martin-Garcia, J. M., Andujar-Sanchez, M., Ortiz-Salmeron, E., Neira, J. L., and Camara-Artigas, A. (2014) Electrostatic Effects in the Folding of the SH3 Domain of the c-Src Tyrosine Kinase: pH-Dependence in 3D-Domain Swapping and Amyloid Formation, *PloS one 9*

47. Harford, C., and Sarkar, B. (1997) Amino terminal Cu(II)- and Ni(II)-binding (ATCUN) motif of proteins and peptides: Metal binding, DNA cleavage, and other properties, *Accounts Chem Res 30*, 123-130

48. Bal, W., Sokolowska, M., Kurowska, E., and Faller, P. (2013) Binding of transition metal ions to albumin: Sites, affinities and rates, *Bba-Gen Subjects 1830*, 5444-5455

49. Neupane, K. P., Aldous, A. R., and Kritzer, J. A. (2014) Macrocyclization of the ATCUN motif controls metal binding and catalysis, *Abstr Pap Am Chem S 247*

50. Sankararamakrishnan, R., Verma, S., and Kumar, S. (2005) ATCUN-like metal-binding motifs in proteins: Identification and characterization by crystal structure and sequence analysis, *Proteins 58*, 211-221

51. Kritzer, J. A., Neupane, K. P., and Aldous, A. R. (2013) Design of Macrocyclic ATCUN Peptides as Redox Catalysts, *Biopolymers 100*, 281-281

52. Chung, K. C. C., Cao, L., Dias, A. V., Pickering, I. J., George, G. N., and Zamble, D. B. (2008) A High-Affinity Metal-Binding Peptide from Escherichia coli HypB, *J Am Chem Soc 130*, 14056-+

53. Choudhury, S. B., Lee, J. W., Davidson, G., Yim, Y. I., Bose, K., Sharma, M. L., Kang, S. O., Cabelli, D. E., and Maroney, M. J. (1999) Examination of the nickel site structure and reaction mechanism in Streptomyces seoulensis superoxide dismutase, *Biochemistry 38*, 3744-3752. (10.1021/bi982537j)

54. Wuerges, J., Lee, J. W., Yim, Y. I., Yim, H. S., Kang, S. O., and Djinovic Carugo, K. (2004) Crystal structure of nickel-containing superoxide dismutase reveals another type of active site, *Proc Natl Acad Sci U S A 101*, 8569-8574. (10.1073/pnas.0308514101)

55. van Vliet, A. H., Kuipers, E. J., Waidner, B., Davies, B. J., de Vries, N., Penn, C. W., Vandenbroucke-Grauls, C. M., Kist, M., Bereswill, S., and Kusters, J. G. (2001) Nickel-responsive induction of urease expression in Helicobacter pylori is mediated at the transcriptional level, *Infect Immun 69*, 4891-4897. (10.1128/IAI.69.8.4891-4897.2001)

56. Contreras, M., Thiberge, J. M., Mandrand-Berthelot, M. A., and Labigne, A. (2003) Characterization of the roles of NikR, a nickel-responsive pleiotropic autoregulator of Helicobacter pylori, *Molecular microbiology 49*, 947-963

57. Bury-Mone, S., Skouloubris, S., Labigne, A., and De Reuse, H. (2001) The Helicobacter pylori UreI protein: role in adaptation to acidity and identification of residues essential for its activity and for acid activation, *Molecular microbiology 42*, 1021-1034

58. Scott, D. R., Marcus, E. A., Weeks, D. L., and Sachs, G. (2002) Mechanisms of acid resistance due to the urease system of Helicobacter pylori, *Gastroenterology 123*, 187-195

59. Mehta, N., Benoit, S., and Maier, R. J. (2003) Roles of conserved nucleotide-binding domains in accessory proteins, HypB and UreG, in the maturation of nickel-enzymes required for efficient Helicobacter pylori colonization, *Microbial Pathogenesis 35*, 229-234. (10.1016/s0882-4010(03)00151-7)

60. Carter, E. L., Flugga, N., Boer, J. L., Mulrooney, S. B., and Hausinger, R. P. (2009) Interplay of metal ions and urease, *Metallomics : integrated biometal science 1*, 207-221. (10.1039/b903311d)

61. Benoit, S., and Maier, R. J. (2003) Dependence of Helicobacter pylori Urease Activity on the Nickel-Sequestering Ability of the UreE Accessory Protein, *Journal of bacteriology 185*, 4787-4795. (10.1128/jb.185.16.4787-4795.2003)

62. Baltrus, D. A., Amieva, M. R., Covacci, A., Lowe, T. M., Merrell, D. S., Ottemann, K. M., Stein, M., Salama, N. R., and Guillemin, K. (2009) The Complete Genome Sequence of Helicobacter pylori Strain G27, *Journal of bacteriology 191*, 447-448. (10.1128/Jb.01416-08)

63. Joyce, E. A., Gilbert, J. V., Eaton, K. A., Plaut, A., and Wright, A. (2001) Differential gene expression from two transcriptional units in the cag pathogenicity island of Helicobacter pylori, *Infection and Immunity 69*, 4202-4209

64. Copass, M., Grandi, G., and Rappuoli, R. (1997) Introduction of unmarked mutations in the Helicobacter pylori vacA gene with a sucrose sensitivity marker, *Infection and immunity 65*, 1949-1952

65. Horton, R. M., Ho, S. N., Pullen, J. K., Hunt, H. D., Cai, Z., and Pease, L. R. (1993) Gene splicing by overlap extension, *Methods in enzymology 217*, 270-279

66. Herbst, R. W., Perovic, I., Martin-Diaconescu, V., O'Brien, K., Chivers, P. T., Pochapsky, S. S., Pochapsky, T. C., and Maroney, M. J. (2010) Communication between the zinc and nickel sites in dimeric HypA: metal recognition and pH sensing, *Journal of the American Chemical Society 132*, 10338-10351. (10.1021/ja1005724)

67. Horton, R. M., Ho, S. N., Pullen, J. K., Hunt, H. D., Cai, Z. L., and Pease, L. R. (1993) Gene-Splicing by Overlap Extension, *Method Enzymol 217*, 270-279

68. McGee, D. J., May, C. A., Garner, R. M., Himpsl, J. M., and Mobley, H. L. (1999) Isolation of Helicobacter pylori genes that modulate urease activity, *Journal of bacteriology 181*, 2477-2484

69. Weatherb.Mw. (1967) Phenol-Hypochlorite Reaction for Determination of Ammonia, *Analytical chemistry 39*, 971-&. (Doi 10.1021/Ac60252a045)

70. Hendrickson, W. A., Horton, J. R., and Lemaster, D. M. (1990) Selenomethionyl Proteins Produced for Analysis by Multiwavelength Anomalous Diffraction (Mad) - a Vehicle for Direct Determination of 3-Dimensional Structure, *Embo J 9*, 1665-1672

71. Webb, S. M. (2005) SIXpack: a graphical user interface for XAS analysis using IFEFFIT, *Phys Scripta T115*, 1011-1014

72. Ravel, B., and Newville, M. (2005) ATHENA, ARTEMIS, HEPHAESTUS: data analysis for X-ray absorption spectroscopy using IFEFFIT, *Journal of synchrotron radiation 12*, 537-541. (10.1107/S0909049505012719)

73. Newville, M., Līviņš, P., Yacoby, Y., Rehr, J., and Stern, E. (1993) Near-edge x-ray-absorption fine structure of Pb: A comparison of theory and experiment, *Physical Review B 47*, 14126-14131. (10.1103/PhysRevB.47.14126)

74. Padden, K. M., Krebs, J. F., MacBeth, C. E., Scarrow, R. C., and Borovik, A. S. (2001) Immobilized metal complexes in porous organic hosts: Development of a material for the selective and reversible binding of nitric oxide, *J Am Chem Soc 123*, 1072-1079. (Doi 10.1021/Ja003282b)

75. Newville, M. (2001) EXAFS analysis using FEFF and FEFFIT, *Journal of synchrotron radiation 8*, 96-100. (Doi 10.1107/S0909049500016290)

76. Ankudinov, A. L., Ravel, B., Rehr, J. J., and Conradson, S. D. (1998) Real-space multiple-scattering calculation and interpretation of x-ray-absorption near-edge structure, *Physical Review B 58*, 7565-7576. (DOI 10.1103/PhysRevB.58.7565)

77. Hough, M. A., and Hasnain, S. S. (2003) Structure of fully reduced bovine copper zinc superoxide dismutase at 1.15 angstrom, *Structure 11*, 937-946. (10.1016/S0969-2126(03)00155-2)

CHAPTER 4

NICKEL- AND PH-DEPENDENT INTERACTIONS REVEAL THAT HYPA AND $UREE_2$ ACT AS CO-METALLOCHAPERONES IN NICKEL-DELIVERY TO *HELICOBACTER PYLORI* UREASE

This chapter will be submitted for publication: Hu, H. Q. and Maroney, M. J. (2017) Nickel- and pH-dependent interactions reveal that HypA and $UreE_2$ act as co-metallochaperones in nickel-delivery to *Helicobacter pylori* urease. *ACS Chemical Biology*.

4.1 Introduction

Helicobacter pylori is a successful human pathogen that colonizes the stomach and causes chronic gastritis, ulcers, and cancers.[1, 2] Despite thriving in the niche environment of the acidic stomach, *H. pylori* is a neutrophilic bacterium. One of the adaptations that allow for successful colonization in the acidic stomach is the ability to rapidly increase urease activity upon acid shock.[3] Urease catalyzes the hydrolysis of urea to carbamate (spontaneously hydrolyzing to ammonia and carbon dioxide) and ammonia, which neutralizes the intracellular pH of the bacterium in acidic environments.[4] Acid readiness is ensured by a plentiful supply of apo-urease protein, which accounts for 7 – 10% of the total nascent proteins synthesized by *H. pylori* at both neutral and acidic pH conditions.[5] Activation of urease involves the assembly of the complex di-nickel active sites, which requires the accessory proteins UreEFGH as well as hydrogenase-associated accessory proteins HypA and HypB in *H. pylori*.[6, 7] The function of the accessory proteins in urease maturation has been extensively studied and reviewed for *H. pylori* and other organisms.[6]

Of these accessory proteins, UreE, has been identified as a Ni-metallochaperone responsible for acquiring and specifically delivering Ni^{2+} for urease activation.[6] *H. pylori* UreE is a homodimer ($UreE_2$), where a six-coordinate Ni site is formed at the dimer interface using a labile C-terminal motif.[8] The interfacial $UreE_2$ site has a relatively high-affinity for Ni^{2+} with an apparent dissociation constant (K_d) of 0.15 ± 0.01 μM, as measured by isothermal titration calorimetry (ITC).[9] However, purified $UreE_2$ has been known to demonstrate disorder and/or partial degradation at the C-terminal Ni-binding motif,[8, 10, 11] which may reduce the ability of *H.*

pylori $UreE_2$ to sequester Ni. Additionally, UreE in *H. pylori* lacks a His-rich tail commonly found in other known UreE proteins[12] resulting in a lower Ni-binding capacity of one Ni^{2+} per dimer[8-10, 12] compared to up to six Ni^{2+} per dimer in *K. aerogenes* $UreE_2$.[6, 13, 14] Appending His-rich tails derived from homologues to the *H. pylori* UreE protein sequence increases the Ni-binding capacity of the protein variants and the urease activities of corresponding *H. pylori* isostrains. [12] Where other UreE homologues have evolved superior Ni-sequestration ability, *H. pylori* UreE seems obviously lacking.

Urease activity in *H. pylori* also requires another known Ni-metallochaperone, HypA,[15] which is typically associated with the maturation of the Ni-containing enzyme, NiFe-hydrogenase.[16] Interruption of the *hypA* gene [11, 15, 17] or diminishing its Ni-binding ability by site-directed mutagenesis [11, 18] have been known to abolish urease activity and acid survival of the cells. WT-like urease activity in *hypA*-interruption strains of *H. pylori* can be restored by Ni-supplementation in the growth media,[15] but cannot rescue *ureE*-interruption strains.[19] These phenotypes suggest that while both HypA and $UreE_2$ are involved in delivery of Ni^{2+} to *H. pylori* apo-urease, Ni^{2+} insertion specifically requires $UreE_2$, potentially due to protein-protein interactions with downstream urease accessory proteins in a maturation complex, as observed in other bacterial strains.[6]

Purified HypA protein has been shown to interact with $UreE_2$, forming a stable complex that can outcompete complex formation with UreG,[20] an accessory protein in the urease maturation cascade that is characterized as a GTPase.[21-23] In contrast, alternate studies using N-terminally modified HypA (where cleavage of an affinity tag left a Gly-Ser overhang at the N-terminal Ni-binding motif; henceforth referred to as GSHypA) found that the GSHypA-$UreE_2$ complex dissociates in favor of a $UreG_2$-$UreE_2$ complex in the presence of Mg and GTP.[24]

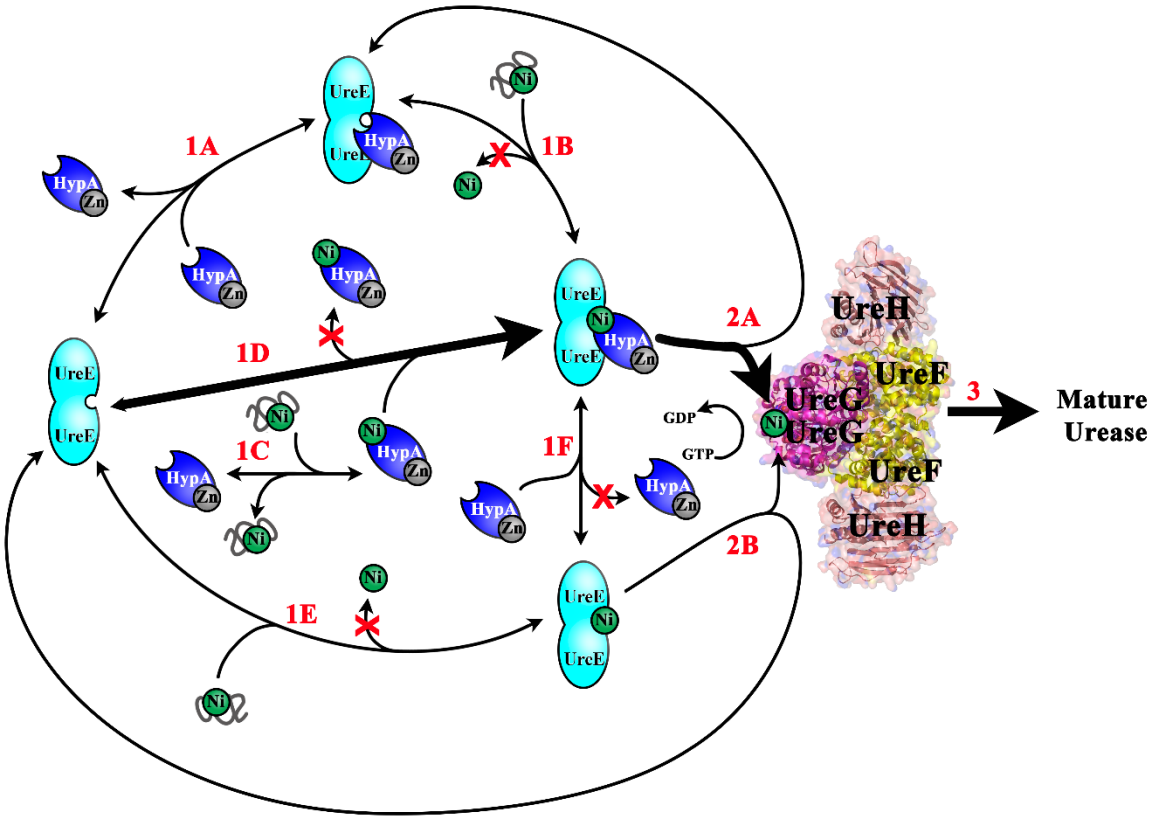

Figure 4.1: Model of Ni-transfer paths between *H. pylori* HypA and $UreE_2$.
Possible paths (steps labeled in red) of Ni-transfer between HypA and $UreE_2$ in the urease maturation process culminating with delivery of Ni to the urease maturation complex (PDB ID 4HI0[21]). Gray squiggles surrounding Ni represents the available Ni within the cell that are loosely coordinated by proteins, peptides, or small molecules. Paths marked with a red X have sub-micromolar apparent dissociation constants (K_d), indicating the complex is unlikely to dissociate.

H. pylori HypA has been extensively characterized and has been found to be a monomeric protein that contains a structural Zn-site, as well as a Ni-binding site with moderate affinity (K_d ~1 μM).[11, 25-27] The Ni-binding to HypA is approximately one order of magnitude weaker than that of $UreE_2$, and with both proteins serving the same function of Ni^{2+} acquisition and delivery, the requirement of HypA in *H. pylori* urease maturation seems redundant and confounding. The disparity in the Ni-binding affinities between HypA and $UreE_2$ led to a current model in the literature[24] that suggests that HypA first acquires Ni^{2+}, possibly by direct interaction with the Ni importer, (Figure 4.1, path 1C), and then transfers it to $UreE_2$ (Figure 4.1, path 1D) through protein-protein interactions.[19, 24] Subsequently, HypA dissociates (Figure 4.1, path 1F) from the complex leaving Ni-$UreE_2$ to interact with UreG (Figure 4.1, path 2B) in delivering Ni^{2+}

to *apo*-urease.[24] However, early *in vitro* and *in vivo* attempts to show Ni-transfer between HypA and $UreE_2$ yielded ambiguous results.[19] Ni-transfer from GSHypA to UreE has been demonstrated using a Ni-specific cross-linking dye after SDS-PAGE separation of the two proteins,[28] however other N-terminally modified HypA variants (H2A and M1_H2insL, hereafter known as L2*HypA) have been known to abrogate or weaken Ni-binding.[11, 18] Additionally, separation of the tightly bound Ni-GSHypA-$UreE_2$ complex requires denaturing conditions[28] or additional cofactors (such as Mg, GTP, and $UreG_2$).[24]

As a mechanism accounting for the HypA-requirement in *H. pylori* urease maturation, the HypA Ni^{2+} acquisition and handoff to $UreE_2$ is unsatisfactory in two respects. First, the *in vitro* studies of the HypA-$UreE_2$ interaction reported thus far have been performed under neutral pH conditions, which may miss key aspects of the mechanism of Ni-delivery for urease maturation that are critical for the survival of *H. pylori* under acid shock (with internal pH ~ 6.3).[29-31] Second, the studies performed thus far at neutral pH indicate that the HypA-$UreE_2$ complex is stable with or without Ni^{2+}, which renders spontaneous HypA dissociation from the complex unlikely. Even with $UreE_2$ binding more tightly to Ni^{2+} than HypA, the strong protein-protein interaction would hamper the hand-off mode of Ni-transfer that is a feature of the current model. The goal of the studies presented here is to elucidate the role(s) of HypA in Ni^{2+} delivery to the urease maturation pathway in *H. pylori*, and specifically to add studies performed under conditions that mimic acid shock (*i.e.*, at pH 6.3).

4.2 Results

4.2.1 Apo--ZnHypA-$UreE_2$ interactions are not altered by acid shock conditions

Although *H. pylori* has a specific Ni-chaperone for urease, $UreE_2$, the full activation of urease requires another Ni-chaperone, HypA.[15] One possible mechanism is that the HypA-$UreE_2$ interaction (Figure 4.1, Path 1A and 1D) is enhanced by acidic pH, recruiting HypA to the urease maturation pathway through protein-protein interactions under acidic shock conditions. To assess the pH effects on the interaction between apo-ZnHypA or Ni-ZnHypA with $UreE_2$, size exclusion

chromatography in tandem with multi-angle light-scattering (SEC-MALS) and ITC titrations were performed under neutral (pH 7.2) conditions and conditions that approximate acid shock (pH 6.3). [29-31]

Prior studies of the N-terminally modified GSHypA and $UreE_2$ mixture by SEC and Static Light Scattering performed only at pH 7.2 indicated the formation of a stable complex of GSHypA-$UreE_2$ with a mass of 51 kDa.[28] To confirm that this complex remains stable under acid shock conditions, SEC-MALS was used to determine the masses of peaks resolved from a mixture containing a three-fold excess of apo-ZnHypA to apo-$UreE_2$ at both pH 7.2 and 6.3. Two peaks were clearly resolved for the mixture at both pH conditions with elution volumes of 7.2 – 7.3 and 8.5 – 8.7 mL (APPENDIX 3, Figure A3.1). The peak at 8.5 – 8.7 mL overlaps with the peak for isolated apo-ZnHypA, has a molecular mass of 13 kDa, and is therefore attributable to the excess apo-ZnHypA protein in the mixture. The peak at 7.2 – 7.3 mL has a molecular mass of 51 kDa, which is distinct from either apo-ZnHypA or apo-$UreE_2$ alone (with elution volume at 7.6 – 7.8 mL and a mass of 38 kDa), and match the mass of the previously characterized GSHypA-$UreE_2$ complex.[28] This peak is therefore assigned to a HypA-$UreE_2$ complex.

The formation of the apo-ZnHypA-$UreE_2$ complex was also by assessed by the titration of apo-ZnHypA into apo-$UreE_2$ and measured by ITC. Single isotherm binding curves were detected at both pH 7.2 and 6.3 (Figure 4.2, left) and best fitted by OneSite models with apparent dissociation constant (K_d) values of 0.90 ± 0.44 μM and 1.2 ± 0.3 μM, respectively (Table 4.1). These K_d values corroborate prior ITC studies of GSHypA binding to apo-$UreE_2$ performed at neutral pH, and the low-affinity binding event detected by bio-layer interferometry (BLI) at similar pH.[20, 28] The change in pH from 7.2 to 6.3 did not affect the overall binding of apo-ZnHypA to apo-$UreE_2$, suggesting that acid shock conditions do not alter the interaction between these proteins in the absence of Ni.

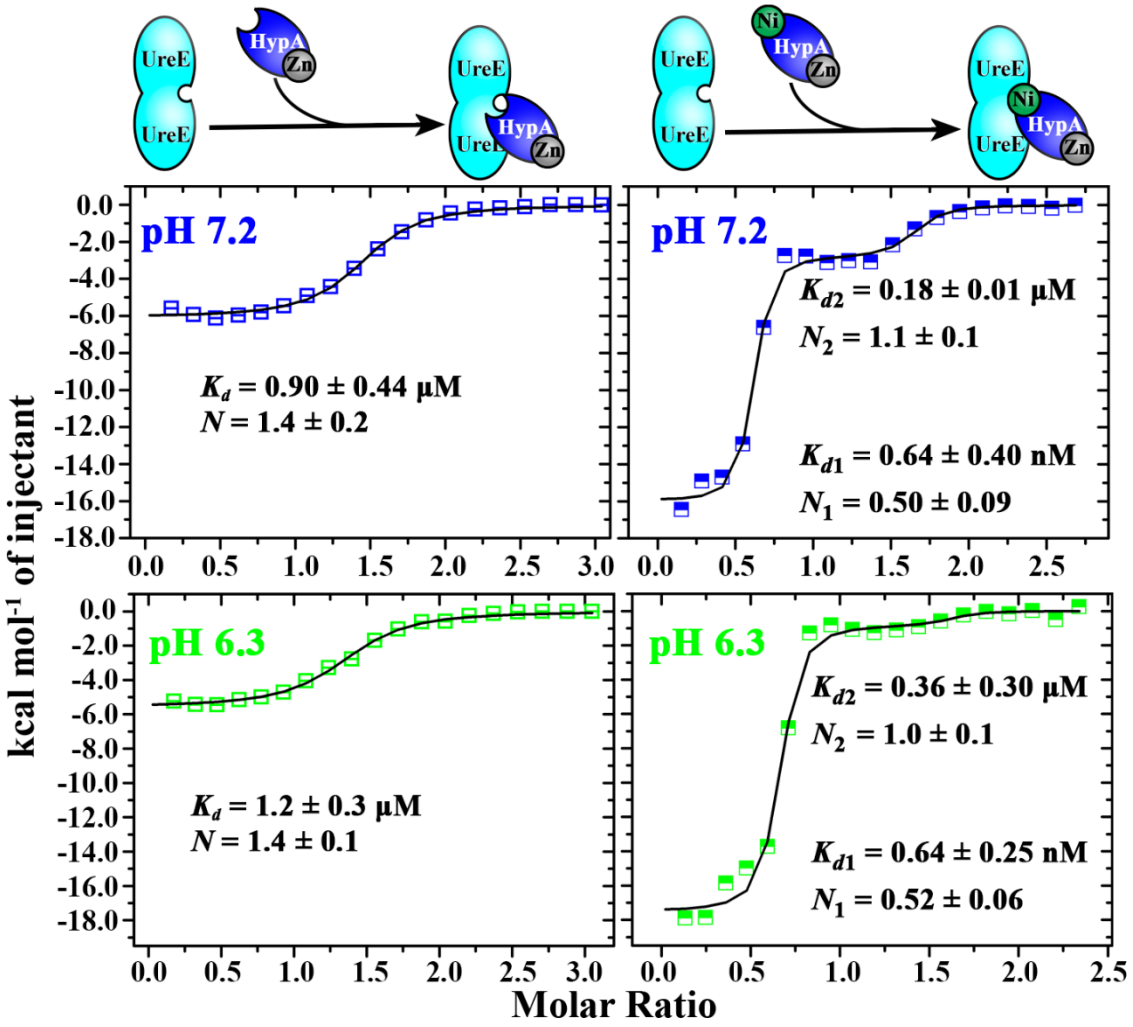

Figure 4.2: ITC isotherms of HypA binding to UreE$_2$.
ITC binding isotherms resulting from the titration of apo-ZnHypA (open squares) into apo-UreE$_2$ and Ni-ZnHypA (half-filled squares) into apo-UreE$_2$, with cartoon representations of each titration shown above the curves. Titrations were performed at pH 7.2 (blue) and 6.3 (green). Data are shown in colored symbols and fits in black lines. Titration curves were graphed to the same y-scale for visual comparison. Data were fitted to OneSite or TwoSites models as described in the text. See method Section 4.5.3 for detail fitting procedures and APPENDIX 3, Figure A3.2 for raw ITC thermograms.

Table 4.1: Summary of HypA titration into $UreE_2$

Binding Partners	pH 7.2		pH 6.3	
	K_d (M)	N (Sites)	K_d (M)	N (Sites)
	ITC			
Apo-ZnHypA	$(9.0 \pm 4.4) \times 10^{-7}$	1.4 ± 0.2	$(1.2 \pm 0.3) \times 10^{-6}$	1.4 ± 0.1
Ni-ZnHypA	$(1.8 \pm 0.1) \times 10^{-7}$	1.1 ± 0.1	$(3.6 \pm 3.0) \times 10^{-7}$	1.0 ± 0.1
	$(6.4 \pm 4.0) \times 10^{-10}$	0.50 ± 0.09	$(6.4 \pm 2.5) \times 10^{-10}$	0.52 ± 0.06
	Δ Fluorescence (NHS640-$UreE_2$)			
Apo-ZnHypA	$(2.7 \pm 0.5) \times 10^{-6}$	1:1	$(1.8 \pm 0.2) \times 10^{-6}$	1:1
Ni-ZnHypA*	$(2.0 \pm 0.9) \times 10^{-8}$	1:1	$(4.5 \pm 2.6) \times 10^{-9}$	*(H)* 1.4 ± 0.6

Results were the average of three or more independent titrations. ITC data fitted with Microcal analysis for One- or TwoSites models. Δ Fluorescence binding fitted with mass action function assuming 1:1 binding; or with the Hill Equation with Hill coefficient (*H*) as indicated. See method Sections 4.5.3 and 4.5.4 for fitting detail.
* = Measured in Ni-saturating conditions (with 1 μM Ni^{2+} in the buffer)

Fluorescence intensity change was used to further address apo-ZnHypA-$UreE_2$ binding. Primary amines in purified recombinant apo-$UreE_2$ were labeled with a fluorophore (NHS640-$UreE_2$) and then mixed with increasing concentrations of apo-ZnHypA, and the fluorescence of each mixture was then measured using a NanoTemper NT.115. Fluorescence intensity increases from apo-ZnHypA titration into apo-NHS640-$UreE_2$ were fitted to a modified mass action function, assuming a single binding site, to obtain K_d values of 2.7 ± 0.5 μM at pH 7.2 and 1.8 ± 0.2 μM at pH 6.3 (Figure 4.3 left panels and Table 4.1). These fluorescence binding results corroborate the ITC results and support a single observable binding event between apo-ZnHypA and apo-$UreE_2$ (Table 4.1). Protein-protein interactions between apo-ZnHypA and apo-$UreE_2$ remain the same at pH 7.2 and 6.3, indicating pH-dependent changes in the protein interactions is unlikely to contribute to enhanced urease activity under acid shock conditions *in vivo* in the absence of Ni.

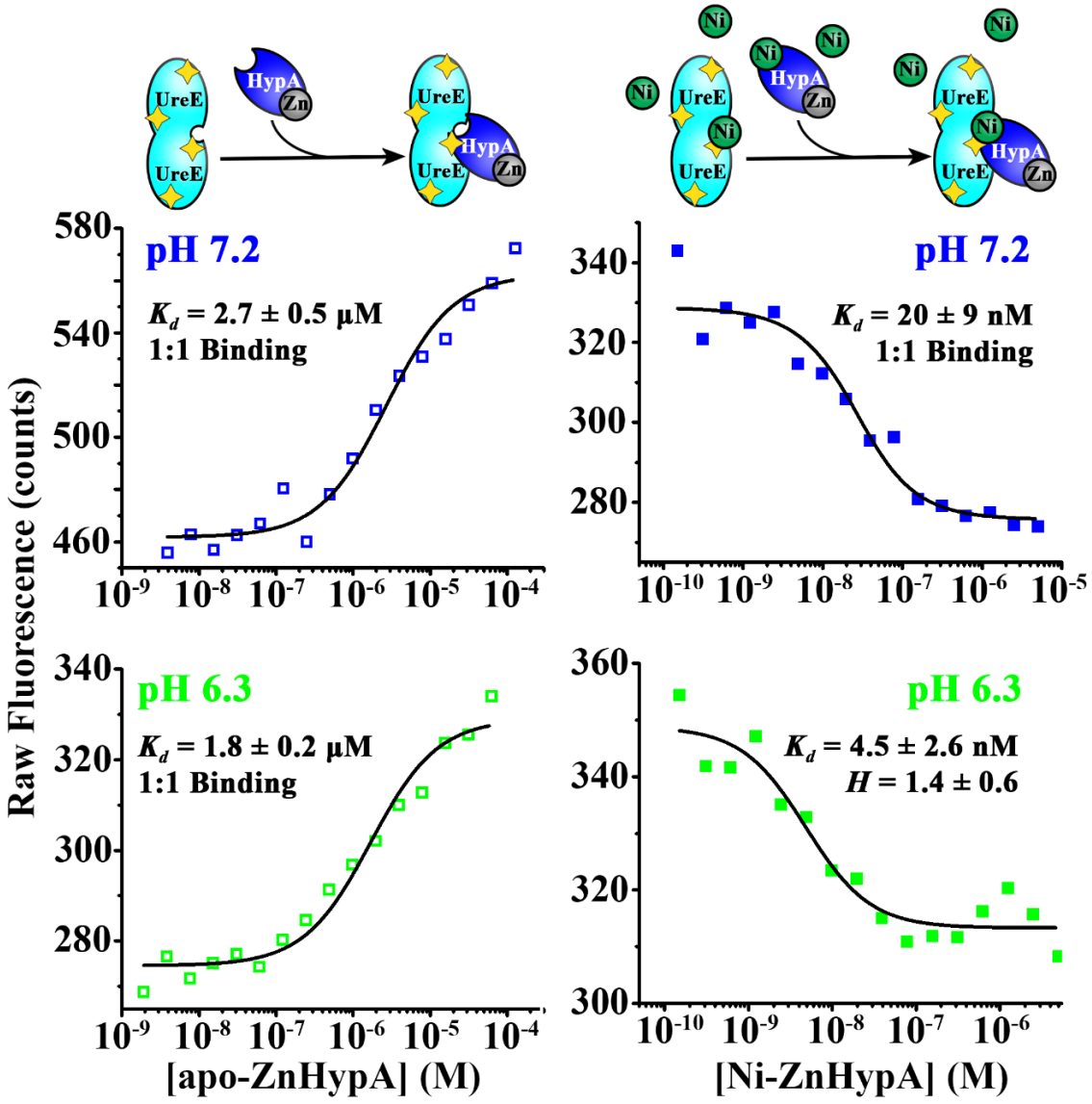

Figure 4.3: Fluorescence binding curve of HypA to NHS640-UreE$_2$
Titration were performed at pH 7.2 (blue) and 6.3 (green). Cartoon representations of each titration are shown above the binding curves, where fluorophores are represented as yellow stars. Apo-ZnHypA titrations into NHS640-UreE$_2$ (open squares) were performed in buffer without Ni, and Ni-ZnHypA titration into NHS-640-UreE$_2$ (filled squares) were performed with 1 µM Ni^{2+} in the buffer. Fluorescence data (colored symbols) were fitted (black lines) with the mass action function for the binding of apo-ZnHypA to NHS640-UreE$_2$ at both pH, and for Ni-ZnHypA binding to NHS640-UreE$_2$ at pH 7.2, assuming 1:1 binding. A Hill Equation was used to fit the Ni-ZnHypA binding to NHS640-UreE$_2$ at pH 6.3. See method Section 4.5.4 for fit details.

4.2.2 Low pH not favor Ni^{2+} binding to HypA over $UreE_2$

Another possible mechanism for requiring HypA in *H. pylori* urease maturation is that under acid shock conditions, Ni^{2+} binding to HypA (Figure 4.1 path 1C) may be favored over $UreE_2$ (Figure 4.1 path 1E). Prior studies have established that Ni binds to $UreE_2$ approximately one order of magnitude tighter than HypA at neutral pH,[9, 26, 28] but Ni^{2+} binding to $UreE_2$ has not been studied at conditions resembling acid shock. Using identical buffers, the Ni^{2+} binding to HypA and $UreE_2$ under neutral (pH 7.2) or acid shock (pH 6.3) conditions were compared. $NiCl_2$ was dissolved in buffers at pH 7.2 or 6.3, and then titrated into either apo-$UreE_2$ or apo-ZnHypA in the same buffer, monitoring the heat of binding using ITC. A single isotherm was observed for Ni^{2+} binding to either apo-ZnHypA or apo-$UreE_2$, and the data were best fit by OneSite models, as summarized in Table 4.2, with example data and fits shown in Figure 4.4.

The moderate change of expected cytoplasmic pH of *H. pylori* under neutral (pH 7.2) and acid shock (pH 6.3) conditions did not significantly alter the Ni^{2+} binding of either $UreE_2$ or HypA individually. At both pH conditions tested, UreE bound to Ni^{2+} at least one order of magnitude tighter than HypA. The K_d for Ni^{2+} binding to $UreE_2$ were best fit to 67 ± 15 nM at pH 7.2 and 53 ± 25 nM at pH 6.3, which are indistinguishable values and within the range of previously reported values measured at pH 7.[9] Apo-ZnHypA bound Ni^{2+} with more moderate affinities (K_d = 0.97 ± 0.26 μM at pH 7.2; 1.6 ± 0.8 μM at pH 6.3) that are also indistinguishable in both neutral and acidic conditions, and in agreement with prior reports.[11, 26]

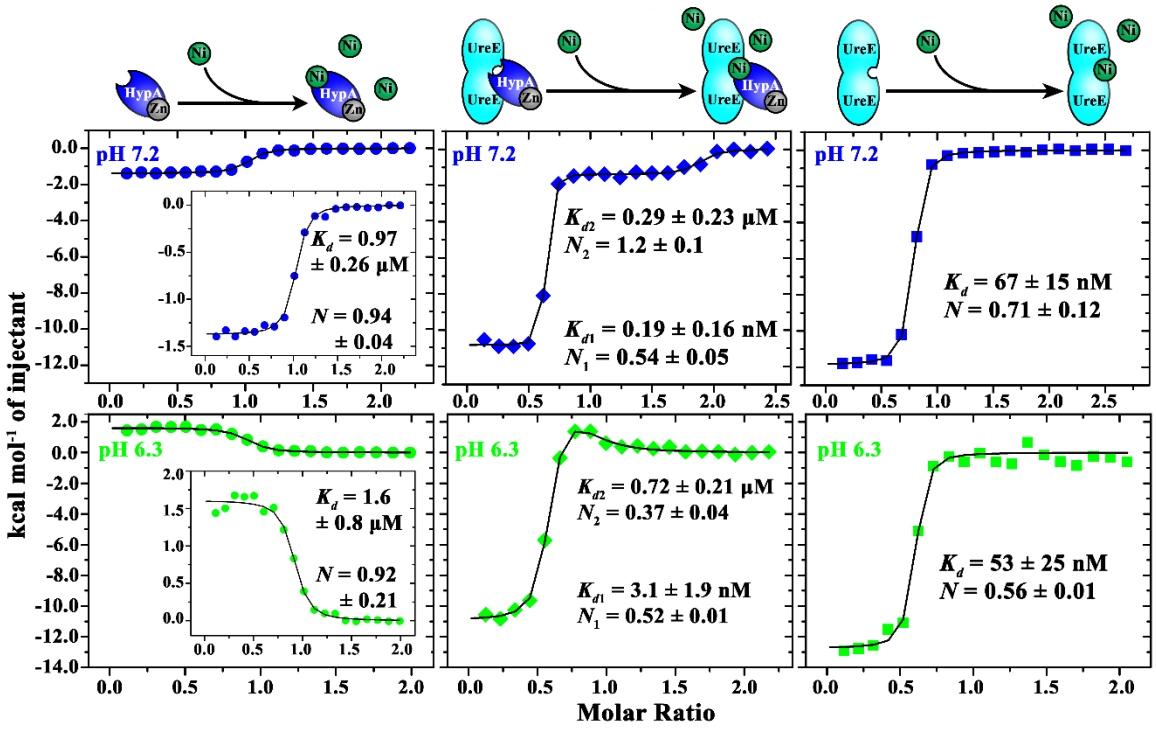

Figure 4.4: ITC binding isotherms of Ni^{2+} titration into proteins
Titration of Ni^{2+} into HypA (circles), $UreE_2$ (squares), and HypA-$UreE_2$ complex (diamonds) with data in color and fits in black lines. Titrations were performed at pH 7.2 (blue) and 6.3 (green) and isotherms were graphed to the same y-scale for visual comparison. With insets showing properly scaled isotherms for Ni^{2+} binding to HypA. Ni^{2+} binding to HypA or $UreE_2$ were fitted with OneSite models, and Ni^{2+} binding to the HypA-$UreE_2$ complex were fitted to TwoSites models (see text and Section 4.5.3 for detail fitting procedures and APPENDIX 3, Figure A3.2 for raw ITC thermograms).

The ITC data also reveal that the capacity for Ni-binding was reduced in $UreE_2$ (Table 4.2). $UreE_2$ was found to bind less than one Ni^{2+} per dimer with the number of sites (*N*) fitted to 0.71 ± 0.12 at pH 7.2, and 0.56 ± 0.01 at pH 6.3. As previously reported, the C-terminal motif (close to the Ni-binding site) of purified *H. pylori* UreE degrades slowly over time,[8, 9, 11] which affects the number of sites available for Ni-binding. However, the *N* values determined in our fits are consistent with approximately one Ni-site per UreE dimer and is consistent with previously reported crystal structures[8, 10] and Ni K-edge X-ray absorption spectroscopy data.[8]

Apo-ZnHypA bound one Ni^{2+} per monomer, as expected, with *N* fitted to 0.94 ± 0.4 and 0.92 ± 0.21 at pH 7.2 and 6.3, respectively. This result contradicts a previous report of HypA binding one Ni^{2+} per monomer at pH 7.2 and one Ni^{2+} per dimer at pH 6.3.[26] This discrepancy

could be attributed to buffer system differences, where the presence of reducing agents in the buffer used in these studies prevented sulfur oxidation, and therefore better maintained the native Zn-bound state of HypA, or possibly due to the use of re-folded protein in the prior studies.

Table 4.2: Summary of ITC results from Ni titration into HypA and UreE

Binding Partners	pH 7.2		pH 6.3	
	K_d (M)	N (Sites)	K_d (M)	N (Sites)
Apo,Zn-HypA	$(9.7 \pm 2.6) \times 10^{-7}$	0.94 ± 0.04	$(1.6 \pm 0.8) \times 10^{-6}$	0.92 ± 0.21
Apo-$UreE_2$	$(6.7 \pm 1.5) \times 10^{-8}$	0.71 ± 0.12	$(5.3 \pm 2.5) \times 10^{-8}$	0.56 ± 0.01
*HypA-$UreE_2$	$(2.9 \pm 2.3) \times 10^{-7}$	1.2 ± 0.1	$(7.2 \pm 2.1) \times 10^{-7}$	0.37 ± 0.04
	$(1.9 \pm 1.6) \times 10^{-10}$	0.54 ± 0.05	$(3.1 \pm 1.9) \times 10^{-9}$	0.52 ± 0.01

Results represent the average and standard deviation from three or more independent titrations unless otherwise noted. See Section 4.5.3 for fit details.
* = Result represent the average and range from two independent titrations

4.2.3 Ni^{2+} binding to HypA-$UreE_2$ complex is enhanced at neutral and acid shock pH

Our results indicate that Ni^{2+} binding to HypA was not favored over $UreE_2$ under acidic conditions, ruling out pH-dependent changes in the Ni affinities of the two metallochaperones as a possible mechanism for the HypA-requirement in *H. pylori* urease maturation. However, since HypA and $UreE_2$ are known to form a tight complex,[11, 19] the interaction of Ni^{2+} with the complex (Figure 4.1, path 1B) may be drastically different as compared to each protein individually (Figure 4.1, paths 1C and 1E). ITC was used to measure the Ni^{2+} binding to the HypA-$UreE_2$ complex under neutral (pH 7.2) and acid shock (pH 6.3) conditions to assess whether Ni-binding is enhanced in the preformed protein complex. The formation of the HypA-$UreE_2$ complex under the conditions used in these titrations was confirmed by protein-protein titrations and SEC-MALS (see Table 4.1, and Figure 4.2 and Figure 4.3 left panels, and APPENDIX 3 Figure A3.1). Two distinct isotherms were observed in the titration of Ni^{2+} into the HypA-$UreE_2$ complex at both pH 7.2 and 6.3, and were best fitted to models that featured two independent sites (Figure 4.4 middle panels, Table 4.2). Fits for a single binding site produced statistically and visually poor fits for the data (APPENDIX 3, Figure A3.3).

At neutral pH, Ni^{2+} binding to the preformed HypA-$UreE_2$ complex was best fitted to two binding events. The lower affinity binding event (K_{d2} = 0.29 ± 0.23 μM and N_2 = 1.2 ± 0.1 sites) feature a K_d value in-between that of Ni^{2+} binding to HypA and $UreE_2$ individually. The higher affinity binding event (K_{d1} = 0.19 ± 0.16 nM and N_1 = 0.54 ± 0.05 sites) feature a K_d value that is almost three orders of magnitude tighter than Ni^{2+} binding to $UreE_2$ (Figure 4.4, Table 4.2). Under acidic conditions, the two isotherms for Ni^{2+} binding to the HypA-$UreE_2$ complex were also modeled with two binding events [K_{d1} = 3.1 ± 1.9 nM (N_1 = 0.52 ± 0.01 sites) and K_{d2} = 0.72 ± 0.21 μM (N_2 = 0.37 ± 0.4 sites)]. The higher affinity binding is one order of magnitude tighter than Ni^{2+} binding to $UreE_2$, and the lower affinity binding features a K_d value similar to the Ni^{2+} binding to HypA (Figure 4.4 and Table 4.2). Thus, in contrast to the situation at neutral pH, Ni^{2+} binding to the preformed HypA-UreE complex under acid shock conditions is only slightly enhanced relative to Ni^{2+} binding to the two isolated proteins.

Although HypA has only a moderate affinity towards Ni^{2+} (~1 μM, see Table 4.2), it appears to play a crucial role in the high affinity Ni-binding event observed in the apo-ZnHypA-$UreE_2$ complex. Disruption of the native Ni-binding site in HypA by site-directed mutagenesis was used to investigate the contribution of HypA to the high-affinity (K_{d1} ~ 0.2 – 3 nM, Table 4.2) binding events observed in Ni^{2+} titration into the ZnHypA-$UreE_2$ complex. A previously characterized HypA variant, L2*HypA, was shown to bind Ni^{2+} at a lowered affinity (K_d ~ 20 – 60 μM) compared to WT-HypA (K_d ~ 1 μM) without affecting the binding affinity to $UreE_2$.[11] Indeed, the L2*HypA closely resembles the GSHypA variant in Ni-binding affinity (K_d ~ 14 μM),[28] Ni-site structure, and magnetic properties.[11, 27] Ni^{2+} titration of the ZnL2*HypA-$UreE_2$ complex was measured by ITC (APPENDIX 3, Figure A3.4). A single isotherm was observed at pH 7.2 (K_d = 17 ± 2 nM and N = 0.49 ± 0.002 sites) and pH 6.3 (K_d = 27 ± 5 nM and N = 0.48 ± 0.003 sites), with affinities that are similar to Ni^{2+} binding to apo-$UreE_2$ alone (Figure 4.4, Table 4.2). The higher affinity binding event observed in the Ni titration into ZnWTHypA-$UreE_2$ (K_d ~ 0.2 – 3 nM, see Table 4.2) is absent. Thus, the loss of this higher affinity binding event upon the

disruption of the native HypA Ni-binding site suggests that the Ni-binding ligands in HypA are essential for forming a high affinity site in the HypA-$UreE_2$ complex.

4.2.4 Ni-ZnHypA enhances protein interactions under both neutral and acid shock pH

ITC was used to monitor the interaction between HypA and $UreE_2$ when Ni-ZnHypA was titrated into apo-$UreE_2$ under neutral (pH 7.2) and acid shock (pH 6.3) conditions (Figure 4.1, path 1D). The results are consistent with a series of complex interactions that are reflected in at least two distinct isotherms under both neutral and acidic conditions. TwoSites models were used to fit the titrations at both pH values and reveal two binding events (Figure 4.2, right). The tighter binding events were best fitted with K_d values of 0.64 ± 0.40 nM (N = 0.50 ± 0.09 sites) at pH 7.2, and 0.64 ± 0.25 nM (N = 0.52 ± 0.06 sites) at pH 6.3, both of which are three orders of magnitude tighter than the binding of the two apo-proteins observed in the absence of Ni^{2+} (Table 4.1). These K_d values are in the same order of magnitude as the high affinity binding events observed in the titration of Ni into the ZnHypA-$UreE_2$ complex, although it is unclear whether the same binding events precipitated these observed isotherms. The lower affinity events were best fitted with K_d values of 0.18 ± 0.01 μM (N = 1.1 ± 0.1 sites) at pH 7.2, and 0.36 ± 0.30 μM (N = 1.0 ± 0.1) sites at pH 6.3 (Table 4.1), which are within the range of Ni^{2+} binding to apo-$UreE_2$ (Table 4.2). The tighter binding events (with K_d values in the sub-nM to low-nM range) are only observed in the presence of both Ni and the HypA-$UreE_2$ complex (*i.e.*, in the titrations of Ni-ZnHypA into apo-$UreE_2$; or in the titrations of Ni^{2+} into the apo-ZnHypA-$UreE_2$ complexes). This suggests that the tight interactions are due to the formation of a new Ni-binding site formed by the ZnHypA-$UreE_2$ complex that was absent in the individual proteins.

4.2.5 High-affinity interaction between HypA and $UreE_2$ persists with Ni-bound $UreE_2$

ITC detects all the processes that result in heat change during a titration, including any metal binding/unbinding and changes to protein conformation. Thus, to simplify the processes observed in the titration of Ni-ZnHypA into apo-$UreE_2$, the titration was repeated under saturating Ni^{2+} conditions using fluorescence change as a detection method. The fluorescence

change of Ni-NHS640-$UreE_2$ was measured upon titration with unlabeled Ni-ZnHypA under both neutral (pH 7.2) and acid shock (pH 6.3) conditions in the presence of excess Ni^{2+} (1 μM) in the buffer (Figure 4.3 and Table 4.1). In this approach, the signal is derived exclusively from fluorophores bound to the surface of Ni-NHS640-$UreE_2$ at nM concentration, where the $UreE_2$ Ni-binding site is saturated. The release or rebinding of Ni^{2+} or rearrangements in HypA is not detectible by this method unless the process directly affects the surface of the Ni-NHS640-$UreE_2$. This experimental design allowed for the detected signals to be unambiguously assigned to protein-protein interactions in the presence of Ni.

The Ni-NHS640-$UreE_2$ fluorescence intensities decrease with increasing concentration of Ni-ZnHypA, which is opposite to the effect observed for the apo-ZnHypA interaction with apo-NHS640-$UreE_2$ (Figure 4.3). The reversal of the fluorescence intensity changes in response to increasing concentrations of HypA indicates that interactions that occur in the Ni-bound proteins are distinct from the binding events in the apo-proteins. One possible mechanism for the Ni-ZnHypA-dependent decrease in fluorescence is the release and/or rebinding of Ni to the Ni-NHS640-$UreE_2$.

The changes in fluorescence intensities were plotted against the concentration of Ni-ZnHypA and to generate binding curves. At pH 7.2, the binding of Ni-ZnHypA to Ni-NHS640-$UreE_2$ was fitted to a modified mass action function, assuming a single binding site, resulting in K_d of 20 ± 9 nM. The binding at pH 6.3 was best fitted with the Hill's equation resulting in K_d of 4.5 ± 2.6 nM with Hill coefficient (H) of 1.4 ± 0.6, suggesting cooperativity in binding. These K_d values are at least two orders of magnitude tighter than the apo-protein interactions measured by fluorescence at both pH values ($K_d \sim 2$ μM). These observations unambiguously establish that a HypA-$UreE_2$ complex occurs under saturating Ni^{2+} conditions, and that the affinity between Ni-ZnHypA and Ni-$UreE_2$ was *increased* under both neutral and acid shock conditions. Further, the complex is about 10-fold tighter under acid shock conditions. These enhanced interactions

provide a possible mechanism for increased Ni delivery to apo-urease under acid shock conditions, and suggest a more involved role for HypA beyond the handing off Ni^{2+} to $UreE_2$.

4.2.6 Ni^{2+} and apo-ZnHypA does not dissociates from the Ni-ZnHypA-$UreE_2$ complex in size exclusion chromatography

To assess the stability of the HypA-$UreE_2$ complex with Ni bound, particularly its ability to retain Ni^{2+} ions under dilute conditions, the SEC-MALS experiment described above for the interaction of apo-ZnHypA and apo-$UreE_2$ was repeated using Ni-ZnHypA.

A three-fold excess of Ni-ZnHypA was mixed with apo-$UreE_2$ under neutral (pH 7.2) and acidic (pH 6.3) conditions, and then separated and analyzed by SEC-MALS. The results shown in Figure 4.5 are essentially identical to those obtained using apo-ZnHypA (APPENDIX 3, Figure A3.1), and featured two resolved peaks at similar elution volumes. The first peak centered at elution volumes of 7.1 – 7.3 mL corresponds to a molecular mass of 51 kDa at both pH 7.2 and 6.3, and is assigned to the stable complex of ZnHypA-$UreE_2$, with or without Ni^{2+} bound. A second smaller peak eluted at 8.5 – 8.7 mL and overlaps with the peak of HypA alone. This smaller peak has a molecular mass of 13 kDa both pH values, and is assigned to the excess HypA separated from the mixture, with or without Ni^{2+} bound.

To assess whether metals remain bound to the resolved protein peaks, each peak was collected and analyzed for metal content using inductively coupled plasma optical emission spectroscopy (ICP-OES). Since properly folded HypA contains a structural Zn-site,[17, 25, 26, 32] comparing the Ni:Zn ratio of each peak is a convenient way to accurately assess the Ni retention and stoichiometry compared with the amount of HypA in the sample. The 51 kDa HypA-$UreE_2$ complex contained 0.36 ± 0.06 μM Ni with a Ni:Zn ratio of 1.07 at pH 7.2; and had a 0.10 ± 0.05 μM Ni concentration with a Ni:Zn ratio of 1.33 at pH 6.3. These results show that Ni is retained in the protein complex and this complex is stable at sub-micromolar concentrations (Figure 4.1, Path 1B). The peak corresponding to excess Ni-ZnHypA contained 0.72 ± 0.05 μM Ni with a Ni:Zn ratio of 0.85 at pH 7.2; and contained 0.38 ± 0.03 μM Ni with a Ni:Zn ratio of 0.98 at pH

6.3, demonstrating that Ni-ZnHypA also retains Ni under these conditions at close to 1:1 ratios (Figure 4.1, Path 1F). Together these data indicate that the Ni-ZnHypA-$UreE_2$ complex is stable at sub-micromolar concentrations, suggesting that this complex is unlikely to dissociate within the cell without other disruptions.

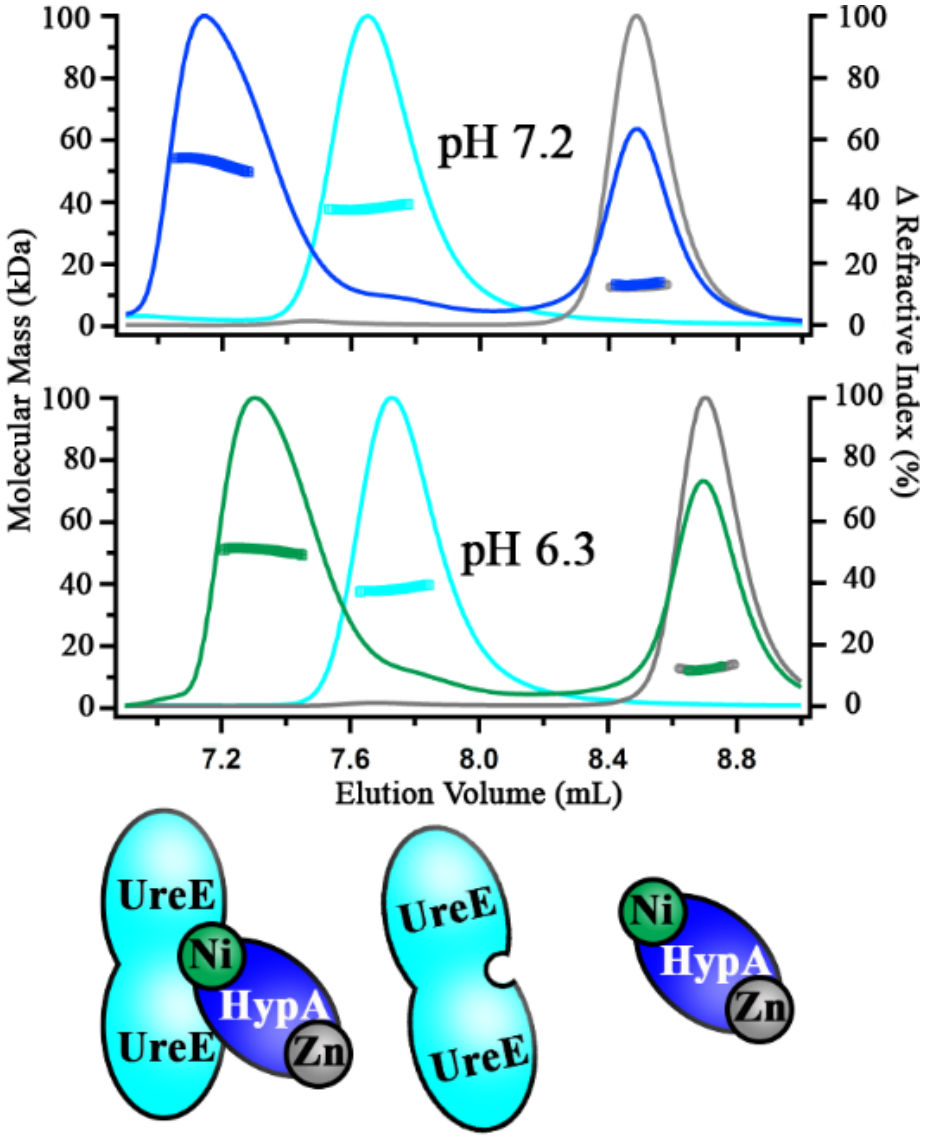

Figure 4.5: SEC-MALS analyses of Ni-ZnHypA-$UreE_2$ complexes
Chromatographs of Ni-ZnHypA (gray lines), $UreE_2$ (cyan lines), and a 3:1 mixture of Ni-ZnHypA with $UreE_2$ at pH 7.2 (blue line, upper panel) and at pH 6.3 (green line, lower panel) separated by SEC. The deconvoluted molecular masses from MALS analyses are graphed on the center of each peak. See Section 4.5.5 for detailed analysis method. Cartoon representation of the individual proteins and complexes are shown below each set of peaks.

4.2.7 Binding to HypA slows the degradation of UreE

One potential role of HypA in ensuring proper Ni-delivery to the urease maturation pathway in *H. pylori* is to stabilize $UreE_2$. The C-terminal domain of *H. pylori* UreE protein has been known to be disordered or degrade over time producing two distinct bands on SDS-PAGE (APPENDIX 3, Figure A3.5).[8, 10, 11] LC-MS analysis of partially degraded UreE protein identified the full-length protein at 19407.3 Da (theoretical mass = 19407.5 Da) and a major degradation product at 18504.4 Da corresponding to UreE with eight residues missing from the C-terminus (theoretical mass = 18504.5 Da) producing a UreEΔ163-170 fragment. A similar *H. pylori* UreE variant, UreEΔ158-170, has been shown to lose the ability to interact with the N-terminally modified GSHypA,[28] indicating the C-terminal domain of UreE is critical for interaction with HypA. We hypothesize that the tight complex formed between native ZnHypA-$UreE_2$ both in the absence and presence of Ni (Figure 4.2 and Figure 4.3, Table 4.1) may stabilize the disordered C-terminus of $UreE_2$, therefore slowing its degradation. To test this hypothesis, the stability of purified $UreE_2$ was monitored in the presence and absence of ZnHypA, with and without of Ni^{2+}, at pH 7.2 and 6.3.

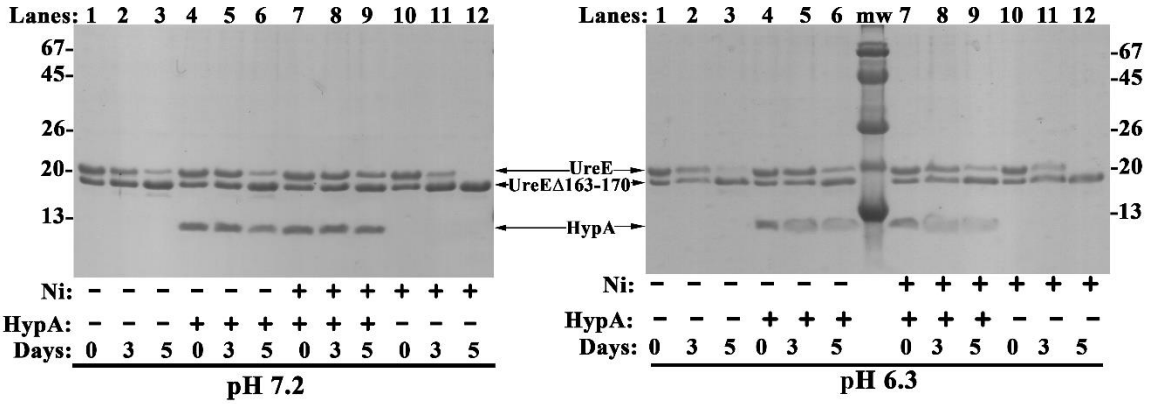

Figure 4.6: SDS-PAGE of time-dependent UreE degradation
Degradation of the UreE at room temperature was monitored at pH 7.2 (left) and 6.3 (right), in the presence and absence of one molar equivalent of ZnHypA and two molar equivalents of Ni^{2+} as indicated at the bottom of the gel. The molecular weight positions of HypA and UreE [separated into full-length peptide (UreE) and degraded peptide (UreEΔ163-170)] are marked with arrows.

At pH 7.2 and in the absence of Ni, the presence of UreEΔ163-170 fragment increases proportionally to the disappearance of full-length UreE between 0 – 5 days at 20˚C (Figure 4.6 left, lanes 1 – 3). Addition of Ni^{2+} to UreE slightly enhances the appearance of the degraded fragment (Figure 4.6, left, lanes 10 – 12). Whereas addition of ZnHypA in the absence (Figure 4.6, lanes left 4 – 6) and presence (Figure 4.6 left, lanes 7 – 9) of Ni^{2+} reduced the appearance of the degraded fragment in the same time frame. Complex formation with ZnHypA also reduced the degradation of UreE under acid shock conditions (pH 6.3), however the effects were less prominent as the ZnHypA protein also degraded over the 3 – 5-day period (Figure 4.6 right, lanes 4 – 6 and 8 – 10). These observations demonstrate that formation of the ZnHypA-$UreE_2$ complex protected the of the labile UreE C-terminal domain from degradation and therefore enhances urease maturation by ensuring the availability of full-length UreE.

4.3 Discussion

Understanding the mechanism of urease maturation in *H. pylori* is of interest both because of the unique adaptations that carefully control urease activity, and the health issues posed by the pervasiveness of the pathogen infecting the mucous layer of the stomach.[1, 2, 33] One of these adaptations encompasses the conundrum of the HypA-requirement for urease maturation, despite the presence of the urease-specific Ni-metallochaperone: $UreE_2$.[15, 34] Using a biophysical approach, the studies presented above address the role of pH in the relevant Ni-protein and protein-protein interactions, and extend current knowledge to include studies that mimic acid shock conditions.

Several hypothetical mechanisms might account for why HypA is needed to achieve full urease activation in *H. pylori*.[11, 12, 15, 17-19, 28] As the requirement for higher urease activity is most acute under acidic shock, the demand for Ni-insertion into urease would also increase at low pH. Changes in the Ni-binding affinities of the isolated proteins at low pH (Figure 4.1, Paths 1C and 1E) were ruled out by titrations conducted at both pH 7.2 and 6.3, the estimate of the internal pH of *H. pylori* under neutral or acid shock conditions (Table 4.2).[29-31]

Under neutral pH conditions, *H. pylori* HypA and UreE dimers are known to form a stable complex both as apo-proteins[11, 20] and in the presence of metals,[20, 24] raising the possibility that nickel availability for urease maturation is significantly improved in the HypA-$UreE_2$ complex compared to $UreE_2$ alone. Improvements in Ni-binding could occur via enhanced Ni interaction with the preformed HypA-$UreE_2$ complex (Figure 4.1, Path 1B) compared to either protein individually or by enhancing protein-protein complex formation in the presence of Ni^{2+} (Figure 4.1, Path 1D), particularly at low pH. The results of our studies shown above establish that while Ni^{2+} binding to the pre-formed ZnHypA-$UreE_2$ complex (Figure 4.1, Path 1B) is significantly enhanced relative to $UreE_2$ alone at neutral pH, it is only slightly increased at pH 6.3 (Table 4.2). Thus, enhancing the Ni-binding in HypA-$UreE_2$ (Figure 4.1, Path 1B) would not be a likely mechanism for increasing Ni delivery to urease under acid shock conditions.

Enhancing the HypA and $UreE_2$ protein-protein interactions (Figure 4.1, Paths 1A and 1D) under acid shock conditions can also improve Ni delivery to the urease maturation pathway. This was addressed by examining the interaction of apo-ZnHypA and Ni-ZnHypA with $UreE_2$ as a function of pH. The results establish that a single binding event with K_d ~ 1 - 2 μM accounts for the formation of the apo-ZnHypA-$UreE_2$ complex (Table 4.1), which is stable and has the same protein stoichiometry at both pH values (APPENDIX 3, Figure A3.1). However, use of Ni-ZnHypA in the titrations reveals a more complicated binding process that is characterized by at least two binding events, one high-affinity event with K_d ~ 0.6 nM that is not observed in the titration using apo-ZnHypA and not pH-dependent, and a lower affinity binding event with low μM K_d that is also not pH-dependent and is similar to the binding of apo-ZnHypA to apo-$UreE_2$ (Table 4.1). Thus, the enhanced interaction between Ni-ZnHypA and $UreE_2$ (Figure 4.1, Path 1D) is a major pathway for potentially increasing Ni delivery to the urease maturation pathway.

Prior studies of the HypA-$UreE_2$ interaction at neutral pH with biolayer interferometry (BLI) and surface plasmon resonance (SPR) demonstrated the presence of two binding events

(with reported dissociation constants of 5.4 nM and 1.1 μM), which were attributed to initial binding at higher affinity followed by a conformational change at lower affinity.[20] The K_d values reported above (Table 4.1) generally agree with the lower-affinity binding event observed in prior SPR and BLI studies,[20] but the previously reported high-affinity site was not detected using the apo-proteins. Addition of Ni^{2+} or Zn^{2+} ions to the binding studies did not affect the binding of HypA and UreE in the BLI and SPR studies,[20] but use of Ni-ZnHypA in the titrations presented above resulted in the observation of a high-affinity binding event by ITC with nM affinity (similar to the high-affinity binding event observed by BLI and SPR). This high-affinity binding event is clearly associated with the presence of Ni^{2+} by the studies presented here. Both the BLI and SPR experiments feature tethering of HypA to a surface, which given its small size (13 kDa) and complexity (binding Zn, Ni, and protein partners), could alter its interaction with $UreE_2$.

Prior studies of interactions between HypA and $UreE_2$ were also performed using the N-terminally modified GSHypA.[28] In contrast to the current study, ITC measurements of GSHypA interaction with $UreE_2$ produced single isotherms (K_d ~ 1 μM), regardless of metal loading of GSHypA (apo, Zn-bound, or Ni-Zn-bound) or the metal loading of $UreE_2$ (apo, Zn-bound, or Ni-bound).[28] The high-affinity binding events (K_d ~ 0.6 nM) that were observed in the current studies between (Ni-ZnHypA and apo-$UreE_2$) and in previous BLI and SPR studies (between tethered-HypA and $UreE_2$ in the presence and absence of metals)[20] were absent in the GSHypA studies.[28] These observations point to a loss of function in the N-terminally modified GSHypA in Ni-binding, which also interferes with the Ni-site formation in the HypA-$UreE_2$ complex. This was confirmed by the missing high-affinity binding event when Ni was titrated into the ZnL2*HypA-$UreE_2$ complex (APPENDIX 3, Figure A3.4).

In our ITC studies of Ni-ZnHypA binding to apo-$UreE_2$, both isotherms observed were distinct from the apo-ZnHypA interaction with $UreE_2$ (Figure 4.2) and therefore cannot be definitively attributed to the same interactions. The isotherms observed for Ni-ZnHypA interactions with apo-$UreE_2$ could be the results of combinations of multiple events with distinct

heat changes. Some possible interaction events include Ni transfer to $UreE_2$ from HypA, and/or the dissociation of HypA from Ni-$UreE_2$ after Ni-transfer, and/or Ni-enhanced HypA-$UreE_2$ interaction (thermodynamically distinct from the interactions in apo-forms), and/or Ni site and protein rearrangements in one or both protein partners.

The number of potential mechanistic steps, each with unknown thermodynamic parameters, render the unambiguous assignments of the isotherms to specific events improbable. However, the complexities of the Ni-ZnHypA interaction with apo-$UreE_2$ were partially clarified by probing some of the possible events that may be involved. To remove transfer of Ni^{2+} from HypA to $UreE_2$ from the process, titrations were carried out under conditions where both the HypA and $UreE_2$ Ni-binding sites are saturated with Ni^{2+}. Since HypA has been hypothesized to bind and then transfer Ni^{2+} to $UreE_2$,[24, 28] one anticipated outcome was that the HypA-$UreE_2$ complex would not form with Ni-$UreE_2$, or that the protein-protein affinities would be reduced. However, titration yielded an unexpected outcome: compared to apo protein-protein interactions with K_d ~ 2 μM at both pH, the affinity of the HypA-$UreE_2$ complex is markedly enhanced under saturating Ni^{2+} concentrations with K_d = 20 ± 9 nM at pH 7.2, and K_d = 4.5 ± 2.9 nM at pH 6.3 (Figure 4.3 and Table 4.1). The pH dependency indicates that the complex is about 10-fold tighter under acidic conditions. In addition, SEC-MALS showed that the complex stoichiometry under these conditions (1 HypA: 1 $UreE_2$) was not affected by pH (Figure 4.5). The complex was separated chromatographically and analyzed for Ni and Zn content, which showed that Ni-ZnHypA-$UreE_2$ contained a Ni:Zn ration of 1.1:1 at pH 7.2, and 1.3:1 at pH 6.3. The results are consistent with the formation of a HypA-$UreE_2$ protein complex containing a single tight Ni-binding site, since the Ni content is equal to the Zn content of the HypA protein present in the complex.

A long-standing hypothesis in the field proposes that HypA acquires and then delivers Ni^{2+} to $UreE_2$ (Figure 4.1, path 1C and 1D).[19, 24] Prior *in vitro* and *in vivo* experiments performed to elucidate Ni-transfer from HypA to $UreE_2$ yielded ambiguous results indicating that $UreE_2$ was

able to acquire Ni^{2+} directly as well as from HypA.[19] Transfer of Ni from GSHypA to $UreE_2$ was demonstrated with Ni-specific cross-linking and then forcibly separating the protein complex under denaturing conditions, in support of the hypothesis that HypA transfers Ni^{2+} to $UreE_2$, which has the tighter Ni-binding affinity of the two isolated proteins.[28] This hypothesis suggests that Ni-$UreE_2$ may no longer interact with apo-ZnHypA following the transfer, or that the interaction would weaken significantly (Figure 4.1 Path 1F). However, the Ni-ZnHypA-$UreE_2$ complex remains intact in SEC at sub-micromolar concentrations, indicating that neither Ni^{2+} or ZnHypA are likely dissociates from this tight complex (Figure 4.5) without further disruptions.

The results presented here are more consistent with an alternative mechanism wherein a tight protein complex is formed between Ni-ZnHypA and $UreE_2$ (K_d ~ low nM, Figure 4.1 path 1D) that has higher affinity than the complex formation between apo-ZnHypA and $UreE_2$ (K_d ~ 1 μM, Figure 4.1 path 1A). This complex creates a single novel Ni-binding site with higher affinity (K_d ~ 0.2 – 3 nM, Figure 4.1 path 1B) than either Ni^{2+} binding to HypA (K_d ~ 1 μM, Figure 4.1 path 1C) or $UreE_2$ (K_d ~ 60 nM, Figure 4.1 path 1E) individually. This mechanism explains the observation of a high-affinity binding event observed in the titration of Ni-ZnHypA into $UreE_2$ shown here (Figure 4.2 and Figure 4.3, Table 4.1), and possibly also those observed by BLI and SPR.[20] The fact that the Ni-ZnHypA-$UreE_2$ complex contains a new tight Ni-binding site, rather than the weaker Ni-binding sites associated with the isolated protein, suggests that it is located at an interface and is composed of ligands from both proteins in the complex. The shared Ni-ligands hypothesis is supported by the loss of the high affinity Ni binding event when the native HypA Ni-site in the complex is was altered by substituting with the L2*-HypA variant (APPENDIX 3, Figure A3.4). The formation of the complex also reduced the hydrolysis of the UreE peptides in the complex (Figure 4.6), thereby increasing the stability of the Ni delivery system and providing another mechanism for control of Ni incorporation into UreE. The fact that the Ni-ZnHypA-$UreE_2$ complex formation is enhanced at pH 6.3 (Figure 4.3) provides a possible mechanism for increased Ni delivery to the urease maturation pathway under acid shock conditions.

Prior studies in BLI experiments demonstrated that HypA outcompetes UreG (urease accessory protein with GTP hydrolysis activity) for binding to $UreE_2$.[20] In contrast, size exclusion chromatography of protein mixtures found that formation of the $UreE_2$-$UreG_2$ complex was favored over GSHypA-$UreE_2$ in the presence of GTP and Mg^{2+}.[24] The same study also found that GTP-hydrolysis by UreG was significantly enhanced by the presence of the Ni-GSHypA-$UreE_2$ or Ni-$UreE_2$, but to a lesser degree with either Ni-GSHypA or Ni^{2+}.[24] Taken together, the disruption of the tight Ni-ZnHypA-$UreE_2$ complex likely requires Ni- and GTP-induced dimerization of UreG, which favors GTP-hydrolysis.[21] The requirement of GTP-bound $UreG_2$ for disrupting the Ni-ZnHypA-$UreE_2$ complex likely enhances the fidelity of Ni delivery to the urease maturation pathway. In this way, the results of this study, along with previous studies,[19, 20, 24] indicate that HypA and $UreE_2$ act as co-metallochaperone that form the Ni-ZnHypA-$UreE_2$ complex, offering both tight Ni-coordination and fidelity of release, for Ni delivery to apo-urease in *H. pylori*.

4.4 Conclusions

The results presented here suggest that a ZnHypA-$UreE_2$ complex acts as an enhanced Ni-metallochaperone for delivering Ni^{2+} to the urease maturation pathway in *H. pylori*. Unlike UreE in other urease-containing organisms, the short C-terminal Ni-binding motif in *H. pylori* UreE has a lower Ni-binding capacity[12] and tends to be degraded.[8-11] With Ni^{2+} binding at the dimer interface in Ni-$UreE_2$, even the degradation/instability of the C-terminal Ni-binding motif in just one subunit in the $UreE_2$ would hamper its ability to retain Ni^{2+}. Given the high level of expression of apo-urease in *H. pylori* at both neutral and low pH, the low Ni-binding capacity in *H. pylori* $UreE_2$ may be an additional mechanism for preventing over-activation of urease at neutral pH. The formation of the HypA-$UreE_2$ complex stabilizes and slows the degradation of the C-terminal domain of UreE proteins. This level of control would require a Ni-metallochaperone enhancer, such as HypA, for $UreE_2$ under acid-shock conditions. Indeed, acid-induced up-regulation of *hypA* has been previously reported.[30, 35] The current studies demonstrate

that HypA binding to $UreE_2$ enhances the affinity, capacity, and retention of Ni^{2+} in the complex. This complex does not dissociate at sub-micromolar concentrations, as HypA dissociation was previously shown to require GTP-bound $UreG_2$ or denaturing conditions.[24, 28] This mechanism ensures delivery of Ni^{2+} to the urease maturation cascade, and resolves the HypA-requirement in *H. pylori* urease maturation by establishing its role as a co-metallochaperone in Ni-delivery to apo-urease.

4.5 Methods

4.5.1 Protein overexpression, purification, and preparation

Untagged WT-HypA and L2*-HypA proteins were overexpressed in *E. coli* strain DL41 (DE3) pLysS transformed with the PJI110 plasmid, and then purified using ion exchange and size exclusion columns as previously described.[11]

Overexpression of the untagged WT-$UreE_2$ proteins was achieved from *E. coli* expression cell lines transformed with the *pET15b::HpureE* plasmid[9], generously donated from Professor Stephano Ciurli's lab (Univ. of Bologna). The *pET15b::HpureE* plasmid was first amplified and the open-reading frame was confirmed to match the reported *H. pylori* G27 UreE protein sequence (GenBank Accession: Number ABM16833) prior to transformation into DL41 (DE3) pLysS or BL21 (DE3) pLysS cell lines. Transformed cells were plated on LB-agar plates supplemented with a final concentration of 100 μg/mL of ampicillin (Amp) and 34 μg/mL of chloramphenicol (Cam) and were used for overexpression within one month of transformation. A single colony selected from the transformed plate was used to inoculate small scale (50 – 150 mL) aliquots of sterile liquid LB culture media supplemented with Amp and Cam and grown at 37 ˚C with shaking (200 rpm) until saturation (> 6 hours). A 1:100 dilution of the small saturated culture was scaled to a large (1 or 2 L) culture using sterile liquid LB culture supplemented with only Amp and then grown at 37˚C with shaking until the OD_{600} reached ~0.6 (approximately 3 hours). Protein overexpression was induced by addition of isopropyl β-D-1-thiogalactopyranoside (IPTG) to a final concentration of 0.4 mM and then dropping the temperature to 25˚ C for 5

hours. Cells were separated from residual media by centrifugation at 5,500 x g for 8 minutes and then resuspended in SP A Buffer (20 mM HEPES, 1 mM TCEP, pH 7.2) and then phenylmethylsulfonyl fluoride (PMSF) and SigmaFast EDTA-free protease inhibitor cocktail (Sigma) was added to the resuspended cells to a final concentration of 1mM prior to freezing and storage at -80 ˚C.

Cells were thawed in a 30˚C water bath and were lysed upon thawing. PMSF was added to the lysate to 2 mM final concentration. The genomic DNA in the cell lysate was cleared by digestion with 20 μL of 10 mg/mL DNase I (Worthington) per liter of culture for 30 minutes in a 30˚C water bath. The insoluble fraction was removed from the lysate by centrifugation at 15,000 x g for 30 minutes. The soluble clarified lysate from 2 L of cells was diluted to 50 mL with SP A Buffer for purification using an AKTA FPLC system (Amersham Biosciences/GE Healthcare Life Sciences) equipped with a packed column (9 mL column volume) of SP Sepharose High-Performance resin (GE Healthcare Life Sciences). The SP Sepharose column was first pre-conditioned with 3 column volumes of SP A Buffer, followed by 3 column volumes of SP B Buffer (20 mM HEPES, 1 M NaCl, 1 mM TCEP, pH 7.2), and then washed with SP A buffer until the conductance was stabilized. The clarified diluted lysate is applied to the SP Sepharose column at 3 mL/min, following which nonspecifically bound proteins were washed off with 5 column volumes of 5% SP B Buffer. The bound proteins were eluted using a linear gradient of SP B Buffer from 5 – 60% over 10 column volumes. $UreE_2$ protein typically elutes off the column between 17 – 27% SP B Buffer. Fractions collected from SP Sepharose columns were separated on 16% SDS-PAGE to confirm the presence of $UreE_2$ protein.

Fractions containing $UreE_2$ were further purified using a 120-mL column volume HiLoad Superdex 75 16/60 column (GE Healthcare Life Sciences) pre-equilibrated with GF Buffer (20 mM HEPES, 200 mM NaCl, 1mM TCEP, pH 7.2). Combined fractions from SP Sepharose were loaded onto the HiLoad Superdex 75 at no more than 3 mL (5 – 10 mg/mL) per column and all fractions were collected and analyzed using 16% SDS-PAGE, with $UreE_2$ typically coming off

the column starting at 81 mL after injection. Fractions were assessed for purity and were re-loaded onto the HiLoad Superdex75 column for additional purification as needed. Pure fractions were pooled and then concentrated using a Vivaspin 20 (Sartorius) centrifugal concentrator with a 10-kDa MWCO. Purity and quality of the protein was reassessed by 16% SDS-PAGE (APPENDIX 3, Figure A3.5) and quantified using the Odyssey CLx Imaging System (LI-COR), with only fractions at >90% purity used for experiments. The actual mass of the purified protein was confirmed by ESI Mass Spec to be 19408.84 Da (theoretical mass of 19407.5).

Purified proteins were concentrated to 0.2 – 1.2 mM and then flash frozen with liquid N_2 and stored at -80 ˚C (for up to one year) and were rapidly thawed in a room temperature water bath as needed for experiments. All protein samples used for experiments were prepared by rapidly buffer exchanging concentrated protein using 0.5 mL Zeba Spin Desalting Columns with a 7-kDa MWCO pre-equilibrated with the desired buffer at Ph 7.2 or 6.3 as needed. Protein concentration as well as metal analysis were remeasured to account for any protein loss prior to final dilution of the proteins into to the appropriate concentration for experiments. For all experiments involving Ni-ZnHypA, the apo-ZnHypA protein was first reconstituted with two molar equivalents of Ni^{2+} with excess Ni^{2+} removed by Chelex 100 resin[11] prior to desalting into appropriate buffers for experiments. All samples of Ni-ZnHypA proteins used in experiments contain 0.8 – 1.1 Zn and 0.9 – 1.0 Ni per HypA. Each batch of $UreE_2$ used in experiments was confirmed to be less than 2% metal loaded (Ni or Zn) as measured by ICP-OES (see below).

4.5.2 Inductively coupled plasma-optical emission spectroscopy (ICP-OES)

ICP-OES was used to analyze the metal content (Ni, Cu, and Zn) of protein and metal solutions with sample preparation and method as previously described (3.4.15).[11] Analyses of the metal concentrations of the HypA-$UreE_2$ complexes were also performed using ICP-OES, where peak fraction collected from SEC-MALS (*vide infra*) was directly analyzed without further dilution.

4.5.3 Isothermal titration calorimetry (ITC)

ITC measurements of Ni-protein and protein-protein interactions were performed as previously described[11] using an Auto-ITC200 (MicroCal) with slight modifications. ITC experiments were performed in GF Buffer or NTP Buffer (20mM HEPES, 100 mM NaCl, 100 mM KCl, 5 mM $MgCl_2$, 1 mM TCEP) with the final pH adjusted to 7.2 or 6.3 and then filtered through a 0.22 μm membrane. No changes were observed in isotherms obtained from experiments performed in either GF Buffer or NTP Buffer (APPENDIX 3, Figure A3.6).

All proteins used in ITC experiments were prepared as described (*vide supra*). All Ni^{2+} solutions used for titration into protein or protein complexes were diluted from a stock of 500 mM $NiCl_2$ (in MilliQ water) into the same buffer as the protein solutions in the cell. The metal concentrations of each metal in the appropriate buffer solution used in ITC experiments were confirmed by ICP-OES.

ITC titrations were performed at 25˚C with the reference cell filled with the same buffer as the experiment. Each titration curve was the result of one injection of 0.4 μL, followed by 19 injections of 2.0 μL from the syringe into the cell with 150 – 600 seconds between each injection, depending on the baseline. For each set of interactions, the heat of dilution was established by injecting the appropriate buffer into the cell filled with the same protein or protein complexes.

The results from ITC titrations were fitted with the MicroCal ITC Analysis Module in Origin 7.0. Raw ITC data was first baseline corrected and then integrated to produce the initial ΔH curve, from which the averaged ΔH from the heat of dilutions from buffer injections was subtracted to produce the final ΔH curve for each titration. The first injection (0.4 μL) was excluded from use in fitting as appropriate (it is typically used to eliminate equilibration artifacts). The remaining data points were fitted to OneSite and/or TwoSites models to produce the best χ^2 values and visually appropriate fits. The inverses of the fitted *K* values were taken as the apparent dissociation constants (K_d) values. The reported K_d values and associated errors

reported were the averages and standard deviations of three or more independent ITC titrations (unless otherwise noted) for each interaction.

4.5.4 Fluorescence protein-protein interaction

Fluorescence measurements of protein-protein interactions were performed in MST Buffer (20 mM HEPES, 100 mM NaCl, 100 mM KCl, 5 mM $MgCl_2$, 1mM TCEP, and 0.02% Tween 20) at pH 7.2 or 6.3 for Apo-ZnHypA titrations into $UreE_2$, and with an additional 1 μM $NiCl_2$ added for Ni-ZnHypA titrations into $UreE_2$. HypA protein samples were prepared as described in the Protein overexpression, purification, and preparation section (*vide supra*). Purified $UreE_2$ was labeled with the amine reactive Monolith Protein Labeling Kit Red-NHS (MO-L001, NanoTemper Technologies) by reacting a solution of a 3:1 dye:protein ratio for 30 minutes in the dark. Excess dye was removed using a 0.5 mL Zeba Spin Desalting Column with a 7-kDa MWCO that was pre-equilibrated with MST buffer at pH 7.2 or 6.3. Protein concentrations and dye:protein ratios were re-evaluated using UV-Vis (with protein absorbance at 260nm and dye absorbance at 650nm) after dye removal to account for protein loss in the column. The resulting NHS640-$UreE_2$ protein sample was rapidly frozen with liquid N_2 in small aliquots and stored at -80˚C and used for experiments within one year. Both HypA and NHS640-$UreE_2$ proteins were centrifuged at 15,000 x g for 15 minutes to pellet potential aggregates prior to dilution to the appropriate concentration for protein-protein titration experiments.

Titration samples of HypA into NHS640-$UreE_2$ were prepared by serial dilution of the HypA protein into the appropriate MST Buffer and then adding equal volumes of NHS640-UreE to each HypA sample. The resulting titration series contains 16 samples with a constant concentration of fluorescently labeled NHS640-$UreE_2$ (15 – 17 nM) and increasing concentrations of HypA from sub-nM to μM range. The protein samples were loaded into Monolith NT.115 premium coated capillaries (MO-K005, NanoTemper Technologies) and the fluorescence of each tube was measured using the Monolith NT.115 Nano-Green/Red instrument at 50 – 100% LED power for 5 seconds. In each titration series, the initial fluorescence of

NHS640-$UreE_2$ changed by 10% or more with increasing concentrations of HypA. The raw fluorescence counts collected for each data point in the titration curve was plotted against the concentration of HypA and then fitted using the NanoTemper MO.Affinity Analysis software (MO-S001A). A modified version of the mass action function was used to fit each titration curve:

$$F(L) = Unbound + \frac{(Bound - Unblund)}{2} * \left(TargetConc + L + K_d - \sqrt{(TargetConc + L + K_d)^2 - 4 * TargetConc * L}\right) \quad \text{Eq. 4.1}$$

Fits were also performed for each set of data using the Hill's Equation:

$$F(L) = Unbound + \left(\frac{(Bound - Unbound)}{1 + \left(\frac{K_d}{L}\right)^H}\right) \quad \text{Eq. 4.2}$$

where L is the variable concentration of HypA, *Unbound* is the concentration of free $UreE_2$, and *Bound* is the concentration of the HypA-$UreE_2$ complex, *TargetConc* is the concentration of total $UreE_2$, K_d is the apparent dissociation constant of the HypA-$UreE_2$ complex, and H is the Hill coefficient. In each case the total $UreE_2$ concentration (*TargetConc*) is known and set as a constant for fitting. In each case, best χ^2 values and visually appropriate fits were reported. The reported K_d values and associated errors for each set of interactions were the averages and standard deviations from three or more independent titrations.

To rule out the possibilities of that the observed HypA-dependent fluorescence change was caused by pipetting errors, protein aggregation, or NHS640-$UreE_2$ sticking to the tubing at high- and low- HypA concentrations, SD tests were performed for each titration. The SD tests involves removal of potential aggregates from select samples by centrifugation, followed by reducing and denaturing the samples with SD-mix (8% SDS, 80mM DTT) and heat to disrupt all interactions with the fluorescently labeled molecule. The resulting samples should have the same fluorescent signal for high and low concentrations of the non-fluorescent ligands in the titration series. SD tests were performed for samples containing the highest and lowest concentration of HypA in the HypA-NHS640-$UreE_2$ titration series. These samples were centrifuged for 15

minutes at 15,000 x g to pellet any protein aggregates, and then a 10 μL aliquot of each sample was removed and mixed with 10 μL of SD-mix and then heated at 90 ˚C for 5 minutes. The SD-treated samples were cooled to room temperature and then loaded into Monolith NT.115 standard coated capillaries (MO-K002, NanoTemper Technologies) and the fluorescence of the SD-treated samples were measured alongside the corresponding native samples. The results show similar levels of fluorescence in SD-treated samples with high- and low-HypA concentrations, and 10% or more change in fluorescence in the corresponding native samples (APPENDIX 3, Figure A3.7). These results confirmed that the HypA-dependent fluorescence changes in NHS640-$UreE_2$ were the results of HypA-$UreE_2$ interactions and not a result of pipetting errors, protein aggregation, or protein sticking to tubing.

4.5.5 Size exclusion chromatography with multi-angle light scattering (SEC-MALS)

SEC-MALS was performed using a modified version of a previously described method.[11] The instrument setup consisted of a combination of an Agilent HPLC running a TSKgel G2000SWxL column (Tosoh Bioscience) attached to the DAWN HELEOS II light scattering detector (Wyatt Technology) and the Optilab T-rEX refractometer (Wyatt Technology). Experiments were performed at 25 ˚C, with the system was equilibrated with NTP Buffer at pH 7.2 or 6.3 at 0.5 mL/min. Individual proteins were prepared as described in the protein overexpression, purification, and preparation method section (*vide supra*). An injection volume of 50 μL was used for all samples analyzed, with the protein concentration at 75 μM for Apo- or Ni-ZnHypA individually, 25 μM for $UreE_2$ individually, and 75 μM of Apo- or Ni-ZnHypA combined with 25 μM $UreE_2$ for protein complexes. Proteins eluting off the column were monitored by multiple channels on the instrument including: UV at 280nm, light-scattering at 664 nm with multiple angled (13 – 157.8˚) detectors, and refractive index at 658 nm. Each chromatograph was processed using the Astra 6 software package (Wyatt Technology) as previously described.[11] The system and data processing method was calibrated by measuring the absolute mass of bovine serum albumin (expected 66.5 kDa, SEC-MALS 64.9 kDa) to ensure

accurate mass determination. Peaks from injections of protein complexes were manually collected following the last module (Optilab T-rEX) in the instrument set-up according to the changes in refractive index measurement with each collected peak range from 0.5 – 0.9 mL in total volume depending on the broadness of the peak. Collected peak samples were analyzed with ICP-OES to deduce the metal content of individual HypA and HypA-$UreE_2$ complexes.

4.6 References

1. Gobert, A. P., and Wilson, K. T. (2016) The Immune Battle against Helicobacter pylori Infection: NO Offense, *Trends Microbiol 24*, 366-376. (10.1016/j.tim.2016.02.005)

2. Eusebi, L. H., Zagari, R. M., and Bazzoli, F. (2014) Epidemiology of Helicobacter pylori infection, *Helicobacter 19 Suppl 1*, 1-5. (10.1111/hel.12165)

3. Fischer, F., and De Reuse, H. (2016) Adaptation of *Helicobacter pylori* Metabolism to Persistent Gastric Colonization, In *Helicobacter pylori Research From Bench to Bedside* (Steffen Backert, Y. Y., Ed.), pp 29-56, Springer, Japan.

4. Stingl, K., and De Reuse, H. (2005) Staying alive overdosed: how does Helicobacter pylori control urease activity?, *International journal of medical microbiology : IJMM 295*, 307-315. (10.1016/j.ijmm.2005.06.006)

5. Bauerfeind, P., Garner, R., Dunn, B. E., and Mobley, H. L. T. (1997) Synthesis and activity of Helicobacter pylori urease and catalase at low pH, *Gut 40*, 25-30

6. Farrugia, M. A., Macomber, L., and Hausinger, R. P. (2013) Biosynthesis of the Urease Metallocenter, *Journal of Biological Chemistry 288*, 13178-13185. (10.1074/jbc.R112.446526)

7. Maroney, M. J., and Ciurli, S. (2014) Nonredox nickel enzymes, *Chemical reviews 114*, 4206-4228. (10.1021/cr4004488)

8. Banaszak, K., Martin-Diaconescu, V., Bellucci, M., Zambelli, B., Rypniewski, W., Maroney, M. J., and Ciurli, S. (2012) Crystallographic and X-ray absorption spectroscopic characterization of Helicobacter pylori UreE bound to Ni(2)(+) and Zn(2)(+) reveals a role for the disordered C-terminal arm in metal trafficking, *The Biochemical journal 441*, 1017-1026. (10.1042/BJ20111659)

9. Bellucci, M., Zambelli, B., Musiani, F., Turano, P., and Ciurli, S. (2009) Helicobacter pylori UreE, a urease accessory protein: specific Ni(2+)- and Zn(2+)-binding properties and interaction with its cognate UreG, *The Biochemical journal 422*, 91-100. (10.1042/BJ20090434)

10. Shi, R., Munger, C., Asinas, A., Benoit, S. L., Miller, E., Matte, A., Maier, R. J., and Cygler, M. (2010) Crystal structures of apo and metal-bound forms of the UreE protein from Helicobacter pylori: role of multiple metal binding sites, *Biochemistry 49*, 7080-7088. (10.1021/bi100372h)

11. Hu, H. Q., Johnson, R. C., Merrell, D. S., and Maroney, M. J. (2017) Nickel Ligation of the N-Terminal Amine of HypA Is Required for Urease Maturation in Helicobacter pylori, *Biochemistry 56*, 1105-1116. (10.1021/acs.biochem.6b00912)

12. Benoit, S., and Maier, R. J. (2003) Dependence of Helicobacter pylori Urease Activity on the Nickel-Sequestering Ability of the UreE Accessory Protein, *Journal of bacteriology 185*, 4787-4795. (10.1128/jb.185.16.4787-4795.2003)

13. Lee, M. H., Pankratz, H. S., Wang, S., Scott, R. A., Finnegan, M. G., Johnson, M. K., Ippolito, J. A., Christianson, D. W., and Hausinger, R. P. (1993) Purification and characterization of Klebsiella aerogenes UreE protein: a nickel-binding protein that functions in urease metallocenter assembly, *Protein Sci 2*, 1042-1052. (10.1002/pro.5560020617)

14. Colpas, G. J., Brayman, T. G., Ming, L. J., and Hausinger, R. P. (1999) Identification of metal-binding residues in the Klebsiella aerogenes urease nickel metallochaperone, UreE, *Biochemistry 38*, 4078-4088. (10.1021/bi982435t)

15. Olson, J. W., Mehta, N. S., and Maier, R. J. (2001) Requirement of nickel metabolism proteins HypA and HypB for full activity of both hydrogenase and urease in Helicobacter pylori (vol 39, pg 176, 2001), *Molecular microbiology 40*, 270-270. (DOI 10.1046/j.1365-2958.2001.02397.x)

16. Casalot, L., and Rousset, M. (2001) Maturation of the [NiFe] hydrogenases, *Trends Microbiol 9*, 228-237

17. Johnson, R. C., Hu, H. Q., Merrell, D. S., and Maroney, M. J. (2015) Dynamic HypA zinc site is essential for acid viability and proper urease maturation in Helicobacter pylori, *Metallomics : integrated biometal science 7*, 674-682. (10.1039/c4mt00306c)

18. Mehta, N., Olson, J. W., and Maier, R. J. (2003) Characterization of Helicobacter pylori Nickel Metabolism Accessory Proteins Needed for Maturation of both Urease and Hydrogenase, *Journal of bacteriology 185*, 726-734. (10.1128/jb.185.3.726-734.2003)

19. Benoit, S. L., Mehta, N., Weinberg, M. V., Maier, C., and Maier, R. J. (2007) Interaction between the Helicobacter pylori accessory proteins HypA and UreE is needed for urease maturation, *Microbiology 153*, 1474-1482. (10.1099/mic.0.2006/003228-0)

20. Benoit, S. L., McMurry, J. L., Hill, S. A., and Maier, R. J. (2012) Helicobacter pylori hydrogenase accessory protein HypA and urease accessory protein UreG compete with each other for UreE recognition, *Biochimica et biophysica acta 1820*, 1519-1525. (10.1016/j.bbagen.2012.06.002)

21. Fong, Y. H., Wong, H. C., Yuen, M. H., Lau, P. H., Chen, Y. W., and Wong, K. B. (2013) Structure of UreG/UreF/UreH complex reveals how urease accessory proteins facilitate maturation of Helicobacter pylori urease, *PLoS Biol 11*, e1001678. (10.1371/journal.pbio.1001678)

22. Zambelli, B., Turano, P., Musiani, F., Neyroz, P., and Ciurli, S. (2009) Zn2+-linked dimerization of UreG from Helicobacter pylori, a chaperone involved in nickel trafficking and urease activation, *Proteins 74*, 222-239. (10.1002/prot.22205)

23. Voland, P., Weeks, D. L., Marcus, E. A., Prinz, C., Sachs, G., and Scott, D. (2003) Interactions among the seven Helicobacter pylori proteins encoded by the urease gene cluster, *American journal of physiology. Gastrointestinal and liver physiology 284*, G96-G106. (10.1152/ajpgi.00160.2002)

24. Yang, X., Li, H., Lai, T. P., and Sun, H. (2015) UreE-UreG complex facilitates nickel transfer and preactivates GTPase of UreG in Helicobacter pylori, *The Journal of biological chemistry 290*, 12474-12485. (10.1074/jbc.M114.632364)

25. Kennedy, D. C., Herbst, R. W., Iwig, J. S., Chivers, P. T., and Maroney, M. J. (2007) A dynamic Zn site in Helicobacter pylori HypA: A potential mechanism for metal-specific protein activity, *J Am Chem Soc 129*, 16-17. (Doi 10.1021/Ja066958x)

26. Herbst, R. W., Perovic, I., Martin-Diaconescu, V., O'Brien, K., Chivers, P. T., Pochapsky, S. S., Pochapsky, T. C., and Maroney, M. J. (2010) Communication between the Zinc and Nickel Sites in Dimeric HypA: Metal Recognition and pH Sensing, *J Am Chem Soc 132*, 10338-10351. (Doi 10.1021/Ja1005724)

27. Xia, W., Li, H. Y., Sze, K. H., and Sun, H. Z. (2009) Structure of a Nickel Chaperone, HypA, from Helicobacter pylori Reveals Two Distinct Metal Binding Sites, *J Am Chem Soc 131*, 10031-10040. (Doi 10.1021/Ja900543y)

28. Yang, X., Li, H., Cheng, T., Xia, W., Lai, Y. T., and Sun, H. (2014) Nickel translocation between metallochaperones HypA and UreE in Helicobacter pylori, *Metallomics : integrated biometal science 6*, 1731-1736. (10.1039/c4mt00134f)

29. Sachs, G., Weeks, D. L., Wen, Y., Marcus, E. A., Scott, D. R., and Melchers, K. (2005) Acid acclimation by Helicobacter pylori, *Physiology 20*, 429-438. (DOI 10.1152/physiol.00032.2005)

30. Wen, Y., Marcus, E. A., Matrubutham, U., Gleeson, M. A., Scott, D. R., and Sachs, G. (2003) Acid-Adaptive Genes of Helicobacter pylori, *Infection and Immunity 71*, 5921-5939. (10.1128/iai.71.10.5921-5939.2003)

31. Scott, D. R., Marcus, E. A., Weeks, D. L., and Sachs, G. (2002) Mechanisms of acid resistance due to the urease system of Helicobacter pylori, *Gastroenterology 123*, 187-195

32. Xia, W., Li, H., Yang, X., Wong, K. B., and Sun, H. (2012) Metallo-GTPase HypB from Helicobacter pylori and its interaction with nickel chaperone protein HypA, *The Journal of biological chemistry 287*, 6753-6763. (10.1074/jbc.M111.287581)

33. Schreiber, S., Konradt, M., Groll, C., Scheid, P., Hanauer, G., Werling, H. O., Josenhans, C., and Suerbaum, S. (2004) The spatial orientation of Helicobacter pylori in the gastric mucus, *Proc Natl Acad Sci U S A 101*, 5024-5029. (10.1073/pnas.0308386101)

34. Maier, R. J., Benoit, S. L., and Seshadri, S. (2007) Nickel-binding and accessory proteins facilitating Ni-enzyme maturation in Helicobacter pylori, *Biometals : an international journal on the role of metal ions in biology, biochemistry, and medicine 20*, 655-664. (10.1007/s10534-006-9061-8)

35. Bury-Mone, S., Skouloubris, S., Labigne, A., and De Reuse, H. (2001) The Helicobacter pylori UreI protein: role in adaptation to acidity and identification of residues essential for its activity and for acid activation, *Molecular microbiology 42*, 1021-1034

CHAPTER 5

CONCLUSIONS AND FUTURE DIRECTIONS

5.1 Discussions and conclusions

The abundant use of the Ni-dependent enzyme, urease, is one of the major adaptations that allow the human pathogen *Helicobacter pylori* to colonize the acidic human stomach,[1-4] ensuring the rapid activation of enzyme upon acid stress by insertion of Ni into the urease active site.[5] In addition to the urease-specific accessory proteins UreEFGH, the full activation of urease also required the accessory proteins HypA and HypB, which are associated with Ni insertion into the NiFe-hydrogenase (H_2ase).[5, 6] Thus, the accessory proteins HypA and HypB are pivotal for the maturation of Ni-dependent enzymes within *H. pylori*.

While the role of HypB (discussed in APPENDIX 1) in urease maturation remain uncertain,[7-9] the link between the Ni-metallochaperone HypA and the urease maturation pathway was established through its direct interaction with the urease-specific Ni-metallochaperone, $UreE_2$.[10-13] The small HypA protein (13 kDa) contains two conserved metal sites, the structural Zn site involving two CXXC motifs, as well as the Ni site using the N-terminal MHE-motif.[14-18] The work presented in this dissertation seeks to further explore the role of the Ni-metallochaperone HypA in the Ni-dependent acid adaptions of *H. pylori*. Our findings were summarized in the model shown in Figure 5.1.

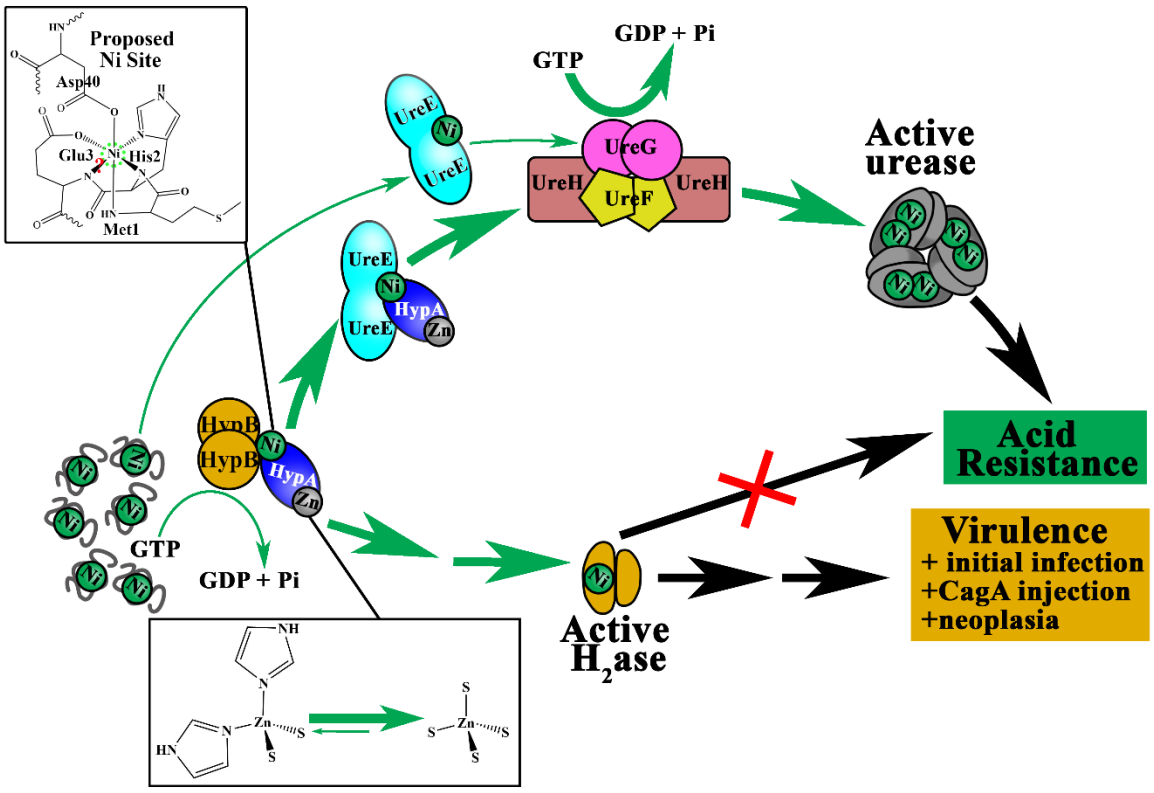

Figure 5.1: Model summarizing the role of HypA in *H. pylori* Ni enzyme maturation. The available Ni pool within the cells bound by proteins, peptides, or small molecules (represented as squiggles). Ni-trafficking pathways are shown in green arrows and pathways to other cellular processes are shown in black arrows, where thin arrows represent minor pathways. The red X indicates the lack of a contribution for H_2ase in the acid resistance mechanisms in *H. pylori*. Proposed HypA Ni and Zn sites are shown in boxes.

5.1.1 Hydrogenase is not required for acid adaptation in *H. pylori*

The only other Ni-dependent enzyme in *H. pylori*, NiFe-H_2ase, has been characterized as a membrane-bound enzyme that oxidizes molecular H_2 (presumably produced by intestinal flora in the host) to protons and electrons.[19, 20] H_2ase has also been shown to be increase initial colonization density in Mongolian gerbil infection models.[20, 21] While this phenotype was attributed to its use of H_2 as an alternate energy source,[20] its potential contribution to acid adaptability was not addressed until our present study. A variant strain of *H. pylori* G27 that lack H_2ase activity was created, by deleting the *hydB* gene, which coded for the Ni-containing large subunit of H_2ase. H_2ase and urease assays confirmed that the Δ*hydB* strain exhibit WT-like in urease activity CHAPTER 2, Figure 2.2B), but does not have H_2-oxidation activity (CHAPTER

2, Figure 2.2A). In acid shock challenge, the Δ*hydB* strain also exhibit WT-like survival (CHAPTER 2, Figure 2.3D), whereas the urease-deficient strain (Δ*ureB*) did not survive the acid challenge. These results were independently verified in the Δ*hydABCDE* strain in the *H. pylori* 26695 background (CHAPTER 2, Figure 2.4).

Our results indicate that H_2ase is not part of the acid adaptive mechanism in *H. pylori*. The initial boost in infection density observed in Mongolian gerbils with H_2ase-active strains were not a result of increased acid adaptations, and are more likely related to the coupling of H_2ase activity to increased activity in the *H. pylori* type IV secretion system (T4SS) in modifying the host immune system.[21] Since both H_2ase and urease rely on the presence of HypA for Ni-insertion, these two enzymes must compete for activation.

5.1.2 Proper HypA metal site structures are important for Ni-enzyme maturation and acid survival

Previous structural characterizations of Ni-bound *H. pylori* HypA indicated that the Zn site coordination is dynamic, changing from an averaged $Zn(Cys)_4$ site at pH 7.2 to a $Zn(Cys)_2(His)_2$ site at pH 6.3 (CHAPTER 1, Figure 1.6**)**.[15] Structural changes were lost with ligand substitution or loss of any of the Cys residues that constituted the conserved CXXC (C74, C77, C91, C94) motifs, or the loss of either of the flanking His residues (H79 or H95) (CHAPTER 3, Figure 3.1).[16] The endogenous *hypA* gene in *H. pylori* was replaced with the coding sequences for the HypA Zn site variants. These *hypA* Zn site variant strains were then tested for acid survival, as well as H_2ase and urease activities.[18] Our results show that the non-conserved His residues are generally not important for acid survival or enzymatic activities (CHAPTER 3, Figure 3.3).[18] The conserved Cys residues are generally important for enzymatic activities, but only the C74D, C91A, and C94A variant strains were deficient in acid survival (CHAPTER 3, Figure 3.2 Figure 3.3**)**[18] These results indicate that although mutation of any Cys residues in the CXXC motifs resulted in the same averaged structure at the Zn site [$Zn(Cys)_2(His)_2$], certain positions in the CXXC motifs are more significant than others in enzyme maturation.[18] Taken together, our

studies suggest that the proper Zn site coordination in HypA is required for efficient maturation of urease and H_2ase, and that the residues that are important for the maturation of urease are also important for H_2ase. Additionally, full urease activation is not necessary for short term acid survival (1 hour at pH 2.3, with 5 mM urea supplement).[18]

The Ni coordination to the N-terminal amine of HypA was also established and its effects were investigated. The L2*-HypA variant was created, wherein an Leu residue was inserted between the conserved Met1 and His2 residue, thereby extending the N-terminal amine one residue further away from the known Ni-binding site. Structural and magnetic property studies show that the L2*-HypA variant is five-coordinate and diamagnetic, having lost two N/O-ligands (presumably contributed by the protein), one of which was replaced by a buffer anion as compared to WT (CHAPTER 3, Table 3.1 and Figure 3.7**)**, which is six-coordinate and paramagnetic.[17] This change in coordination and magnetic properties in L2* is similar to a previously characterized N-terminal extension variant GSHypA (Gly-Ser overhang at the N-terminus leftover from cleavage of an affinity tag).[14] *H. pylori* strains expressing the L2*-HypA protein are also deficient in acid survival, and lack H_2ase and urease activities (CHAPTER 3, Figure 3.8 and Figure 3.9**)**.[17] This phenotypic deficiency is best explained by a decrease in Ni-binding affinity by one order of magnitude compared to WT-HypA (CHAPTER 3, Table 3.2, and Figure 3.11 and Figure 3.12).[17] While the affinity of the protein-protein interactions between apo-ZnHypA and apo-$UreE_2$ (CHAPTER 3, Table 3.2 and Figure 3.10**)** were unaffected by the L2* mutation.[17]

5.1.3 HypA and $UreE_2$ act as co-metallochaperone in delivering Ni for urease maturation

HypA has been hypothesized to hand-off Ni to $UreE_2$ in the urease maturation pathway,[13] enabling Ni-$UreE_2$ to deliver Ni to the rest of the maturation complex: UreH-$UreG_2$-$UreF_2$-UreH.[22] However, the HypA-$UreE_2$ complex does not appear to dissociate without either denaturation[13] or the presence of $UreG_2$ (along with Mg^{2+} and GTP),[23] indicating a more involved role than the Ni hand-off mechanism. We systematically investigated the interaction of Ni with

HypA, $UreE_2$, and the HypA-$UreE_2$ complex (CHAPTER 4, Table 4.2, and Figure 4.4), as well as the protein-protein interactions between HypA and $UreE_2$ with and without Ni (CHAPTER 4, Table 4.1, and Figure 4.2 and Figure 4.3), at pH conditions that simulate the internal pH of *H. pylori* at neutral (pH 7.2) and under acid shock (pH 6.3) conditions. We found a new Ni-binding site was formed in the HypA-$UreE_2$ complex that is tighter than Ni-binding to either protein individually (CHAPTER 4, Figure 4.4**)**. Contrary to the prediction of a Ni hand-off mechanism from HypA to $UreE_2$, Ni-ZnHypA interactions with Ni-$UreE_2$ persisted and are enhanced compared to the interactions of the two apo-proteins (CHAPTER 4, Figure 4.3). Moreover, the Ni-ZnHypA-$UreE_2$ complex is stable at sub-micromolar concentrations (CHAPTER 4, Figure 4.5), with neither Ni or apo-ZnHypA dissociating from the complex, as expected from a simple Ni hand-off mechanism. Our results indicate that HypA and $UreE_2$ form a tight complex, which act as co-metallochaperones in Ni delivery to the urease maturation pathway. In prior studies, the dissociation of the GSHypA-$UreE_2$ complex was promoted by the presence of $UreG_2$ (along with Mg^{2+} and GTP),[23] which would ensure the fidelity in Ni delivery to the urease maturation pathway.

5.2 Future Directions

The role of HypA as a co-metallochaperone along with $UreE_2$ in Ni delivery, as well as the importance of the unmodified metal sites within HypA, in the activation of urease confirmed that Ni delivery involving HypA is an essential part of the post-translational regulation of urease activation in *H. pylori*. With the abundance of apo-urease produced at both neutral and acidic pH,[4] the multi-level regulation of its activity is essential for the survival and adaptability of the cell in the host stomach.[24] Alternately, *H. pylori* may divert Ni to the H_2ase maturation pathway. Based on infection studies in Mongolian gerbil models, elevation of H_2ase activity is associated with more virulent infections (increase initial infection density; and prolong inflammation and host cell transformation in *cagA*-positive strains).[20, 21] Understanding the underlying mechanisms of diverging Ni co-factors between H_2ase and urease may lead to better treatments and/or more

effective eradications of particularly virulent strains if *H. pylori*. The future directions suggested here pertain to additional layers in the regulation of urease and H_2ase activities within *H. pylori* by controlling Ni availability.

5.2.1 $UreE_2$ stability as a mechanism for controlling urease activity

Ni supplementation in the growth media can restore the urease activity to Δ*hypA* strains but not in Δ*ureE* strains of *H. pylori*.[6] However, purified *H. pylori* $UreE_2$ proteins have been documented to be degraded at the C-terminal motif,[17, 25, 26] which resulted in loss of interaction with HypA and potential loss of Ni-binding.[13] Formation of the HypA-$UreE_2$ complex have been shown to stabilized $UreE_2$ (CHAPTER 4, Figure 4.6) and slow the degradation at both neutral and acidic pH, in the presence and absence of Ni. This observation led us to the hypothesis that the C-terminal degradation of $UreE_2$ is part of the mechanism for controlling the activity of urease. To further test this hypothesis, the stability of the UreE peptide(s) should be tested *in vivo*.

One of the most unambiguous ways to test the stability of the UreE peptide is through Western blotting of the whole cell lysate. The full-length and C-terminally degraded UreE peptides separate into discrete bands in 16% SDS-PAGE (CHAPTER 4, Figure 4.6) in relatively dilute conditions. Therefore, SDS-PAGE can be used to separate these peptides in whole cell lysate. *H. pylori* cells grown at neutral and acidic pH should be compared for the relative abundance and ratio of full-length versus C-terminally degraded UreE peptide. Since the *hypA* gene is transcriptionally upregulated in acid stress, it is expected that the HypA protein levels would be increased under acidic growth conditions. Therefore, the ratio of full-length UreE peptide to C-terminally degraded peptide is expected to be greater in cultures grown under acid conditions compared to those grown under neutral conditions. Western Blots of an invariable cellular protein, UreB, and HypA proteins should also be conducted as a control for loading, as well as confirming the expected increase in UreB and HypA levels under acidic growth. Anti-UreE,[27] anti-HypA,[10] and anti-UreB[7] antibodies were previously described from work in the Maier lab (University of Georgia, Athens, GA).

To confirm the role of HypA in stabilizing the UreE peptide, a variant strain of *H. pylori* should be constructed that constitutively overexpresses (OX) the WT-HypA or Ni-binding deficient variant of HypA (such as L2*-HypA). Additional controls would include the *hypA::kan-sacB* strain, which do not express a functional HypA peptide. All cells should be grown at the same pH conditions (neutral) and in media with a consistent and known concentration of Ni. The ratio of full-length to C-terminally degraded UreE peptides in the *hypA*-OX strains is expected to be higher than WT (G27 parental) strain, and the *hypA::kan-sacB* strain is expected to have the lowest full-length $UreE_2$. It is unclear whether the strain overexpressing the L2*-HypA protein would protect UreE from degradation, although it is expected to, since N-terminally modified HypA (GSHypA[13] and L2*-HypA[17]) persisted in forming tight complexes with $UreE_2$. Thus far the protection of UreE by complex formation with HypA does not appear to be Ni-dependent (CHAPTER 4, Figure 4.6), although Ni-dependence should be reevaluated within the cell. The urease activity assays of these strains should be tested to confirm the expected increase in urease activity in strains overexpressing the WT-HypA protein.

5.2.2 High affinity Ni-binding site in the HypA-$UreE_2$ complex

We observe a tight binding event (K_d ~ 0.2 – 3 nM) in the titration of Ni into the preformed apo-ZnHypA-$UreE_2$ complex that was not observed in the binding of Ni to either proteins individually (CHAPTER 4, Table 4.2). This binding event was not observed in the titration of Ni into the L2*-HypA-$UreE_2$ complex, where the Ni site in HypA was disrupted. The interaction of Ni-ZnHypA with apo-$UreE_2$ also produced a tight binding event (K_d ~ 0.6 nM) that was absent from the interaction of the apo-proteins (CHAPTER 4, Table 4.1). These events point to the formation of a unique high-affinity Ni-binding site within the ZnHypA-$UreE_2$ complex that involves ligands from both proteins (i.e. at an interfacial site).

The structural characterization of this potential new Ni site would further support the role of HypA and $UreE_2$ as co-metallochaperones in Ni-delivery. XAS studies of the Ni sites in Ni-

ZnHypA[15-17] and Ni-UreE$_2$[28] indicate that these proteins each form six-coordinate complexes with Ni, containing all N/O ligands. XAS characterizations of the Ni-ZnHypA-UreE$_2$ complex compared to the Ni complex with either protein should reveal whether this new high-affinity site is unique. The Ni-ZnHypA-UreE$_2$ Ni K-edge is expected to be different from Ni-complex with either protein alone (Figure 5.2).

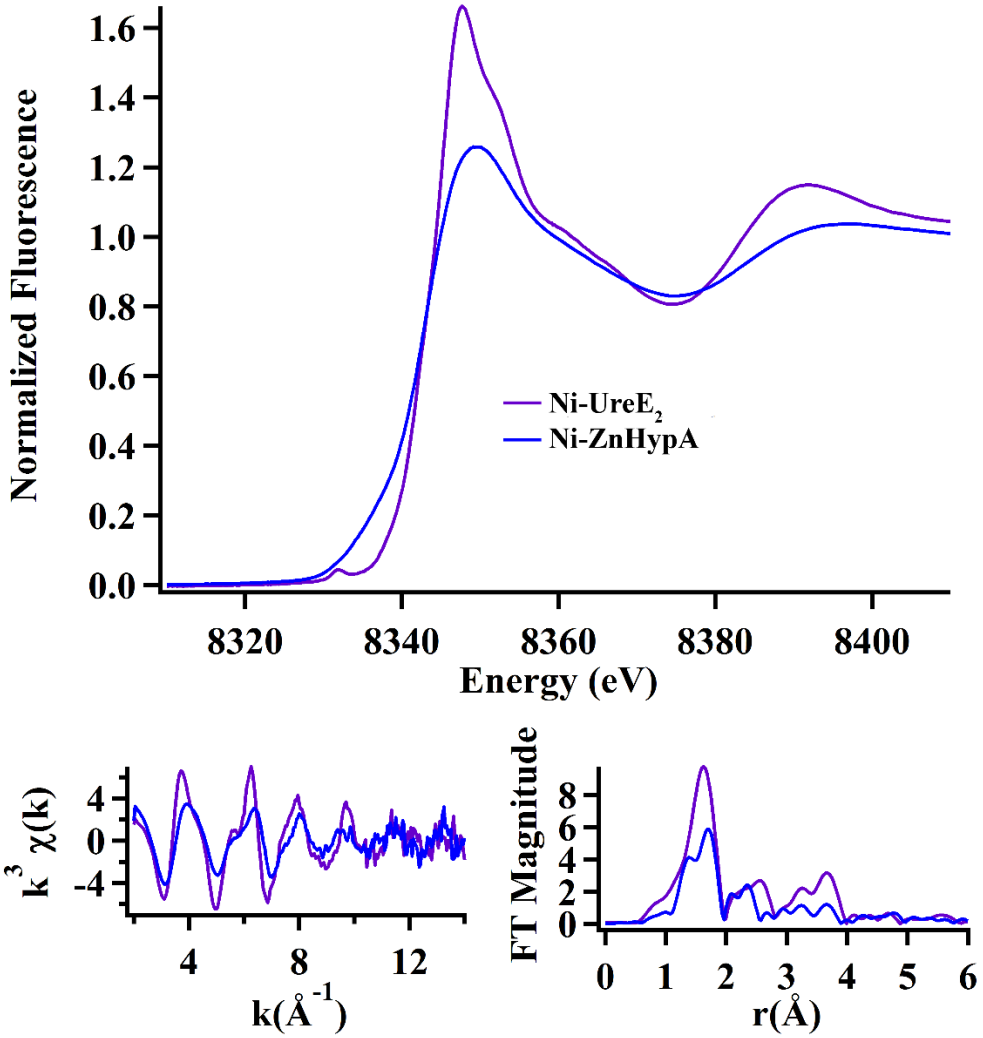

Figure 5.2: XAS Ni K-edge overlay of Ni-UreE$_2$ and Ni-ZnHypA.
Comparison of published Ni K-edge XANES (top) and EXAFS (bottom) spectra [k^3-weighted unfiltered EXAFS data (left) and Fourier-transformed data (right)] for Ni-complexes with *H. pylori* UreE$_2$[28] and HypA[17].

We expect that the ligands from each protein contribute to the formation of the new Ni site within the Ni-ZnHypA-UreE$_2$ complex. This hypothesis was supported by the loss of the high-affinity binding site when Ni was titrated into the ZnL2*HypA-UreE$_2$ complex, resulting in

a single binding event (K_d ~ 20 nM) with affinities similar to Ni binding to $UreE_2$ (K_d ~ 60 nM) alone (APPENDIX 3, Figure A3.4). Additionally, replacing the endogenous *hypA* gene with L2*-*hypA* resulted in loss of urease activity (CHAPTER3, Figure 3.9) and acid survival (CHAPTER 3, Figure 3.8) in *H. pylori* cultures, indicating that the N-terminal amine plays a crucial role in the urease maturation pathway. Comparison of the Ni K-edges of the Ni-ZnWTHypA-$UreE_2$ and the Ni-ZnL2*HypA-$UreE_2$ complexes will definitively reveal whether the N-terminal amine is a ligand in the new Ni-ZnHypA-$UreE_2$ complex. Additionally, comparison of the Ni K-edge of the Ni-ZnL2*HypA-$UreE_2$ complex with the Ni-$UreE_2$ will definitively reveal whether the loss of the N-terminal amine as a potential ligand prevents the formation of the high-affinity Ni site formed by the HypA-$UreE_2$ complex.

The Ni site within the Ni-ZnHypA-$UreE_2$ complex may also be explored using variant proteins of $UreE_2$, such as H102K and H152A. The H152A variant was previously characterized to have lower affinity for Ni compared to WT-$UreE_2$, whereas the H102K variant did not bind Ni.[26, 28] The Ni titration into ZnHypA-$UreE_2$ with either of these two variants would reveal whether one or both of these ligands are involved in the formation of the new Ni site. Additionally, biophysical characterizations of the interaction between the HypA protein with these two $UreE_2$ variants would reveal the role of each potential ligand.

In addition to these biophysical and spectroscopic studies of the Ni-ZnHypA-$UreE_2$ complex, efforts to crystalize the complex should be attempted. The crystal structures of $UreE_2$ had already been solved.[25, 28] Although the Ni-binding domain of the protein has been disordered due to degradation of the $UreE_2$ C-terminal domain,[25, 28] mutagenesis and XAS were used to confirm the side-chain of His152 as a Ni-binding ligand.[28] We have found that formation of the ZnHypA-$UreE_2$ complex with or without Ni can slow the degradation process of the $UreE_2$ protein (CHAPTER 4, Figure 4.6). This finding indicated that co-crystallization of these two proteins may prove to be a valuable tool for gaining structural information. Firstly, co-expression of the HypA and UreE proteins in *E. coli* could be accomplished using the *pETDuet* vectors

(EMD Millipore). The purified HypA-$UreE_2$ complexes from these cells should therefore have minimal degradation in the C-terminal domain of UreE. Since the crystallization conditions for $UreE_2$ has already been published,[25, 28] the same conditions should be used to attempt to crystalize the HypA-$UreE_2$ complex. Success in crystallizing this complex, especially with Ni-bound, will provide validation of the biochemical data as well as a wealth of information regarding the urease maturation process.

5.2.3 Role of HypB in Ni-enzyme maturation

Although both *hypA* and *hypB* are required for the maturation of H_2ase and urease in *H. pylori*,[6] the role of HypB remain uncertain. Similar to the requirement of HypA, the HypB-requirement for maturation of *H. pylori* urease is only necessary when Ni is abundant.[6] HypB is small GTPase in the G3E family and part of the SIMIBI class of P-loop NTPases.[29, 30] Studies involving the GTPase-deficient K59A-*hypB* strain of *H. pylori* indicate that the GTP-turnover activity in HypB is more important for H_2ase activation than urease (discussed in APPENDIX 1).[7] The GTPase activity of the protein has been notoriously sluggish *in vitro*, leading to hypotheses that additional cofactors are required to boost its activity.[7, 29-31] Recently, potassium (100 mM KCl) was shown to boost the GTPase activity of HypB by one order of magnitude, whereas excessive (200 μM) Ni and Zn was found to reduce this activity.[30] Although our own studies along with others in literature[31] support that lower concentrations of Ni (5 μM) does not negatively affect the GTPase activity of HypB, and the addition of 5 μM of Ni along with stoichiometric concentrations of HypA improves the GTP turnover rate (APPENDIX 1, Table A1.2 and Figure A1.9).

One hypothesis that may explain this phenomenon is that HypB interacts with HypA and the Ni-storage proteins within the cells (Figure 5.1), where the presence of both HypA and Ni stimulates the GTPase turnover in HypB to release Ni for the urease maturation pathway. This hypothesis is supported by the interaction between *H. pylori* HypB with known Ni-storage

proteins, Hpn and Hpn2.[32] Hpn appears to be important for upregulating urease activity in Ni abundant conditions, whereas Hpn2 appears to suppress urease activation in low Ni conditions.[32, 33] Several *in vitro* experiments can be used to characterized the interactions between Hpn, HypA, and HypB.

The His- and Cys-rich Hpn protein (7 kDa monomer) have been known to form large oligomers after purification (> 500 kDa) without the presence of 500 mM of imidazole and 5 mM of DTT.[32] These large oligomers were predicted to be also present inside the cell.[32] These large oligomers prevent many traditional biochemical techniques that probe its direct interactions with HypB. However, the Ni content of proteins can be used to directly monitor whether HypB can release Ni from the Hpn oligomers.

First, Hpn must be purified[32] and then bound to Ni with all excess Ni removed from the buffer. A portion of the Ni-Hpn complex can be mixed with apo-HypB, and then the HypB protein can be separated from the Ni-Hpn oligomers after an appropriate incubation period. This could be accomplished by either using a Zeba Spin desalting column at 40 kDa MWCO or a Vivaspin protein concentrator at 100 kDa MWCO. The separated fractions should be evaluated by 20% SDS-PAGE to ensure proper separation of the two proteins. The recovered HypB protein should be evaluated by ICP to determine whether it was able to extract Ni from the Ni-Hpn complex. Alternatively, SEC can be used for separating the HypB and Ni-Hpn mixture, although the large Ni-Hpn oligomers may negatively affect the reproducibility and longevity of the column. The separation techniques used will concentrate or dilute the Ni content of the protein complexes, and therefore all fractions must be meticulously collected and then assess as a percentage of total available Ni in the system.

This experiment should be performed in the presence of buffers that promote GTPase turnover in HypB (20 mM HEPES, 100 mM NaCl, 100 mM KCl, 5 mM $MgCl_2$, and 1 mM TCEP), and the experiment should be repeated at pH 7.2 and 6.3 with and without the presence of GTP or GDP. Although bacteria two-hybrid assays did not find direct interactions between HypA

and either Hpn or Hpn2,[32] it is possible that HypA can still directly bind Ni from the Ni-Hpn complex. Therefore, the separation techniques should also be repeated using HypA alone. Our preliminary results indicate that the presence of HypA and Ni together can stimulate GTP-turnover in HypB (APPENDIX 1, Table A1.2 and Figure A1.9). Therefore, we predict that adding Apo-ZnHypA and apo-HypB together to the Ni-Hpn oligomers would simulate additional release of Ni, which should be tested directly. These experiments can also be repeated with the previously characterized GTPase-deficient HypB variant, K59A-HypB.

Systematic deletion of the *hpn*, *hypB*, and *hypA* genes from the *H. pylori* genome can be used to assess whether the interaction between HypB and Hpn is linked to the Ni enzyme maturation pathway. The Δ*hypA* and Δ*hypB* effects on urease and hydrogenase activities were observed in various strain of *H. pylori* (43504, 26695, G27),[6, 8, 17, 18] at least two of which should be selected for additional deletion of the *hpn* gene. The control strains of WT, Δ*hydB*, and Δ*ureB*; the single-gene mutants Δ*hypB,* K59A-*hypB,* and Δ*hpn*; and double-mutants Δ*hpn*-Δ*hypB* and Δ*hpn*-K59A-*hypB* would be assessed for urease and hydrogenase activities as well as acid survivals in the presence and absence of 5 μM of Ni added to the growth media. The Δ*hpn* strain is expected not to have deleterious effects on the acid survival, urease, or H_2ase activities with or without Ni supplementation.[32] The Δ*hypB* or K59A-Δ*hypB* are expected to be acid sensitive, urease- and H_2ase-deficient, which is expected to be rescued to varying extents with 5 μM of Ni added to the growth media. However, the Ni-supplementation is not expected to rescue the Δ*hpn*-Δ*hypB* and Δ*hpn*-K59A-*hypB* strains, in acid survival, urease or H_2ase activities. These studies should be repeated with Δ*hypA* and *hypA*-overexpression strains to assess the effect of HypA to the system.

These same assays can be repeated alongside Hpn2 proteins and Δ*hpn2* variants strains of *H. pylori*. Although the Hpn2 protein properties have been extensively studied,[34] but its interaction with HypB is less robust and dependent on the Gln-rich C-terminal region of the

protein. Additionally, the *hpn2* gene appear to negatively regulate urease activity, where the Δ*hpn2* strains appear to have increased urease activities compared to WT (B128) strain.[32]

5.3 References

1. Fischer, F., and De Reuse, H. (2016) Adaptation of *Helicobacter pylori* Metabolism to Persistent Gastric Colonization, In *Helicobacter pylori Research From Bench to Bedside* (Steffen Backert, Y. Y., Ed.), pp 29-56, Springer, Japan.

2. Salama, N. R., Hartung, M. L., and Muller, A. (2013) Life in the human stomach: persistence strategies of the bacterial pathogen Helicobacter pylori, *Nat Rev Microbiol 11*, 385-399. (10.1038/nrmicro3016)

3. Sachs, G., Weeks, D. L., Wen, Y., Marcus, E. A., Scott, D. R., and Melchers, K. (2005) Acid acclimation by Helicobacter pylori, *Physiology 20*, 429-438. (DOI 10.1152/physiol.00032.2005)

4. Bauerfeind, P., Garner, R., Dunn, B. E., and Mobley, H. L. T. (1997) Synthesis and activity of Helicobacter pylori urease and catalase at low pH, *Gut 40*, 25-30

5. Maier, R. J., Benoit, S. L., and Seshadri, S. (2007) Nickel-binding and accessory proteins facilitating Ni-enzyme maturation in Helicobacter pylori, *Biometals : an international journal on the role of metal ions in biology, biochemistry, and medicine 20*, 655-664. (10.1007/s10534-006-9061-8)

6. Olson, J. W., Mehta, N. S., and Maier, R. J. (2001) Requirement of nickel metabolism proteins HypA and HypB for full activity of both hydrogenase and urease in Helicobacter pylori (vol 39, pg 176, 2001), *Molecular microbiology 40*, 270-270. (DOI 10.1046/j.1365-2958.2001.02397.x)

7. Mehta, N., Benoit, S., and Maier, R. J. (2003) Roles of conserved nucleotide-binding domains in accessory proteins, HypB and UreG, in the maturation of nickel-enzymes required for efficient Helicobacter pylori colonization, *Microbial Pathogenesis 35*, 229-234. (10.1016/s0882-4010(03)00151-7)

8. Benanti, E. L., and Chivers, P. T. (2009) An intact urease assembly pathway is required to compete with NikR for nickel ions in Helicobacter pylori, *Journal of bacteriology 191*, 2405-2408. (10.1128/JB.01657-08)

9. Stingl, K., Schauer, K., Ecobichon, C., Labigne, A., Lenormand, P., Rousselle, J. C., Namane, A., and de Reuse, H. (2008) In Vivo Interactome of Helicobacter pylori Urease Revealed by Tandem Affinity Purification, *Mol Cell Proteomics 7*, 2429-2441. (DOI 10.1074/mcp.M800160-MCP200)

10. Mehta, N., Olson, J. W., and Maier, R. J. (2003) Characterization of Helicobacter pylori Nickel Metabolism Accessory Proteins Needed for Maturation of both Urease and Hydrogenase, *Journal of bacteriology 185*, 726-734. (10.1128/jb.185.3.726-734.2003)

11. Benoit, S. L., Mehta, N., Weinberg, M. V., Maier, C., and Maier, R. J. (2007) Interaction between the Helicobacter pylori accessory proteins HypA and UreE is needed for urease maturation, *Microbiology 153*, 1474-1482. (10.1099/mic.0.2006/003228-0)

12. Benoit, S. L., McMurry, J. L., Hill, S. A., and Maier, R. J. (2012) Helicobacter pylori hydrogenase accessory protein HypA and urease accessory protein UreG compete with each other for UreE recognition, *Biochimica et biophysica acta 1820*, 1519-1525. (10.1016/j.bbagen.2012.06.002)

13. Yang, X., Li, H., Cheng, T., Xia, W., Lai, Y. T., and Sun, H. (2014) Nickel translocation between metallochaperones HypA and UreE in Helicobacter pylori, *Metallomics : integrated biometal science 6*, 1731-1736. (10.1039/c4mt00134f)

14. Xia, W., Li, H. Y., Sze, K. H., and Sun, H. Z. (2009) Structure of a Nickel Chaperone, HypA, from Helicobacter pylori Reveals Two Distinct Metal Binding Sites, *J Am Chem Soc 131*, 10031-10040. (Doi 10.1021/Ja900543y)

15. Kennedy, D. C., Herbst, R. W., Iwig, J. S., Chivers, P. T., and Maroney, M. J. (2007) A dynamic Zn site in Helicobacter pylori HypA: A potential mechanism for metal-specific protein activity, *J Am Chem Soc 129*, 16-17. (Doi 10.1021/Ja066958x)

16. Herbst, R. W., Perovic, I., Martin-Diaconescu, V., O'Brien, K., Chivers, P. T., Pochapsky, S. S., Pochapsky, T. C., and Maroney, M. J. (2010) Communication between the Zinc and Nickel Sites in Dimeric HypA: Metal Recognition and pH Sensing, *J Am Chem Soc 132*, 10338-10351. (Doi 10.1021/Ja1005724)

17. Hu, H. Q., Johnson, R. C., Merrell, D. S., and Maroney, M. J. (2017) Nickel Ligation of the N-Terminal Amine of HypA Is Required for Urease Maturation in Helicobacter pylori, *Biochemistry 56*, 1105-1116. (10.1021/acs.biochem.6b00912)

18. Johnson, R. C., Hu, H. Q., Merrell, D. S., and Maroney, M. J. (2015) Dynamic HypA zinc site is essential for acid viability and proper urease maturation in Helicobacter pylori, *Metallomics : integrated biometal science 7*, 674-682. (10.1039/c4mt00306c)

19. Benoit, S. L., and Maier, R. J. (2008) Hydrogen and nickel metabolism in helicobacter species, *Ann N Y Acad Sci 1125*, 242-251. (10.1196/annals.1419.014)

20. Olson, J. W., and Maier, R. J. (2002) Molecular hydrogen as an energy source for Helicobacter pylori, *Science 298*, 1788-1790. (10.1126/science.1077123)

21. Wang, G., Romero-Gallo, J., Benoit, S. L., Piazuelo, M. B., Dominguez, R. L., Morgan, D. R., Peek, R. M., Jr., and Maier, R. J. (2016) Hydrogen Metabolism in Helicobacter pylori Plays a Role in Gastric Carcinogenesis through Facilitating CagA Translocation, *MBio 7*. (10.1128/mBio.01022-16)

22. Fong, Y. H., Wong, H. C., Yuen, M. H., Lau, P. H., Chen, Y. W., and Wong, K. B. (2013) Structure of UreG/UreF/UreH complex reveals how urease accessory proteins facilitate maturation of Helicobacter pylori urease, *PLoS Biol 11*, e1001678. (10.1371/journal.pbio.1001678)

23. Yang, X., Li, H., Lai, T. P., and Sun, H. (2015) UreE-UreG complex facilitates nickel transfer and preactivates GTPase of UreG in Helicobacter pylori, *The Journal of biological chemistry 290*, 12474-12485. (10.1074/jbc.M114.632364)

24. Stingl, K., and De Reuse, H. (2005) Staying alive overdosed: how does Helicobacter pylori control urease activity?, *International journal of medical microbiology : IJMM 295*, 307-315. (10.1016/j.ijmm.2005.06.006)

25. Shi, R., Munger, C., Asinas, A., Benoit, S. L., Miller, E., Matte, A., Maier, R. J., and Cygler, M. (2010) Crystal structures of apo and metal-bound forms of the UreE protein from Helicobacter pylori: role of multiple metal binding sites, *Biochemistry 49*, 7080-7088. (10.1021/bi100372h)

26. Bellucci, M., Zambelli, B., Musiani, F., Turano, P., and Ciurli, S. (2009) Helicobacter pylori UreE, a urease accessory protein: specific Ni(2+)- and Zn(2+)-binding properties and interaction with its cognate UreG, *The Biochemical journal 422*, 91-100. (10.1042/BJ20090434)

27. Benoit, S., and Maier, R. J. (2003) Dependence of Helicobacter pylori Urease Activity on the Nickel-Sequestering Ability of the UreE Accessory Protein, *Journal of bacteriology 185*, 4787-4795. (10.1128/jb.185.16.4787-4795.2003)

28. Banaszak, K., Martin-Diaconescu, V., Bellucci, M., Zambelli, B., Rypniewski, W., Maroney, M. J., and Ciurli, S. (2012) Crystallographic and X-ray absorption spectroscopic characterization of Helicobacter pylori UreE bound to Ni(2)(+) and Zn(2)(+) reveals a role for the disordered C-terminal arm in metal trafficking, *The Biochemical journal 441*, 1017-1026. (10.1042/BJ20111659)

29. Sydor, A. M., Liu, J., and Zamble, D. B. (2011) Effects of metal on the biochemical properties of Helicobacter pylori HypB, a maturation factor of [NiFe]-hydrogenase and urease, *Journal of bacteriology 193*, 1359-1368. (10.1128/JB.01333-10)

30. Sydor, A. M., Lebrette, H., Ariyakumaran, R., Cavazza, C., and Zamble, D. B. (2014) Relationship between Ni(II) and Zn(II) coordination and nucleotide binding by the Helicobacter pylori [NiFe]-hydrogenase and urease maturation factor HypB, *The Journal of biological chemistry 289*, 3828-3841. (10.1074/jbc.M113.502781)

31. Xia, W., Li, H., Yang, X., Wong, K. B., and Sun, H. (2012) Metallo-GTPase HypB from Helicobacter pylori and its interaction with nickel chaperone protein HypA, *The Journal of biological chemistry 287*, 6753-6763. (10.1074/jbc.M111.287581)

32. Vinella, D., Fischer, F., Vorontsov, E., Gallaud, J., Malosse, C., Michel, V., Cavazza, C., Robbe-Saule, M., Richaud, P., Chamot-Rooke, J., Brochier-Armanet, C., and De Reuse, H. (2015) Evolution of Helicobacter: Acquisition by Gastric Species of Two Histidine-Rich Proteins Essential for Colonization, *PLoS Pathog 11*, e1005312. (10.1371/journal.ppat.1005312)

33. Ge, R., Watt, R. M., Sun, X., Tanner, J. A., He, Q. Y., Huang, J. D., and Sun, H. (2006) Expression and characterization of a histidine-rich protein, Hpn: potential for Ni2+ storage in Helicobacter pylori, *The Biochemical journal 393*, 285-293. (10.1042/BJ20051160)

34. Zeng, Y. B., Yang, N., and Sun, H. (2011) Metal-binding properties of an Hpn-like histidine-rich protein, *Chemistry 17*, 5852-5860. (10.1002/chem.201100279)

APPENDIX 1

STRUCTURE, ACTIVITY, AND INTERACTIONS OF *HELICOBACTER PYLORI* HYPB

A1.1 Introduction

The *Helicobacter pylori hypA* and *hypB* genes are required for the maturation of NiFe-hydrogenase (H_2ase),[1] and the full maturation of urease under conditions where Ni is not supplemented in the media.[1, 2] The focus of this dissertation has been on the structure, Ni-protein and protein-protein interactions, and cellular function of the HypA protein in the maturation of H_2ase and urease. Whereas the role of HypB in enzyme maturation has remained mysterious, despite its known function as a small GTPase.[3-8]

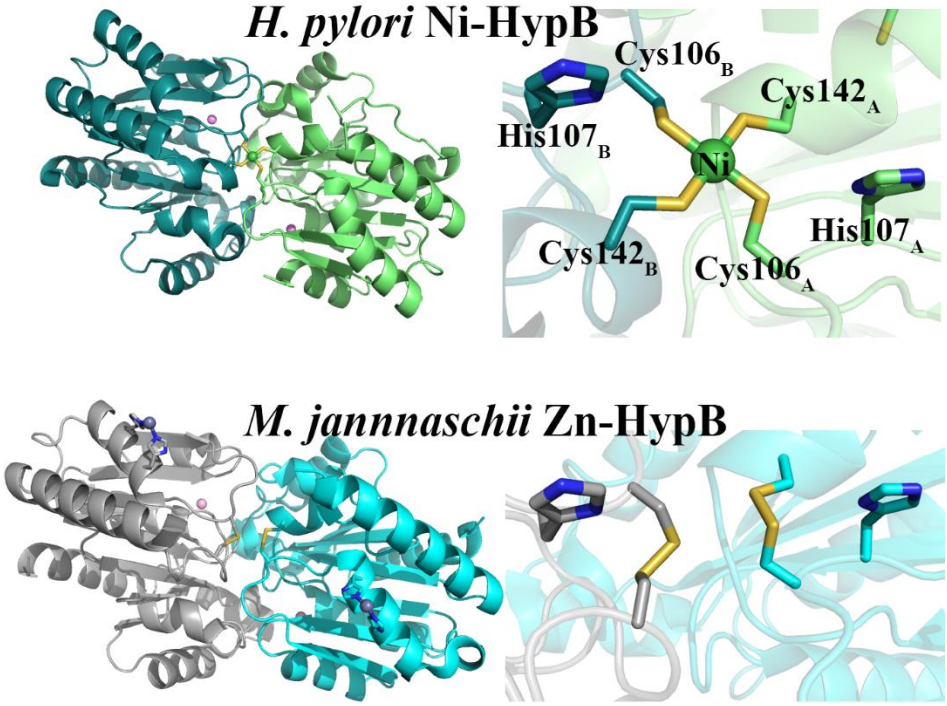

Figure A1.1: HypB crystal structures
Crystal structures of dimeric Ni-bound HypB from *H. pylori* (Top, PDB ID 4LPS)[6] with subunits shown in cartoon and colored in teal and light green, Ni (green) and Mg (pink) shown as spheres. The close-up views of the Ni site at the dimer interface are shown to the right with the side chains of potential Ni-binding residues shown as sticks. The crystal structure of Zn-bound HypB from *Methanocaldococcus jannaschii* (bottom, PDB ID 2HF9)[9] is also shown, where subunits are shown in cartoon and colored in light gray and cyan, with Zn (gray) and Mg (pink) shown as spheres. The close-up of the interfacial residues corresponding to Ni-binding site in *H. pylori* HypB are shown to the right.

HypB is small GTPase in the G3E family and part of the SIMIBI class of P-loop NTPases.[6, 7] The HypB protein is purified as a monomer and forms homodimers in the presence of Ni and nucleotides (GTP or GDP).[6-8] A crystal structure of *H. pylori* HypB (Figure A1.1)[6] shows that Ni binds at the dimer interface, coordinating two Cys residues (Cys106 and Cys142) from each monomer with a His residue (His107) from each monomer close by.[6] However, UV-absorption (at 350 nm) studies of Ni titration into HypB indicate that it could bind up to one Ni per monomer without nucleotide present, and only one Ni per dimer in the presence of nucleotide.[6] A crystal structure of the *M. jannaschii* HypB (PDB 2HF9)[9] bound to Zn indicate an alternate metal binding site well away from the interfacial Ni-binding site. It is unclear if oligomeric state or metal binding affects the interaction of *H. pylori* HypB with other protein binding partners in the Ni trafficking system.[4, 8] Although HypA and HypB interaction have been characterized using crosslinking studies,[2] the interaction is weak (K_d ~ 60 μM by ITC).[8]

An active site mutant strain, K59A-*hypB*, was used in prior studies to investigate the role of *H. pylori* HypB GTPase activity in either urease or H_2ase maturations.[5] These studies found that the GTPase activity of HypB is essential for both the maturation of both urease and H_2ase in low Ni conditions.[5] However, in Ni abundant conditions (5 μM Ni supplement in growth media) urease activity was fully recovered and H_2ase activity was partially restored, despite the lack of GTPase activity in the K59A-*hypB* mutant variant.[5] Whereas in *hypB* deletion strains, 5 μM Ni supplement in growth media fully rescued the urease activity of the strain, but not the H_2ase activity.[2] These observations indicate *H. pylori* HypB is also involved in Ni acquisition, like HypA. Moreover, the GTPase activity of *H. pylori* HypB appears to be more important in H_2ase maturation than in urease maturation.

This appendix summarizes the work that we have done on the HypB protein to elucidate its potential role in the maturation pathway of H_2ase and urease. Most of the work performed on HypB is based on the hypothesis of a pH-dependent prioritization of the maturation of H_2ase and

urease, which could be reflected in the preferential interactions between HypA-$UreE_2$ or HypA-HypB (Figure A1.2).

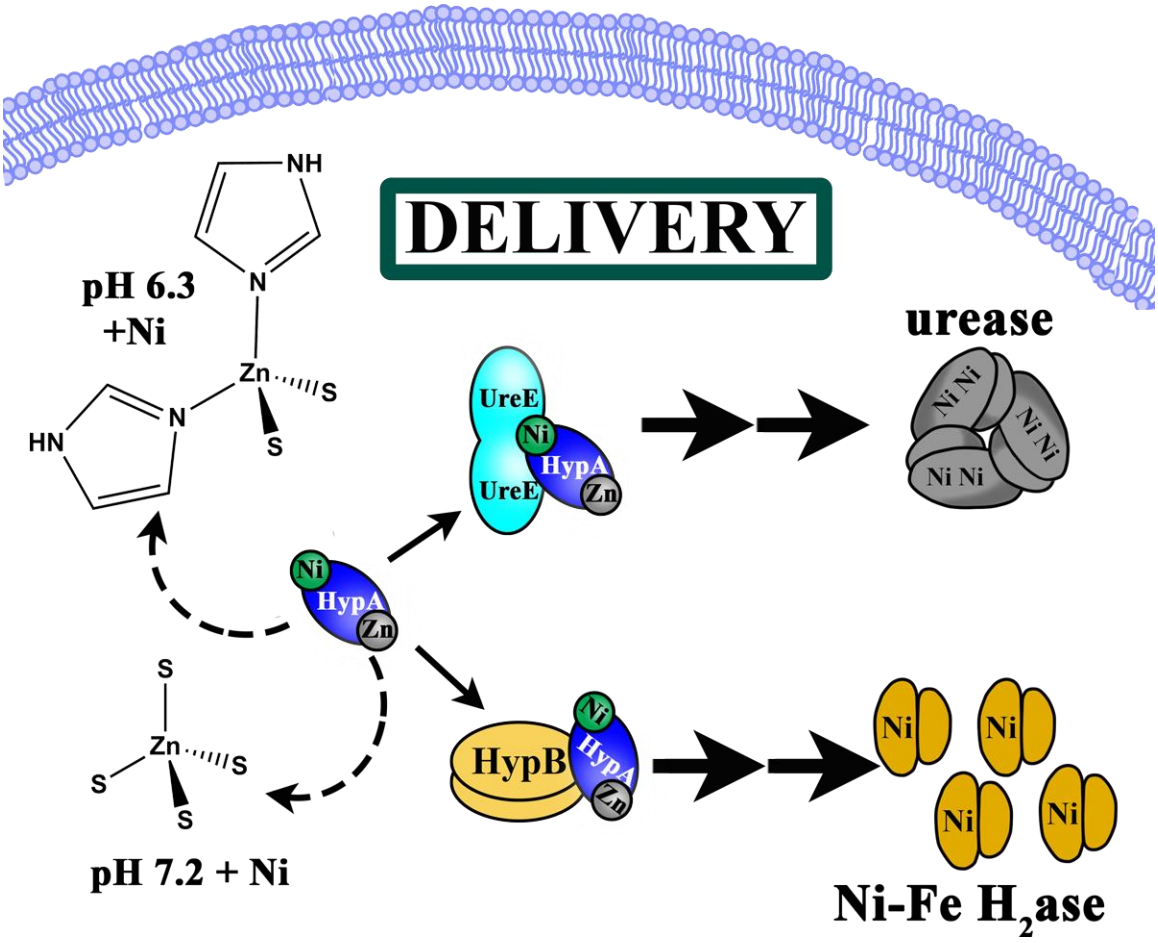

Figure A1.2: Hypothesis of pH-dependent maturation of urease and H_2ase
The pH-dependent Zn site structural changes in HypA was proposed to alter its overall structure, leading to preferential interaction with either UreE or HypB, culminating in pH- and Ni-dependent maturation of urease and H_2ase.

A1.2 Results

A1.2.1 *H. pylori* HypA and HypB do not form stable complexes in SEC

H. pylori HypA and HypB interactions were initially characterized using Immunoblots that identified a cross-linked HypA-HypB complex.[2] The *in vivo* interactions between the two proteins were also observed using GFP-fragment complementation assays by expression of the two fusion proteins in *E. coli*.[8] We initially predict that the *H. pylori* HypA-HypB complex could be purified as a complex for structure and functional analyses. However, equimolar mixtures of

apo-ZnHypA and apo-HypB produced two peaks on size exclusion chromatography (SEC) that overlapped precisely with the two individual proteins (Figure A1.3) and no other higher molecular weight peak that indicated a stable HypA-HypB complex. The lack of HypA-HypB complex formation in SEC is unusual, The HypA-HypB complex (without nucleotides) from *Archaeoglobus fulgidus*;[10] and several high molecular weight complexes variations were observed for HypA and the ATP-binding form of $HypB_{AT}$ from *Thermococcus kodakarensis*.[11]

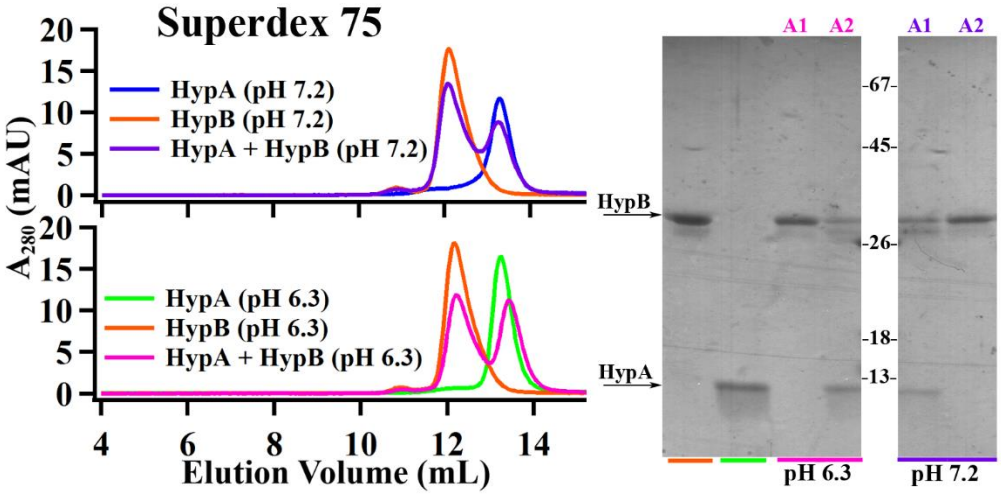

Figure A1.3: SEC of apo-ZnHypA and apo-HypB
Superdex 75 10/300 GL column was used to separate 100 µL of protein samples: 40 µM of apo-ZnHypA, 40 µM of apo-HypB, or a mixture of 20 µM each of the two proteins using GF buffer (20 mM HEPES, 200 mM NaCl, 1 mM TCEP at pH 7.2 or 6.3) as the mobile phase. SDS-PAGE of the protein fractions (A1 and A2) collected from resolution of each mixture and the positions of HypA and HypB are as shown on the gels.

These relatively resolved peaks of purified *H. pylori* HypA and HypB mixtures indicate that it may be possible to elucidate the direction of potential Ni-transfer between the two proteins. Therefore, the experiment was repeated at pH 7.2 with two mixtures containing equimolar amounts of either (1) Ni-ZnHypA and apo-HypB or (2) apo-ZnHypA and Ni-HypB (Figure A1.3). The resolution of these two mixtures resulted in chromatographs that resemble the mixture of apo proteins, where HypA and HypB proteins are well-resolved into two peaks with minimum overlap. Five fractions were collected from the two peaks and then SDS-PAGE was used to analyze the protein content of each fraction, revealing that fractions A1 – A3 consisted primarily of HypB, and fractions A4 and A5 consisted primarily of HypA (Figure A1.4).

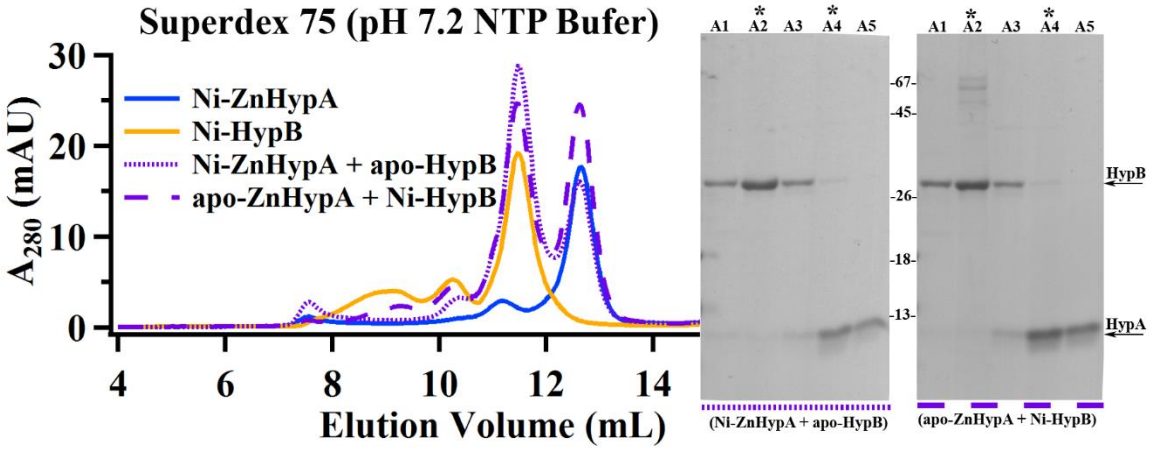

Figure A1.4: SEC of Ni-bound HypA and HypB mixtures
Superdex 75 10/300 GL column was used to separate 100 µL of protein samples: 40 µM of Ni-ZnHypA, 40 µM of Ni-HypB, a mixture of 20 µM each of the Ni-ZnHypA and apo-HypB, and a mixture of 20 µM each of the apo-ZnHypA and Ni-HypB using NTP buffer (20 mM HEPES, 100 mM NaCl,100 mM KCl, 5 mM $MgCl_2$, 1 mM TCEP at pH 7.2 or 6.3) as the mobile phase. SDS-PAGE of protein fractions collected (A1 – A5) from the two resolved mixtures as labeled on each gel. The position of the HypA and HypB proteins are as labeled on the gel. The fractions A2 (primarily HypB) and A4 (primarily HypA) from each mixture were additionally analyzed by ICP-OES (lane marked with *****) with results shown in Table A1.1.

These most concentrated fractions (A2 and A4) from each resolved mixture was analyzed for metal content by ICP-OES. Metal analysis was also performed on the individual proteins before loading onto the column and the main fraction collected after the column. ICP results were summarized in Table A1.1. The metal analyses of Ni-HypB proteins before loading onto the SEC column and the fraction collected after indicated that the HypB protein does not retain Ni through the SEC separation, instead it has a tendency of picking up Zn from the buffer. This observation was unexpected but not unreasonable, given that Ni bound at the homodimer interface, where the HypB protein was clearly separated into monomers through the SEC column resulting in the loss of Ni. Zn-binding in HypB was presumed not to involve the Cys residues at the dimer interface and favored the monomeric conformation,[9] hence HypB was able to pick up the trace amount of Zn within the mobile phase (< 1 ppb Zn, the limit of detection of our ICP-OES standards). In contrast, HypA retained both Ni and Zn through the SEC column, where the ratio of Ni:Zn is closer to one. The initial high Ni:Zn ratio of the in the Ni-ZnHypA protein was attributed to excess Ni loosely bound to the protein despite treatment with Chelex 100 resin. The metal

analyses of the HypA and HypB mixtures, resulted in Ni ending up with HypA, which is explained by the results from the individual proteins. The tendency of HypB to lose Ni in SEC may be altered by the presence of nucleotides, which were reported to stabilize the HypB dimer.[6, 8] Additionally, protein concentration may also affect the oligomeric state of HypB, as it was also reported that higher concentrations of HypB eluted as dimers with a full equivalent of Ni added from SEC.[7]

Table A1.1: ICP-OES results of SEC fractions from HypA and HypB Mixtures

Protein Samples	Before or after SEC?	Protein Fraction by SDS-PAGE	Ni (μM)	Zn (μM)	Ni:Zn
apo-ZnHypA	Before	HypA	0.78	15	0.05
	After		0.00	1.7	No Ni
Ni-ZnHypA	Before	HypA	33	13	2.5
	After		0.80	1.1	0.73
apo-HypB	Before	HypB	0.22	0.00	No Zn
	After		0.00	0.67	No Ni
Ni-HypB	Before	HypB	18	0.00	No Zn
	After		0.00	0.23	No Ni
Ni-ZnHypA + apo-HypB	After *	HypB	0.00	1.1	No Ni
Ni-ZnHypA + apo-HypB	After *	HypA	0.65	1.1	0.61
apo-ZnHypA + Ni-HypB	After *	HypB	0.00	0.81	No Ni
apo-ZnHypA + Ni-HypB	After *	HypA	1.3	2.2	0.61

* = the same fractions collected in SEC and represented in SDS-PAGE in Figure A1.4

A1.2.2 HypB binds Ni with similar affinity compared to HypA

Next, we investigated the Ni-binding of HypB using isothermal titration chromatography (ITC). Titrations of $NiCl_2$ (dissolved in buffer) into apo-HypB in GF buffer (20 mM HEPES, 200 mM NaCl, 1 mM TCEP) at pH 7.2 resulted in a clear single isotherm (Figure A1.5) that was best fitted with a K_d of 1.3 ± 0.3 μM with N of 0.44 ± 0.003 sites (from the average and standard deviation of three independent titrations). The K_d is similar to the Ni binding to HypA (K_d ~ 1 μM), however, HypB only binds ~0.5 Ni per protein as opposed to a full Ni in HypA. The N ~ 0.5 sites is consistent with the crystal structure of *H. pylori* Ni-$(HypB)_2$ (PDB 4LPS, Figure A1.1 Top panel), indicating that Ni bound at the homodimer interface coordinating residues from each

monomer.[6] Ni binding to HypB was much weaker at pH 6.3 (Figure A1.5), with a K_d of 43 ± 8 μM and N of 0.30 ± 0.06 site (from the average and range of two independent titrations), compared to HypA (K_d ~ 1 μM). The K_d for Ni binding to HypB as determined by ITC titrations were consistent with those determined from UV-Vis absorption changes (K_d ~ 1.7 μM),[8] but is approximately one order of magnitude less tight than those derived from competition assays with Mag-Fura-2 (K_d ~ 0.2 – 0.3 μM).[6] However, the Mag-Fure-2 competition assays were fitted with a model assuming one Ni binding per monomer,[6] which was not observed in our ITC studies.

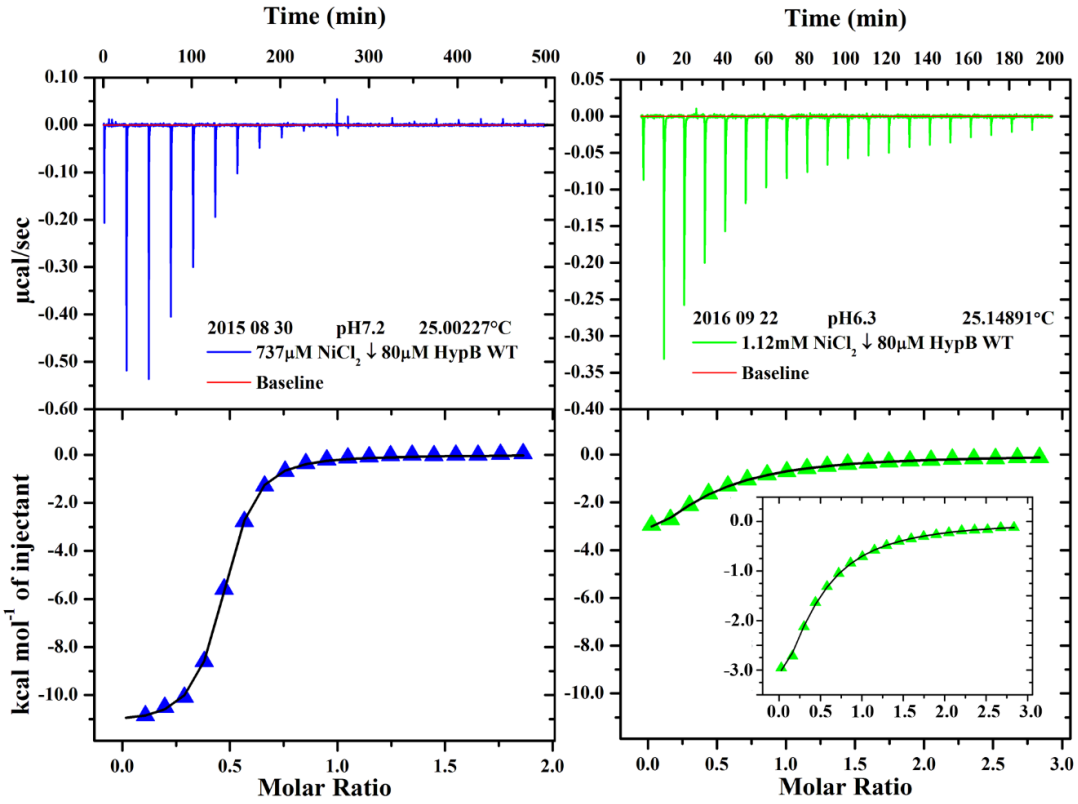

Figure A1.5: ITC of Ni binding to HypB
$NiCl_2$ titrated into apo-HypB at pH 7.2 (blue) and 6.3 (green) were monitored by ITC with raw data graphed on top panels and corresponding ΔH graphed on the bottom panels (data in color and fits in black lines). See methods in A1.3.3for detail fitting methods.

The similarity in K_d between Ni binding to HypA and HypB suggested that the two proteins should be able to compete for Ni. However, the SEC experiments clearly indicated that HypA ended up with all the Ni. Since, the SEC experiments with Ni-HypB were injected at 100 μL of 40 μM (monomer) and then diluted over the column (with ~ 22 mL column volume), the

resulting concentration of the eluted peak is likely to be low. The low concentration may have contributed to its failure to maintain dimeric conformation/hold onto Ni. Future experiments with SEC of HypB should be performed with higher protein concentrations.

A1.2.3 Weak interaction between HypA and HypB

A1.2.3.1 ITC

Prior reports of HypA interactions with HypB in NMR and ITC show that the two proteins interact with relatively low affinity (K_d ~ 60 μM). Our own attempts to monitor the ITC from HypA titrated into HypB (from two independent trials) or the reverse titration (from a single trial) did not yield appreciable isotherms (Figure A1.6). However, when Ni-ZnHypA was titrated into apo-HypB, a low affinity isotherm was detected, which was best fitted with a K_d of 23 ± 4 μM with N of 0.34 ± 0.04 site (from a single trial, Figure A1.6). It is unclear whether the presence of nucleotide would improve this interaction, or the potential interaction between HypA and the GTP/GDP-bound Ni-$HypB_2$.

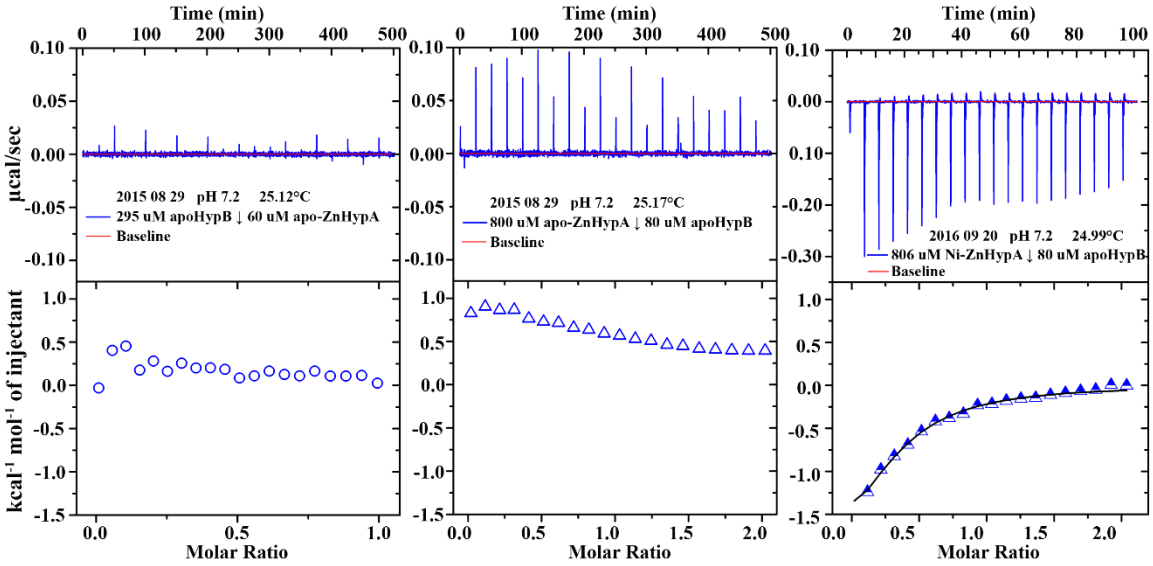

Figure A1.6: ITC of HypA-HypB interactions
ApoHypB WT titrated into apo-ZnHypA WT (left, circles) and apo-ZnHypA titrated into apoHypB WT (middle, open triangles) did not produce clear isotherms in ITC. Ni-ZnHypA WT titrated into apoHypB WT (right, half-filled triangles) produced an isotherm that was fitted with a OneSite model (black line). See method Section A1.3.3 for detail fitting methods.

A1.2.3.2 Thermophoresis

The interactions between HypA and HypB were also investigated using microscale thermophoresis using the NanoTemper NT.115. In the first demonstration (September 2010), HypA (purified by a previous post-doc) was labeled. Unlabeled apo-HypB was serial diluted and then added to tubes containing constant amounts (50 nM) of fluorescently-labeled HypA, creating a titration series, which was monitored by the NT.115. This series was repeated in the presence of 10-fold excess of Ni (as compared to HypA), following a 10-minute incubation, was also monitored by the NT.115. The thermophoresis data from these two titrations were fitted by the scientists from NanoTemper, accumulating in a report that indicated that apoHypB bound to HypA with an apparent K_d of 1.8 ± 0.4 μM, and in the presence of excess Ni the K_d was improved by approximately three-fold to 0.65 ± 0.2 μM.

A second demonstration (November 2012) from NanoTemper was performed with fluorescently labeled HypB. Increasing concentrations of apo-ZnHypA (0.61 nM – 20 μM) was added to a constant concentration of fluorescently-labeled HypB (100 nM) at pH 7.2, and the thermophoresis was monitored by the NT.115. The experiment was repeated at pH 6.3, but with lower concentrations of both proteins (constant 29.3 nM of fluorescently labeled HypB; and 0.3 nM – 10 μM of unlabeled apo-ZnHypA). The data generated were also fitted by the NanoTemper representative, which reported an apparent K_d of 66 ± 9 nM at pH 7.2; and 0.45 ± 0.03 μM at pH 6.3. So far, both demonstrations were performed in GF buffer (20 mM HEPES, 200 mM NaCl, 1 mM TCEP, at pH 7.2 or 6.3) using standard capillaries.

The results from the NanoTemper demonstrations of HypA-HypB interactions did not agree with the reported literature values from ITC titrations of GSHypA (N-terminally modified HypA) into HypB (K_d ~ 60 μM).[8] The binding events with high-to-moderate affinity observed in thermophoresis was also absent from our own ITC studies of unmodified HypA interaction with HypB, with or without Ni present (Figure A1.6).

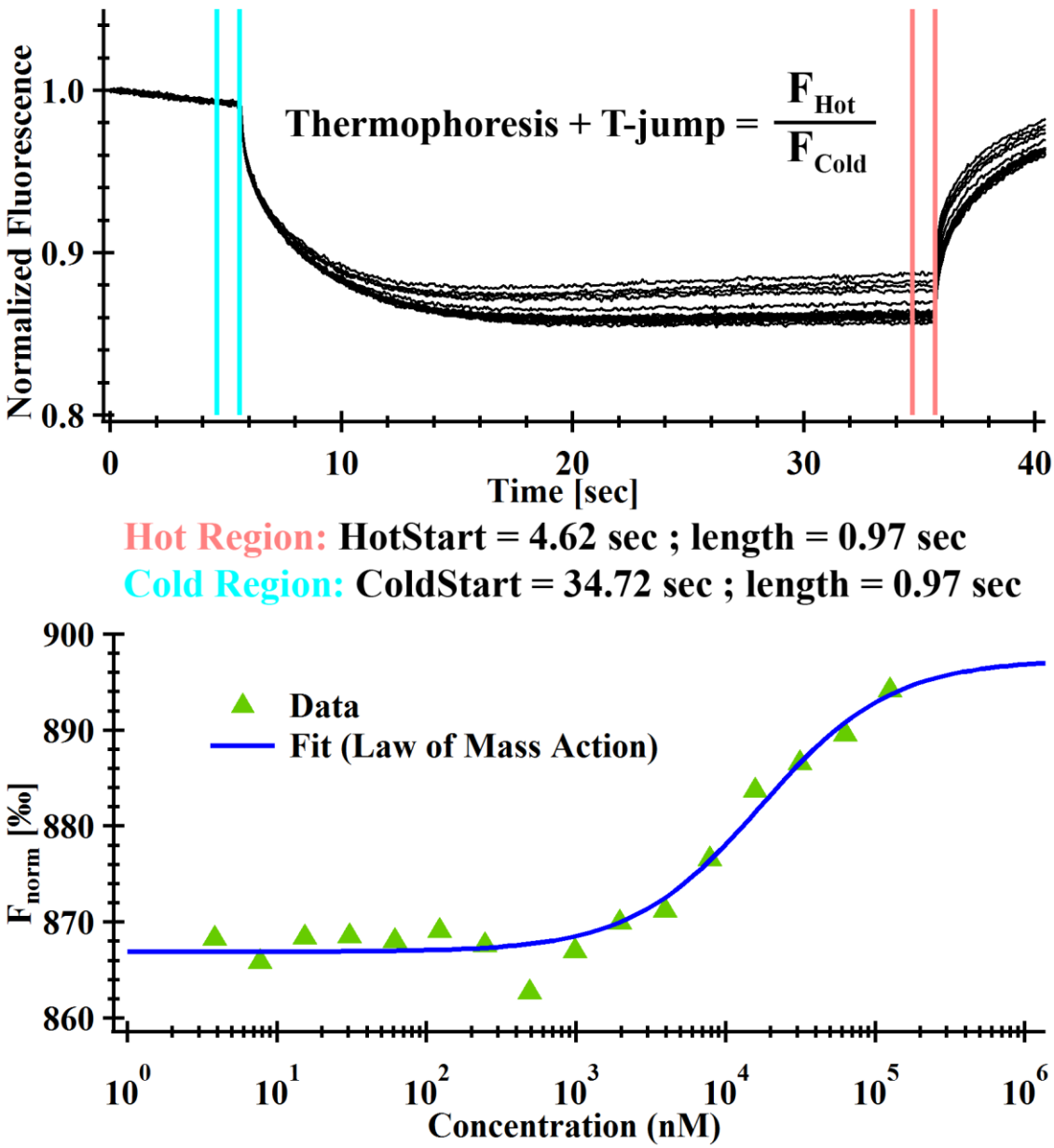

Figure A1.7: Summary of data analysis for thermophoresis experiments
Titration series containing serially diluted unlabeled binding partners (HypA, in most experiments) were mixed with equal amounts of fluorescently labeled molecules (in this case, NHS640-HypB), and loaded into capillary tubes and scanned for fluorescence using the NT.115, which produces fluorescence Time-traces (upper panel). The thermophoresis + T-jump from each trace was graphed against the concentration of the unlabeled molecule (HypA) to produce the binding curve (lower panel), which was fitted with the Law of Mass Action.

Experiments with the NT.115 continued after acquiring the instrument, from which three additional sets of data were acquired for the HypA-HypB interactions using relatively consistent buffer and titration conditions. Primarily, apo-HypB were labeled with NHS-640, which targeted

the free amines on the surface of the protein, and then free fluorophores were removed using a desalting column. The labeled NHS640-HypB were diluted into the binding buffer (20 mM HEPES, 200 mM NaCl, 1 mM TCEP, 0.02% Tween20, at pH 7.2 or 6.3) to check for fluorescent response. Unlabeled HypA is then serially diluted and then mixed with a constant concentration of the NHS640-HypB protein and then the fluorescence of the mixtures in the dilutions series were read by the NT.115. These mixtures were typically excited at a consistent power, and the fluorescence of the mixture was monitored while the IR laser is powered on and off at regular intervals to capture the thermophoresis of the fluorescent molecules in each mixture (Figure A1.7). The change in thermophoresis plus T-jump of each mixture was plotted to evaluate for the occurrence of a binding event. The thermophoresis plus T-jump is defined as the accumulated fluorescence intensities from one second of the hot/cold, where the "cold" fluorescence was taken immediately prior to turning on the IR laser, and "hot" fluorescence was taken immediately prior to turning off the IR laser (Figure A1.7).

Of the three sets of HypA titration into NHS640-HypB that was performed, the response from thermophoresis was inconsistent, resulting in three vastly different K_d values from the fitted data. Example binding curves from each set of data are shown in Figure A1.8, with the summary of all binding data collected shown in Table A1.2. The binding of unlabeled apo-ZnHypA to NHS640-HypB at pH 7.2 (Figure A1.8, Jun 2015) initially produced well-defined binding curves, however, attempts to repeat this initial data failed to produce data with similar quality. Instead, low amplitude and noisy curves were observed, including reversal of the direction of the binding curve in one instance (Figure A1.8, Aug 2016). The corresponding K_d values from the fits of these curves are equally unreliable. This inconsistency was also true for experiments conducted at pH 6.3 (Table A1.2). These inconsistencies may have resulted from the fluorescent labeling of HypB. The HypB protein have been known to form homodimers under certain conditions, and it is unclear whether fluorescent labeling of the monomeric form would have prevented some of

these interactions. It is also unclear whether the fluorescent labeling would interrupt interaction with HypA.

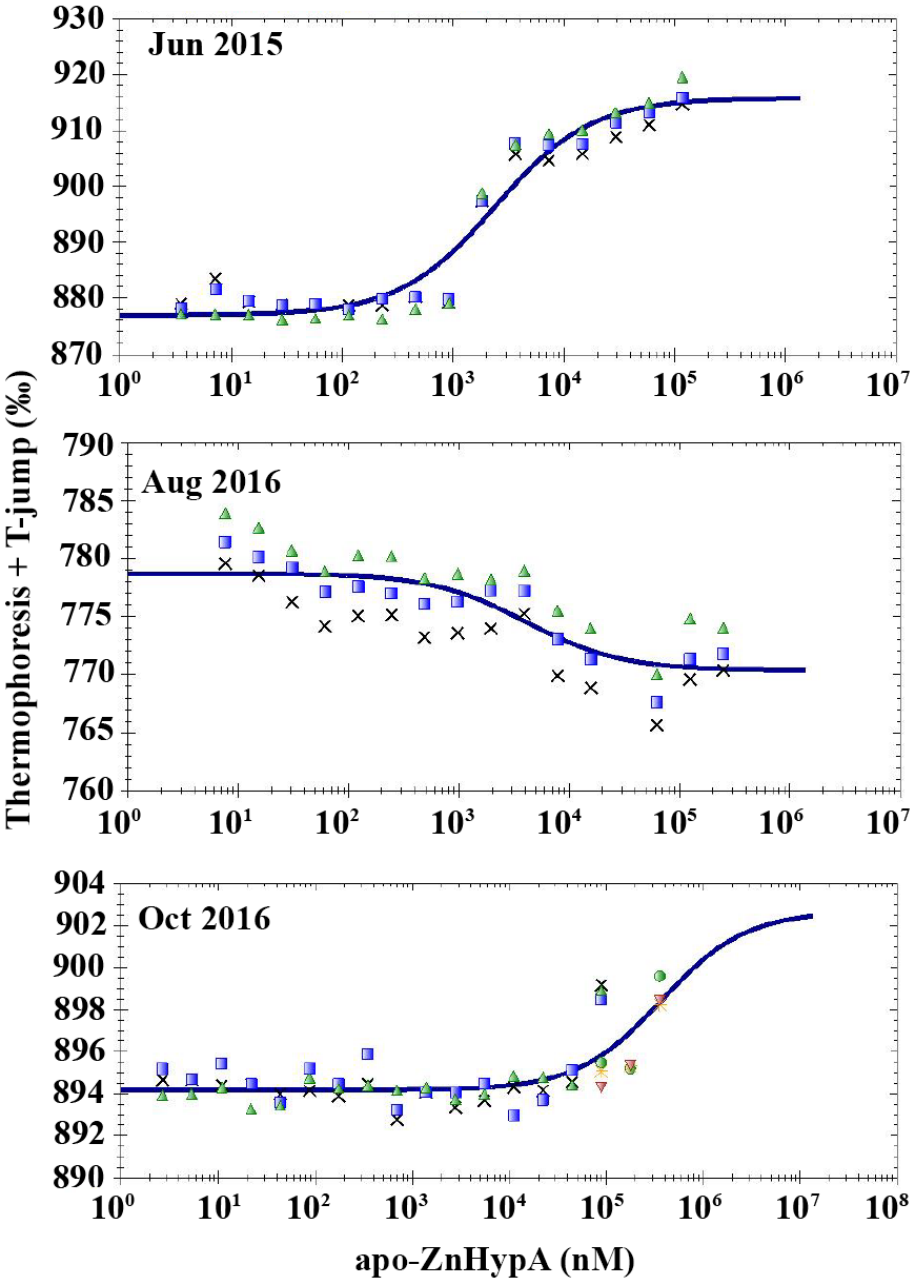

Figure A1.8: Thermophoresis plus T-jump binding curves of HypA and NHS640-HypB
The binding of apo-ZnHypA to NHS640-HypB was inconsistent and irreproducible. The square, triangle, and x-symbols represent three different scans of the same dilution series. Higher concentration samples in the same dilution series were added to the Oct 2016 curve represented as inverted triangle and yellow *.

Table A1.2: Summary of thermophoresis data for HypA binding to NHS640-HypB

pH	Ligand	[HypA] used	NHS640-HypB (nM)	Date	Laser Power	MST Power	Amplitude (‰)	K_d (μM)	Notes
6.3	Apo-ZnHypA	3.8 nM - 125 μM	40.2	6/5/15	70%	40%	27.99	23.4 ± 2.2	
		3.8 nM - 125 μM	14.8	10/22/16	50%	40%	3.31	2.53 ± 0.88	1,2,3
	Ni-ZnHypAWT	22 nM - 184 μM	14.8	10/22/16	50%	80%	Low	No Fit	2,4
7.2	Apo-ZnHypAWT	3.6 nM - 177 μM	47.5	6/3/15	70%	40%	38.94	2.37 ± 0.31	
		7.6 nM - 250 μM	47.5	8/26/16	50%	100%	8.36	4.05 ± 1.21	2,3
		2.7 nM - 354 μM	15.9	10/22/16	50%	40%	8.51	369 ± 56	1,2,3
	Ni-ZnHypAWT	13 nM - 207 μM	15.9	10/22/16	50%	80%	35.37	105 ± 19	1

Notes: 1 = no saturation; 2 = low amplitude; 3 = noisy data; 4 = apparent aggregation

The early experiments with thermophoresis (early demos from NanoTemper and Jun 2015) found that the HypA-HypB interaction may be high affinity. This was contradictory to the ITC results, which found that *H. pylori* HypA and HypB interact at much lower affinities than initially expected. This was also confirmed by other studies that no observable interactions for HypA and HypB using Biolayer Interferometry or surface plasmon resonance.[12] It also agreed with the low affinity interaction found between the N-terminally modified GSHypA and HypB by ITC ($K_d \sim 60$ μM).[8]

Thermophoresis is an excellent technique for observing transient interactions between biomolecules, however, additional experiments using this technique may be best conducted with fluorescently labeled HypA. This was utilized in the first demonstrations from NanoTemper (September 2012) that found fluorescently-labeled HypA interactions with unlabeled HypB. This method offers higher levels of control for the oligomeric state of the HypB used for titrations. The HypA protein appears to be primarily monomeric in solution and would be less likely to affect the interactions between the two proteins. Labeling of HypA under neutral conditions using the NHS640 kit from NanoTemper would result in modification of amines of arginine and lysine residues and should not affect the N-terminal amine. However, Ni titration into the NHS640-HypA should be used as a control for the availability of the N-terminal amine for Ni-binding since it was characterized as an essential ligand (L2*-HypA variant discussed in CHAPTER 3).

A1.2.4 HypA and Ni enhances HypB GTPase activity

The poor GTPase activity in HypB was enhanced by addition of potassium and reducing agents,[6, 7] resulting in the NTP buffer (20 mM HEPES, 100 mM NaCl, 100 mM KCl, 5 mM $MgCl_2$, 1 mM TCEP, at pH 7.2). Using this buffer, the activity of HypB was assayed using malachite green method modified from previous reports.[7, 13, 14] Firstly, Ni was reported to reduce the GTPase activity of HypB in one incident,[6] and to enhance it in another.[8] Our own finding suggests that moderate amount of Ni (5 μM) can slightly enhance the activity of HypB, whereas high concentration (200 μM) reduces the GTPase activity (Figure A1.9A, Table A1.3). The addition of an equimolar amount of HypA slightly enhances the GTPase activity at pH 6.3 but has no affect at pH 7.2 (Figure A1.9, and Table A1.3). The addition of both HypA and low concentrations of Ni seem to enhance the GTPase activity of HypB at both pH values (Figure A1.9, Table A1.3).

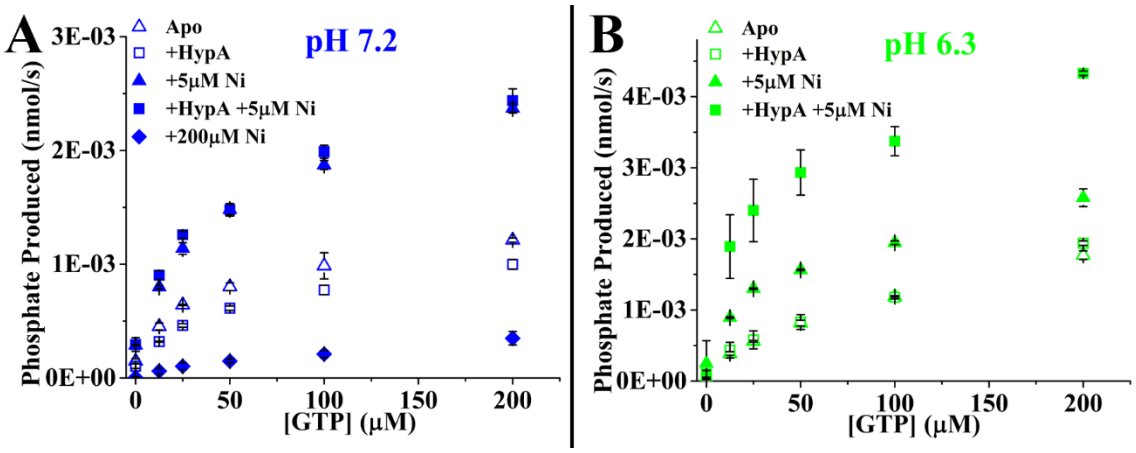

Figure A1.9: HypB GTPase activity
Phosphate produced by 2 μM of apo-HypB (open triangle), with addition 2 μM of apo-ZnHypA (open square), with addition of 5 μM of Ni (closed triangle), or with addition of 2 μM of apo-ZnHypA and 5 μM of Ni (closed square), at pH 7.2 (A, blue) and 6.3 (B, green). Phosphate production of 2 μM of apo-HypB with addition 200 μM of Ni at pH 7.2 (closed diamond) was also shown in panel A.

Table A1.3: HypB GTPase Activity Summary

Conditions	pH 7.2			pH 6.3		
	K_{cat} (x 10^{-3} sec^{-1})	K_M (μM)	K_{cat}/K_M (M^{-1} s^{-1})	K_{cat} (x 10^{-3} sec^{-1})	K_M (μM)	K_{cat}/K_M (M^{-1} s^{-1})
Apo	0.86 ± 0.03	29 ± 3	30 ± 10	2.67 ± 0.54	249 ± 79	11 ± 7
+ 5 μM Ni	1.64 ± 0.12	33 ± 8	50 ± 15	3.60 ± 0.57	387 ± 88	9.3 ± 6.5
+ 200 μM Ni	0.81 ± 0.16	438 ± 140	1.9 ± 1.1	ND	ND	ND
+ HypA	0.66 ± 0.07	31 ± 7	21 ± 10	1.46 ± 0.10	23 ± 5	64 ± 21
+ HypA + 5 μM Ni	1.50 ± 0.01	25 ± 6	60 ± 22	3.24 ± 0.14	39 ± 10	83 ± 14

Measured in NTP buffer (20 mM HEPES, 100 mM NaCl, 100 mM KCl, 5 mM $MgCl_2$, 1 mM TCEP) at the indicated pH.

The addition of HypA and Ni together appear to enhance the GTP turnover of HypB by 2 – 3 folds, which is very slight. However, due to the propensity of HypB to dimerize in the presence of Ni and nucleotide, there may be a concentration dependence to the GTPase activity of HypB. The K_d for Ni-binding in HypB is ~ 1 μM (see above) at pH 7.2 and significantly weaker at pH 6.3 (K_d ~ 40 μM, see above), therefore the enhancement at pH 6.3 is likely due to the involvement of HypA, which shows little pH-dependence in Ni-binding affinity (K_d ~ 1 – 2 μM, CHAPTER 4, Figure 4.4 and Table 4.2). The acid-enhanced of HypB GTPase activity involving the presence of Ni and HypA suggest a potential mechanism for urease maturation under these conditions.

A1.2.5 Ni K-edge of HypA-HypB complex

Due to the disparate structures of the Ni-HypA and Ni-$HypB_2$ site, Ni K-edge is an attractive method for exploring the metal site created in the complex. XAS samples were collected for a 1:1 mixture of apo-ZnHypA and Ni-$HypB_2$ in XBr buffer (20 mM HEPES, 200 mM NaBr, 1mM TCEP) at pH 7.2, which resulted in Ni K-edge spectra that is a combination of the Ni K-edge spectra from each of the individual proteins (Figure A1.10A). The Least Squares Fitting module from SIXPack was used to fit the XANES of the mixture using the individual Ni K-edge of Ni-ZnHypA WT and Ni-$HypB_2$ WT as component standards in the linear combination fit. The results indicate a 69% character from the Ni-ZnHypA WT and a 30% character from the Ni-

$HypB_2$ WT character (Figure A1.10B). Since the Ni started off in the Ni-$HypB_2$ WT, a change in the XANES in the 1:1 mixture indicated that either some of the Ni have been transferred to HypA or a new Ni site was formed that combined the characteristics of both proteins. In the opposing experiment, where a 1:1 mixture of Ni-ZnHypA WT was combined with apo-HypB WT (monomer), yielded similar results. The least squares fitted results indicated that the mixture retained 65% character of the Ni-ZnHypA WT and 33% of the character from the Ni-$HypB_2$ WT XANES spectra (Figure A1.10C).

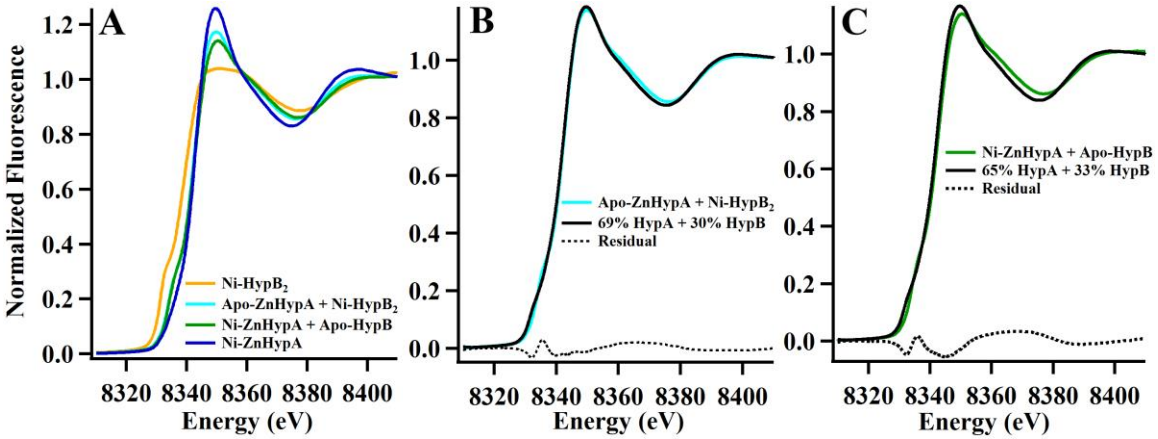

Figure A1.10: XANES of Ni K-edge of HypA, HypB, and HypA-HypB mixtures
Overlay of the individual Ni K-edge spectra of Ni-ZnHypA WT, Ni-$HypB_2$, and 1:1 mixtures of apo:Ni of the two proteins (A). The XANES of Ni-ZnHypA and Ni-$HypB_2$ were used in linear combination to produce least square fits for the 1:1 mixture of apo-ZnHypA + Ni-$HypB_2$ (B), and the 1:1 mixture of Ni-ZnHypA + apo-HypB (C).

It is still unclear whether these spectra represent a new site or an uneven mixture of the two types of Ni sites in solution. Additionally, the physiological relevance of this mixture is unclear, since the buffer conditions used do not favor the active conformations of HypB (does not contain K^+, Mg^{2+}, or nucleotides). The addition of these components may favor the adaptation of an alternate conformation for HypB or otherwise alter the Ni sites in HypB or in the distributions of Ni in the HypA-HypB mixtures. Since the HypA and HypB mixtures separate into separate peaks in SEC, it is possible that the Ni has distributed between the two proteins, with HypA retaining slightly more Ni due to the 1:1 stoichiometry of binding.

It is possible that HypB GTP-turnover cycle rely on formation and then dissociation of the homodimer, which is aided by the presence of Ni and HypA. This type of mechanism is favored by some members of the SIMIBI (signal recognition particle, MinD, and BioD) -type NTP-binding proteins,[15] of which HypB is also a member.[16] Presuming that HypB follow a homodimer formation/dissociation cycle in GTP-hydrolysis, which is supported by the fact that dimer formation is favored in the presence of Ni and nucleotide,[6, 8] and that HypA and Ni stimulate GTPase activity (Figure A1.9 and Table A1.3), the role of HypA remains unclear. HypA may act as an activator (in handing off Ni to Ni-$HypB_2$) or an effector (in receiving Ni from Ni-$HypB_2$) in the GTP-hydrolysis cycle. The Ni binding affinity of the individual protein suggests that this may be a pH-dependent phenomenon, where HypA may be more prone to receive Ni from HypB at lower pH. With either Ni transfer mechanism, the interaction between *H. pylori* HypA and HypB is likely to be transient and difficult to quantitate *in vitro*. A Ni-transfer mechanism suggests the combined Ni site structure of the HypA-HypB complex is likely to be short-lived and dynamic *in vivo*. Hence, is vitally important to first elucidate the nature of interaction between HypA and HypB and the GTP-hydrolysis mechanism of HypB.

A1.2.6 Ni K-edge XAS of HypB

The Ni-$HypB_2$ complex was prepared in Br buffer (20 mM HEPES, 200 mM NaBr, 1mM TCEP) at pH 7.2, and the Ni K-edge XAS spectrum was collected at NSLS beamline X3B. Systematic fitting was performed as previously described.[17, 18] The shape of the XANES spectrum suggested coordination of heavy atoms (such as sulfur) with a broad $1s \rightarrow 4p_z$ transition (plus shakedown) that indicated a four- or five-coordinate Ni site (Figure A1.10A).[19] The Ni K-edge EXAFS spectra were fitted using SIXpack to a best fit containing four S-Cys ligands and a single His-imidazole ligand (Figure A1.11 and Table A1.4).

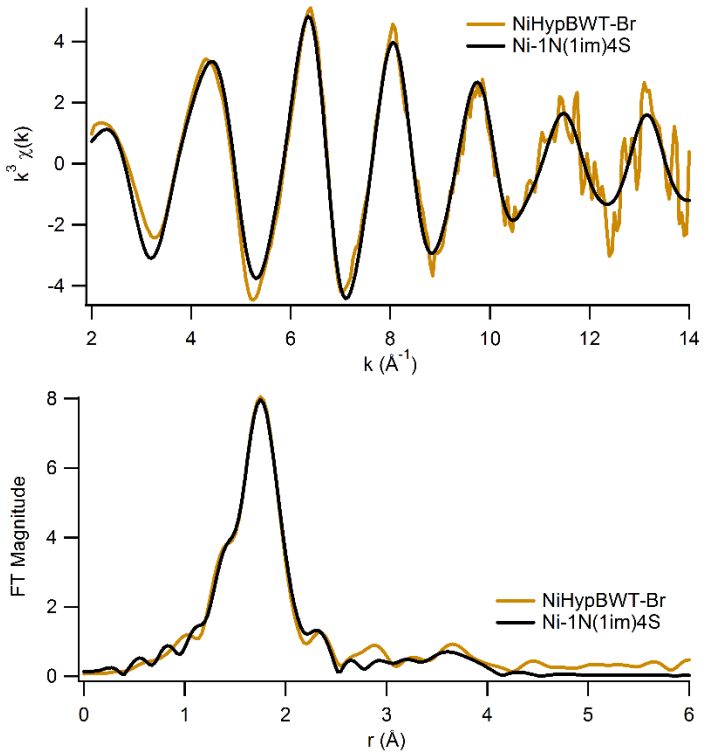

Figure A1.11: EXAFS spectra and best fit for Ni-HypB$_2$
Data and best fit model of the Ni K-edge EXAFS represented in k^3-weighted unfiltered data (top) and Fourier-transformed (k = 2 – 14 Å^{-1}) data uncorrected for phase shifts (bottom) for Ni-HypB$_2$ in 20 mM HEPES, 200 mM NaBr, 1mM TCEP (pH 7.2).

Table A1.4: EXAFS analysis of Ni-HypB$_2$

Shell	r (Å)	σ^2 (x10^{-3} Å^2)	ΔE_o (eV)	R factor	Reduced χ^2
4S	2.19(1)	9(1)	-12(2)	0.0713	67.14
3S	2.20(1)	7(0)			
1S	2.56(4)	15(6)	-11(2)	0.0376	17.03
1 N/O	2.32(2)	1(2)			
4S	2.21(1)	9(1)	-11(2)	0.0539	24.40
1 N/O (Imid)	2.07(1)	0(1)			
4S	2.18(1)	10(1)	-11(1)	0.0103	8.57

Uncertainties in the fitted parameters are shown in parentheses. Unacceptable values are shown in red and the best fit highlighted in orange. See method Section A1.3.6 for fitting method.

A1.3 Methods

A1.3.1 Protein overexpression and purification

The HypB protein was overexpressed from the DL41 (DE3) pLysS *E. coli* cells transformed with the *Hp* WT*hypB*-pET22b plasmid (pET22b vector containing the WT *hypB* coding sequence from *H. pylori* strain 26695). Single colonies were selected from freshly transformed cells grown on LB-agar plates supplemented with 34 μg/mL chloramphenicol (Cam) and 100 μg/mL ampicillin (Amp), and then grown in 150 mL of sterile liquid LB supplemented with Cam/Amp until saturation (>6 hours, shaking at 200 RPM at 37 ˚C). Large scale (typically 2L in a 5L growth flask) sterile LB media supplemented with Amp only with 1:100 (typically 20 mL) of the saturated culture of *Hp* WT*hypB*-pET22B plasmid and allow to grow at 37 ˚C shaking at 200 RPM to OD_{600} of ~0.8 (2.5 – 3.5 hours). Protein overexpression was induced by addition of isopropyl β-D-1-thiogalacopyranoside (IPTG) to a final concentration of 0.8 mM, and then dropping the temperature to 25 ˚C for three hours. Cells containing the WT HypB proteins were pelleted by centrifugation at 5500 x g for 10 minutes, and then resuspended with 10 mL of QA buffer (20 mM Tris, 1 mM TCEP, pH 7.2) per liter of cells. Phenylmethylsulfonyl fluoride (PMSF) was added to the resuspended cells to a final concentration of 1 mM and mixed thoroughly by vortexing, and then immediately stored in the -80 ˚C freezer for no more than 2 years.

Frozen cells were removed from the -80 ˚C freezer and then thawed in a 30 – 35 ˚C water bath. Cells were lysed upon one freeze-thaw cycle due to release of lysozymes from the expression of the included pLysS plasmid. Deoxyribonuclease I (frozen stock in 10 mg/mL with 40% glycerol) were added to the cell lysate at 10 μL per liter of cell culture along with 2 mM (final concentration) of PMSF, and then thoroughly mixed by vortex. The cell lysates were returned to the water bath for 30 minutes to allow for digestion of the genomic DNA in the lysate. The digested lysate was pelleted by centrifugation at 15,000 x g to remove insoluble materials,

and then the soluble part of the lysate was filtered through a 0.22 μm membrane filter and then stored on ice (for no more than 3 hours) prior to column loading.

The overexpressed HypB protein was purified by a Q Sepharose column and then a HiLoad Superdex 75 16/60 on an ÄKTA FPLC system at room temperature. The packed Q Sepharose column (12 mL column volume) was the first step of purifying HypB protein. The column should be freshly conditioned by first washing with three column volumes of QA buffer, followed by three column volumes of QB buffer (20 mM Tris, 1 M NaCl, 1 mM TCEP, pH 7.2), and then another three to five column volumes of QA buffer until the conductance of the flow through is minimized and stabilized. All fractions should be collected for analyses by SDS-PAGE from the onset of loading protein onto the column. The clarified lysate from 1.5 L of cell culture was diluted with QA buffer to a final volume of 50 mL for loading onto the Q Sepharose columns with 12 mL bed volume. The diluted clarified lysate was loaded onto the column at a flow rate (usually 1.5 mL/min) that does not exceed an overall pressure of 0.3 MPa within the column. After loading, the Q Sepharose column was washed with 3 – 5 column volumes of QA buffer to remove loosely bound proteins until the conductance of the flow through is stabilized. The bound HypB protein was eluted off the column using a 0 – 20% QB gradient, after which 3 – 4 column volumes of 100% QB buffer was used to wash off all other proteins from the column. Although HypB protein continue to elute at high salt concentrations beyond 20% QB, the high amount of impurities in the higher salt fractions render the additional purification of HypB from these fractions improbable.

All collected fractions should be evaluated using SDS-PAGE (Figure A1.12A). The fractions containing the highest concentrations of HypB (with relatively few other contaminant proteins) was selected for further purification on the Hiload Superdex 75 16/60 column. These fractions were treated with ~ 20 mM EDTA overnight at 4 ˚C prior to loading onto the gel filtration column. Using only the most concentrated fractions (as indicated on Figure A1.12A) the fractions from the Q Sepharose columns did not need to be concentrated for the HiLoad Superdex

75 column. Typically, 2 – 3 HiLoad Superdex 75 columns should be run per each Q Sepharose column with no more than 3.5 mL loaded per column, which was pre-equilibrated with 3 column volumes of GF buffer (20 mM HEPES, 200 mM NaCl, 1 mM TCEP, pH 7.2). Pure HypB eluted from the HiLoad Superdex 75 16/60 column between 78 – 90 mL after injection. Collected fractions were evaluated by SDS-PAGE (Figure A1.12B) to evaluate purity. Only proteins with >90% pure were used for experiments. The concentration of the purified HypB was measured by UV-Vis spectroscopy using the extinction coefficient of 7,450 M^{-1} cm^{-1}.[7] Protein was also evaluated for metal content by ICP-OES to ensure no metals were present.

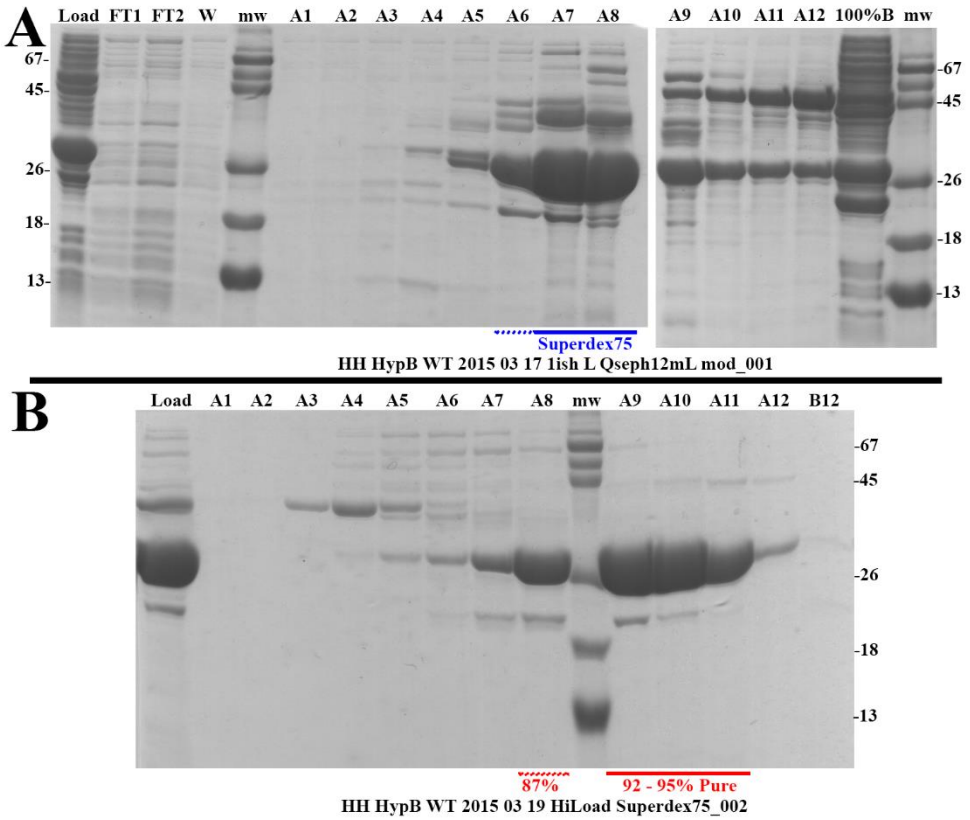

Figure A1.12: HypB Purification gel
Fractions from Q Sepharose column (A) and HiLoad Superdex 75 column (B) from the purification of HypB protein. Fraction numbers are labeled on top of each gel. The blue lines underscore fractions that were further purified in the Superdex 75 column, and the red lines underscore fractions that were considered pure and used for experiments (>90% pure) or were further purified with additional columns (red dashed line, <90% pure).

A1.3.2 Size exclusion chromatography

SEC was performed on the AKTA FPLC using a Superdex 75 GL 10/300 column. Pure HypA or HypB protein were first evaluated by SDS-PAGE and then ICP-OES to ensure the proper purity and metal content. Ni-bound HypA was prepared as previously described, and Ni-bound HypB was prepared as described for the XAS sample preparations (see below).

A1.3.3 Isothermal titration calorimetry

ITC was performed on the Auto-ITC200 using purified apo-HypB protein in GF buffer (20 mM HEPES, 20 mM NaCl, 1 mM TCEP) at either pH 7.2 or 6.3. Ni stock used for titration into apo-HypB was prepared by diluting a concentrated aqueous $NiCl_2$ solution (500 mM) into GF buffer to a final concentration between 0.8 and 1.2 mM for use in titration. The actual concentration of Ni used for fitting was determined by ICP-OES. Apo-ZnHypA and Ni-ZnHypA used in ITC experiments were prepared as previously described.[20] ITC experiments were performed and the resulting data were fitted using the MicroCal analysis module as previously described.[20]

A1.3.4 Microscale thermophoresis

Microscale thermophoresis was used to monitor interaction between purified HypA and HypB protein using the Monolith NT.115 instrument (NanoTemper). The experiment involved labeling either HypA or HypB with the NHS640-RED labeling kit (NanoTemper), which selectively labels amine functional groups with a proprietary fluorophore. In the first demonstration with NanoTemper (September 2010), the HypA protein was labeled with the NHS640 fluorophore (as performed by previous post-doc and NanoTemper specialists). All subsequent experiments were performed with NHS640-labeled HypB. Apo-HypB protein was diluted to 20 μM using the provided NHS labeling buffer and then mixed with 3:1 excess of the freshly prepared NHS640 dye, and incubated in the dark for 30 minutes. Excess NHS640 dyes were removed from the labeled NHS640-HypB proteins either using the gravity desalting columns that were part of the labeling kit or by using the 0.5 mL Zeba Spin desalting column

with a 7 kDa MWCO, which were pre-equilibrated with GF buffer at the appropriate pH. Freshly labeled HypB were evaluated by UV-Vis for protein concentration (A_{280}, ε = 7,450 M^{-1} cm^{-1}) and NHS640 dye concentration (A_{650}, ε = 250,000 M^{-1} cm^{-1}). Labeling efficiency was calculated by the ratio of dye/protein (typically less than 0.3), which indicated that there are typically fewer than one label per HypB protein. The fluorescent intensity of the NHS640-HypB was tested by diluting the protein in the binding buffer (20 mM HEPES, 20 mM NaCl, 1 mM TCEP, 0.02% Tween20, at pH 7.2 or 6.3) at a dilution factor of 1:100 up to 1:400, and then loaded into the appropriate capillaries and scanned with the Red LED (between 20 – 100% power). The concentration of NHS640-HypB and LED power was adjusted to produce the desirable response of between 150 – 500 RFU fluorescence, which was required for data collection using thermophoresis. The protein was separated into small aliquots and rapidly frozen with liquid nitrogen and stored at -80 ˚C for up to one year and thawed for use as needed.

The HypA purified protein used in thermophoresis titrations were prepared as previously described.[20] The concentrated HypA protein (usually > 1 mM) was diluted in half using the 2XBinding buffer (20 mM HEPES, 20 mM NaCl, 1 mM TCEP, 0.04% Tween20, at pH 7.2 or 6.3), and then used as a stock for binding studies. A 1:1 serial dilution of the HypA protein was prepared in 10 μL aliquots in 16 microtubes, which was mixed with 10 μL of the NHS640-HypB diluted to the appropriate concentration (15 – 50 nM) for the fluorescence experiment. After a 10-minute incubation time at room temperature, the proteins mixtures were loaded into Premium coated (previously known as hydrophilic coated) capillaries. The capillaries were loaded onto the scanning tray and the fluorescence was captured by the NT.115 using a fixed % LED power, where the IR laser (at fixed % MST power) was powered on following a cycle of: 5 seconds off, 30 seconds on, and 5 seconds off (Figure A1.7 top panel). The captured fluorescence from all titration samples were normalized, and the Thermophoresis plus T-jump was calculated for each sample in the titration series. The thermophoresis plus T-jump (Figure A1.7) is the ratio of the normalized fluorescence from 0.97 second immediately prior to turning on the IR laser (at T =

4.62 seconds) and immediately prior to turning off the IR laser (at T = 34.72 seconds). The thermophoresis plus T-jump (Figure A1.7 bottom panel) were plotted against the concentration of unlabeled HypA used in each titration sample to create the binding curve. Three scans were performed for each titration reported to ensure that photobleaching does not occur within the sample. The three sets of collected data were fitted in a single titration curve. The binding curve was fitted with the law of mass action:

$$F(L) = Unbound + \frac{(Bound - Unblund)}{2} * \left(TargetConc + L + K_d - \sqrt{(TargetConc + L + K_d)^2 - 4 * TargetConc * L}\right)$$

Where *L* is the variable concentration of HypA, *Unbound* is the concentration of free $UreE_2$, and *Bound* is the concentration of the HypA-$UreE_2$ complex, *TargetConc* is the concentration of total $UreE_2$, and K_d is the apparent dissociation constant of the HypA-$UreE_2$ complex. In each case the total $UreE_2$ concentration (*TargetConc*) is known and set as a constant for fitting. The reported K_d for each titration were the result of independently prepared titration series, which were quite different from trial to trial, and does not appear to be reproducible.

A1.3.5 GTPase assays

GTPase assays were performed in triplicates by adding a final concentration of 2 μM of HypB protein in NTP buffer (20 mM HEPES, 100 mM NaCl, 100 mM KCl, 5 mM $MgCl_2$, 1 mM TCEP, at pH 7.2 or 6.3) to 0 – 200 μM of GTP (prepared in the same buffer). In assays performed in the presence of Ni, a final concentration of 5 μM or 200 μM of $NiCl_2$ was added to the GTP solution, and reaction was initiated by addition of HypB. In assays performed in the presence of HypA, a final concentration of 2 μM of apo-ZnHypA protein was added to the GTP solutions and the reaction was initiated by addition of HypB. In assays performed in the presence of Ni and HypA, a final concentration of 2 μM of apo-ZnHypA protein and 5 μM of $NiCl_2$ was added to the GTP solutions and the reaction was initiated by addition of HypB. Blank assays (where only NTP buffer was added in place of HypB enzyme) were performed alongside each set of enzymatic assays, from which the background phosphate amount was subtracted. After addition of HypB, reaction mixture was incubated at room temperature for 30 minutes and then was terminated by

addition of MG-MO solution (see below) for determination of phosphate production using by color development. Linearity of response of phosphate production using 2 μM of HypB per assay was confirmed from 15 to 90 minutes (R^2 = 0.998) at the highest concentration of substrate used for assays (200 μM).

Phosphate production from GTPase assays were evaluated using a modified version of the malachite green colorimetric assay for detection of phosphates.[13, 14] First a malachite green stock solution was prepared by dissolving 0.44 g of malachite green oxalate in a 16.7% sulfuric acid, resulting in an orange "MG" solution of 0.122% malachite green stock that was stored in foil wrapped glass bottles for up to one year. A 7.5% "MO" stock solution was also prepared by dissolving 0.975 g of ammonium molybdate tetrahydrate in MilliQ water, which was stored for up to 2 weeks. The green "MG-MO" solution was freshly prepared on the day of the GTPase assay by mixing one part "MG" with four parts "MO" solutions together and then adding Tween20 to a final concentration of 0.17%. The amount of phosphate in solution was monitored by adding 200 μL of MG-MO solution to 800 μL of standard or unknown sample with and incubating at room temperature for 30 minutes, and the assessed by UV-Vis absorption at 630 nm.

A phosphate standard curve was prepared concurrently with each set of GTPase assay performed and used for quantitating the amount of phosphate produced in each assayed sample. The phosphate standards were prepared from a 1000 ppm phosphate standard from RICCA chemical company. The stock was serially diluted into 800 μL standard solutions in NTP Buffer that produced linear response (A_{630}) ranging from 0.313 – 20 nmol PO_4^{3-} in solution. The phosphate production rate of HypB were calculated for each set of substrate concentrations (0 – 200 μM) and then fitted using the Michaelis-Menton equation in Origin 2016. The reported GTPase activities for HypB in each condition (apo-, with HypA, with 5 μM Ni, with 200 μM Ni, with 5 μM Ni and HypA) at each pH were the results from fitting the response from triplicate experiments.

A1.3.6 X-ray absorption spectroscopy (XAS)

Ni-$HypB_2$ WT XAS samples were prepared at room temperature by reconstituting the purified apo-HypB protein with two molar-equivalents of $NiCl_2$ added at 0.5-equivalent intervals allowing 20 minutes between each addition for equilibration. Excess Ni^{2+} was removed by treating with equal volumes of Chelex 100 resin (sodium form) for 45 minutes at room temperature, and then concentrating the reconstituted protein using an Amicon Ultra-0.5mL 3-kDa MWCO spin concentrator at 10,000 x g. The resulting sample was assessed for protein concentration and then analyzed for metal content by ICP-OES, with the final XAS sample containing 3 mM of HypB (by monomer concentration) and 1.4 mM of Ni, indicating a Ni-$HypB_2$ complex.

The 1:1 mixtures of apo-ZnHypA WT and Ni-$HypB_2$ WT was prepared from the above described sample, where an equimolar of the prepared Ni-$HypB_2$ WT sample was mixed with apo-ZnHypA WT sample (prepared as described in CHAPTER 3, Section 3.4.8) and incubated for 30 minutes at room temperature prior to concentrating. The final sample has a Ni-Zn-HypA-HypB ratio of 0.46-0.76-1-1. The 1:1 mixture of Ni-ZnHypA WT with apo-HypB was prepared from metallated Ni-ZnHypA WT sample (prepared as described in CHAPTER 3, Section 3.4.8) mixed with equimolar amount of apo-HypB monomer, incubated at room temperature for 30 minutes prior to concentrating. The final sample has a Ni-Zn-HypA-HypB ratio of 1.3-1.3-1-1.

XAS data collection was performed as previously described at NSLS beamline X3B using the dedicated ring conditions.[21] Data processing and normalization were performed using SIXpack[22] software package built on the IFEFFIT[23] engine as previously described.[21] EXAFS analyses was also performed using SIXpack as previously described.[17, 18] The 1:1 mixtures of HypA and HypB were fitted with the "Least Sq. Fitting" module within SIXpack, where the XANES region (8310 – 8410 eV) of the Ni-ZnHypA WT spectra (see Figure A1.10) and Ni-$HypB_2$ WT (see Figure A1.10) were used as components in linear least square fits to the mixture data.

A1.4 References

1. Maier, R. J., Benoit, S. L., and Seshadri, S. (2007) Nickel-binding and accessory proteins facilitating Ni-enzyme maturation in Helicobacter pylori, *Biometals : an international journal on the role of metal ions in biology, biochemistry, and medicine 20*, 655-664. (10.1007/s10534-006-9061-8)

2. Olson, J. W., Mehta, N. S., and Maier, R. J. (2001) Requirement of nickel metabolism proteins HypA and HypB for full activity of both hydrogenase and urease in Helicobacter pylori (vol 39, pg 176, 2001), *Molecular microbiology 40*, 270-270. (DOI 10.1046/j.1365-2958.2001.02397.x)

3. Casalot, L., and Rousset, M. (2001) Maturation of the [NiFe] hydrogenases, *Trends Microbiol 9*, 228-237

4. Mehta, N., Olson, J. W., and Maier, R. J. (2003) Characterization of Helicobacter pylori Nickel Metabolism Accessory Proteins Needed for Maturation of both Urease and Hydrogenase, *Journal of bacteriology 185*, 726-734. (10.1128/jb.185.3.726-734.2003)

5. Mehta, N., Benoit, S., and Maier, R. J. (2003) Roles of conserved nucleotide-binding domains in accessory proteins, HypB and UreG, in the maturation of nickel-enzymes required for efficient Helicobacter pylori colonization, *Microbial Pathogenesis 35*, 229-234. (10.1016/s0882-4010(03)00151-7)

6. Sydor, A. M., Lebrette, H., Ariyakumaran, R., Cavazza, C., and Zamble, D. B. (2014) Relationship between Ni(II) and Zn(II) coordination and nucleotide binding by the Helicobacter pylori [NiFe]-hydrogenase and urease maturation factor HypB, *The Journal of biological chemistry 289*, 3828-3841. (10.1074/jbc.M113.502781)

7. Sydor, A. M., Liu, J., and Zamble, D. B. (2011) Effects of metal on the biochemical properties of Helicobacter pylori HypB, a maturation factor of [NiFe]-hydrogenase and urease, *Journal of bacteriology 193*, 1359-1368. (10.1128/JB.01333-10)

8. Xia, W., Li, H., Yang, X., Wong, K. B., and Sun, H. (2012) Metallo-GTPase HypB from Helicobacter pylori and its interaction with nickel chaperone protein HypA, *The Journal of biological chemistry 287*, 6753-6763. (10.1074/jbc.M111.287581)

9. Gasper, R., Scrima, A., and Wittinghofer, A. (2006) Structural insights into HypB, a GTP-binding protein that regulates metal binding, *The Journal of biological chemistry 281*, 27492-27502. (10.1074/jbc.M600809200)

10. Chan, K. H., Lee, K. M., and Wong, K. B. (2012) Interaction between hydrogenase maturation factors HypA and HypB is required for [NiFe]-hydrogenase maturation, *PloS one 7*, e32592. (10.1371/journal.pone.0032592)

11. Watanabe, S., Kawashima, T., Nishitani, Y., Kanai, T., Wada, T., Inaba, K., Atomi, H., Imanaka, T., and Miki, K. (2015) Structural basis of a Ni acquisition cycle for [NiFe] hydrogenase by Ni-metallochaperone HypA and its enhancer, *Proc Natl Acad Sci U S A 112*, 7701-7706. (10.1073/pnas.1503102112)

12. Benoit, S. L., McMurry, J. L., Hill, S. A., and Maier, R. J. (2012) Helicobacter pylori hydrogenase accessory protein HypA and urease accessory protein UreG compete with each other for UreE recognition, *Biochimica et biophysica acta 1820*, 1519-1525. (10.1016/j.bbagen.2012.06.002)

13. Hohenwallner, W., and Wimmer, E. (1973) The Malachite green micromethod for the determination of inorganic phosphate, *Clinica chimica acta; international journal of clinical chemistry 45*, 169-175

14. Baykov, A. A., Evtushenko, O. A., and Avaeva, S. M. (1988) A malachite green procedure for orthophosphate determination and its use in alkaline phosphatase-based enzyme immunoassay, *Analytical biochemistry 171*, 266-270

15. Bange, G., and Sinning, I. (2013) SIMIBI twins in protein targeting and localization, *Nat Struct Mol Biol 20*, 776-780. (10.1038/nsmb.2605)

16. Leipe, D. D., Wolf, Y. I., Koonin, E. V., and Aravind, L. (2002) Classification and evolution of P-loop GTPases and related ATPases, *Journal of molecular biology 317*, 41-72. (10.1006/jmbi.2001.5378)

17. Higgins, K. A., Hu, H. Q., Chivers, P. T., and Maroney, M. J. (2013) Effects of select histidine to cysteine mutations on transcriptional regulation by Escherichia coli RcnR, *Biochemistry 52*, 84-97. (10.1021/bi300886q)

18. Higgins, K. A., Chivers, P. T., and Maroney, M. J. (2012) Role of the N-terminus in determining metal-specific responses in the E. coli Ni- and Co-responsive metalloregulator, RcnR, *J Am Chem Soc 134*, 7081-7093. (10.1021/ja300834b)

19. Colpas, G. J., Maroney, M. J., Bagyinka, C., Kumar, M., Willis, W. S., Suib, S. L., Baidya, N., and Mascharak, P. K. (1991) X-Ray Spectroscopic Studies of Nickel-Complexes, with Application to the Structure of Nickel Sites in Hydrogenases, *Inorg Chem 30*, 920-928. (Doi 10.1021/Ic00005a010)

20. Johnson, R. C., Hu, H. Q., Merrell, D. S., and Maroney, M. J. (2015) Dynamic HypA zinc site is essential for acid viability and proper urease maturation in Helicobacter pylori, *Metallomics : integrated biometal science 7*, 674-682. (10.1039/c4mt00306c)

21. Hu, H. Q., Johnson, R. C., Merrell, D. S., and Maroney, M. J. (2017) Nickel Ligation of the N-Terminal Amine of HypA Is Required for Urease Maturation in Helicobacter pylori, *Biochemistry 56*, 1105-1116. (10.1021/acs.biochem.6b00912)

22. Webb, S. M. (2005) SIXpack: a graphical user interface for XAS analysis using IFEFFIT, *Phys Scripta T115*, 1011-1014

23. Newville, M. (2001) EXAFS analysis using FEFF and FEFFIT, *Journal of synchrotron radiation 8*, 96-100. (Doi 10.1107/S0909049500016290)

APPENDIX 2

SUPPORTING DATA FOR HYPA N-TERMINAL NI BINDING

Table A2.1: Selected fits for WT-HypA Ni-complex (in buffer with NaBr)

Shell	r (Å)	σ^2 (x 10^{-3} Å^2)	ΔE_o (eV)	χ^2	Reduced χ^2	#Var	R factor
6 N/O	2.10 (2)	14 (2)	3 (1)	3442.01	175.26	3	9.61%
3 N/O	2.31 (3)	19 (8)					
3 N/O	2.09 (1)	5 (1)	5 (1)	2264.20	128.36	5	6.92%
4 N (1 Imid0˚)	2.10 (1)	5 (2)					
	1.93 (3)						
BBAm	1.98 (3)	6 (4)	2 (1)	2629.07	149.04	5	4.76%
1 N/O	2.21 (5)	4 (8)					
3 N (1 Imid0˚)	2.08 (2)	3 (2)					
	1.92 (3)						
BBAm	1.97 (3)	6 (3)	2 (1)	2096.62	134.06	7	3.53%

Uncertainties in the fitted parameters are shown in parentheses (see Section 3.4.9 for detailed fit methods). Numbers in red are unacceptable values. The best fit is highlighted in orange. Alternative good fits are highlighted in yellow.

Table A2.2: Selected fits for the L2*-HypA Ni-complex (in buffer with NaBr)

Shell	r (Å)	σ^2 (x 10^{-3} Å^2)	ΔE_o (eV)	χ^2	Reduced χ^2	#Var	R factor
5 N/O	1.92 (3)	17 (2)	-1 (2)	6206.92	316.04	3	19.68%
3 N/O	1.89 (2)	6 (2)					
2 N/O	1.78 (25)	55 (94)	-4 (6)	4604.52	261.03	5	14.69%
2 N/O	1.86 (1)	1 (1)					
1 N/O	2.06 (2)	2 (3)					
1 Imid7˚	2.45 (2)	3 (3)					
1 Imid7˚	1.96 (3)	4 (4)	0 (1)	1356.41	99.45	9	3.57%
3N (1 Imid0˚)	2.01 (1)	11 (4)					
	1.83 (1)						
BBAm	1.88 (1)	1 (1)	1 (1)	3638.43	206.26	5	8.85%
1N/O	2.04 (3)	4 (4)					
1Br	2.42 (2)	11 (3)					
1 Imid7˚	1.94 (4)	5 (5)					
	1.82 (1)						
BBAm	1.87 (1)	1 (1)	0 (1)	1747.12	128.09	9	3.49%

Uncertainties in the fitted parameters are shown in parentheses (see Section 3.4.9 for detailed fit methods). Numbers in red are unacceptable values. The best fit is highlighted in orange. Alternative good fits are highlighted in yellow.

Table A2.3: Select fits for the L2*-HypA Ni-complex (in buffer with NaCl)

Shell	r (Å)	σ^2 (x 10^{-3} Å^2)	ΔE_0 (eV)	χ^2	Reduced χ^2	#Var	R factor
5 N/O	1.96 (2)	16 (2)	1 (1)	2768.07	140.94	3	12.98%
4 N/O	1.93 (2)	11 (2)					
1 N/O	2.13 (5)	3 (5)	1 (1)	2726.65	154.57	5	9.90%
1 N/O	1.85 (2)	1 (2)					
4 N/O (1 Imid0˚)	2.00 (2)	9 (2)	2 (1)	1703.74	96.59	5	9.01%
1S/Cl	2.26 (2)	8 (2)					
4N (1 Imid0˚)	1.88 (1)	9 (1)	-4 (1)	1136.75	64.44	5	4.90%
1 N/O	1.86 (3)	2 (3)					
2 N (1 Imid0˚)	2.03 (5)	9 (7)					
	1.93 (6)						
BBAm	1.98 (6)	13 (11)	2 (2)	1736.28	111.02	7	8.48%
1 S/Cl	2.25(2)	10 (3)					
2 N (1 Imid0˚)	1.95 (6)	15 (5)					
	1.84 (2)						
BBAm	1.89 (2)	6 (3)	-2 (1)	1063.53	68.00	7	4.24%
1 N/O	2.05 (3)	2 (3)					
1 Imid0˚	1.99 (5)	7 (6)					
	1.85 (2)						
BBAm	1.90 (2)	2 (1)	1 (1)	1616.67	103.37	7	7.99%

Uncertainties in the fitted parameters are shown in parentheses (see Section 3.4.9 for detailed fit methods). The best fit is highlighted in orange. Alternative good fits are highlighted in yellow.

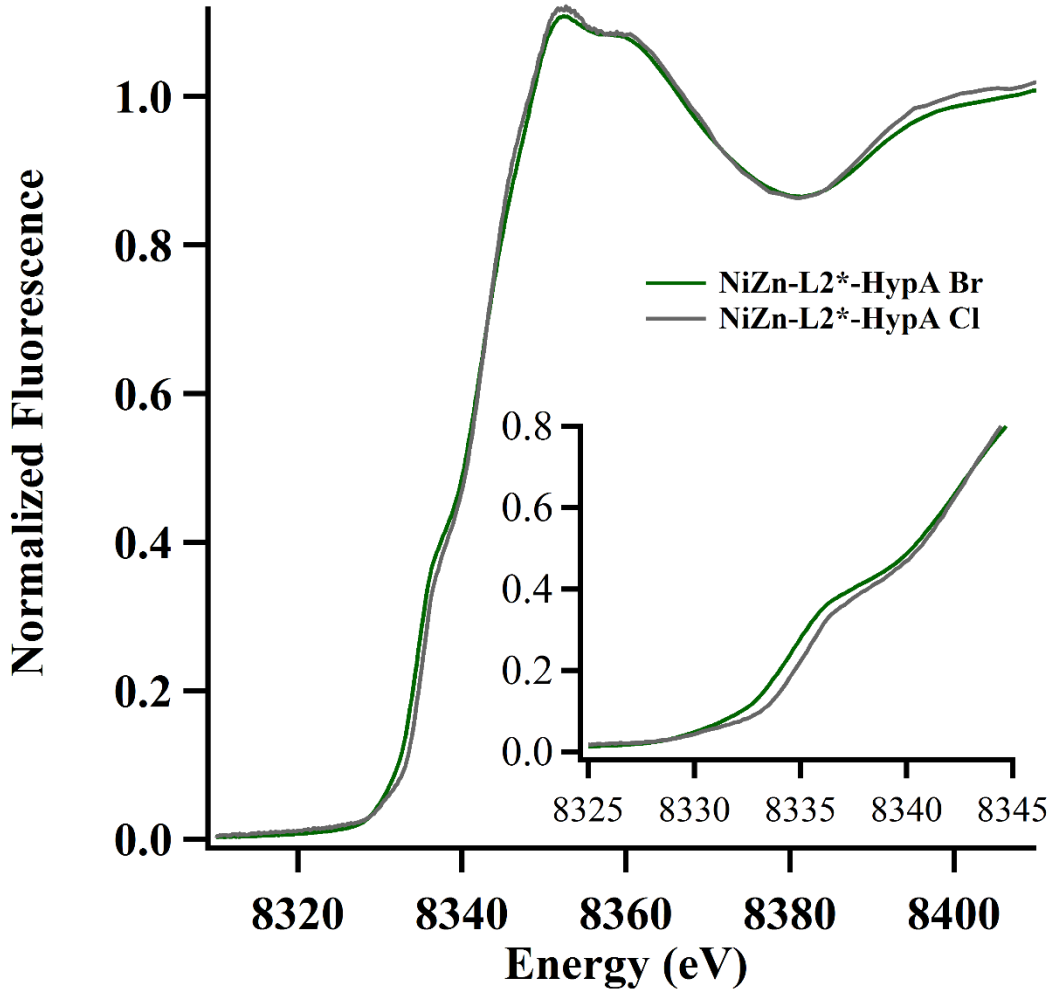

Figure A2.1: XANES overlay of Ni K-edge of Ni-ZnL2*HypA
Overlay of XANES region of the normalized Ni K-edge of Ni-ZnL2*-HypA in buffer with NaBr (in green) and NaCl (in gray) with 1s → $4p_z$ region enlarged in inset.

Table A2.4: Best fits for EXAFS of Zn-complexes with WT- and L2*-HypA (in buffer with NaBr)

HypA	Shell	r (Å)	σ^2 (x 10^{-3} Å^2)	ΔE_o (eV)	R factor	Reduced χ^2
WT	4S	2.33 (5)	4 (0)	-4 (1)	1.89%	569.52
	1 N (1 imid2˚)	2.18 (2)	4 (4)			
	3S	2.34 (1)	2 (0)	-4 (1)	2.45%	759.10
	1 N (1 imid2˚)	2.12 (2)	2 (2)			
	4S	2.33 (1)	3 (1)	-6 (1)	3.57%	978.25
L2*	4S	2.34 (1)	4 (0)	-4 (1)	1.73%	281.58
	1 N (1 imid2˚)	2.18 (2)	2 (3)			
	3S	2.34 (1)	2 (0)	-3 (1)	2.34%	375.00
	1 N (1 imid2˚)	2.13 (2)	2 (3)			
	4S	2.33 (5)	4 (0)	-6 (1)	3.50%	538.16

Uncertainties in the fitted parameters are shown in parentheses (see Section 3.4.9 for detailed fit methods). The best fit is highlighted in orange. Alternative good fits are highlighted in yellow.

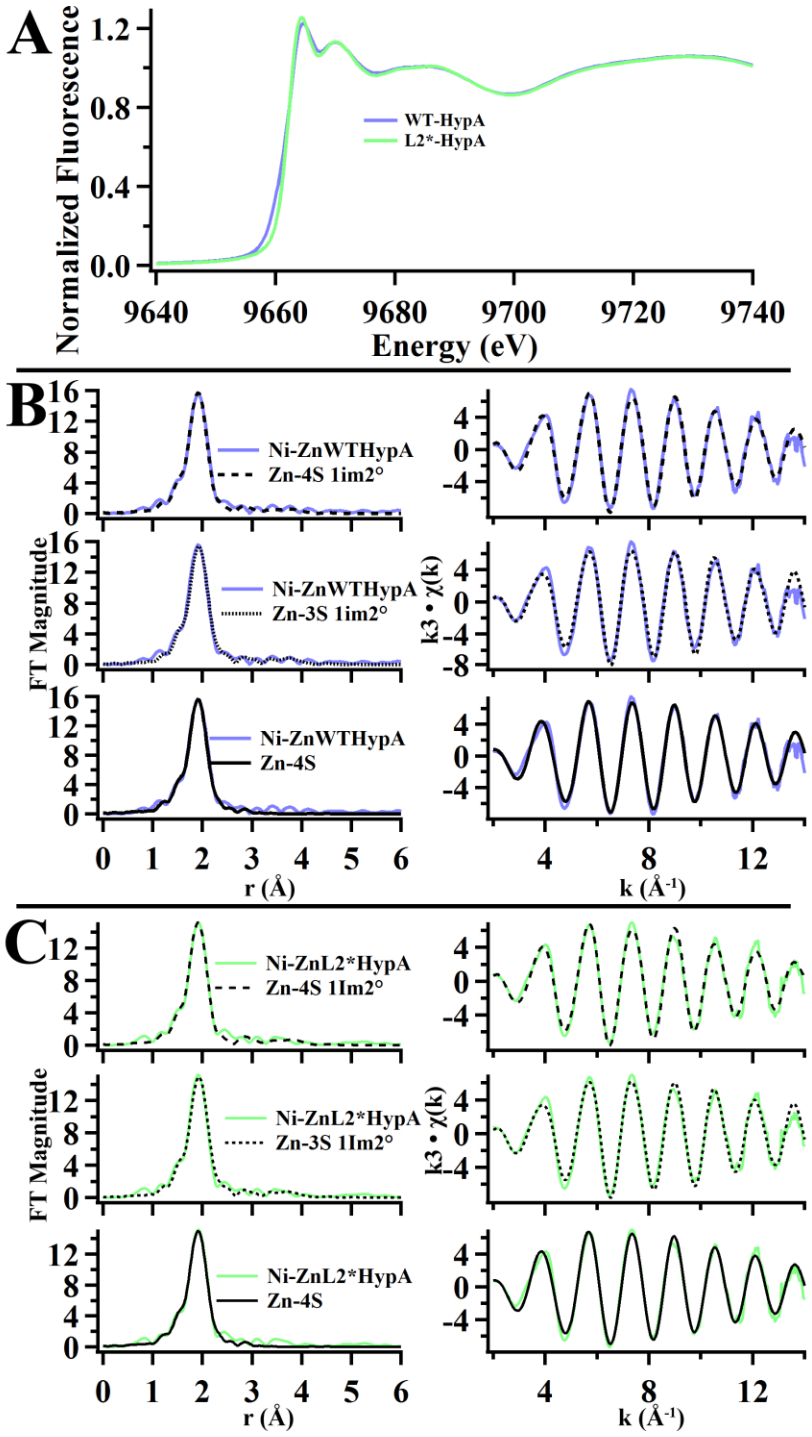

Figure A2.2: Zn K-edge of WT- and L2*-HypA

Zn-site XANES overlay and EXAFS plus best fits for Ni-ZnHypA complexes in buffer with NaBr.(A) Overlay of XANES region of the normalized Zn K-edge of Ni-ZnWTHypA (light blue) and Ni-ZnL2*HypA (light green). EXAFS data (in color) and best fit models (in black) of the Zn K-edge EXAFS region (k = 2 – 14 $Å^{-1}$) represented in unfiltered k^3•χ(k) and non-phased corrected Fourier transformed χ(r) for Ni-ZnWTHypA (B) and Ni-ZnL2*HypA (C) in buffer with NaBr.

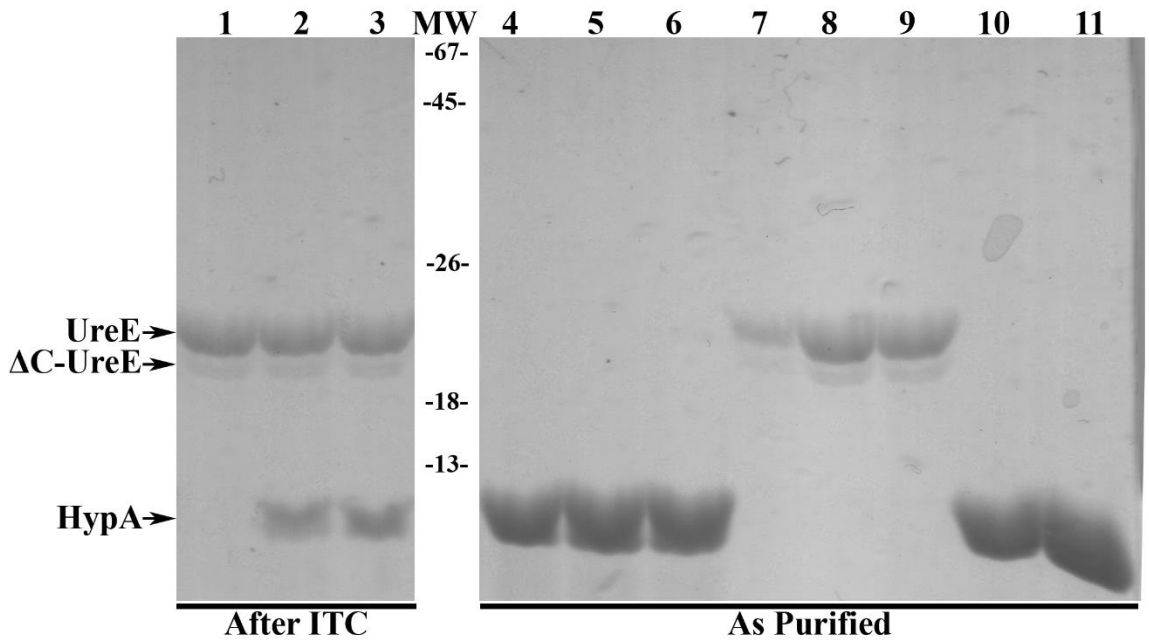

Figure A2.3: SDS-PAGE of protein used in WT- and L2*-HypA titration into UreE
Example of SDS-PAGE showing the purity and integrity of proteins. Sample recovered after ITC experiments of Ni (lane 1), WT-HypA (lane 2), or L2*-HypA (lane 3) titration into $UreE_2$; and as purified proteins of WT-HypA (lanes 4 – 6), L2*-HypA (lanes 10 and 11), and WT-$UreE_2$ (lanes 7 – 9). All lanes containing UreE (calculated molecular weight of 19.4 kDa) is always observed with a small fraction that migrate at a slightly lower molecular weight, which represents the fraction of the protein that has lost 8-residues from the C-terminus as confirmed by ESI-Mass Spec. The position of full length UreE (UreE), C-terminally degraded UreE (ΔC-UreE), and WT- or L2*-HypA (HypA) are as indicated by arrows to the left of the SDS-PAGE.

APPENDIX 3

SUPPORTING DATA FOR HYPA UREE$_2$ INTERACTIONS

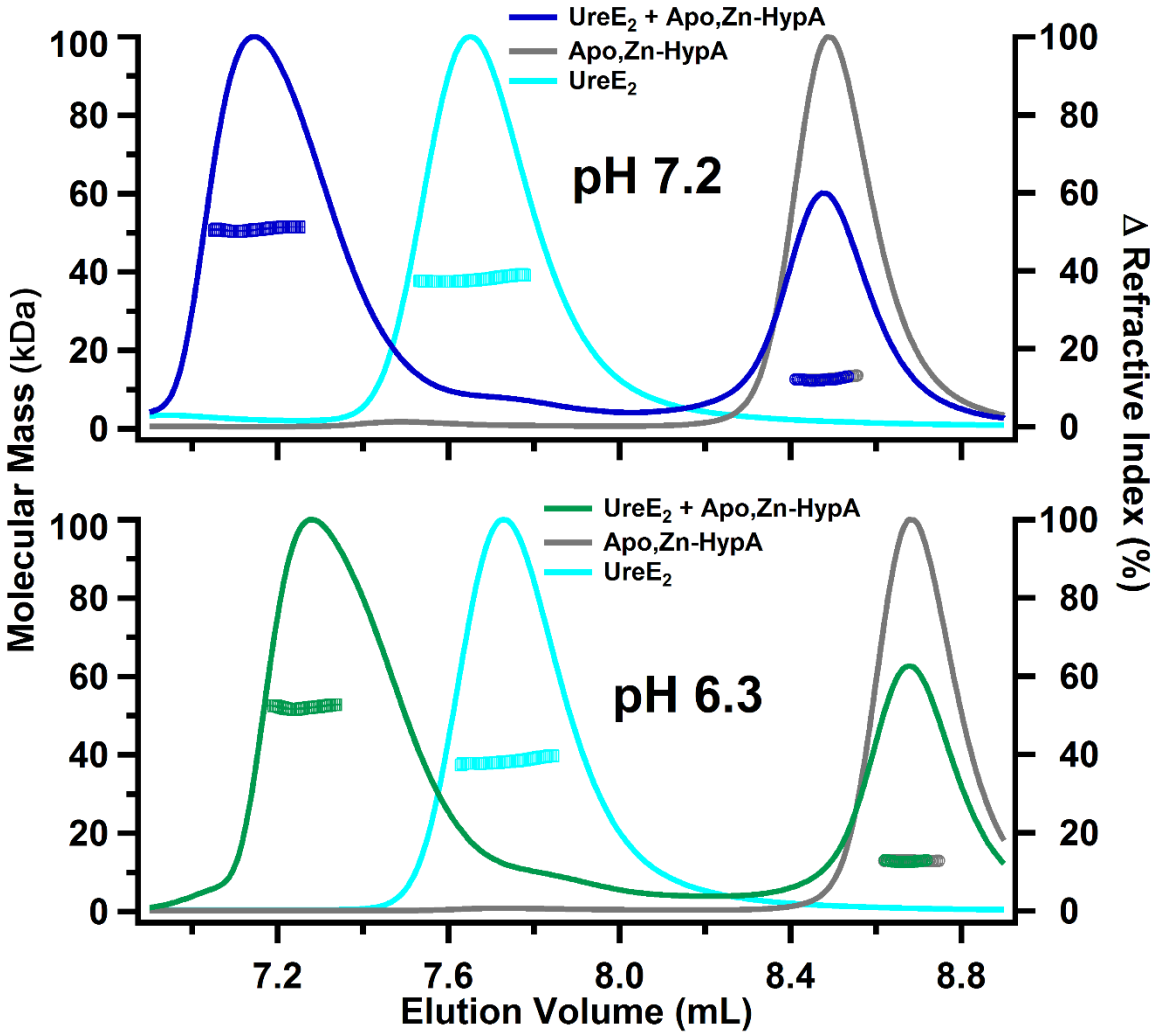

Figure A3.1: SEC-MALS analysis of proteins
Representative size exclusion chromatography and multi-angle light scattering (SEC-MALS) chromatographs of apo-ZnHypA (gray lines), apo-UreE (cyan lines, and 3:1 mixture of apo-ZnHypA with apo-UreE$_2$ at pH 7.2 (blue, upper panel) and pH 6.3 (green, lower panel). Deconvoluted masses of the protein or protein complexes are shown in the middle of each peak.

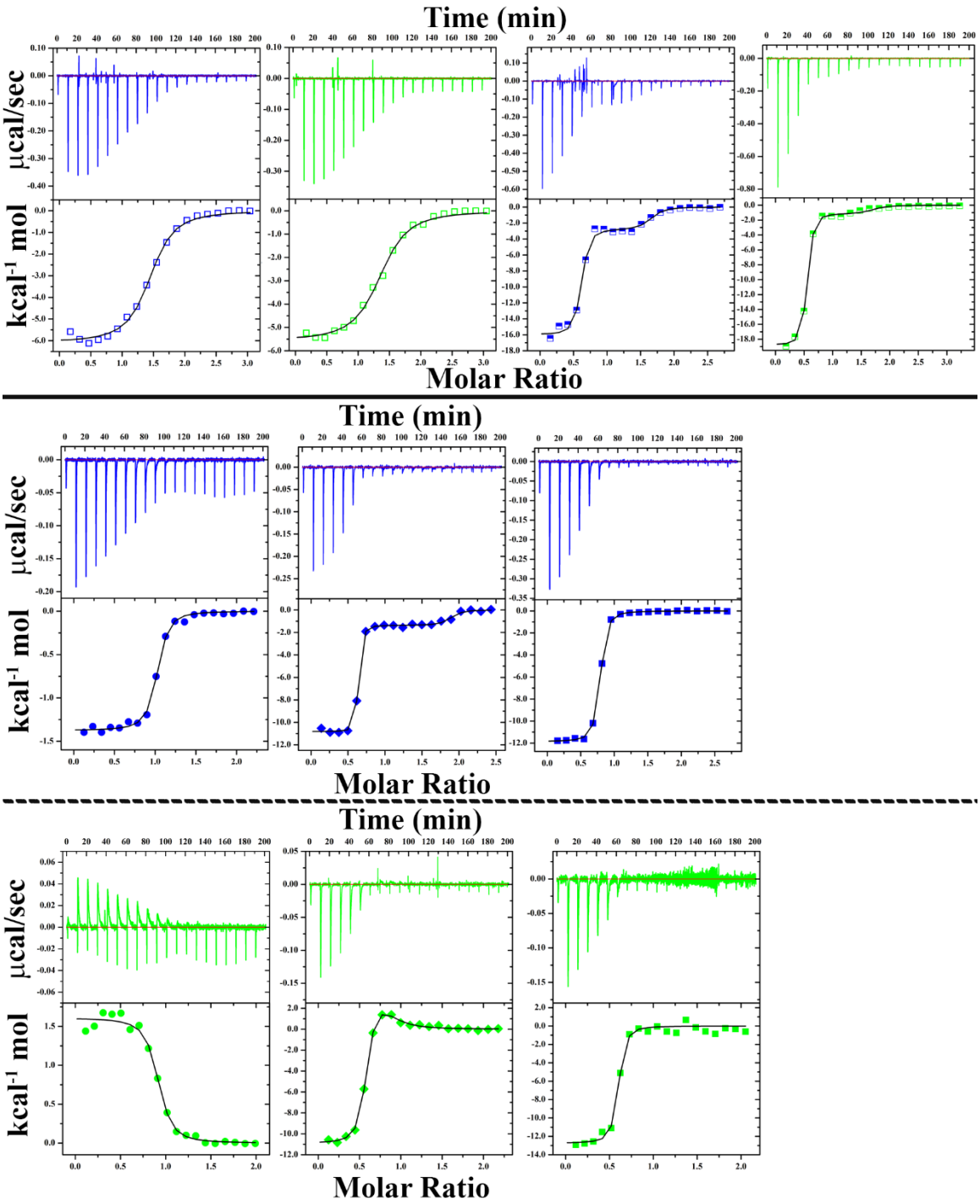

Figure A3.2: Raw ITC data and ΔH

Isothermal titration calorimetry (ITC) raw data and corresponding ΔH binding isotherms of apo-ZnHypA titrations into apoUreE$_2$ (open squares); Ni-ZnHypA titrations into apoUreE$_2$ (half-filled squares); and Ni titration into apo-ZnHypA (filled circles), apoUreE2 (filled squares), and apo-ZnHypA-UreE2 protein complex (filled diamonds) performed at pH 7.2 (blue) and 6.3 (green).

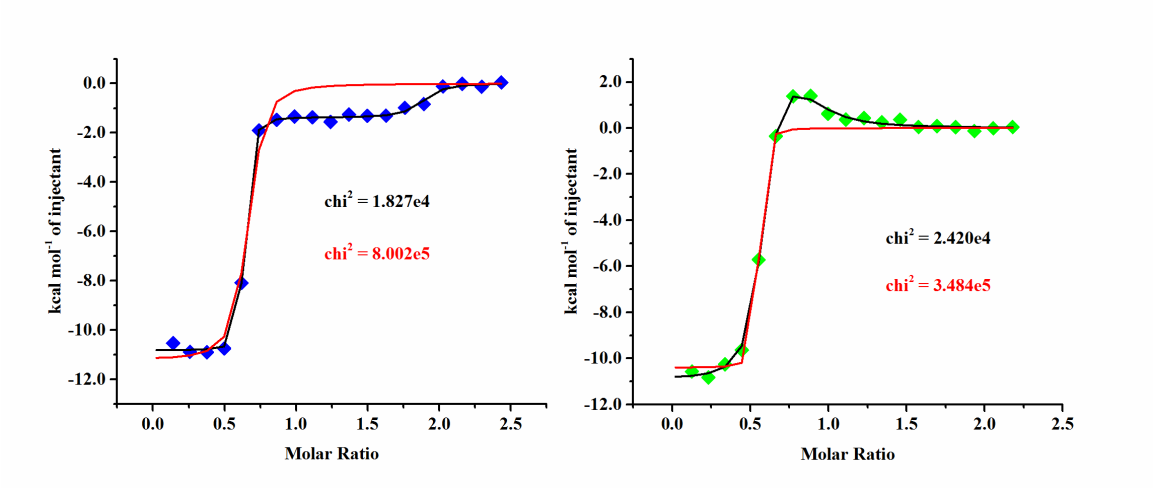

Figure A3.3: ITC TwoSites versus OneSite Fits of Ni binding to apo-ZnHypA-UreE$_2$
Comparison of fitting models with TwoSites (black line) and OneSite (red line) of ITC data for Ni^{2+} binding to the preformed ZnHypA-UreE$_2$ complex at pH 7.2 (blue) and 6.3 (green). The goodness of fit parameter, chi^2, for each fit is displayed in corresponding colors.

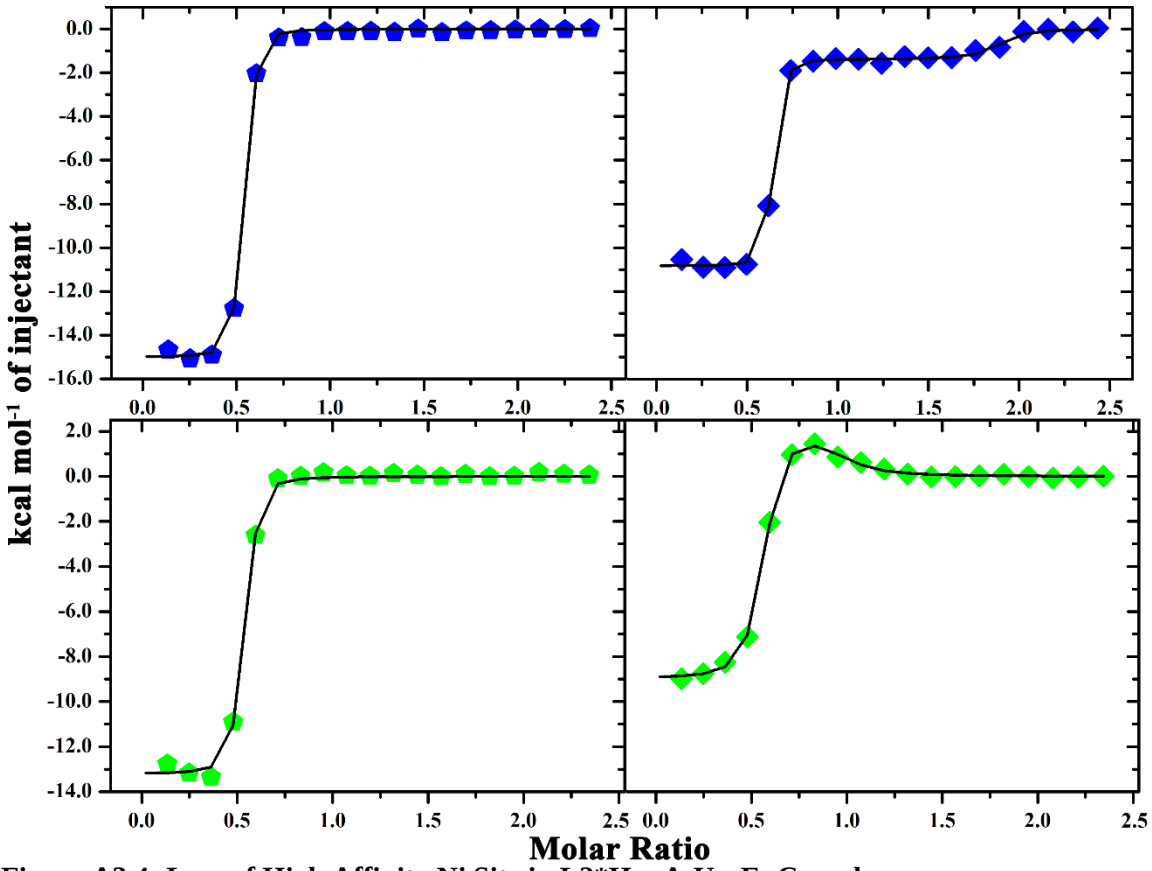

Figure A3.4: Loss of High Affinity Ni Site in L2*HypA-UreE$_2$ Complex

Loss of high affinity binding site in Ni^{2+} titration into the preformed complex of ZnHypA-UreE$_2$ complex when WTHypA (diamonds) is replaced with N-terminal variant L2*HypA (pentagons) at pH 7.2 (blue) and 6.3 (green).

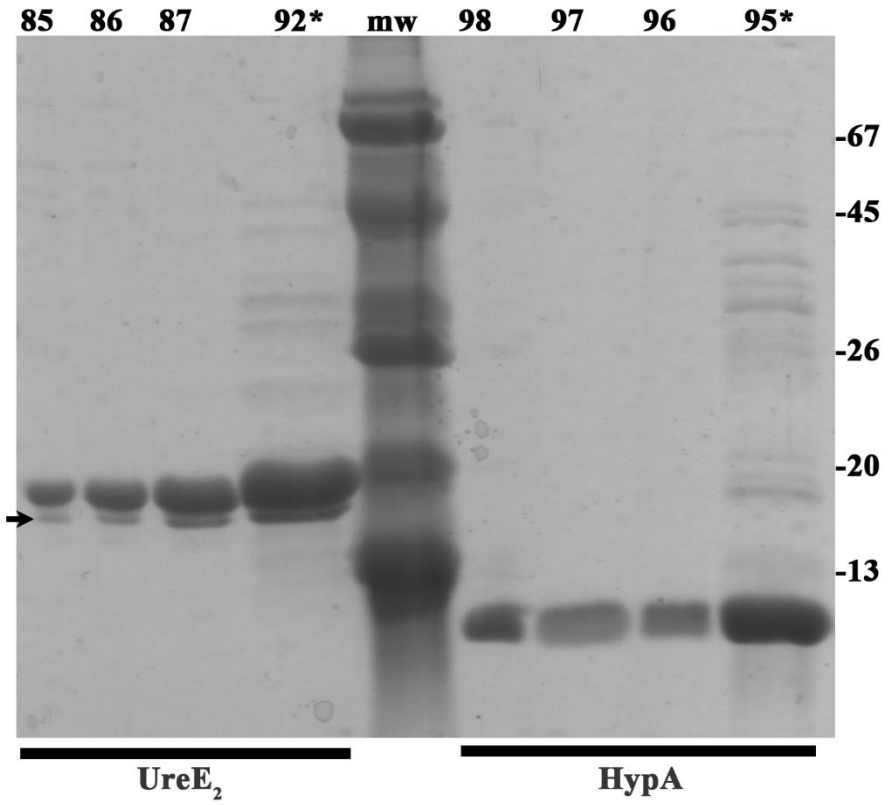

Figure A3.5: SDS-PAGE of Purified UreE and HypA Proteins
SDS-PAGE showing the purity of the purified $UreE_2$ (left) and HypA (right) from the HiLoad Superdex 75 column with the elution volume of the fractions labeled at the top of each lane. (***** indicates the fractions that were not used for experiments, and the black arrow indicates the band corresponding to degradation of purified *Hp*UreE protein at the C-terminal Ni-binding motif).

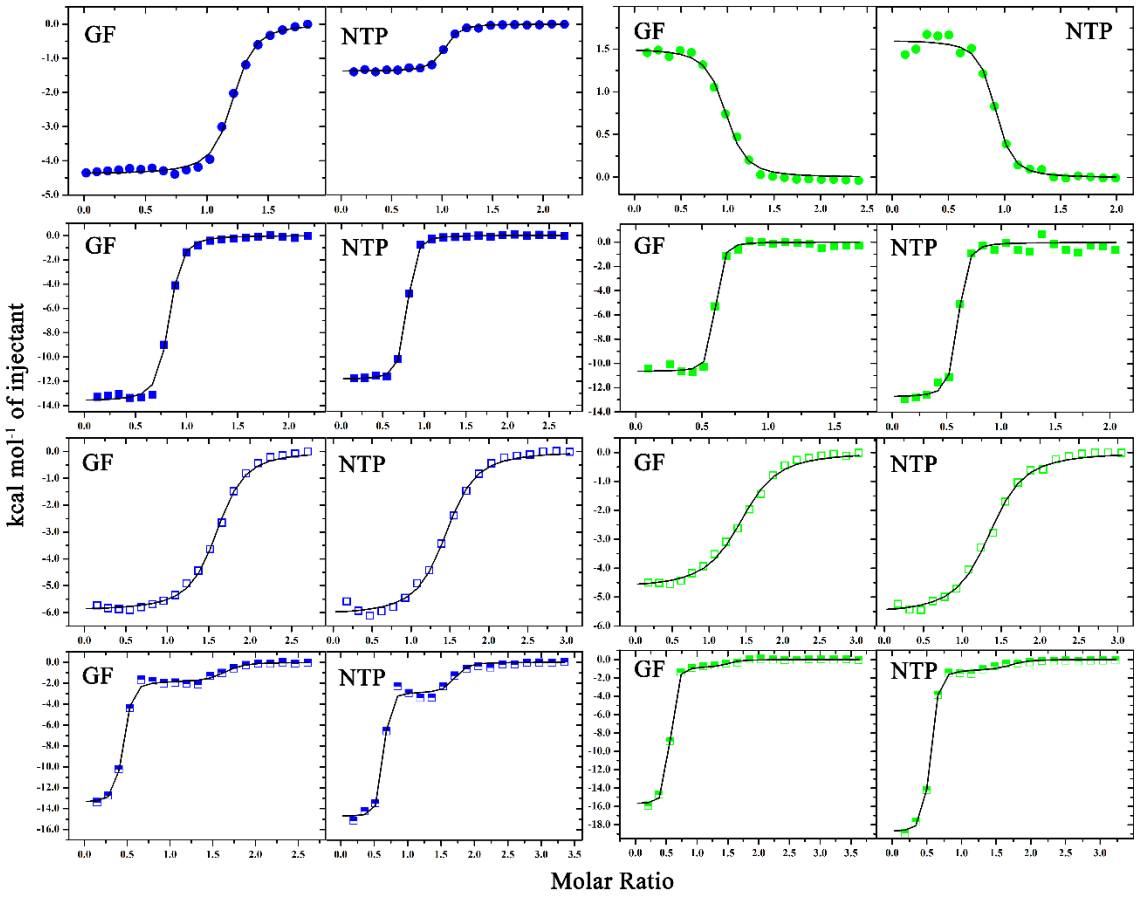

Figure A3.6: Comparison of ITC isotherms performed in GF and NTP Buffers
Representative ITC binding isotherms of parallel titrations performed in GF buffer (20 mM HEPES, 200 mM NaCl, 1 mM TCEP) and NTP buffer (20 mM HEPES, 100 mM NaCl, 100 mM KCl, 5 mM $MgCl_2$, 1 mM TCEP) demonstrating lack of significant differences in titrations performed between the two buffers. Shown are titrations performed at pH 7.2 (blue) and 6.3 (green) of Ni^{2+} titrations into HypA (circles) and $UreE_2$ (filled squares), apo-ZnHypA titration into UreE2 (open squares), and Ni-ZnHypA titration into $UreE_2$ (half-filled squares) with fits (black lines).

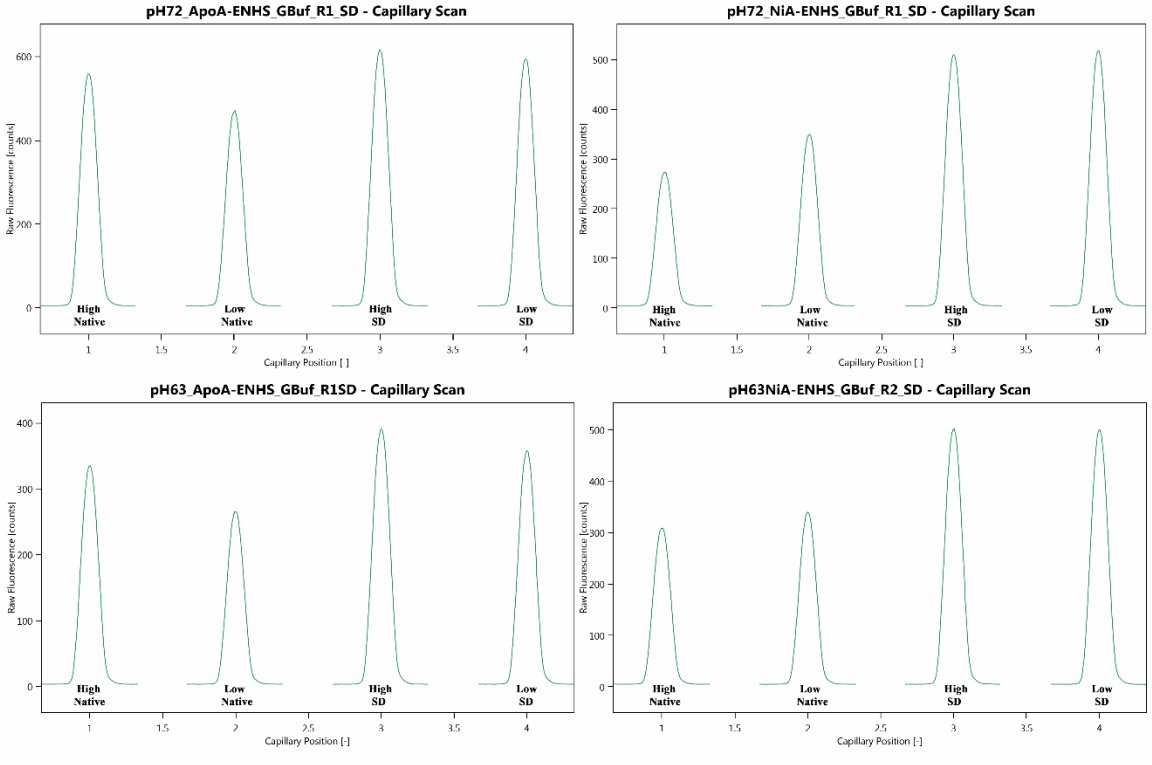

Figure A3.7: SD Test Control for Fluorescence Binding
Fluorescence response of parallel samples of native and denatured (SD = heat-treated with SDS and DTT) titration samples containing equal concentrations of NHS640-UreE_2 mixed with high- and low-concentrations of HypA.

BIBLIOGRAPHY

1. Abraham, L. O., Li, Y., and Zamble, D. B. (2006) The metal- and DNA-binding activities of Helicobacter pylori NikR, *Journal of inorganic biochemistry 100*, 1005-1014. (10.1016/j.jinorgbio.2005.10.014)

2. Akada, J. K., Shirai, M., Takeuchi, H., Tsuda, M., and Nakazawa, T. (2000) Identification of the urease operon in Helicobacter pylori and its control by mRNA decay in response to pH, *Molecular microbiology 36*, 1071-1084

3. Allan, E., Clayton, C. L., McLaren, A., Wallace, D. M., and Wren, B. W. (2001) Characterization of the low-pH responses of Helicobacter pylori using genomic DNA arrays, *Microbiology 147*, 2285-2292. (10.1099/00221287-147-8-2285)

4. Andersson, M., Wittgren, B., and Wahlund, K. G. (2003) Accuracy in multiangle light scattering measurements for molar mass and radius estimations. Model calculations and experiments, *Anal Chem 75*, 4279-4291

5. Ang, S., Lee, C. Z., Peck, K., Sindici, M., Matrubutham, U., Gleeson, M. A., and Wang, J. T. (2001) Acid-induced gene expression in Helicobacter pylori: study in genomic scale by microarray, *Infect Immun 69*, 1679-1686. (10.1128/IAI.69.3.1679-1686.2001)

6. Ankudinov, A. L., Ravel, B., Rehr, J. J., and Conradson, S. D. (1998) Real-space multiple-scattering calculation and interpretation of x-ray-absorption near-edge structure, *Physical Review B 58*, 7565-7576. (DOI 10.1103/PhysRevB.58.7565)

7. Arnold, I. C., Dehzad, N., Reuter, S., Martin, H., Becher, B., Taube, C., and Muller, A. (2011) Helicobacter pylori infection prevents allergic asthma in mouse models through the induction of regulatory T cells, *J Clin Invest 121*, 3088-3093. (10.1172/JCI45041)

8. Ba, L. A., Doering, M., Burkholz, T., and Jacob, C. (2009) Metal trafficking: from maintaining the metal homeostasis to future drug design, *Metallomics : integrated biometal science 1*, 292-311. (10.1039/b904533c)

9. Bacarizo, J., Martinez-Rodriguez, S., Martin-Garcia, J. M., Andujar-Sanchez, M., Ortiz-Salmeron, E., Neira, J. L., and Camara-Artigas, A. (2014) Electrostatic Effects in the Folding of the SH3 Domain of the c-Src Tyrosine Kinase: pH-Dependence in 3D-Domain Swapping and Amyloid Formation, *PloS one 9*

10. Bal, W., Sokolowska, M., Kurowska, E., and Faller, P. (2013) Binding of transition metal ions to albumin: Sites, affinities and rates, *Bba-Gen Subjects 1830*, 5444-5455

11. Baltrus, D. A., Amieva, M. R., Covacci, A., Lowe, T. M., Merrell, D. S., Ottemann, K. M., Stein, M., Salama, N. R., and Guillemin, K. (2009) The Complete Genome Sequence of Helicobacter pylori Strain G27, *Journal of bacteriology 191*, 447-448. (10.1128/Jb.01416-08)

12. Baltrus, D. A., Amieva, M. R., Covacci, A., Lowe, T. M., Merrell, D. S., Ottemann, K. M., Stein, M., Salama, N. R., and Guillemin, K. (2009) The complete genome sequence of Helicobacter pylori strain G27, *J Bacteriol 191*, 447-448. (10.1128/JB.01416-08)

13. Banaszak, K., Martin-Diaconescu, V., Bellucci, M., Zambelli, B., Rypniewski, W., Maroney, M. J., and Ciurli, S. (2012) Crystallographic and X-ray absorption spectroscopic characterization of Helicobacter pylori UreE bound to Ni(2)(+) and Zn(2)(+) reveals a role for the disordered C-terminal arm in metal trafficking, *The Biochemical journal 441*, 1017-1026. (10.1042/BJ20111659)

14. Bange, G., and Sinning, I. (2013) SIMIBI twins in protein targeting and localization, *Nat Struct Mol Biol 20*, 776-780. (10.1038/nsmb.2605)

15. Barondeau, D. P., Kassmann, C. J., Bruns, C. K., Tainer, J. A., and Getzoff, E. D. (2004) Nickel superoxide dismutase structure and mechanism, *Biochemistry 43*, 8038-8047. (10.1012/bi0496081)

16. Bauerfeind, P., Garner, R., Dunn, B. E., and Mobley, H. L. T. (1997) Synthesis and activity of Helicobacter pylori urease and catalase at low pH, *Gut 40*, 25-30

17. Baykov, A. A., Evtushenko, O. A., and Avaeva, S. M. (1988) A malachite green procedure for orthophosphate determination and its use in alkaline phosphatase-based enzyme immunoassay, *Analytical biochemistry 171*, 266-270

18. Bellucci, M., Zambelli, B., Musiani, F., Turano, P., and Ciurli, S. (2009) Helicobacter pylori UreE, a urease accessory protein: specific Ni(2+)- and Zn(2+)-binding properties and interaction with its cognate UreG, *The Biochemical journal 422*, 91-100. (10.1042/BJ20090434)

19. Benanti, E. L., and Chivers, P. T. (2009) An intact urease assembly pathway is required to compete with NikR for nickel ions in Helicobacter pylori, *Journal of bacteriology 191*, 2405-2408. (10.1128/JB.01657-08)

20. Benoit, S., and Maier, R. J. (2003) Dependence of Helicobacter pylori Urease Activity on the Nickel-Sequestering Ability of the UreE Accessory Protein, *Journal of bacteriology 185*, 4787-4795. (10.1128/jb.185.16.4787-4795.2003)

21. Benoit, S. L., and Maier, R. J. (2008) Hydrogen and nickel metabolism in helicobacter species, *Ann N Y Acad Sci 1125*, 242-251. (10.1196/annals.1419.014)

22. Benoit, S. L., and Maier, R. J. (2014) Twin-arginine translocation system in Helicobacter pylori: TatC, but not TatB, is essential for viability, *MBio 5*, e01016-01013. (10.1128/mBio.01016-13)

23. Benoit, S. L., McMurry, J. L., Hill, S. A., and Maier, R. J. (2012) Helicobacter pylori hydrogenase accessory protein HypA and urease accessory protein UreG compete with each other for UreE recognition, *Biochimica et biophysica acta 1820*, 1519-1525. (10.1016/j.bbagen.2012.06.002)

24. Benoit, S. L., Mehta, N., Weinberg, M. V., Maier, C., and Maier, R. J. (2007) Interaction between the Helicobacter pylori accessory proteins HypA and UreE is needed for urease maturation, *Microbiology 153*, 1474-1482. (10.1099/mic.0.2006/003228-0)

25. Blum, F. C., Hu, H. Q., Servetas, S. L., Benoit, S. L., Maier, R. J., Maroney, M. J., and Merrell, D. S. (2017) Structure-function analyses of metal-binding sites of HypA reveal residues important for hydrogenase maturation in Helicobacter pylori, *PloS one 12*, e0183260. (10.1371/journal.pone.0183260)

26. Boyer, M. E., Stapleton, J. A., Kuchenreuther, J. M., Wang, C. W., and Swartz, J. R. (2008) Cell-free synthesis and maturation of [FeFe] hydrogenases, *Biotechnol Bioeng 99*, 59-67

27. Bury-Mone, S., Mendz, G. L., Ball, G. E., Thibonnier, M., Stingl, K., Ecobichon, C., Ave, P., Huerre, M., Labigne, A., Thiberge, J. M., and De Reuse, H. (2008) Roles of alpha and beta carbonic anhydrases of Helicobacter pylori in the urease-dependent response to acidity and in colonization of the murine gastric mucosa, *Infect Immun 76*, 497-509. (10.1128/IAI.00993-07)

28. Bury-Mone, S., Skouloubris, S., Labigne, A., and De Reuse, H. (2001) The Helicobacter pylori UreI protein: role in adaptation to acidity and identification of residues essential for its activity and for acid activation, *Molecular microbiology 42*, 1021-1034

29. Bury-Mone, S., Thiberge, J. M., Contreras, M., Maitournam, A., Labigne, A., and De Reuse, H. (2004) Responsiveness to acidity via metal ion regulators mediates virulence in the gastric pathogen Helicobacter pylori, *Molecular microbiology 53*, 623-638. (10.1111/j.1365-2958.2004.04137.x)

30. Campecino, J. O., Dudycz, L. W., Tumelty, D., Berg, V., Cabelli, D. E., and Maroney, M. J. (2015) A Semisynthetic Strategy Leads to Alteration of the Backbone Amidate Ligand in the NiSOD Active Site, *J Am Chem Soc 137*, 9044-9052

31. Carpenter, B. M., McDaniel, T. K., Whitmire, J. M., Gancz, H., Guidotti, S., Censini, S., and Merrell, D. S. (2007) Expanding the Helicobacter pylori genetic toolbox: modification of an endogenous plasmid for use as a transcriptional reporter and complementation vector, *Appl Environ Microbiol 73*, 7506-7514. (10.1128/AEM.01084-07)

32. Carpenter, B. M., West, A. L., Gancz, H., Servetas, S. L., Pich, O. Q., Gilbreath, J. J., Hallinger, D. R., Forsyth, M. H., Merrell, D. S., and Michel, S. L. (2015) Crosstalk between the HpArsRS two-component system and HpNikR is necessary for maximal activation of urease transcription, *Front Microbiol 6*, 558. (10.3389/fmicb.2015.00558)

33. Carter, E. L., Flugga, N., Boer, J. L., Mulrooney, S. B., and Hausinger, R. P. (2009) Interplay of metal ions and urease, *Metallomics : integrated biometal science 1*, 207-221. (10.1039/b903311d)

34. Casalot, L., and Rousset, M. (2001) Maturation of the [NiFe] hydrogenases, *Trends Microbiol 9*, 228-237

35. Chan, K. H., Lee, K. M., and Wong, K. B. (2012) Interaction between hydrogenase maturation factors HypA and HypB is required for [NiFe]-hydrogenase maturation, *PloS one 7*, e32592. (10.1371/journal.pone.0032592)

36. Cheng, T., Li, H., Xia, W., and Sun, H. (2012) Multifaceted SlyD from Helicobacter pylori: implication in [NiFe] hydrogenase maturation, *Journal of biological inorganic chemistry : JBIC : a publication of the Society of Biological Inorganic Chemistry 17*, 331-343. (10.1007/s00775-011-0855-y)

37. Cheng, T., Li, H., Yang, X., Xia, W., and Sun, H. (2013) Interaction of SlyD with HypB of Helicobacter pylori facilitates nickel trafficking, *Metallomics : integrated biometal science 5*, 804-807. (10.1039/c3mt00014a)

38. Chivers, P. T., Benanti, E. L., Heil-Chapdelaine, V., Iwig, J. S., and Rowe, J. L. (2012) Identification of Ni-(L-His)(2) as a substrate for NikABCDE-dependent nickel uptake in Escherichia coli, *Metallomics : integrated biometal science 4*, 1043-1050. (10.1039/c2mt20139a)

39. Choudhury, S. B., Lee, J. W., Davidson, G., Yim, Y. I., Bose, K., Sharma, M. L., Kang, S. O., Cabelli, D. E., and Maroney, M. J. (1999) Examination of the nickel site structure and reaction mechanism in Streptomyces seoulensis superoxide dismutase, *Biochemistry 38*, 3744-3752. (10.1021/bi982537j)

40. Chuang, M. H., Wu, M. S., Lin, J. T., and Chiou, S. H. (2005) Proteomic analysis of proteins expressed by Helicobacter pylori under oxidative stress, *Proteomics 5*, 3895-3901. (10.1002/pmic.200401232)

41. Chung, K. C. C., Cao, L., Dias, A. V., Pickering, I. J., George, G. N., and Zamble, D. B. (2008) A High-Affinity Metal-Binding Peptide from Escherichia coli HypB, *J Am Chem Soc 130*, 14056-+

42. Colpas, G. J., Brayman, T. G., Ming, L. J., and Hausinger, R. P. (1999) Identification of metal-binding residues in the Klebsiella aerogenes urease nickel metallochaperone, UreE, *Biochemistry 38*, 4078-4088. (10.1021/bi982435t)

43. Colpas, G. J., Maroney, M. J., Bagyinka, C., Kumar, M., Willis, W. S., Suib, S. L., Baidya, N., and Mascharak, P. K. (1991) X-Ray Spectroscopic Studies of Nickel-Complexes, with Application to the Structure of Nickel Sites in Hydrogenases, *Inorg Chem 30*, 920-928. (Doi 10.1021/Ic00005a010)

44. Contreras, M., Thiberge, J. M., Mandrand-Berthelot, M. A., and Labigne, A. (2003) Characterization of the roles of NikR, a nickel-responsive pleiotropic autoregulator of Helicobacter pylori, *Molecular microbiology 49*, 947-963

45. Copass, M., Grandi, G., and Rappuoli, R. (1997) Introduction of unmarked mutations in the Helicobacter pylori vacA gene with a sucrose sensitivity marker, *Infection and immunity 65*, 1949-1952

46. Croxen, M. A., Sisson, G., Melano, R., and Hoffman, P. S. (2006) The Helicobacter pylori chemotaxis receptor TlpB (HP0103) is required for pH taxis and for colonization of the gastric mucosa, *Journal of bacteriology 188*, 2656-2665. (10.1128/JB.188.7.2656-2665.2006)

47. Dian, C., Schauer, K., Kapp, U., McSweeney, S. M., Labigne, A., and Terradot, L. (2006) Structural basis of the nickel response in Helicobacter pylori: crystal structures of HpNikR in Apo and nickel-bound states, *Journal of molecular biology 361*, 715-730. (10.1016/j.jmb.2006.06.058)

48. Dorer, M. S., Cohen, I. E., Sessler, T. H., Fero, J., and Salama, N. R. (2013) Natural competence promotes Helicobacter pylori chronic infection, *Infect Immun 81*, 209-215. (10.1128/IAI.01042-12)

49. Dorer, M. S., Fero, J., and Salama, N. R. (2010) DNA damage triggers genetic exchange in Helicobacter pylori, *PLoS Pathog 6*, e1001026. (10.1371/journal.ppat.1001026)

50. Dorer, M. S., Sessler, T. H., and Salama, N. R. (2011) Recombination and DNA repair in Helicobacter pylori, *Annu Rev Microbiol 65*, 329-348. (10.1146/annurev-micro-090110-102931)

51. Eaton, K. A., Brooks, C. L., Morgan, D. R., and Krakowka, S. (1991) Essential Role of Urease in Pathogenesis of Gastritis Induced by Helicobacter-Pylori in Gnotobiotic Piglets, *Infection and Immunity 59*, 2470-2475

52. Eaton, K. A., and Krakowka, S. (1994) Effect of Gastric Ph on Urease-Dependent Colonization of Gnotobiotic Piglets by Helicobacter-Pylori, *Infection and Immunity 62*, 3604-3607

53. Eaton, K. A., Suerbaum, S., Josenhans, C., and Krakowka, S. (1996) Colonization of gnotobiotic piglets by Helicobacter pylori deficient in two flagellin genes, *Infect Immun 64*, 2445-2448

54. Ernst, F. D., Kuipers, E. J., Heijens, A., Sarwari, R., Stoof, J., Penn, C. W., Kusters, J. G., and van Vliet, A. H. (2005) The nickel-responsive regulator NikR controls activation and repression of gene transcription in Helicobacter pylori, *Infect Immun 73*, 7252-7258. (10.1128/IAI.73.11.7252-7258.2005)

55. Ernst, F. D., Stoof, J., Horrevoets, W. M., Kuipers, E. J., Kusters, J. G., and van Vliet, A. H. (2006) NikR mediates nickel-responsive transcriptional repression of the Helicobacter pylori outer membrane proteins FecA3 (HP1400) and FrpB4 (HP1512), *Infect Immun 74*, 6821-6828. (10.1128/IAI.01196-06)

56. Eusebi, L. H., Zagari, R. M., and Bazzoli, F. (2014) Epidemiology of Helicobacter pylori infection, *Helicobacter 19 Suppl 1*, 1-5. (10.1111/hel.12165)

57. Evans, D. F. (1959) The Determination of the Paramagnetic Susceptibility of Substances in Solution by Nuclear Magnetic Resonance, *J Chem Soc*, 2003-2005. (Doi 10.1039/Jr9590002003)

58. Farrugia, M. A., Macomber, L., and Hausinger, R. P. (2013) Biosynthesis of the Urease Metallocenter, *Journal of Biological Chemistry 288*, 13178-13185. (10.1074/jbc.R112.446526)

59. Fischer, F., and De Reuse, H. (2016) Adaptation of *Helicobacter pylori* Metabolism to Persistent Gastric Colonization, In *Helicobacter pylori Research From Bench to Bedside* (Steffen Backert, Y. Y., Ed.), pp 29-56, Springer, Japan.

60. Fong, Y. H., Wong, H. C., Yuen, M. H., Lau, P. H., Chen, Y. W., and Wong, K. B. (2013) Structure of UreG/UreF/UreH complex reveals how urease accessory proteins facilitate maturation of Helicobacter pylori urease, *PLoS Biol 11*, e1001678. (10.1371/journal.pbio.1001678)

61. Foynes, S., Dorrell, N., Ward, S. J., Stabler, R. A., McColm, A. A., Rycroft, A. N., and Wren, B. W. (2000) Helicobacter pylori possesses two CheY response regulators and a histidine kinase sensor, CheA, which are essential for chemotaxis and colonization of the gastric mucosa, *Infect Immun 68*, 2016-2023

62. Gasper, R., Scrima, A., and Wittinghofer, A. (2006) Structural insights into HypB, a GTP-binding protein that regulates metal binding, *The Journal of biological chemistry 281*, 27492-27502. (10.1074/jbc.M600809200)

63. Ge, R., Watt, R. M., Sun, X., Tanner, J. A., He, Q. Y., Huang, J. D., and Sun, H. (2006) Expression and characterization of a histidine-rich protein, Hpn: potential for Ni2+ storage in Helicobacter pylori, *The Biochemical journal 393*, 285-293. (10.1042/BJ20051160)

64. Ge, R. G., Wang, D. X., Hao, M. C., and Sun, X. S. (2013) Nickel trafficking system responsible for urease maturation in Helicobacter pylori, *World journal of gastroenterology : WJG 19*, 8211-8218. (10.3748/wjg.v19.i45.8211)

65. Giri, N. C. (2013) Structural Investigations of Early Intermediates and Nickel Inhibition Complexes of Human DNA and Histone Demethylases, In *Chemistry*, p 343, University of Massachusetts Amherst, UMASS Amherst.

66. Giri, N. C., Sun, H., Chen, H., Costa, M., and Maroney, M. J. (2011) X-ray absorption spectroscopy structural investigation of early intermediates in the mechanism of DNA repair by human ABH2, *Biochemistry 50*, 5067-5076. (10.1021/bi101668x)

67. Gobert, A. P., and Wilson, K. T. (2016) The Immune Battle against Helicobacter pylori Infection: NO Offense, *Trends Microbiol 24*, 366-376. (10.1016/j.tim.2016.02.005)

68. Goodwin, C. S., and Armstrong, J. A. (1990) Microbiological aspects of Helicobacter pylori (Campylobacter pylori), *Eur J Clin Microbiol Infect Dis 9*, 1-13

69. Harford, C., and Sarkar, B. (1997) Amino terminal Cu(II)- and Ni(II)-binding (ATCUN) motif of proteins and peptides: Metal binding, DNA cleavage, and other properties, *Accounts Chem Res 30*, 123-130

70. Hayes, E. T., Wilks, J. C., Sanfilippo, P., Yohannes, E., Tate, D. P., Jones, B. D., Radmacher, M. D., BonDurant, S. S., and Slonczewski, J. L. (2006) Oxygen limitation modulates pH regulation of catabolism and hydrogenases, multidrug transporters, and envelope composition in Escherichia coli K-12, *BMC Microbiol 6*, 89. (10.1186/1471-2180-6-89)

71. Hendrickson, W. A., Horton, J. R., and Lemaster, D. M. (1990) Selenomethionyl Proteins Produced for Analysis by Multiwavelength Anomalous Diffraction (Mad) - a Vehicle for Direct Determination of 3-Dimensional Structure, *Embo J 9*, 1665-1672

72. Herbst, R. W. (2010) Structure and Function in a Nickel Metallochaperone, HypA and Nickel Dependent Superoxide Dismutase, In *Department of Chemistry*, p 184, University of Massachusetts Amherst, UMASS Amherst.

73. Herbst, R. W., Perovic, I., Martin-Diaconescu, V., O'Brien, K., Chivers, P. T., Pochapsky, S. S., Pochapsky, T. C., and Maroney, M. J. (2010) Communication between the zinc and nickel sites in dimeric HypA: metal recognition and pH sensing, *Journal of the American Chemical Society 132*, 10338-10351. (10.1021/ja1005724)

74. Herbst, R. W., Perovic, I., Martin-Diaconescu, V., O'Brien, K., Chivers, P. T., Pochapsky, S. S., Pochapsky, T. C., and Maroney, M. J. (2010) Communication between the Zinc and Nickel Sites in Dimeric HypA: Metal Recognition and pH Sensing, *J Am Chem Soc 132*, 10338-10351. (Doi 10.1021/Ja1005724)

75. Higgins, K. A., Carr, C. E., and Maroney, M. J. (2012) Specific metal recognition in nickel trafficking, *Biochemistry 51*, 7816-7832. (10.1021/bi300981m)

76. Higgins, K. A., Chivers, P. T., and Maroney, M. J. (2012) Role of the N-terminus in determining metal-specific responses in the E. coli Ni- and Co-responsive metalloregulator, RcnR, *J Am Chem Soc 134*, 7081-7093. (10.1021/ja300834b)

77. Higgins, K. A., Hu, H. Q., Chivers, P. T., and Maroney, M. J. (2013) Effects of select histidine to cysteine mutations on transcriptional regulation by Escherichia coli RcnR, *Biochemistry 52*, 84-97. (10.1021/bi300886q)

78. Hohenwallner, W., and Wimmer, E. (1973) The Malachite green micromethod for the determination of inorganic phosphate, *Clinica chimica acta; international journal of clinical chemistry 45*, 169-175

79. Horton, R. M., Ho, S. N., Pullen, J. K., Hunt, H. D., Cai, Z., and Pease, L. R. (1993) Gene splicing by overlap extension, *Methods in enzymology 217*, 270-279

80. Horton, R. M., Ho, S. N., Pullen, J. K., Hunt, H. D., Cai, Z. L., and Pease, L. R. (1993) Gene-Splicing by Overlap Extension, *Method Enzymol 217*, 270-279

81. Hough, M. A., and Hasnain, S. S. (2003) Structure of fully reduced bovine copper zinc superoxide dismutase at 1.15 angstrom, *Structure 11*, 937-946. (10.1016/S0969-2126(03)00155-2)

82. Hu, H. Q., Johnson, R. C., Merrell, D. S., and Maroney, M. J. (2017) Nickel Ligation of the N-Terminal Amine of HypA Is Required for Urease Maturation in Helicobacter pylori, *Biochemistry 56*, 1105-1116. (10.1021/acs.biochem.6b00912)

83. Johnson, R. C., Hu, H. Q., Merrell, D. S., and Maroney, M. J. (2015) Dynamic HypA zinc site is essential for acid viability and proper urease maturation in Helicobacter pylori, *Metallomics : integrated biometal science 7*, 674-682. (10.1039/c4mt00306c)

84. Joyce, E. A., Gilbert, J. V., Eaton, K. A., Plaut, A., and Wright, A. (2001) Differential gene expression from two transcriptional units in the cag pathogenicity island of Helicobacter pylori, *Infection and immunity 69*, 4202-4209. (10.1128/IAI.69.7.4202-4209.2001)

85. Joyce, E. A., Gilbert, J. V., Eaton, K. A., Plaut, A., and Wright, A. (2001) Differential gene expression from two transcriptional units in the cag pathogenicity island of Helicobacter pylori, *Infection and Immunity 69*, 4202-4209

86. Kang, D., Gong, Y., Zhu, Y., Li, A., Dong, N., Piao, Y., and Yuan, Y. (2013) The biological activity of H. pylori SlyD in vitro, *Helicobacter 18*, 347-355. (10.1111/hel.12057)

87. Kang, J., and Blaser, M. J. (2006) Bacterial populations as perfect gases: genomic integrity and diversification tensions in Helicobacter pylori, *Nat Rev Microbiol 4*, 826-836. (10.1038/nrmicro1528)

88. Kennedy, D. C., Herbst, R. W., Iwig, J. S., Chivers, P. T., and Maroney, M. J. (2007) A dynamic Zn site in Helicobacter pylori HypA: A potential mechanism for metal-specific protein activity, *J Am Chem Soc 129*, 16-17. (Doi 10.1021/Ja066958x)

89. Kodaman, N., Pazos, A., Schneider, B. G., Piazuelo, M. B., Mera, R., Sobota, R. S., Sicinschi, L. A., Shaffer, C. L., Romero-Gallo, J., de Sablet, T., Harder, R. H., Bravo, L. E., Peek, R. M., Jr., Wilson, K. T., Cover, T. L., Williams, S. M., and Correa, P. (2014) Human and Helicobacter pylori coevolution shapes the risk of gastric disease, *Proc Natl Acad Sci U S A 111*, 1455-1460. (10.1073/pnas.1318093111)

90. Kritzer, J. A., Neupane, K. P., and Aldous, A. R. (2013) Design of Macrocyclic ATCUN Peptides as Redox Catalysts, *Biopolymers 100*, 281-281

91. Lebwohl, B., Blaser, M. J., Ludvigsson, J. F., Green, P. H., Rundle, A., Sonnenberg, A., and Genta, R. M. (2013) Decreased risk of celiac disease in patients with Helicobacter pylori colonization, *Am J Epidemiol 178*, 1721-1730. (10.1093/aje/kwt234)

92. Leduc, D., Gallaud, J., Stingl, K., and de Reuse, H. (2010) Coupled amino acid deamidase-transport systems essential for Helicobacter pylori colonization, *Infect Immun 78*, 2782-2792. (10.1128/IAI.00149-10)

93. Lee, M. H., Pankratz, H. S., Wang, S., Scott, R. A., Finnegan, M. G., Johnson, M. K., Ippolito, J. A., Christianson, D. W., and Hausinger, R. P. (1993) Purification and characterization of Klebsiella aerogenes UreE protein: a nickel-binding protein that functions in urease metallocenter assembly, *Protein Sci 2*, 1042-1052. (10.1002/pro.5560020617)

94. Leipe, D. D., Wolf, Y. I., Koonin, E. V., and Aravind, L. (2002) Classification and evolution of P-loop GTPases and related ATPases, *Journal of molecular biology 317*, 41-72. (10.1006/jmbi.2001.5378)

95. Lewis, J., and Wilkins, R. G. (1960) *Modern coordination chemistry: principles and methods*, Interscience Publishers, New York,.

96. Li, Y., and Zamble, D. B. (2009) pH-responsive DNA-binding activity of Helicobacter pylori NikR, *Biochemistry 48*, 2486-2496. (10.1021/bi801742r)

97. Liu, Z. F., Chen, C. Y., Tang, W., Zhang, J. Y., Gong, Y. Q., and Jia, J. H. (2006) Gene-expression profiles in gastric epithelial cells stimulated with spiral and coccoid Helicobacter pylori, *J Med Microbiol 55*, 1009-1015. (10.1099/jmm.0.46456-0)

98. Maier, R. J., Benoit, S. L., and Seshadri, S. (2007) Nickel-binding and accessory proteins facilitating Ni-enzyme maturation in Helicobacter pylori, *Biometals : an international journal on the role of metal ions in biology, biochemistry, and medicine 20*, 655-664. (10.1007/s10534-006-9061-8)

99. Maier, R. J., Fu, C., Gilbert, J., Moshiri, F., Olson, J., and Plaut, A. G. (1996) Hydrogen uptake hydrogenase in Helicobacter pylori, *FEMS Microbiol Lett 141*, 71-76

100. Maier, R. J., Olczak, A., Maier, S., Soni, S., and Gunn, J. (2004) Respiratory hydrogen use by Salmonella enterica serovar Typhimurium is essential for virulence, *Infect Immun 72*, 6294-6299. (10.1128/IAI.72.11.6294-6299.2004)

101. Marcus, E. A., Moshfegh, A. P., Sachs, G., and Scott, D. R. (2005) The periplasmic alpha-carbonic anhydrase activity of Helicobacter pylori is essential for acid acclimation, *Journal of bacteriology 187*, 729-738. (10.1128/JB.187.2.729-738.2005)

102. Maroney, M. J., and Ciurli, S. (2014) Nonredox nickel enzymes, *Chemical reviews 114*, 4206-4228. (10.1021/cr4004488)

103. Marshall, B. J., Barrett, L. J., Prakash, C., McCallum, R. W., and Guerrant, R. L. (1990) Urea protects Helicobacter (Campylobacter) pylori from the bactericidal effect of acid, *Gastroenterology 99*, 697-702

104. Marshall, B. J., and Warren, J. R. (1984) Unidentified curved bacilli in the stomach of patients with gastritis and peptic ulceration, *Lancet 1*, 1311-1315

105. Martin-Diaconescu, V., Bellucci, M., Musiani, F., Ciurli, S., and Maroney, M. J. (2012) Unraveling the Helicobacter pylori UreG zinc binding site using X-ray absorption spectroscopy (XAS) and structural modeling, *Journal of biological inorganic chemistry : JBIC : a publication of the Society of Biological Inorganic Chemistry 17*, 353-361. (10.1007/s00775-011-0857-9)

106. McGee, D. J., May, C. A., Garner, R. M., Himpsl, J. M., and Mobley, H. L. (1999) Isolation of Helicobacter pylori genes that modulate urease activity, *Journal of bacteriology 181*, 2477-2484

107. McNorton, M. M., and Maier, R. J. (2012) Roles of H2 uptake hydrogenases in Shigella flexneri acid tolerance, *Microbiology 158*, 2204-2212. (10.1099/mic.0.058248-0)

108. Mehta, N., Benoit, S., and Maier, R. J. (2003) Roles of conserved nucleotide-binding domains in accessory proteins, HypB and UreG, in the maturation of nickel-enzymes required for efficient Helicobacter pylori colonization, *Microbial Pathogenesis 35*, 229-234. (10.1016/s0882-4010(03)00151-7)

109. Mehta, N., Olson, J. W., and Maier, R. J. (2003) Characterization of Helicobacter pylori nickel metabolism accessory proteins needed for maturation of both urease and hydrogenase, *Journal of bacteriology 185*, 726-734

110. Mehta, N., Olson, J. W., and Maier, R. J. (2003) Characterization of Helicobacter pylori Nickel Metabolism Accessory Proteins Needed for Maturation of both Urease and Hydrogenase, *Journal of bacteriology 185*, 726-734. (10.1128/jb.185.3.726-734.2003)

111. Menard, R., Sansonetti, P. J., and Parsot, C. (1993) Nonpolar mutagenesis of the ipa genes defines IpaB, IpaC, and IpaD as effectors of Shigella flexneri entry into epithelial cells, *Journal of bacteriology 175*, 5899-5906

112. Merrell, D. S., Goodrich, M. L., Otto, G., Tompkins, L. S., and Falkow, S. (2003) pH-regulated gene expression of the gastric pathogen Helicobacter pylori, *Infect Immun 71*, 3529-3539

113. Merrell, D. S., Thompson, L. J., Kim, C. C., Mitchell, H., Tompkins, L. S., Lee, A., and Falkow, S. (2003) Growth phase-dependent response of Helicobacter pylori to iron starvation, *Infect Immun 71*, 6510-6525

114. Miles, S., Carpenter, B. M., Gancz, H., and Merrell, D. S. (2010) Helicobacter pylori apo-Fur regulation appears unconserved across species, *Journal of microbiology 48*, 378-386. (10.1007/s12275-010-0022-0)

115. Miller, E. F., and Maier, R. J. (2014) Ammonium metabolism enzymes aid Helicobacter pylori acid resistance, *Journal of bacteriology 196*, 3074-3081. (10.1128/JB.01423-13)

116. Mobley, H. L., Garner, R. M., and Bauerfeind, P. (1995) Helicobacter pylori nickel-transport gene nixA: synthesis of catalytically active urease in Escherichia coli independent of growth conditions, *Molecular microbiology 16*, 97-109

117. Moodley, Y., Linz, B., Bond, R. P., Nieuwoudt, M., Soodyall, H., Schlebusch, C. M., Bernhoft, S., Hale, J., Suerbaum, S., Mugisha, L., van der Merwe, S. W., and Achtman, M. (2012) Age of the association between Helicobacter pylori and man, *PLoS Pathog 8*, e1002693. (10.1371/journal.ppat.1002693)

118. Muller, C., Bahlawane, C., Aubert, S., Delay, C. M., Schauer, K., Michaud-Soret, I., and De Reuse, H. (2011) Hierarchical regulation of the NikR-mediated nickel response in Helicobacter pylori, *Nucleic acids research 39*, 7564-7575. (10.1093/nar/gkr460)

119. Neupane, K. P., Aldous, A. R., and Kritzer, J. A. (2014) Macrocyclization of the ATCUN motif controls metal binding and catalysis, *Abstr Pap Am Chem S 247*

120. Newville, M. (2001) EXAFS analysis using FEFF and FEFFIT, *Journal of synchrotron radiation 8*, 96-100. (Doi 10.1107/S0909049500016290)

121. Newville, M., Līviņš, P., Yacoby, Y., Rehr, J., and Stern, E. (1993) Near-edge x-ray-absorption fine structure of Pb: A comparison of theory and experiment, *Physical Review B 47*, 14126-14131. (10.1103/PhysRevB.47.14126)

122. Noguchi, K., Riggins, D. P., Eldahan, K. C., Kitko, R. D., and Slonczewski, J. L. (2010) Hydrogenase-3 contributes to anaerobic acid resistance of Escherichia coli, *PloS one 5*, e10132. (10.1371/journal.pone.0010132)

123. Olson, J. W., and Maier, R. J. (2002) Molecular hydrogen as an energy source for Helicobacter pylori, *Science 298*, 1788-1790. (10.1126/science.1077123)

124. Olson, J. W., Mehta, N. S., and Maier, R. J. (2001) Requirement of nickel metabolism proteins HypA and HypB for full activity of both hydrogenase and urease in Helicobacter pylori, *Molecular microbiology 39*, 176-182

125. Olson, J. W., Mehta, N. S., and Maier, R. J. (2001) Requirement of nickel metabolism proteins HypA and HypB for full activity of both hydrogenase and urease in Helicobacter pylori (vol 39, pg 176, 2001), *Molecular microbiology 40*, 270-270. (DOI 10.1046/j.1365-2958.2001.02397.x)

126. Orillard, E., Radicella, J. P., and Marsin, S. (2011) Biochemical and cellular characterization of Helicobacter pylori RecA, a protein with high-level constitutive expression, *Journal of bacteriology 193*, 6490-6497. (10.1128/JB.05646-11)

127. Ottemann, K. M., and Lowenthal, A. C. (2002) Helicobacter pylori uses motility for initial colonization and to attain robust infection, *Infect Immun 70*, 1984-1990

128. Padden, K. M., Krebs, J. F., MacBeth, C. E., Scarrow, R. C., and Borovik, A. S. (2001) Immobilized metal complexes in porous organic hosts: Development of a material for the selective and reversible binding of nitric oxide, *J Am Chem Soc 123*, 1072-1079. (Doi 10.1021/Ja003282b)

129. Park, D. H., Laivenieks, M., Guettler, M. V., Jain, M. K., and Zeikus, J. G. (1999) Microbial utilization of electrically reduced neutral red as the sole electron donor for growth and metabolite production, *Appl Environ Microb 65*, 2912-2917

130. Peek, R. M., Jr., and Blaser, M. J. (2002) Helicobacter pylori and gastrointestinal tract adenocarcinomas, *Nat Rev Cancer 2*, 28-37. (10.1038/nrc703)

131. Pflock, M., Finsterer, N., Joseph, B., Mollenkopf, H., Meyer, T. F., and Beier, D. (2006) Characterization of the ArsRS regulon of Helicobacter pylori, involved in acid adaptation, *Journal of bacteriology 188*, 3449-3462. (10.1128/JB.188.10.3449-3462.2006)

132. Pflock, M., Kennard, S., Delany, I., Scarlato, V., and Beier, D. (2005) Acid-induced activation of the urease promoters is mediated directly by the ArsRS two-component system of Helicobacter pylori, *Infect Immun 73*, 6437-6445. (10.1128/IAI.73.10.6437-6445.2005)

133. Ravel, B., and Newville, M. (2005) ATHENA, ARTEMIS, HEPHAESTUS: data analysis for X-ray absorption spectroscopy using IFEFFIT, *Journal of synchrotron radiation 12*, 537-541. (10.1107/S0909049505012719)

134. Ryan, K. C. (2013) Investigation of the Structure/Function Relationship in Nickel Containing Superoxide Dismutase, In *Chemistry*, p 259, University of Massachusetts Amherst, UMASS Amherst.

135. Ryan, K. C., Guce, A. I., Johnson, O. E., Brunold, T. C., Cabelli, D. E., Garman, S. C., and Maroney, M. J. (2015) Nickel superoxide dismutase: structural and functional roles of His1 and its H-bonding network, *Biochemistry 54*, 1016-1027. (10.1021/bi501258u)

136. Sachs, G., Weeks, D. L., Wen, Y., Marcus, E. A., Scott, D. R., and Melchers, K. (2005) Acid acclimation by Helicobacter pylori, *Physiology 20*, 429-438. (DOI 10.1152/physiol.00032.2005)

137. Salama, N., Guillemin, K., McDaniel, T. K., Sherlock, G., Tompkins, L., and Falkow, S. (2000) A whole-genome microarray reveals genetic diversity among Helicobacter pylori strains, *Proc Natl Acad Sci U S A 97*, 14668-14673. (10.1073/pnas.97.26.14668)

138. Salama, N. R., Hartung, M. L., and Muller, A. (2013) Life in the human stomach: persistence strategies of the bacterial pathogen Helicobacter pylori, *Nat Rev Microbiol 11*, 385-399. (10.1038/nrmicro3016)

139. Sankararamakrishnan, R., Verma, S., and Kumar, S. (2005) ATCUN-like metal-binding motifs in proteins: Identification and characterization by crystal structure and sequence analysis, *Proteins 58*, 211-221

140. Sawers, R. G., Jamieson, D. J., Higgins, C. F., and Boxer, D. H. (1986) Characterization and physiological roles of membrane-bound hydrogenase isoenzymes from Salmonella typhimurium, *Journal of bacteriology 168*, 398-404

141. Schauer, K., Gouget, B., Carriere, M., Labigne, A., and de Reuse, H. (2007) Novel nickel transport mechanism across the bacterial outer membrane energized by the TonB/ExbB/ExbD machinery, *Molecular microbiology 63*, 1054-1068. (10.1111/j.1365-2958.2006.05578.x)

142. Schauer, K., Muller, C., Carriere, M., Labigne, A., Cavazza, C., and De Reuse, H. (2010) The Helicobacter pylori GroES cochaperonin HspA functions as a specialized nickel chaperone and sequestration protein through its unique C-terminal extension, *Journal of bacteriology 192*, 1231-1237. (10.1128/JB.01216-09)

143. Schreiber, S., Konradt, M., Groll, C., Scheid, P., Hanauer, G., Werling, H. O., Josenhans, C., and Suerbaum, S. (2004) The spatial orientation of Helicobacter pylori in the gastric mucus, *Proc Natl Acad Sci U S A 101*, 5024-5029. (10.1073/pnas.0308386101)

144. Schreiter, E. R., Sintchak, M. D., Guo, Y., Chivers, P. T., Sauer, R. T., and Drennan, C. L. (2003) Crystal structure of the nickel-responsive transcription factor NikR, *Nature structural biology 10*, 794-799. (10.1038/nsb985)

145. Schubert, E. M. (1992) Utilizing the Evans Method with a Superconducting Nmr Spectrometer in the Undergraduate Laboratory, *J Chem Educ 69*, 62-62

146. Scott, D., Weeks, D., Melchers, K., and Sachs, G. (1998) The life and death of Helicobacter pylori, *Gut 43 Suppl 1*, S56-60

147. Scott, D. R., Marcus, E. A., Weeks, D. L., Lee, A., Melchers, K., and Sachs, G. (2000) Expression of the Helicobacter pylori ureI gene is required for acidic pH activation of cytoplasmic urease, *Infect Immun 68*, 470-477

148. Scott, D. R., Marcus, E. A., Weeks, D. L., and Sachs, G. (2002) Mechanisms of acid resistance due to the urease system of Helicobacter pylori, *Gastroenterology 123*, 187-195

149. Shaik, M. M., Cendron, L., Salamina, M., Ruzzene, M., and Zanotti, G. (2014) Helicobacter pylori periplasmic receptor CeuE (HP1561) modulates its nickel affinity via organic metallophores, *Molecular microbiology 91*, 724-735. (10.1111/mmi.12487)

150. Shao, C., Zhang, Q., Tang, W., Qu, W., Zhou, Y., Sun, Y., Yu, H., and Jia, J. (2008) The changes of proteomes components of Helicobacter pylori in response to acid stress without urea, *Journal of microbiology 46*, 331-337. (10.1007/s12275-008-0062-x)

151. Shi, R., Munger, C., Asinas, A., Benoit, S. L., Miller, E., Matte, A., Maier, R. J., and Cygler, M. (2010) Crystal structures of apo and metal-bound forms of the UreE protein from Helicobacter pylori: role of multiple metal binding sites, *Biochemistry 49*, 7080-7088. (10.1021/bi100372h)

152. Skouloubris, S., Thiberge, J. M., Labigne, A., and De Reuse, H. (1998) The Helicobacter pylori UreI protein is not involved in urease activity but is essential for bacterial survival in vivo, *Infect Immun 66*, 4517-4521

153. Slonczewski, J. L., McGee, D. J., Phillips, J., Kirkpatrick, C., and Mobley, H. L. (2000) pH-dependent protein profiles of Helicobacter pylori analyzed by two-dimensional gels, *Helicobacter 5*, 240-247

154. Sonnenberg, A. (2013) Review article: historic changes of Helicobacter pylori-associated diseases, *Aliment Pharmacol Ther 38*, 329-342. (10.1111/apt.12380)

155. Stahler, F. N., Odenbreit, S., Haas, R., Wilrich, J., Van Vliet, A. H., Kusters, J. G., Kist, M., and Bereswill, S. (2006) The novel Helicobacter pylori CznABC metal efflux pump is required for cadmium, zinc, and nickel resistance, urease modulation, and gastric colonization, *Infect Immun 74*, 3845-3852. (10.1128/IAI.02025-05)

156. Stingl, K., and De Reuse, H. (2005) Staying alive overdosed: how does Helicobacter pylori control urease activity?, *International journal of medical microbiology : IJMM 295*, 307-315. (10.1016/j.ijmm.2005.06.006)

157. Stingl, K., Schauer, K., Ecobichon, C., Labigne, A., Lenormand, P., Rousselle, J. C., Namane, A., and de Reuse, H. (2008) In Vivo Interactome of Helicobacter pylori Urease Revealed by Tandem Affinity Purification, *Mol Cell Proteomics 7*, 2429-2441. (DOI 10.1074/mcp.M800160-MCP200)

158. Stohs, S. J., and Bagchi, D. (1995) Oxidative mechanisms in the toxicity of metal ions, *Free Radic Biol Med 18*, 321-336

159. Sydor, A. M., Lebrette, H., Ariyakumaran, R., Cavazza, C., and Zamble, D. B. (2014) Relationship between Ni(II) and Zn(II) coordination and nucleotide binding by the Helicobacter pylori [NiFe]-hydrogenase and urease maturation factor HypB, *The Journal of biological chemistry 289*, 3828-3841. (10.1074/jbc.M113.502781)

160. Sydor, A. M., Liu, J., and Zamble, D. B. (2011) Effects of metal on the biochemical properties of Helicobacter pylori HypB, a maturation factor of [NiFe]-hydrogenase and urease, *Journal of bacteriology 193*, 1359-1368. (10.1128/JB.01333-10)

161. Tan, S., and Berg, D. E. (2004) Motility of urease-deficient derivatives of Helicobacter pylori, *Journal of bacteriology 186*, 885-888

162. Tomb, J. F., White, O., Kerlavage, A. R., Clayton, R. A., Sutton, G. G., Fleischmann, R. D., Ketchum, K. A., Klenk, H. P., Gill, S., Dougherty, B. A., Nelson, K., Quackenbush, J., Zhou, L., Kirkness, E. F., Peterson, S., Loftus, B., Richardson, D., Dodson, R., Khalak, H. G., Glodek, A., McKenney, K., Fitzegerald, L. M., Lee, N., Adams, M. D., Hickey, E. K., Berg, D. E., Gocayne, J. D., Utterback, T. R., Peterson, J. D., Kelley, J. M., Cotton, M. D., Weidman, J. M., Fujii, C., Bowman, C., Watthey, L., Wallin, E., Hayes, W. S., Borodovsky, M., Karp, P. D., Smith, H. O., Fraser, C. M., and Venter, J. C. (1997) The complete genome sequence of the gastric pathogen Helicobacter pylori, *Nature 388*, 539-547. (10.1038/41483)

163. Torre, L. A., Bray, F., Siegel, R. L., Ferlay, J., Lortet-Tieulent, J., and Jemal, A. (2015) Global cancer statistics, 2012, *CA Cancer J Clin 65*, 87-108. (10.3322/caac.21262)

164. Tsuda, M., Karita, M., Morshed, M. G., Okita, K., and Nakazawa, T. (1994) A urease-negative mutant of Helicobacter pylori constructed by allelic exchange mutagenesis lacks the ability to colonize the nude mouse stomach, *Infect Immun 62*, 3586-3589

165. van Vliet, A. H., Ernst, F. D., and Kusters, J. G. (2004) NikR-mediated regulation of Helicobacter pylori acid adaptation, *Trends Microbiol 12*, 489-494. (10.1016/j.tim.2004.09.005)

166. van Vliet, A. H., Kuipers, E. J., Waidner, B., Davies, B. J., de Vries, N., Penn, C. W., Vandenbroucke-Grauls, C. M., Kist, M., Bereswill, S., and Kusters, J. G. (2001) Nickel-responsive induction of urease expression in Helicobacter pylori is mediated at the transcriptional level, *Infect Immun 69*, 4891-4897. (10.1128/IAI.69.8.4891-4897.2001)

167. Vinella, D., Fischer, F., Vorontsov, E., Gallaud, J., Malosse, C., Michel, V., Cavazza, C., Robbe-Saule, M., Richaud, P., Chamot-Rooke, J., Brochier-Armanet, C., and De Reuse, H. (2015) Evolution of Helicobacter: Acquisition by Gastric Species of Two Histidine-Rich Proteins Essential for Colonization, *PLoS Pathog 11*, e1005312. (10.1371/journal.ppat.1005312)

168. Voland, P., Weeks, D. L., Marcus, E. A., Prinz, C., Sachs, G., and Scott, D. (2003) Interactions among the seven Helicobacter pylori proteins encoded by the urease gene cluster, *American journal of physiology. Gastrointestinal and liver physiology 284*, G96-G106. (10.1152/ajpgi.00160.2002)

169. Wang, G., Alamuri, P., and Maier, R. J. (2006) The diverse antioxidant systems of Helicobacter pylori, *Molecular microbiology 61*, 847-860. (10.1111/j.1365-2958.2006.05302.x)

170. Wang, G., Romero-Gallo, J., Benoit, S. L., Piazuelo, M. B., Dominguez, R. L., Morgan, D. R., Peek, R. M., Jr., and Maier, R. J. (2016) Hydrogen Metabolism in Helicobacter pylori Plays a Role in Gastric Carcinogenesis through Facilitating CagA Translocation, *MBio 7*. (10.1128/mBio.01022-16)

171. Watanabe, S., Arai, T., Matsumi, R., Atomi, H., Imanaka, T., and Miki, K. (2009) Crystal structure of HypA, a nickel-binding metallochaperone for [NiFe] hydrogenase maturation, *Journal of molecular biology 394*, 448-459. (10.1016/j.jmb.2009.09.030)

172. Watanabe, S., Kawashima, T., Nishitani, Y., Kanai, T., Wada, T., Inaba, K., Atomi, H., Imanaka, T., and Miki, K. (2015) Structural basis of a Ni acquisition cycle for [NiFe] hydrogenase by Ni-metallochaperone HypA and its enhancer, *Proc Natl Acad Sci U S A 112*, 7701-7706. (10.1073/pnas.1503102112)

173. Weatherb.Mw. (1967) Phenol-Hypochlorite Reaction for Determination of Ammonia, *Analytical chemistry 39*, 971-&. (Doi 10.1021/Ac60252a045)

174. Weatherburn, M. W. (1967) Phenol-Hypochlorite Reaction for Determination of Ammonia, *Anal Chem 39*, 971-&. (Doi 10.1021/Ac60252a045)

175. Webb, S. M. (2005) SIXpack: a graphical user interface for XAS analysis using IFEFFIT, *Phys Scripta T115*, 1011-1014

176. Wen, Y., Feng, J., Scott, D. R., Marcus, E. A., and Sachs, G. (2007) The HP0165-HP0166 two-component system (ArsRS) regulates acid-induced expression of HP1186 alpha-carbonic anhydrase in Helicobacter pylori by activating the pH-dependent promoter, *Journal of bacteriology 189*, 2426-2434. (10.1128/JB.01492-06)

177. Wen, Y., Marcus, E. A., Matrubutham, U., Gleeson, M. A., Scott, D. R., and Sachs, G. (2003) Acid-Adaptive Genes of Helicobacter pylori, *Infection and Immunity 71*, 5921-5939. (10.1128/iai.71.10.5921-5939.2003)

178. Williams, C. L., Preston, T., Hossack, M., Slater, C., and McColl, K. E. (1996) Helicobacter pylori utilises urea for amino acid synthesis, *FEMS Immunol Med Microbiol 13*, 87-94

179. Wroblewski, L. E., Peek, R. M., Jr., and Wilson, K. T. (2010) Helicobacter pylori and gastric cancer: factors that modulate disease risk, *Clinical microbiology reviews 23*, 713-739. (10.1128/CMR.00011-10)

180. Wuerges, J., Lee, J. W., Yim, Y. I., Yim, H. S., Kang, S. O., and Djinovic Carugo, K. (2004) Crystal structure of nickel-containing superoxide dismutase reveals another type of active site, *Proc Natl Acad Sci U S A 101*, 8569-8574. (10.1073/pnas.0308514101)

181. Xia, W., Li, H., Yang, X., Wong, K. B., and Sun, H. (2012) Metallo-GTPase HypB from Helicobacter pylori and its interaction with nickel chaperone protein HypA, *The Journal of biological chemistry 287*, 6753-6763. (10.1074/jbc.M111.287581)

182. Xia, W., Li, H. Y., Sze, K. H., and Sun, H. Z. (2009) Structure of a Nickel Chaperone, HypA, from Helicobacter pylori Reveals Two Distinct Metal Binding Sites, *J Am Chem Soc 131*, 10031-10040. (Doi 10.1021/Ja900543y)

183. Yang, X., Li, H., Cheng, T., Xia, W., Lai, Y. T., and Sun, H. (2014) Nickel translocation between metallochaperones HypA and UreE in Helicobacter pylori, *Metallomics : integrated biometal science 6*, 1731-1736. (10.1039/c4mt00134f)

184. Yang, X., Li, H., Lai, T. P., and Sun, H. (2015) UreE-UreG complex facilitates nickel transfer and preactivates GTPase of UreG in Helicobacter pylori, *The Journal of biological chemistry 290*, 12474-12485. (10.1074/jbc.M114.632364)

185. Yano, J., and Yachandra, V. K. (2009) X-ray absorption spectroscopy, *Photosynthesis research 102*, 241-254. (10.1007/s11120-009-9473-8)

186. Zambelli, B., Bellucci, M., Danielli, A., Scarlato, V., and Ciurli, S. (2007) The Ni2+ binding properties of Helicobacter pylori NikR, *Chemical communications*, 3649-3651. (10.1039/b706025d)

187. Zambelli, B., Danielli, A., Romagnoli, S., Neyroz, P., Ciurli, S., and Scarlato, V. (2008) High-affinity Ni2+ binding selectively promotes binding of Helicobacter pylori NikR to its target urease promoter, *Journal of molecular biology 383*, 1129-1143. (10.1016/j.jmb.2008.08.066)

188. Zambelli, B., Turano, P., Musiani, F., Neyroz, P., and Ciurli, S. (2009) Zn2+-linked dimerization of UreG from Helicobacter pylori, a chaperone involved in nickel trafficking and urease activation, *Proteins 74*, 222-239. (10.1002/prot.22205)

189. Zbell, A. L., Benoit, S. L., and Maier, R. J. (2007) Differential expression of NiFe uptake-type hydrogenase genes in Salmonella enterica serovar Typhimurium, *Microbiology 153*, 3508-3516. (10.1099/mic.0.2007/009027-0)

190. Zeng, Y. B., Yang, N., and Sun, H. (2011) Metal-binding properties of an Hpn-like histidine-rich protein, *Chemistry 17*, 5852-5860. (10.1002/chem.201100279)

191. Zhu, Y., Chen, M., Gong, Y., Liu, Z., Li, A., Kang, D., Han, F., Liu, J., Liu, J., and Yuan, Y. (2015) Helicobacter pylori FKBP-type PPIase promotes gastric epithelial cell proliferation and anchorage-independent growth through activation of ERK-mediated mitogenic signaling pathway, *FEMS Microbiol Lett 362*. (10.1093/femsle/fnv023)